STRUCTURE-PROPERTY RELATIONSHIPS IN POLYIMIDE-IONENES AND COMPOSITES WITH IONIC LIQUIDS AS GAS SEPARATION MEMBRANES

by

GRAYSON PATRICK DENNIS

JASON E. BARA, COMMITTEE CHAIR
C. HEATH TURNER
PAUL A. RUPAR
STEVEN T. WEINMAN
EVAN K. WUJCIK

A DISSERTATION

Submitted in partial fulfillment of requirements
for the degree of Doctor of Philosophy
in the Department of Chemical and Biological Engineering
in the Graduate School of
The University of Alabama

TUSCALOOSA, ALABAMA

2020

ABSTRACT

Ionic polymers have capabilities to shape the pathway to new membranes and polymer systems that did not exist before. The imidazolium moiety has shown substantial abilities to integrate into a platform for ionic polymers allowing their growth and formation through imidazolium use as a building block. Addition of this component, both ionic and non-ionic, into a polymer matrix has been developed, but the creation of highly tunable, modular polymer structure that contains imidazolium has the potential to surpass previous iterations of ionic compounds and materials in gas separation. After developing a tailorable approach to high performance ionic polymers, we have formed ionic polyimides and polyamides that have been used for various applications such as gas separation, coatings, and films. The ionic polyimides and polyamides which were formed have the potential to be used as CO_2/light gas membranes.

The hardest factor to overcome within membrane separation is the flux-selectivity tradeoff which describes the upper limits of permeability, gases ability to flow through a membrane, and selectivity, one gas's ability over another to permeate. With the addition of these ionic units into the backbone and as "free"-ILs within the polymer matrix, the permeabilities of these materials can be greatly increased. Through systematic design and study of materials, the structure-property relationship of these newly developed ionic polymers can be determined and applied to further the understanding of these unique polymer systems.

DEDICATION

This dissertation is dedicated to my lab group and family, but especially my daughter, Clara, who was born during the preparation of this manuscript. I would also like to give a special shoutout to my wife whom I have been so blessed to have in my life.

LIST OF ABBREVIATIONS AND SYMBOLS

IL	Ionic liquid
P	Permeability
S	Solubility
D	Diffusivity
$\alpha_{i/j}$	Selectivity: the permeability of gas *i* over gas *j*
M_n	Number average molecular weight
$LiTf_2N$	Lithium Bistriflimide
Tf_2N	Bistriflimide
PMDA	Pyromellitic Dianhydride
6FDA	4,4′-(Hexafluoroisopropylidene)diphthalic anhydride
PES	Poly(ethersulfone)
NMP	N-Methyl-2-Pyrrolidone
DMF	Dimethylformamide
DI H_2O	Deionized Water
ODA	Oxydianiline
RT	Room temperature
API	1-(3-aminopropyl)imidazole
TC	Terephtaloyl chloride
IC	Isophthaloyl chloride

K_2CO_3	Potassium Carbonate
MALDI	Matrix assisted Laser Desorption/ionization
TOF	Time of Flight
MS	Mass spectrometry
DSC	Differential scanning Calorimetry
TGA	Thermogravimetric analysis
^{1}H-NMR	Hydrogen-nuclear magnetic resonance
^{13}C-NMR	Carbon-nuclear magnetic resonance
NPT	National pipe thread
PTFE	Teflon
XRD	X-ray diffraction
WAXD	Wide angle x-ray diffraction
λ	Wavelength
d	d-spacing
OEG	Oligo(ethylene glycol)
PEG	Poly(ethylene glycol)
MD	Molecular dynamics
QM	Quantum mechanics
FTIR	Fourier Transform Infrared spectroscopy
IIN	Interpenetrating ionene network
PIL	Polymerizable ionic liquid
T_g	Glass transition temperature
T_m	Melting temperature

Å	Angstrom
CH_4	Methane
N_2	Nitrogen
CO_2	Carbon dioxide
H_2	Hydrogen
BF_4	Tetrafluoroborate
PF_6	Hexafluorophosphate
OTf	Triflate
BETI	Bis(perfluoroethanesulfonyl)imide
C_4mim	1-butyl-3-methylimidazolium
C_2mim	1-ethyl-3-methylimidazolium
VC_4im	1-vinyl-3-butylimidazolium
PEGmim	1-(2-methoxyethyl)-3-methylimidazolium
Bnmim	1-benzyl-3-methylimidazolium
2MeAPI	1-(3-aminopropyl)-2-methylimidazole
PIM	Polymer of Intrinsic Microporosity
PI	Polyimide
MDX	4,4'-methylenebis(2,6-dimethylaniline)
PVDF	Poly(vinylidene fluoride)
SILM	Supported ionic liquid membrane
PMMA	Poly(methyl methacrylate)
pDCXy	1,4-bis(chloromethyl)benzene
mDCXy	1,3-bis(chloromethyl)benzene

oDCXy	1,2-bis(chloromethyl)benzene
Et_2O	Diethylether
THF	Tetrahydrofuran
wt%	Weight percent
kDa	Kilodaltons
X_N	Degree of polymerization, Number average of repeat units
$T_{d,10}$	Temperature at 10% mass loss
$T_{d,25}$	Temperature at 25% mass loss
S-D	Solution-diffusion
BTDA	3,3',4,4'-benzophenonetetracarboxylic dianhydride
PPD	para-phenylenediamine
MDA	4,4'-methylenedianiline
H-bonding	Hydrogen bonding
NH_4OH	Ammonium hydroxide
Et_3N	Triethylamine
MeOH	Methanol
ESP	Electrostatic potential
RDG	Reduced density gradient
GIFP	General interaction property functions
DFT	Density functional theory
SDF	Spatial distribution function
CMat	Connection matrix
SOP	Standard Operating Procedure

CNC	Computer numerical control
SbF_6	Hexafluoro antimonate
dca	Dicyanideamide

ACKNOWLEDGMENTS

Many people have helped and supported me through this pivotal and maybe even treacherous time in my life during my long academic career at The University of Alabama. My advisor, Dr. Jason Bara, has been a tremendous help throughout my graduate experience offering guidance and help wherever I might have needed it. I appreciate that he was able to take me on as a graduate student and foster my growth throughout this time. I especially want to thank him for his attitude toward research and always finding creative solutions with new lab equipment.

I would also like to thank my committee members, Dr. C. Heath Turner, Dr. Paul Rupar, Dr. Steven Weinman, and Dr. Evan Wujcik. You have been a true inspiration for all the incredible accomplishments you have achieved during your times in academia.

My family has been supported me throughout my time at The University of Alabama. Although the distance may be far, your love and support has always made me feel close.

Lastly, my lab mates, Postdocs, graduate, and undergraduate, have been a huge support system during my graduate career. I would like to especially thank Kathryn O'Harra, Irshad Kammakakam, and Sourav Chatterjee for the intellectual conversations and materials because without them I would not have gotten through this. To my undergraduate students, Tristin Jones, Paul Goss, and Colton Duprey, I know y'all will have great success wherever you land.

CONTENTS

LIST OF TABLES

LIST OF FIGURES

LIST OF SCHEMES

CHAPTER 1

INTRODUCTION

Greenhouse gases pose a major threat to the environment since they are the main contributor to the effects of climate change. Through their release, the typical weather patterns have become more extreme due to the effect of CO_2 trapping more energy in the atmosphere. According to the Global Carbon Budget 2019, over 36 billion metric tons of CO_2 are released a year which is consistently rising.[1] To fight the current rising CO_2 levels, CO_2 capturing methods have been employed such as cryogenic distillation[2, 3], amine scrubbing[4-10], and membrane separation[2, 11-18]. Amine scrubbing has been used in the natural gas industry for over 90 years, yet the solvents used to capture CO_2 can degrade and need to be disposed.[8] Cryogenic distillation can recover over 99.9% of gases when it is used, yet the energy cost to acquire the extremely low temperature makes this method very costly. Membrane technologies have flourished since they have moderate capital investment costs, yet very low maintenance. Currently membranes have many advantages when implemented into industrial processes due to their low energy consumption, small scale of equipment, environmentally benign, and ease to be incorporated with existing processes.

Membranes are a highly desirable alternative to current state-of-the-art separation methods such as cryogenic distillation and amine scrubbing due to their low energy input cost, high throughput ability, and versatility.[2, 15, 16, 19, 20] High performance polymers which

contain high free fractional volume (FFV), aromatic, and bulky units such as Tröger's Base[21-24], polymers of intrinsic microporosity[20, 25-28], and aromatic dianhydrides[29-40] (Figure 1.1) have shown advantageous characteristics because of their thermal stability, chemical resistance, and good permeability-selectivity trade-off.

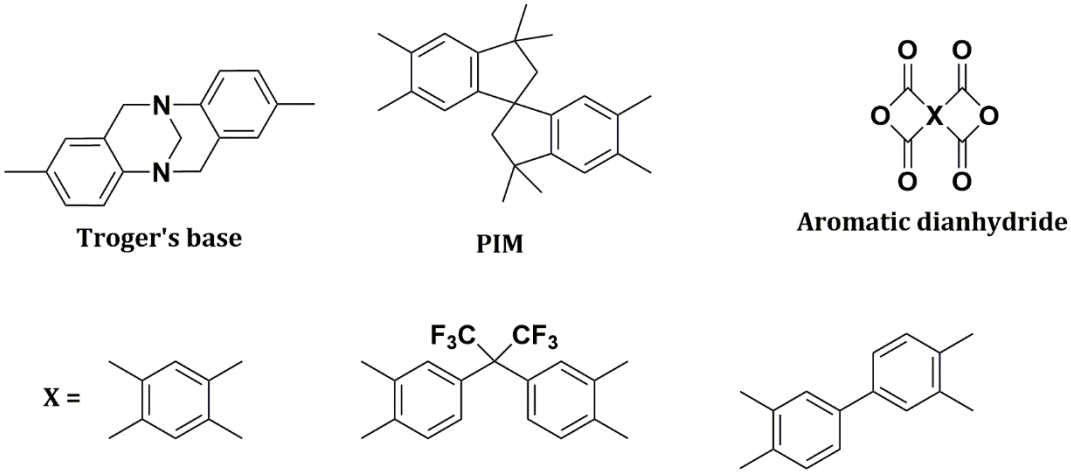

Figure 1.1 Examples of monomeric units used to form high FFV polymers

The dianhydride moiety is used in the formation of polyimides (PIs) which have good CO_2 permeabilities and excellent CO_2/CH_4 and CO_2/N_2 selectivities as well as high thermal stability which is desirable in flue gas separations and natural gas processing.[22, 30, 31, 39, 41-43] The permeability of a gas is a quantitative measure of throughput of gas through a thin membrane, and the selectivity of a membrane is the permeability likelihood of one gas over another to permeate through the membrane. The permeability/selectivity trade-off is a major hurdle to overcome within the gas separation field. As the permeability of a gas through a material increases, the selectivity of that material decreases and vice versa. Lloyd Robeson published the first paper on this characteristic trait of membranes which was dubbed "Robeson's Upper Bound."[44] The plot of permeability (P_i) in barrer versus selectivity ($S_{i/j}$) was denoted the Robeson Plot. This upper bound has been revised in a few

cases as higher permeability membranes are developed as well as the underlying equations refined.[45-47] Determining the permeability and selectivity of a gas separation membrane is integral to judging the viability of that material in the gas separation field.

PIs are formed through the condensation reaction between a dianhydride and a diamine. Two dianhydrides which have shown interest within the research of gas separation of polyimides are pyromellitic dianhydride (PMDA) and 4,4'-(Hexafluoroisopropylidene)diphthalic anhydride (6FDA) (Figure 1.2).

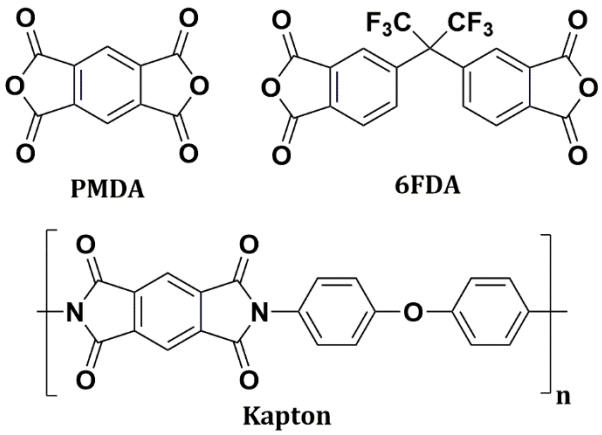

Figure 1.2 Structure of PMDA and 6FDA monomer and commercial polyimide, Kapton®, formed from polymerization of PMDA and ODA

PMDA is used in the formation of Kapton® which is well known for its mechanical, thermal, and chemical capabilities. O'Brien, et al. tested Kapton® from DuPont De Nemours against the same polymer that was polymerized using PMDA and oxydianiline (ODA) (Figure 1.2).[48] Although the materials are theoretically the same and their physical properties were nearly identical (T_g and density), the birefringence was significantly different demonstrating a high degree of orientation in the commercial film. The CO_2 permeability of the synthesized film was significantly higher (2.6 barrer versus 0.3 barrer) in the synthesized film versus the commercial film. The processing methods have a huge effect on the separation abilities

of the resulting polymer. These variables always need to be considered; as the more highly processed a material is, the better the thermal and mechanical properties become due to the alignment and chain-chain interactions of the resulting processed material.

Extensive research has been done utilizing both the PMDA and 6FDA monomers due to the inherent FFV when formed into a polymer backbone, yet research has shown that 6FDA typically outperforms PMDA due to the bulky -CF_3 group as well as its kinked structure.[33, 34, 38-40, 49-59] The Koros group investigated PMDA and 6FDA using three different diamines (Figure 1.3). The 6FDA moiety consistently had higher permeability values than the PMDA moiety when comparing 6FDA and PMDA with the same diamines. The same held true for CO_2/CH_4 selectivity where 6FDA was higher than the PMDA.[50] In another work by Hirayama, et al., 6FDA and PMDA are compared again in the same fashion as the Koros group.[34]

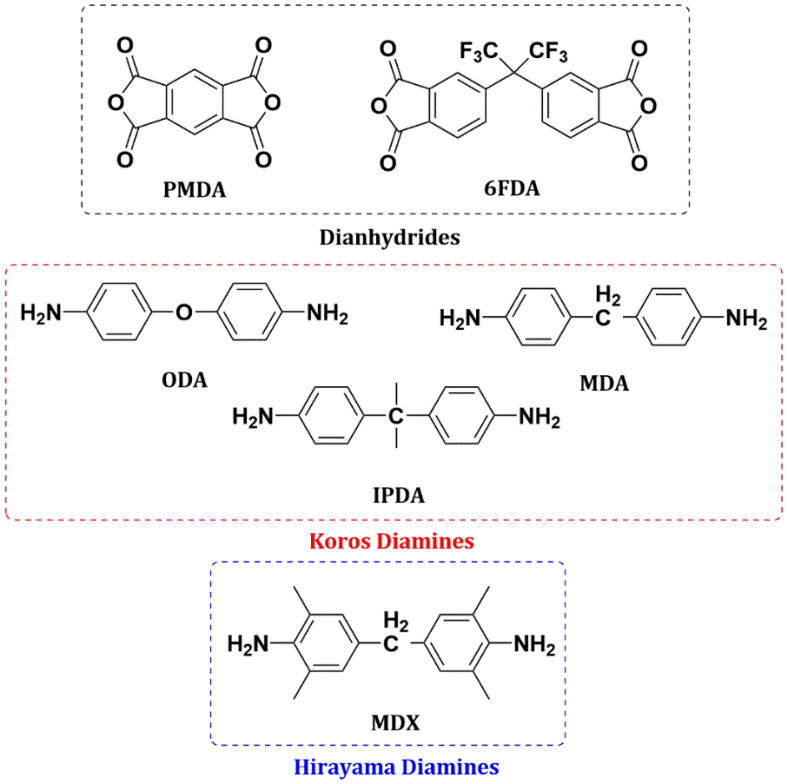

Figure 1.3 Monomers used in Koros polyimides and diamine structure in Hirayama, et al

In their research, two of the materials are kept the same (Figure 1.3), which showed nearly the same results to their predecessors, yet the newly introduced material using the "MDX" linkage caused the PMDA-based material to outperform the 6FDA-based by over 200% in CO_2 permeability.[34] The FFV is typically an indicator of the gas separation factors (permeability, diffusivity, and solubility), and since 6FDA has a kinked structure and bulky $-CF_3$ groups, it should attribute a higher FFV to the overall supramolecular structure. But due to the variable nature of dianhydride and diamine combinations, different dianhydride monomers need to be explored to determine their attribution to the overall structure-property relationship.

Introduction of ionic moieties within high performance polymers has become a growing field due to their CO2 solubility/capacity and compatibility with materials.[15, 60-62]

Ionic polymers in which the ionic moiety is within the polymer backbone have shown promising gas separation ability, yet the complete picture of their structure-property relationship is highly unknown. Many variables exist within ionic polymers such as the backbone formulation (polyelectrolyte, ionomer, or ionene (Figure 1.4)), cation-anion pairings, and specific moieties (alkyl, ether, aromatic, etc).

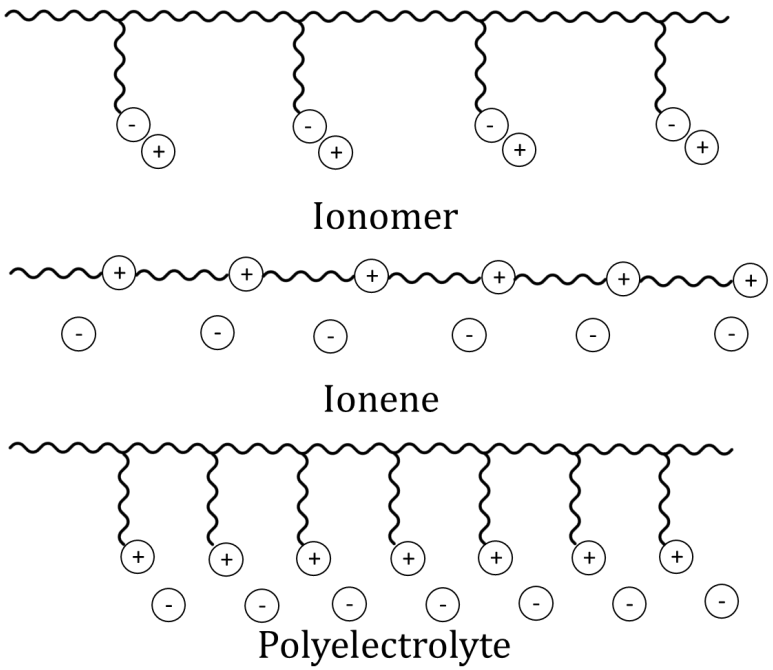

Figure 1.4 Graphical representation of ionomers, ionenes, and polyelectrolytes

The beginnings of ionic materials being used as gas separation membranes occurred when ILs were used as supported ionic liquids membranes (SILMs).[63, 64] This method of production uses highly porous materials such as polyethersulfone (PES), polyethylene glycol (PEG), and polyvinylidene fluoride (PVDF) among others, and the IL is saturated within the pores of these material.[12, 65-71] The CO_2 permeabilities of these SILMs was determined to be >1000 barrers in some cases while still maintaining their selective nature, which fueled investigation for ILs within gas separation. The main caveat, however,

with SILMs was their inability to resist high pressures. An issue also existed with their necessity for a thick membrane formation. Trying to further the investigations into ILs for industrial membrane separations, polymerizable groups were added to ILs to form polymerizable ionic liquids (PILs).[61, 72-83] These ionic materials fall under the polyelectrolyte moniker due to their backbone having IL moieties pendant to the polymer's main chain. PILs were found to have decreased permeabilities compared to the SILM counterparts due to the IL's restricted nature onto a polymer backbone. Even though the PILs had reduced permeabilities, in accordance with the permeability selectivity trade-off, their CO_2 selectivities increased. Along with an increase in selectivity, PILs experienced an increase in viability due to their ability to form thin films upon use of a thermal or photo initiator. However, PILs typically needed a supporting layer to be used as gas separation membranes and they can plasticize under high pressures, both of which hinders their industrial uses.[84] Although SILMs and PILs lack practicality in industrial applications, incorporation of ionic moieties based upon ILs into high performance polymers such as polyimides and polyamides could increase the gas separation ability because of ionic materials properties such as high CO_2 permeabilities and favorable thermal and chemical strengths.

The first known instance of ionic moieties polymerized with polyimide architecture was by Li, et al., yet only copolymers were tested rather than ionic homopolymers.[85] These materials had increasing CO_2 selectivities with increasing molar ionic content, yet since only copolymers were tested, determining the true effects of pure ionic polymers was not demonstrated. In another paper by the same group, block and random copolymers were formed using similar units from the first, yet again only the copolymers were tested for gas

permeabilities.[86] These copolymers again demonstrated increasing CO_2 selectivities although the CO_2 permeability decreased. These were the first instances where an ionic polyimide was polymerized with imidazolium cations directly in the backbone. It should be noted, however, that ionenes featuring tetraalkylammonium ions were the first instance of an ionic polymer being formed in 1933, through the Menshutkin reaction of forming 4° amines using alkylhalides.[87, 88] These examples of ionenes demonstrate two differing synthetic pathways of forming ionic polymers either through a condensation reaction or the Menshutkin reaction.

Our group has demonstrated the possibility of forming ionic polyimides with high number average molecular weight (M_n). Mittenthal, et al. showed that a bisimidazole diimide can be synthesized using a dianhydride and an amino-terminated imidazole.[89] Then quaternary amines are formed using an alkyl α,α'-dihalide through the Menshutkin reaction which causes the halide to be the anion. Anion metathesis is performed to exchange the halide with bistriflimide (Tf_2N). These neat materials demonstrated poor gas permeabilities, but when [C_4mim][Tf_2N] was adsorbed into the polymer matrix, the CO_2 permeabilities increased by over 2200%.[89] O'Harra, et al. has expanded on this concept and polymerized highly aromatic ionic polyimides and ionic polyamides which have also formed membranes with free ILs. They demonstrated that the addition of IL into these ionene materials increased the CO_2 permeabilities in all instances.[90, 91]

Scheme 1.1 Formation of amic acid intermediate from dianhydride and amino-terminated imidazole

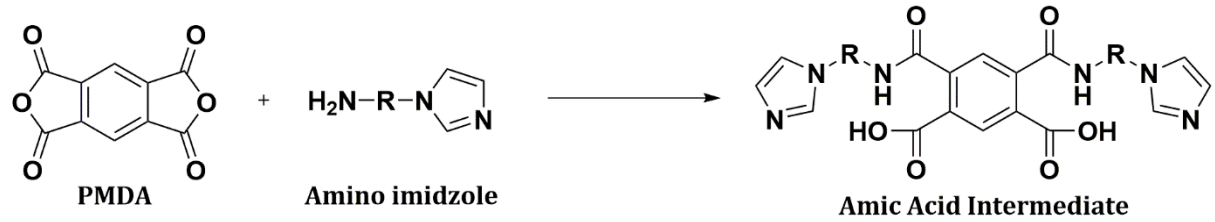

This new, modular synthetic method allows for units with these moieties to be polymerized together and form tens of thousands of different ionic polyimides because of the number of variables that are available in the synthetic schematic. A dianhydride is reacted with two molar equivalents of an amine-terminated imidazole through a condensation reaction. The anhydride rings are reacted via a condensation reaction forming the intermediate amic acid (Scheme 1.1). The amic acid intermediate cyclodehydrates to form a bisimidazole diimide (Scheme 1.2).

Scheme 1.2 Cyclodehydration of amic acid intermediate to form bisimidazole diimide

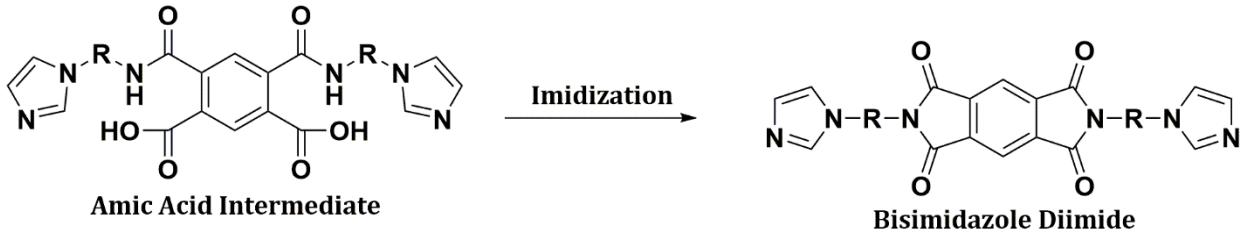

Once the bisimidazole diimide monomer is formed an alkyl-α,α'-dihalide is reacted with the monomer via the Menshutkin reaction, which is used in forming cationic, 4° amines where the halide is the anion (Scheme 1.3). The anions of the newly formed ionic polyimide can be exchanged with other non-coordinating anions ($[BF_4]^-$, $[PF_6]^-$, $[Tf_2N]^-$, $[BETI]^-$, etc) which can have drastic effects on the physical and chemical properties as demonstrated by O'Harra and co-workers in a paper that looks at the anion effects on polyimide ionenes.[92]

Drastic changes occur in the XRD profiles of the materials where crystalline peaks can be seen with smaller non-coordinating anions.

Scheme 1.3 Polymerization scheme of polyimide ionene from bisimidazole diimide and alkyl dihalide

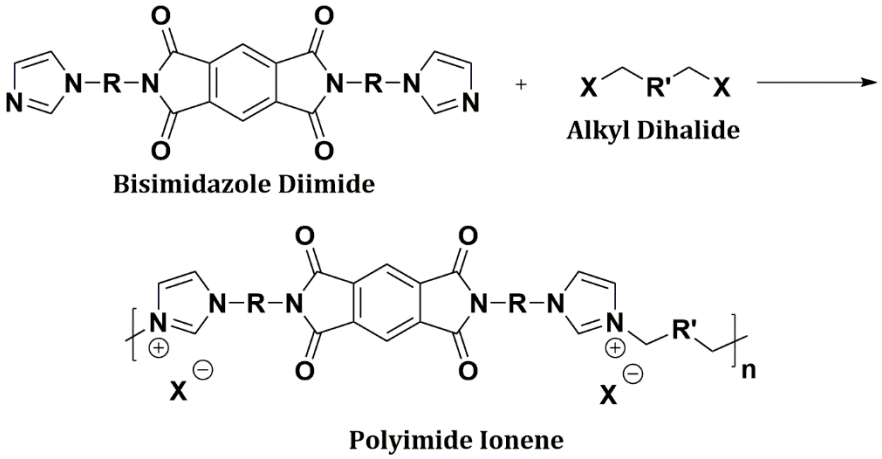

The totality of this work is to investigate the specific interactions and deterministically conclude the structure-property relationships that occur within ionic polyimide membranes and their effects on the gas separation ability. The first aspect investigated is the use of 6FDA as a monomer within our modular ionic polymer design to determine if the aromaticity and bulkier -CF_3, would aid in the gas separation properties. As prior research has demonstrated, 6FDA is known to have advantageous effects on the gas permeabilities of separation membranes, yet at times the effects can be deleterious to the final structuring of the membrane. Since Mittenthal, et al. had investigated a PMDA-based ionene (Figure 1.5), looking toward the introduction this larger and bulkier dianhydride linkage (i.e. 6FDA (Figure 1.5)) is the logical next step. The consensus found that 6FDA + IL composites were not as proficient at gas separation compared to their PMDA + IL composites.[93] Also, the effects of changing the regiochemistry (*para*-, *meta*-, and *ortho*-) was determined to investigate the packing and structuring of the polymer. The

PMDA-based ionic polyimides had distinct qualities which can be seen in the nanostructure of the XRD profile since localized ordering occurs whereas the 6FDA did not have any sort of localized ordering. After the 6FDA linkage was compared to its PMDA counterpart with respect to ionic polymer architecture, other structure-property relationships can be determined such as the effects of C(2) methylation of the imidazolium position.

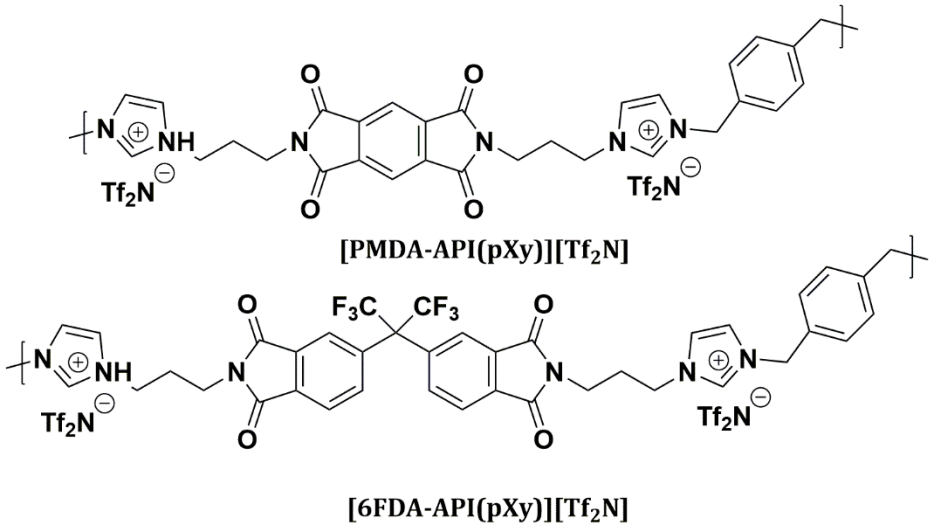

Figure 1.5 Ionic polyimides of interest: [PMDA-API(pXy)][Tf_2N][89] and [6FDA-API(pXy)][Tf_2N][93]

One highly contested effect within ionic liquids is the C(2) position on their structuring and molecular interactions.[94-101] Through rigorous investigation, Fumino, et al. concluded that the C(2) position of the imidazolium cation is integral to the H-bonding effects of the resulting IL.[96, 100] Upon methylation of the C(2) position, the intermolecular interactions tend toward coulombic rather than H-bonding. These same interactions could be integral to the formation of ionic polymers, so investigation of the C(2) position of imidazoliums within ionic polymers can lead to interesting effects on the resulting ionic polyimides formed. Methylation of the C(2) position of the imidazolium has not been

investigated within ionic polyimide architecture where the C(2) position of the imidazolium can have major effects on the structuring of the polymer matrix. Polymers like our previously made ionic polyimides were synthesized containing a methyl group on the C(2) position of the imidazolium moiety (Figure 1.6). Composites of these materials were formed with ionic liquid and their gas separation properties were determined which found that the C(2) position of the imidazolium has a major effect on the chain-chain interaction within the polymer matrix.

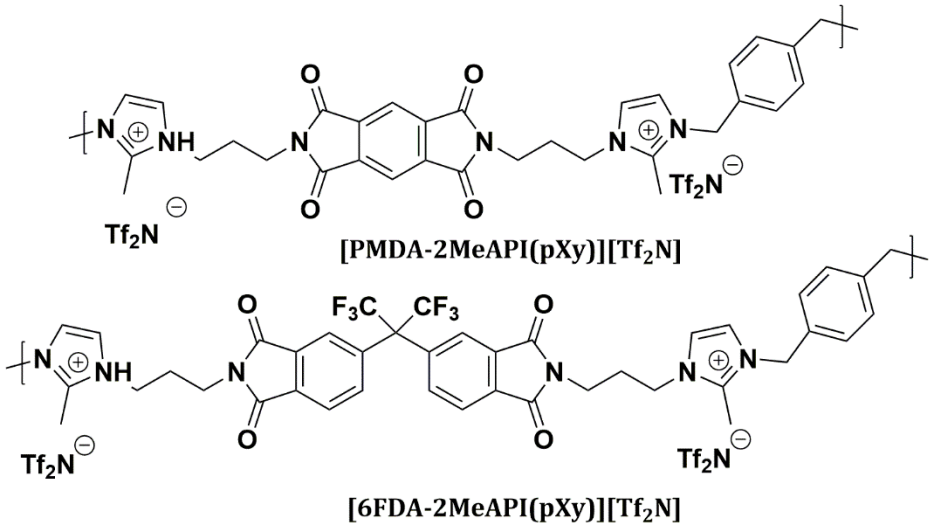

Figure 1.6 Ionic polymers of interest with C(2) methylated

After determination that the C(2) position was integral to the formation of the PMDA-based ionic polyimide, the use of different ILs to determine their effects on the PMDA ionene architecture was the next goal. Along with the IL composites, the regiochemistry of these was also investigated through the lens of XRD to investigate the structure changing xylyl linkages. To previously form films of this material, the PMDA was melt-pressed. The film formation and chain-chain interactions can be heavily influenced by the method with which the film is processed. To determine this effect, the film was made

using a solvent casting method which determined that the structuring occurring due to the IL adsorption was in fact a part of the PMDA ionene structure without IL. Upon investigation of the XRD patterning, the ILs did not have a major influence on the polymer's nanostructure. The gas permeabilities of the neat cast film were substantially higher than the melt-pressed film. Addition of IL did not influence the gas separation ability of the film which shows that the IL structures the film increasing the gas permeabilities.

Other aspects of ionic polymers have been investigated as this modular method allows for not only the formation of polyimide ionenes, but also the formation of polyamide ionenes.[102] These polyamides' gas separation abilities were compared to the other polyimides which showed that the polyamide structuring caused extremely low gas permeability values, yet their selectivity values where high enough to demonstrate capabilities for CO_2/light gas separations. However, it should be noted that these materials experienced very interesting physical characteristics which allowed them to self-heal while also being very elastomeric. Due to the poor permeabilities of the polyamides, this idea was not pursued any further for gas separation. The effects of multiple anions and linkers were also investigated due to the modular polymerization methods and formation of composites with ILs. Lastly, ionenes were dissolved into PILs which forms an interpenetrating ionene network (IIN) that can have implications by increasing the CO_2 permeabilities of the ionene due to the bulk PIL while maintaining gas selectivities of the interpenetrating ionene. This very new and interesting concept allows for easy film formation that combines the properties of PILs while imparting properties of the polymer into the structure. Though some of these concepts are only just being explored, they can help shift and shape the paths with which ionenes and ionic liquids can be used in gas separations.

Our group has investigated a few of the structure-property relationships, so this work only skims the surface of the ionic polymer field. Due to the wide variety of linkages, ionic placement, and charge density, many derivatives can be formulated and polymerized, yet the direction of current ionic research needs a foundation that directs the course of this research area. Herein is a look at the current works that have been explored with ionic polymers, both polyimide- and polyamide-based as well as composite materials formed from the addition of ionic liquids into the ionene polymer matrix.

CHAPTER 2

6FDA-BASED POLYIMIDES AND THEIR IONIC LIQUID COMPOSITES FOR GAS SEPARATION

2.1 Abstract

In recent years, polyimides synthesized from 4,4'-(Hexafluoroisopropylidene)diphthalic anhydride (6FDA) with various diamines have been frequently studied as gas separation membranes. The use of 6FDA in polyimides creates a bent structure than can increase fractional free volume (FFV) and gas permeability. Here, we demonstrate that 6FDA is also a useful building block for polyimide-ionene materials which contain cations directly within the polymer backbone. These new 6FDA-containing polyimide-ionenes were combined with imidazolium ionic liquids (ILs) to determine the structural relationship between regiochemistry and IL as it pertains to membrane formation. The thermal properties of all the derivatives were investigated to determine the relationship between regiochemistry and degradation as well as the intermolecular forces that are present within these structures. The gas separation properties of these 6FDA-containing polyimide-ionene + IL materials were investigated, showing modest CO_2 permeabilities similar to other polyimide-ionenes and CO_2/CH_4 and CO_2/N_2 permselectivities that were relatively higher than other polyimide-ionenes.

Keywords: 6FDA-Ionenes, Ionic Liquid Composites, Gas Separation Membranes

2.2 Introduction

Many forms of polymeric materials have been studied as gas separation membranes as they offer high flexibility, ease of scale-up, and energy efficiency,[1-7] making them competitive with distillation, absorption, and adsorption processes. The key parameters that measure the polymeric membrane gas separation ability are permeability (a normalized measure of flux) and selectivity (the separation factor between two species). Consequently, all glassy polymeric membranes suffer permeability-selectivity trade-off difficulties as quantified by Robeson's so-called upper bound limits.[8, 9]

Polyimides (PIs), synthesized from diamines and dianhydrides, are a well-known class of polymer membrane. Commercial PIs such as Kapton, Ultem, Matrimid, and P84 possess excellent mechanical, chemical, and thermal stability together with moderate gas separation performance, particularly for CO_2 separation in natural gas processing.[10-16]

PIs synthesized from 4,4'-(Hexafluoroisopropylidene)diphthalic anhydride (6FDA) have been observed to have high thermal stability (~500 °C) and better gas separation properties than other PIs[17]. A common dianhydride similar in structure to 6FDA (but not containing -CF_3 groups) is 4,4'-Carbonylbis(phthalic) anhydride. This dianhydride is used in the synthesis of both Matrimid and P84 (Figure 2.1). When comparing these two commercial polyimides to a similar 6FDA-containing polyimide, Sixef (Figure 2.1), the 6FDA-containing polymer had CO_2 permeabilities that were, respectively, over 8x and 50x greater.[18] Kim, et al. utilized two dianhydrides, 6FDA and pyromellitic dianhydride (PMDA), polymerized with various diamines.[4, 19] In both instances, the reported gas permeabilities were higher in the 6FDA derivatives than the PMDA derivatives. The same trend was observed for CO_2/CH_4 selectivities in each membrane. In one example where 6FDA

replaced PMDA, a marginal increase (~20%) in CO_2 permeability was observed in conjunction with a 55% increase in the permselectivity of CO_2/CH_4, which is unusual due to the relationship between permeability and selectivity.[4, 19]

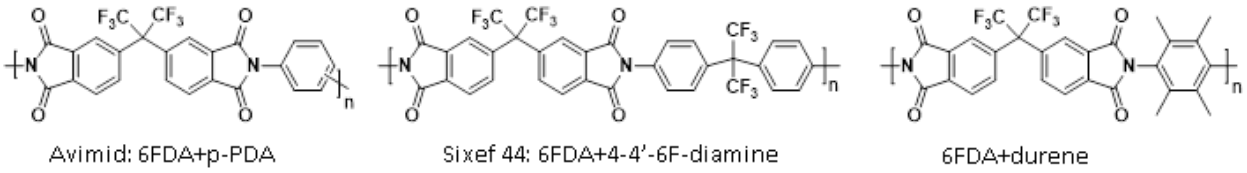

Figure 2.1 Commercially available polyimides synthesized from 6FDA and aromatic diamines

ILs are low temperature molten salts with large and asymmetric organic cations and organic or inorganic anions. ILs have also been of great interest for CO_2 separation because of their physical properties, and unique behaviors when added to polymer gas separation membranes.[20-25] Blending ILs with various polymers, (e.g. PEG[26], PES[27], PMMA[28], PVDF[29], etc.) is a growing trend among the polymer community. Many types of functional groups (ether, alkyl, or aromatic) have been appended to IL cations to influence thermophysical properties (e.g., density, viscosity) as well as CO_2 solubility and selectivity of the bulk ILs and membranes containing ILs.[27, 30, 31]

Our group has reported on new types of PI-ionenes in which imidazolium cations were incorporated into a rigid backbone and studied as CO_2-selective polymer membranes.[32-36] Our modular methods allow for creation of designer polymers through the synthesis of building blocks formed from the reaction of dianhydrides with "imidazole-amines", each of which can be selected from commercially available or novel species. In these methods, the amino terminus of the imidazole-amine selectively reacts with the

dianhydride to form the imide linkage; then α, α'-dihalides (or compounds with similar reactivity) are reacted to form polyimide-ionenes.

Previously, we demonstrated the concept of PI-ionenes by synthesizing a bisimidazole diimide monomer "PMDA-API" (Figure 2.2, left) from 1-(3-aminopropyl)imidazole (API) and PMDA. This bisimidazole diimide monomer was polymerized via the Menshutkin reaction with α, α'-dichloro-*para*-xylene, and the chloride (Cl^-) anions were exchanged to bistriflimide (Tf_2N^-) Membranes of this [PMDA-API(pXy)][Tf_2N] polymer showed CO_2 and H_2 permeabilities of 0.871 barrer and 1.6 barrer, respectively, yet once soaked in [C_4mim][Tf_2N] IL, the composite demonstrated increases in permeability to 20.7 barrer for CO_2 while only increasing H_2 to 5.18 barrer, increasing the selectivity of CO_2/H_2 over 700%.

The PMDA linkage is relatively small and planar, while 6FDA is larger and bent, and the effect of 6FDA in an analogous PI-ionene architecture is of interest as to whether it will increase gas permeability. Thus, we have produced PI-ionenes from bisimidazole a "6FDA-API" diimide monomer formed from 6FDA and API (Figure 2.2, right). The presence of two -CF_3 groups creates torsional strain between the phenyl rings, making a sharp bend in the backbone.

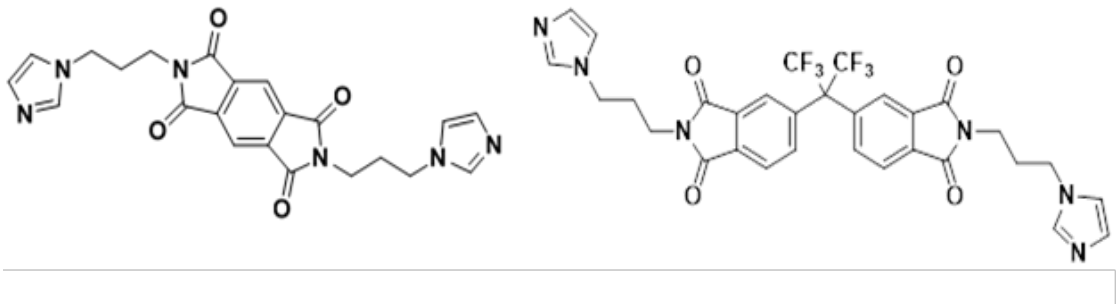

Figure 2.2 Example bisimidazole diimide monomers. Left: PMDA-API. Right: 6FDA-API

Here, we report the synthesis and gas separation properties of 6FDA-containing PI-ionenes including the influence of the regiochemistry of the linker group on the properties of these materials. 6FDA-API was polymerized with three different α,α'-dichloroxylene monomers (i.e., *para*-, *meta*-, and *ortho*-). The resultant PI-ionenes with $[Cl]^-$ anions were exchanged to the $[Tf_2N]^-$ forms, yielding three new PI-ionenes: [6FDA-API(p/m/oXy)][Tf_2N]. Our prior work demonstrated that incorporation of "free" ILs strongly influences the gas permeabilities of PI-ionenes,[36-38] and in this work, we also focus our study on the structural-property relationships and gas transport properties of these new 6FDA-containing PI-ionenes containing three different free ILs: [C_2mim][Tf_2N], [C_4mim][Tf_2N], and [Bnmim][Tf_2N].

2.3 Materials and Methods

2.3.1 Materials

6FDA (>99%) was purchased from Akron Polymer Systems (Akron, OH USA). 1,4-bis(chloromethyl)benzene (pDCXy, >98%), 1,3-bis(chloromethyl)benzene (mDCXy, >96%), 1,2-bis(chloromethyl)benzene (oDCXy, >97%) and 1-(3-aminopropyl)imidazole (API) were purchased from TCI (Portland, OR USA). Lithium bis-trifluoromethanesulfonimide ($LiTf_2N$) was purchased from 3M (Minneapolis, MN USA). N,N-dimethylformamide (DMF, anhydrous), tetrahydrofuran (THF, ACS grade), diethyl ether (Et_2O, ACS grade),and toluene (ACS Grade) were purchased from VWR (Atlanta, GA USA). All materials were used as obtained, without further purification.

2.3.2 Synthesis of 5,5'-(perfluoropropane-2,2-diyl)bis(2-(3-(1H-imidazol-1-yl)propyl)isoindoline-1,3-dione) (6FDA-API)

6FDA-API monomer was synthesized according to our previously published literature procedure, via the condensation of 6FDA (1 eq.) with API (2.05 eq.). The structure and purity of 6FDA-API monomer was confirmed by ^{1}H-NMR, which showed consistent results with published data.[35] The synthesis is demonstrated in Scheme 2.1.

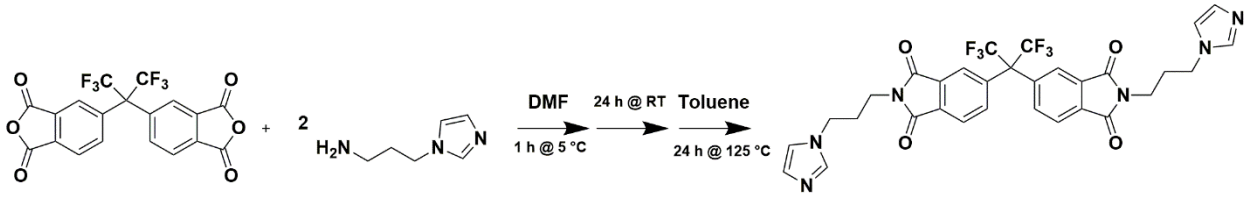

Scheme 2.1 Synthesis of 6FDA-API monomer

2.3.3 Synthesis of 6FDA-Polyimide-Ionenes

6FDA-API was subsequently polymerized with an equimolar amount of an α,α'-dichloroxylene (pDCXy, mDCXy, and oDCXy) to form a xylyl linkage via the Menshutkin reaction, followed by anion exchange from the Cl^- to the $[Tf2N]^-$ salt in H_2O. It should be noted that these ionenes are fully water soluble as the Cl^- salt. Upon exchange to the $[Tf2N]^-$ form, these ionenes are hydrophobic and precipitate. The precipitated polymers were thoroughly washed with water and dried in a vacuum oven.

2.3.3.1 Synthesis of [6FDA-API(pXy)][Tf2N]

6FDA-API (10.00 g, 15.2 mmol) and pDCXy (2.66 g, 15.2 mmol) were added with 50 mL of anhydrous DMF to a round-bottom heavy-walled pressure vessel and sealed. The reaction was heated at 120 °C for 24 h. The reaction was then cooled, the solvent was decanted, and the precipitated solids were dissolved in deionized (DI) H_2O. The polymer-containing solution was poured into DI H_2O containing $LiTf_2N$ (2.5 eq., 10.9 g) to promote

anion exchange. The [6FDA-API(pXy)][Tf2N] PI-ionene was stirred for 24 h at RT. The product was then filtered and dried in a vacuum oven at 120 °C overnight.

To remove low molecular weight content, 100 mL of THF was added to [6FDA-API(pXy)][Tf_2N] and stirred at RT for 4 h. The purified polymer separates as a brown gel, and the THF-rich layer containing residual solvent and oligomeric compounds was decanted. Finally, the polymer was reprecipitated in Et_2O and filtered. Again, the ionene product was dried to yield an off-white powder (15.87 g, 79%).

2.3.3.2 Synthesis of [6FDA-API(mXy)][Tf_2N]

The *meta*- derivative follows the same synthetic procedure as above, utilizing 6FDA-API (10.0 g, 15.2 mmol) and mDCXy (2.66 g, 15.2 mmol). The [6FDA-API(mXy)][Tf_2N] was cleaned via a similar procedure and dried, yielding the product as a tan powder (14.86 g, 74%). ^{1}H NMR (500 MHz, DMSO-d6) δ 9.37 (br, 2H), 8.08 (d, J = 8.04 Hz, 2H), 7.85 (d, J = 8.30 Hz, 2H), 7.80 (dt, J = 1.19 Hz, 4H) 7.69 (br, 2H), 7.50 (m, J = 7.41 Hz, 2H), 7.40 (d, J = 7.48 Hz, 2H), 5.46 (br, 4H), 4.27 (t, J = 7.24 Hz, 4H), 3.63 (t, J = 5.3 Hz, 4H), 2.18 (m, J = 7.59 Hz, 4H).

2.3.3.3 Synthesis of [6FDA-API(oXy)][Tf_2N]

The *ortho*- derivative follows the same synthetic procedure as above, utilizing 6FDA-API (10.0 g, 15.2 mmol) and oDCXy (2.66 g, 15.2 mmol). The [6FDA-API(oXy)][Tf_2N] was cleaned via a similar procedure and dried, yielding the product as a tan powder (14.12 g, 70%). ^{1}H NMR (500 MHz, DMSO-d6) δ 9.21 (br, 2H), 8.08 (d, J = 8.07 Hz, 2H), 7.86 (br, 2H), 7.84 (d, J = 8.65 Hz, 2H), 7.72 (dt, J = 1.20 Hz, 4H), 7.48 (m, J = 2.24, 3.38 Hz, 2H), 7.29 (m, J = 2.18, 3.44 Hz, 2H), 5.59 (br, 4H), 4.27 (t, J = 7.49 Hz, 4H), 3.64 (t, J = 5.4 Hz, 4H), 2.1 (m, J = 2.4, 8.2 Hz, 4H).

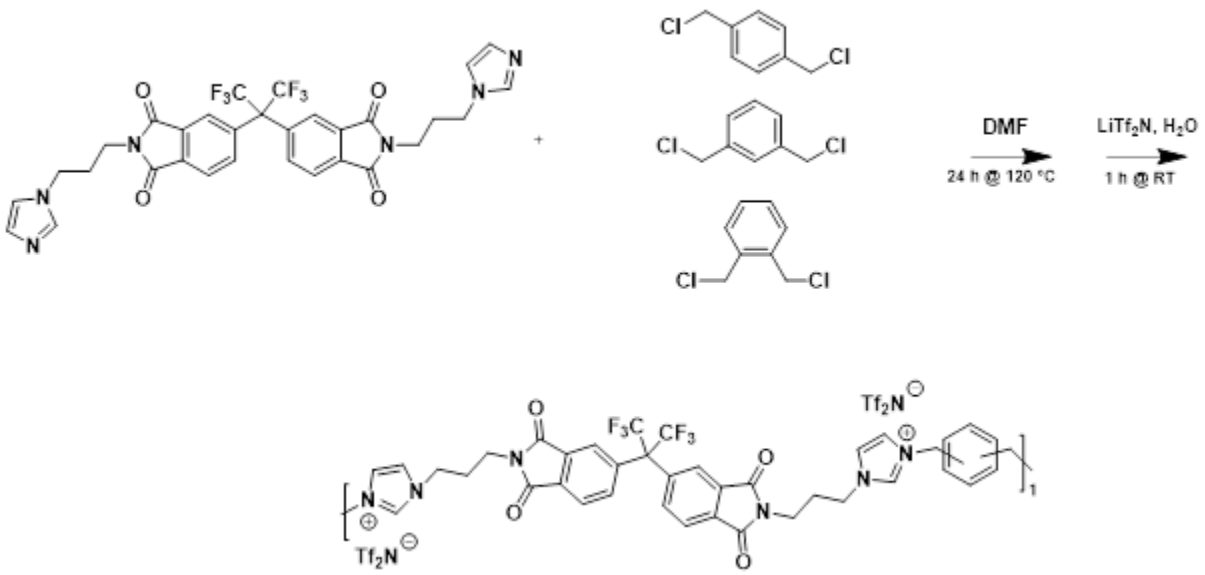

Scheme 2.2 Synthesis of [6FDA-API(p/m/oXy)][Tf_2N]

2.3.4 Membrane Preparation

To produce thin films suitable for use as gas separation membranes, the PI-ionenes (~1.00 g) were dissolved in 10 mL of acetone. 1 molar equivalent of a given IL (either [C_2mim][Tf_2N], [C_4mim][Tf_2N], or [Bnmim][Tf_2N]) was added to the vial, and the solution was homogenized. The solution was filtered through cotton to remove insoluble particulates that can impede membrane formation. The 6FDA-containing PI-ionene + IL solutions were cast onto a glass disc situated in a vacuum chamber. Dynamic vacuum was applied to the chamber and the acetone evaporates leaving a thin, PI-ionene + IL composite film on the glass. To delaminate the membrane from the glass, the membrane was heated to its glass transition temperature (T_g) of ~85 °C for 4 h and then placed into the freezer overnight. An example 6FDA-containing PI-ionene membrane (Figure 2.3), easily peeled from the glass after this procedure. After the final product sat at room temperature in open air to allow condensation from the freezer to dissipate, the membrane was heated again.

Figure 2.3 6FDA-API + IL composite film

2.3.5 Material Characterization

^{1}H-NMR analysis was performed for the both the [6FDA-API(mXy)][Tf_2N] and [6FDA-API(oXy)][Tf_2N] using a Bruker Avance NMR (360 MHz or 500 MHz) (Figures A2.1-2.2). The synthesis and NMR analysis for 6FDA API and [6FDA-API(pXy)][Tf_2N] derivative was outlined in our previous work.[35]

FTIR spectroscopy was performed using a PerkinElmer Spectrum Two spectrometer with the UATR accessory to support that the polymer structures and functional features were formed (Figure A2.7). The spectra were normalized at the carbonyl peak (C=O stretching vibrations at 1720 cm^{-1}). All the materials demonstrated similar peaks which show these as constitutional isomers. The imidazolium ionene formation was confirmed using the main imidazolium stretching vibrations at 1057 cm^{-1}. The ion metathesis of $[Cl]^-$ to $[Tf_2N]^-$ was confirmed via the presence of the sulfonyl (S=O stretching at 1130 cm^{-1} and 1354 cm^{-1}), secondary amine (C-N-C stretch at 725 cm^{-1} and 1105 cm^{-1}), and

trifluoromethyl stretching vibrations (C-F stretch at 1180 cm^{-1} and -CF_3 stretching at 1345 cm^{-1}).

Matrix assisted laser deionization/ionization-time of flight mass spectroscopy (MALDI-TOF MS) was performed on a Bruker Ultraflex to determine the number-average molecular weight (M_N) of each PI-ionene derivative, to confirm that high molecular weights were achieved which would support the formation of robust membranes (Figure A2.3). The repeat unit for these ionenes is 1322.98 g/mol, and Carothers' equation was utilized to derive the corresponding conversion (ρ) and number-average degree of polymerization (X_N).

Wide-angle x-ray diffraction (WAXD) was carried out using a Bruker D8 Discover on each membrane to determine the d-spacing of each material along with their ionic liquid counterparts. The d-spacing was determined by using Bragg's law (Eqn. 1), which states:

$$d = \frac{\lambda}{2*sin\theta} \quad (1)$$

The WAXD was performed in the 5 to 55° 2θ range. The radioactive source is cobalt which corresponds with a Kα of 1.79 Å.

DSC was performed on each neat material using a TA instruments DSC Q20 from 20 to 300 °C at a rate of 10 °C min^{-1} under N_2 environment (Figures A2.4-2.6).

Thermogravimetric analysis (TGA) was conducted utilizing a Seiko TG-DTA 7300 instrument. The mass was monitored as the samples were heated, ramping from room temperature to 700 °C at a rate of 10 °C min^{-1} under an inert atmosphere (Figures 2.5-2.6).

Thicknesses of the films were determined using a Mitutoyo micrometer (Series 293 MDC-MX) at 5 different spots across the membrane area. Kapton® HN films with known thicknesses of 25 μm were used to confirm the accuracy of the Mitutoyo micrometer. Since

the PI-ionene + IL composites were tacky, they would stick to the sintered support disc in the membrane unit, so thicknesses after gas separation could not be confirmed by SEM. To determine the thickness, the film and disc were measured and then the film was dissolved from the disc, and the thickness of the disc was determined using the micrometer. An average of their differences of the membrane-disc and disc was used for the thickness variable within the permeation calculations.

2.3.6 Gas Separation Units

Gas permeation behavior of 6FDA-API PI-ionene + IL composite membranes were analyzed using single gases (H_2, CO_2, N_2, and CH_4) to determine the permeability, solubility, and diffusivity coefficients. Time-lag systems based on the constant-volume/variable-pressure method were used, as described in our previous works.[33, 34, 36, 37] A 47 mm diameter composite membrane was placed onto a sintered disc and placed into the Millipore membrane holder with a 43 mm O-ring. After the feed and permeate were held at dynamic vacuum for 24 h, pure gas was applied to ~3 atm (~44 psia) on the feed while the downstream pressure was at vacuum (~0.01 psia). Through solution diffusion, the gas permeates through the dense membranes while the pressures of both the upstream and downstream were recorded. The pure gas permeations were determined by calculating the linear steady-state increase in pressure of downstream against time (i.e. dp/dt). Eqn. 2 shows the calculation for permeability (P) in units of barrer (10^{-10} cm cm_{stp}^3 s^{-1} $cmHg^{-1}$ cm^{-2}), where V (cm^3) is the downstream volume, l (cm) is the membrane thickness, A (cm^2) is the effective membrane area, T is the temperature in Kelvin and p_o (torr) is the driving force (i.e. the transmembrane pressure differential).

$$P = \frac{273}{76} * \frac{Vl}{ATp_o} * \frac{dp}{dt} \quad \textbf{(2)}$$

The ideal selectivities were determined by dividing the calculated permeabilities of a given gas pair (e.g. P_{CO2}/P_{CH4}).

2.4 Results and Discussion

2.4.1 Synthesis of 6FDA-API + IL Composite Membranes

Both the neat PI-ionenes and the composites with IL were cast and able to form membranes; however, the neat 6FDA-containing PI-ionenes were too brittle, resulting in fractures before and during gas separation testing. This behavior was similar to that which was reported by O'Harra, et. al where a similar material was used.[36] To overcome this issue, the addition of IL was necessary to form films which did not fail during membrane testing. One molar equivalent of [C_2mim][Tf_2N] (22.8 wt%), [C_4mim][Tf_2N] (24.1 wt%), or [Bnmim][Tf_2N] (25.5 wt%) was used, which resulted in membranes that were durable and flexible.

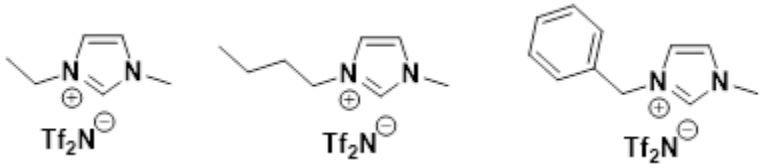

Figure 2.4. Structures of ILs added to PI-ionene to plasticize membranes. Left: [C_2mim][Tf_2N] Middle: [C_4mim][Tf_2N] Right: [Bnmim][Tf_2N]

2.4.2 Material Characterization

The [6FDA-API(pXy)][Tf_2N] polymer had M_N ~100 kDa, which was greater than [6FDA-API(oXy)][Tf_2N] polymer (M_N ~97 kDa) and the [6FDA-API(mXy)][Tf_2N] (M_N ~83 kDa). These values align with our previously reported number average molecular weights.

This corresponds to number average of repeat units (X_N) averages of 63-76 (implying monomer conversions (ρ) ≈ 0.984-0.986).

DSC was performed to determine the T_g of the neat materials, as summarized in Table 2.1 (Figures A2.4-A2.6) The DSC profile for [6FDA-API(pXy)][Tf_2N] indicates a T_g endotherm near 93.5 °C, which is in agreement with previous studies.[35, 36] [6FDA-API(mXy)][Tf_2N] and [6FDA-API(oXy)][Tf_2N] exhibited slightly lower T_g values (83.8 °C and 81.7 °C, respectively) than the *para*-substituted PI-ionene. The *para*-connectivity results in a more linear polymer backbone and may allow for more intermolecular interactions between ionene chains where the overall supramolecular structure can lay flat in sheets, whereas the sterics of the *meta*- and *ortho*-xylyl linkages have a higher propensity to induce bent segments between the 6FDA-API linkage. The more strain between xylyl and API features may cause strain of the propyl segment as well. The polymer's chain-chain interactions directly correlate to T_g, so therefore, when the polymer backbone is bent, the highly strained backbone affects entanglement and inhibits intermolecular interactions bringing about lower T_g. The addition of IL causes no visible glass transitions of the composite materials. The lack of T_g follows the Fox equation where the addition of a material with a lower T_g will depress the composite's T_g based upon the weight fraction.[39]

Table 2.1 T_g and d-spacing values for all neat and composite materials

	[6FDA-API(pXy)][Tf_2N]				**[6FDA-API(mXy)][Tf_2N]**		**[6FDA-API(mXy)][Tf_2N]**	
	Neat	**C_4mim**	**C_2mim**	**Bnmim**	**Neat**	**C_4mim**	**Neat**	**C_4mim**
T_g (°C)	93.5	--	--	--	83.8	--	81.7	--
d-spacing (Å)	5.72	5.33	4.98	4.67	5.88	5.88	5.91	5.88

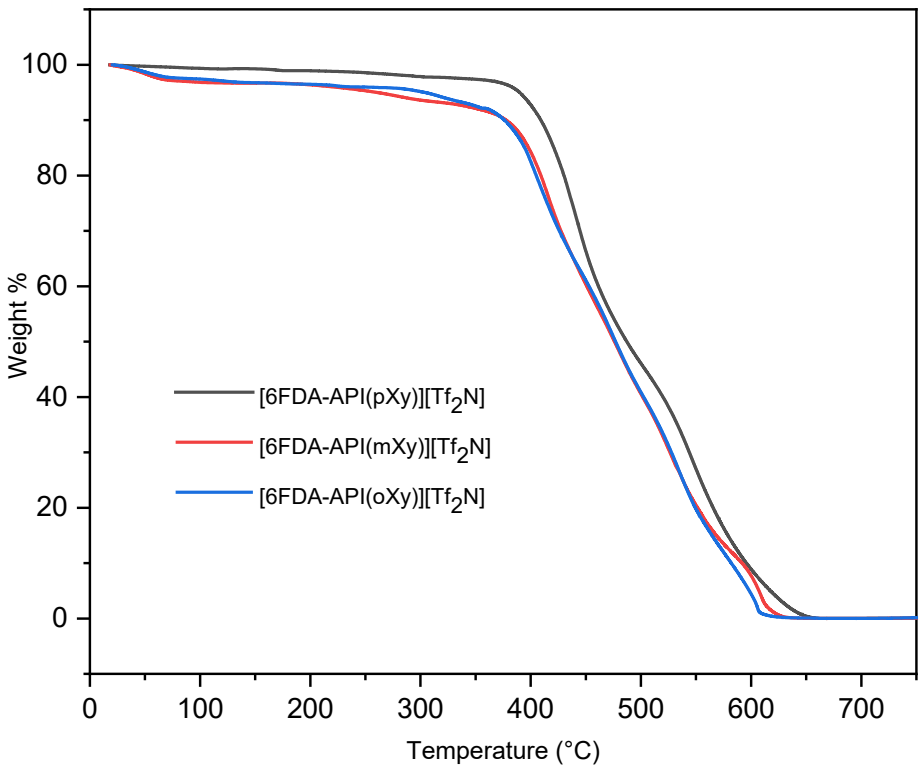

Figure 2.5 TGA curves of neat [6FDA-API(p/m/oXy)][Tf_2N]

TGA was used to demonstrate the thermal stabilities of each ionene, and the thermal decomposition at 10% and 25% degradation/mass loss ($T_{d,10}$ and $T_{d,25}$) were derived (Table 2.2). The thermal degradation behaviors for each 6FDA-containing PI-ionene with [C_4mim][Tf_2N] are displayed in Figure 2.6. Comparison of the neat materials reveals that [6FDA-API(pXy)][Tf_2N] has the highest degradation temperatures whereas [6FDA-API(mXy)][Tf_2N] and [6FDA-API(oXy)][Tf_2N] have very similar $T_{d,10}$ and $T_{d,25}$ values. The similarity of the [6FDA-API(mXy)][Tf_2N] and [6FDA-API(oXy)][Tf_2N] can be attributed to the more strained xylyl linkages compared to [6FDA-API(pXy)][Tf_2N]. [6FDA-API(pXy)][Tf_2N] + [C_4mim][Tf_2N] had the lowest $T_{d,10}$ compared to the other composites. [6FDA-API(mXy)][Tf_2N] + [C_4mim][Tf_2N] and [6FDA-API(oXy)][Tf_2N] + [C_4mim][Tf_2N] are

in agreement with the trends observed in previous ionene materials, such that the $T_{d,10}$ of the *ortho*-linked was less than that of the *meta*-linked.[36] However, it should be noted that the $T_{d,25}$ of all the composite variants corresponded very well with their neat variants following the order of *para*- > *meta*- > *ortho*-. The discrepancy in the $T_{d,10}$ can be associated with the xylyl linkage. [6FDA-API(pXy)][Tf_2N] and [6FDA-API(mXy)][Tf_2N] have similar degradation after 80% mass loss. At $T_{d,25}$, the IL has certainly degraded by 427 °C, and the polymer chains are degrading at this point.

Table 2.2 Temperatures at 10% and 25% mass loss of [6FDA-API(p/m/oXy)][Tf_2N] and [6FDA-API(p/m/oXy)][Tf_2N] + IL composites

	[6FDA-API(pXy)][Tf_2N]				**[6FDA-API(mXy)][Tf_2N]**		**[6FDA-API(oXy)][Tf_2N]**	
	Neat	**C_4mim**	**C_2mim**	**Bnmim**	**Neat**	**C_4mim**	**Neat**	**C_4mim**
$T_{d,10}$	401.5	352	394.5	380.5	377.7	391.5	376.1	376
$T_{d,25}$	435	427	427	426	418	425	414.9	407

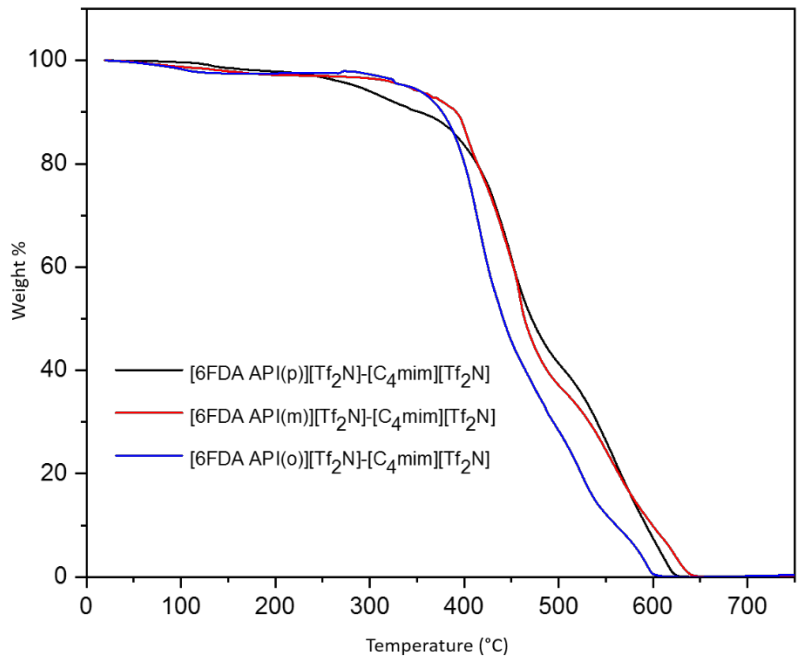

Figure 2.6 TGA curves of [6FDA-API(p/m/oXy)][Tf_2N] composites with 1 eq. [C_4mim][Tf_2N]

Within [6FDA-API(pXy)][Tf_2N], [C_2mim][Tf_2N] and [Bnmim][Tf_2N] IL composites were more stable under thermal stresses, which may indicate that that butyl group of [C_4mim][Tf_2N] degrades or cleaves more readily than the benzyl or ethyl substituents. The [C_2mim][Tf_2N] composite's $T_{d,10}$ was over 40 °C higher than the [6FDA-API(pXy)][Tf_2N] + [C_4mim][Tf_2N], whereas the [Bnmim][Tf_2N] composite's $T_{d,10}$ was 28 °C higher than the [6FDA API(pXy)][Tf_2N] + [C_4mim][Tf_2N] composite. Although these trends would suggest that the [Bnmim][Tf_2N] was the least stable, the benzyl group has a higher degradation temperature compared to the butyl group of the [C_4mim][Tf_2N].

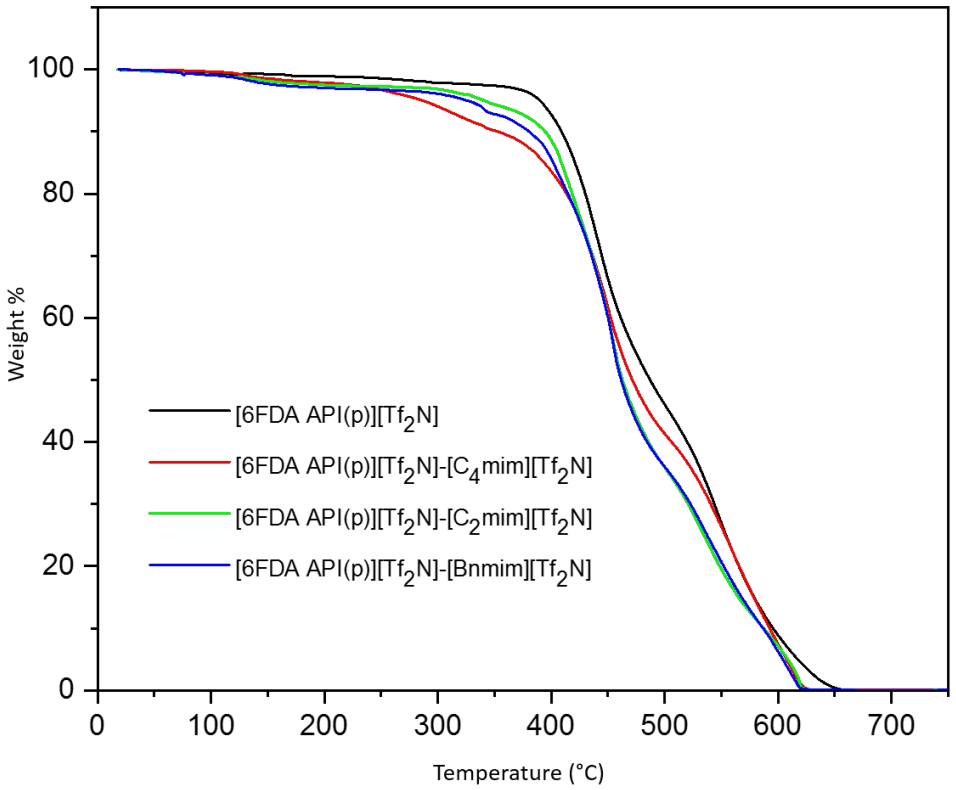

Figure 2.7 TGA curves of [6FDA-API(pXy)][Tf_2N] + ([C_2mim][Tf_2N], [C_4mim][Tf_2N], and [Bnmim][Tf_2N])

The $T_{d,25}$ temperatures were consistent across these systems at 427 °C, yet composite stabilities were depressed 8 °C in comparison to the neat counterpart. This supported that the IL had a considerable effect on the TGA, which is due to the expected onset of IL degradation which occurs at a lower temperature (250 °C). Since the IL in each composite accounts for approximately 23 – 26 % by mass, the $T_{d,25}$ suggests the range where the ionene matrix is degrading.

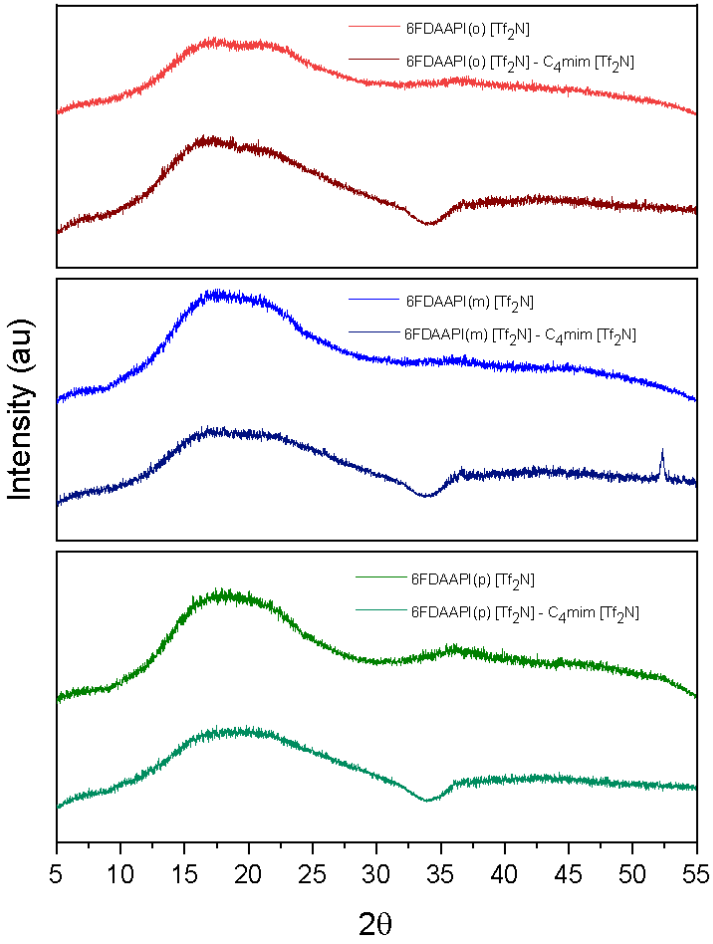

Figure 2.8 Wide-angle X-ray diffraction plots obtained from neat polyimide-ionenes and their [C_4mim][Tf_2N] composite analogues.

XRD profiles were collected for all materials, both neat and with ILs to determine the effects of regiochemistry and IL structure on the interchain spacings and resulting membrane performances. The d-spacings have been shown to correlate to the membrane's intermolecular chain spacings, which can be a predictor of a material's permeability.[40] The d-spacing values were calculated by using the 2θ at the peak of the halo which occurred between 2θ = 17.5-22.1 ° for all the materials. These d-spacing values were consistent with conventional polyimides which tend to be around 5.5 Å which is the median value of the halo.[41] The profiles for 6FDA-containing PI-ionenes and composites with [C_4mim][Tf_2N] are shown in Figure 2.8. The d-spacing values of the neat materials decreased in the order of *para*- < *meta*- < *ortho*-, which was hypothesized since the protruding *ortho*- linkages likely create the most strain between the 6FDA-API segments. The profile of both the [6FDA-API(mXy)][Tf_2N] and [6FDA-API(oXy)][Tf_2N] polymers showed a semi-bimodal halo, which would indicate a slightly lower d-spacing due to the connectivity of each. The change of the xylyl connectivity caused an obvious change to a lower 2θ within the halo. This change is likely due to the xylyl linkage not packing as well with the polymer structure. The addition of [C_4mim][Tf_2N] to the material caused the d-spacing peak to become more prominent.

The addition of [C_2mim][Tf_2N] and [Bnmim][Tf_2N] caused the [6FDA-API(pXy)][Tf_2N] to decrease their d-spacings when compared with the corresponding [C_4mim][Tf_2N] composite. The inclusion of [C_2mim][Tf_2N] resulted in a much broader halo than either of the composites as there was a sharp increase to 14.5 ° where it then peaked at 20.7 °. The [C_2mim][Tf_2N] may be filling in the voids between the chains better than [C_4mim][Tf_2N], which causes the immobility between the chains. The aromaticity of [Bnmim][Tf_2N] could increase the d-spacing by inhibiting chain packing, yet the opposite

behavior was occurred as the addition of an aromatic IL caused the polymer chains to be more tightly packed. The benzyl IL may have allowed for improved stacking interactions with the backbone xylyl groups, which would support the decrease of d-spacing and permeability.

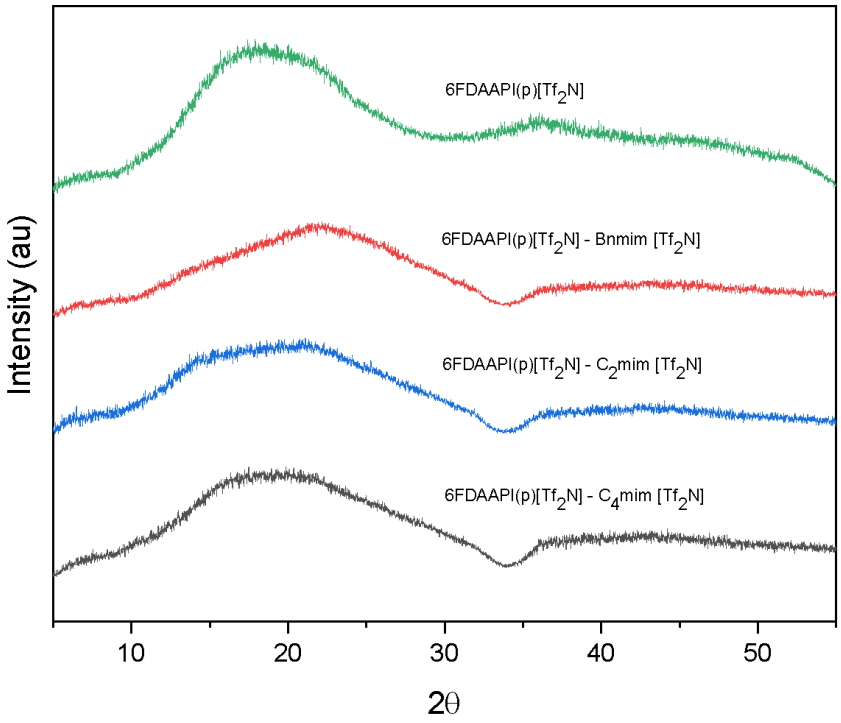

Figure 2.9 Wide-angle X-ray diffraction profiles obtained for neat [6FDA-API(pXy)] [Tf_2N] and composites with various ILs.

2.4.3 Gas Separation Properties

The gas permeabilities of each membrane are reported in Table 2.3. [6FDA-API(pXy)][Tf_2N] + [C_4mim][Tf_2N] showed the highest permeability out of all the composite materials. [6FDA-API(pXy)][Tf_2N] + [Bnmim][Tf_2N] had the lowest permeability values while the [6FDA-API(pXy)][Tf_2N] + [C_2mim][Tf_2N] closely followed. The d-spacings trends observed from changing the IL correlate positively to both their permeabilities and their selectivities. As the d-spacing increased, the permeability increased, and the diffusivity

decreased which was expected. The selectivities of [6FDA-API(pXy)][Tf_2N] with different IL cation structures followed the permeability and selectivity tradeoff, further proving the material's validity which also correlated with a distinct trend to their respective d-spacings. As every permeability decreased, selectivities of all materials increased.

Table 2.3 Permeability (barrer) of [6FDA-API(p/m/oXy)][Tf_2N] + IL composite membranes at 3 atm and 20 °C. Uncertainty represents one standard deviation calculated from at least three replicate experiments

	[6FDA-API(pXy)]						**[6FDA-API(mXy)]**		**[6FDA-API(oXy)]**	
	[C_4mim]		**[C_2mim]**		**[Bnmim]**		**[C_4mim]**		**[C_4mim]**	
N_2	0.20	±0.03	0.08	±0.01	0.04	±0.01	0.05	±0.02	0.13	±0.01
CH_4	0.18	±0.02	0.08	±0.01	0.03	±0.01	0.06	±0.01	0.15	±0.02
H_2	3.59	±0.25	1.72	±0.04	1.32	±0.05	0.88	±0.06	2.62	±0.16
CO_2	6.66	±0.25	3.15	±0.13	1.48	±0.03	1.69	±0.22	5.27	±0.44

The influence of the regiochemistry (*para*-, *meta*-, and *ortho*-) of the xylene linkage shows that the *meta*-connectivity clearly results in the lowest permeability for each gas. Although [C_4mim][Tf_2N] was added to all variants, comparisons can be made between all three composites since the IL is a constant, isolating the effects of the xylyl connectivity on the permeability. The permeabilities of [6FDA-API(pXy)][Tf_2N] and [6FDA-API(oXy)][Tf_2N] were more similar than that of [6FDA-API(mXy)][Tf_2N] which was considerably lower. Even though the d-spacing for [6FDA-API(oXy)][Tf_2N] is higher than [6FDA-API(pXy)][Tf_2N], the halo gives a range of d-spacings, so [6FDA-API(oXy)][Tf_2N] peaks at a higher d-spacing value the halo exists from 2θ = 17.5 - 22.5 °. Though [6FDA-API(mXy)][Tf_2N] exhibited permeability values of only about 33% those of the other materials, both the CO_2 and H_2 selectivities were comparable to both [C_4mim][Tf_2N]

composites. Permeabilities of *meta*-connected isomers were shown to be considerably lower by Coleman et al, so the lower permeabilities of this case is not unusual.[42]

Table 2.4 Permselectivity values for [6FDA-API(p/m/oXy)][Tf_2N] composite membranes

	[6FDA-API(pXy)]			**[6FDA-API(mXy)]**	**[6FDA-API(oXy)]**
	C_4mim	**C_2mim**	**Bnmim**	**C_4mim**	**C_4mim**
CO_2 /N_2	32.9	41.7	41.5	31.6	39.9
CO_2 /CH_4	36.3	40.0	52.3	29.7	36.0
CO_2 /H_2	1.8	1.8	1.1	1.9	2.0
H_2 /N_2	17.7	22.8	36.9	16.5	19.8
H_2 /CH_4	19.5	21.9	46.6	15.4	17.9

Plotting the relevant selectivities (e.g. CO_2/CH_4 and CO_2/N_2) and permeabilities of gas pairs on a logarithmic scale with Robeson's upper bound (Figures 2.10 and 2.11) showed that the membranes from this study are comparable to other ionic polymers reported in literature. The selectivities were also within the range of other ionic polymers but among the more selective ionic materials for both CO_2/N_2 and CO_2/CH_4. With this knowledge, addition of monomeric units associated with higher permeabilities (Tröger's base, spirobisindane, iptycene) introduced within our PI-ionene structures will be the focus of future studies. This may allow for more permeable membranes while maintaining or surpassing typical selectivity values.

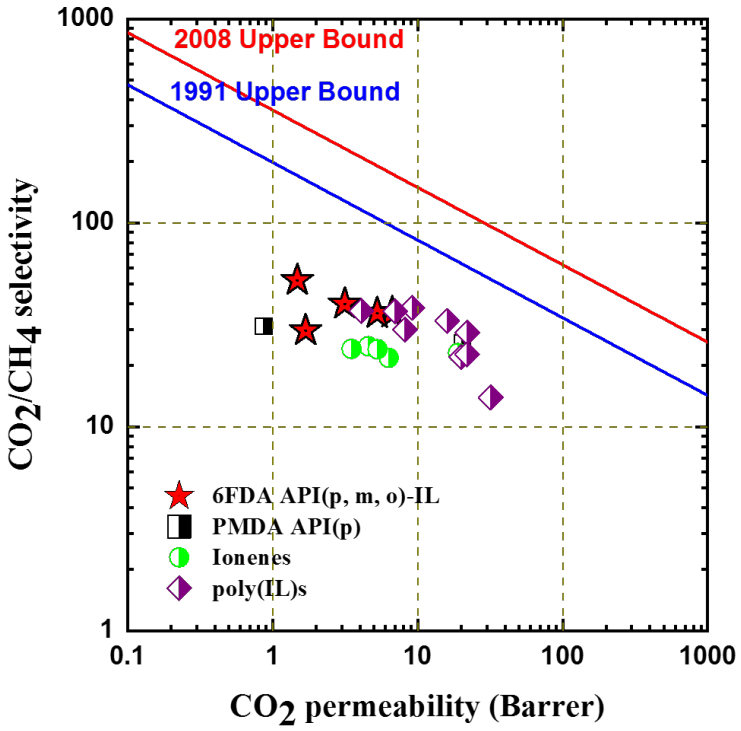

Figure 2.10 Robeson's upper bound Plots of CO_2/N_2 selectivities versus CO_2 permeability of [6FDA-API(p/m/oXy)][Tf_2N], [PMDA-API(pXy)][Tf_2N], various other ionenes, and poly(ILs). Data taken from refs.[33, 36, 43-47]

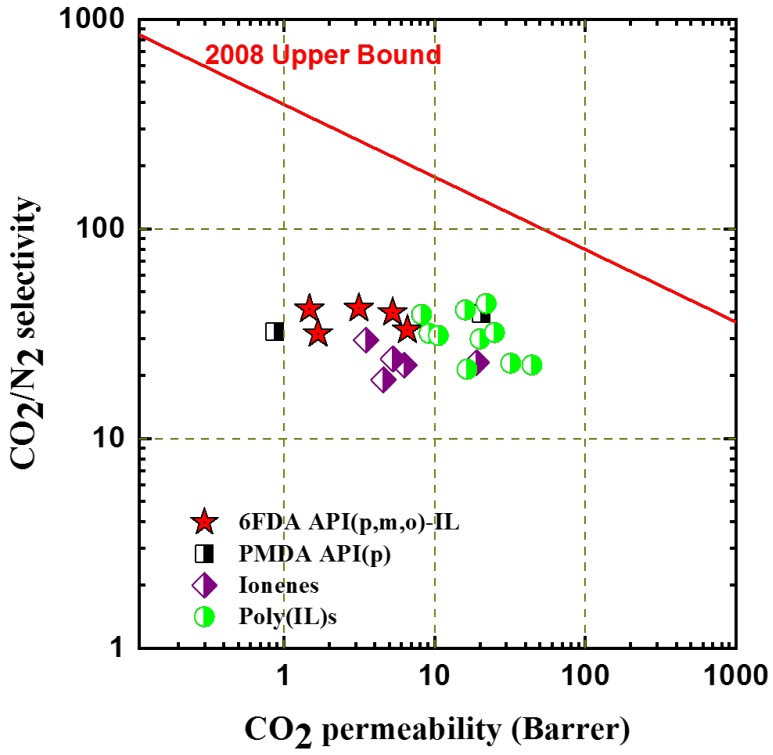

Figure 2.11 Robeson's upper bound Plots of CO_2/CH_4 selectivities versus CO_2 permeability of [6FDA-API(p/m/oXy)][Tf_2N], [PMDA-API(pXy)][Tf_2N], various ionenes, and poly(ILs). Data taken from refs.[33, 36, 43-47]

2.5 Conclusions

In summary, 6FDA-containing PI-ionenes were successfully synthesized and characterized using ^{1}H-NMR, MALDI-TOF MS, XRD, DSC, and TGA. Dense, thin membranes were formed via solvent casting and tested only in this form. Although the neat polymers were not suitable for study as membranes due to their glassy, fragile nature, they were still usable in the form of composites with ILs which helped plasticize the material. Addition of [C_4mim][Tf_2N] did not change the d-spacings of the polymer as seen in the XRDs but slightly enhanced the halo's peaks. The results show that [6FDA-API(pXy)][Tf_2N] +

[C_4mim][Tf_2N] had the highest permeability values when used as a composite whereas [6FDA-API(mXy)][Tf_2N] + [C_4mim][Tf_2N] had the lowest. Since [6FDA-API(pXy)][Tf_2N] demonstrated the best overall permeability value, the effects of two additional ILs with different cation substituents groups were examined. The presence of a smaller alkyl chain [C_2mim][Tf_2N] decreased the permeabilities when compared to [C_4mim][Tf_2N] while [Bnmim][Tf_2N] reduced permeabilities even further like due to the stacking of the aromatic groups. The PI-ionene + IL composite approach clearly offers a vast array of possible material combinations in terms of polymer structures and IL composition. The results here help guide further design as it is clear that the *para*-xylene linkage and [C_4mim][Tf_2N] resulted in the highest gas permeabilities.

2.6. References

1. Baker, R. W., Future Directions of Membrane Gas Separation Technology. *Ind. Eng. Chem. Res.* **2002,** *41* (6), 1393-1411.

2. Bernardo, P.; Drioli, E.; Golemme, G., Membrane Gas Separation: A Review/State of the Art. *Ind. Eng. Chem. Res.* **2009,** *48* (10), 4638-4663.

3. Budd, P. M.; Msayib, K. J.; Tattershall, C. E.; Ghanem, B. S.; Reynolds, K. J.; McKeown, N. B.; Fritsch, D., Gas separation membranes from polymers of intrinsic microporosity. *J. Membr. Sci.* **2005,** *251* (1-2), 263-269.

4. Kim, T. H.; Koros, W. J.; Husk, G. R., Advanced gas separation membrane materials: rigid aromatic polyimides. *Sep. Sci. Technol.* **1988,** *23* (12-13), 1611-26.

5. Sanders, D. F.; Smith, Z. P.; Guo, R.; Robeson, L. M.; McGrath, J. E.; Paul, D. R.; Freeman, B. D., Energy-efficient polymeric gas separation membranes for a sustainable future: A review. *Polymer* **2013,** *54* (18), 4729-4761.

6. Scholes, C. A.; Stevens, G. W.; Kentish, S. E., Membrane gas separation applications in natural gas processing. *Fuel* **2012,** *96*, 15-28.

7. Stern, S. A., Polymers for gas separations: the next decade. *J. Membr. Sci.* **1994,** *94* (1-3), 1-65.

8. Robeson, L. M., Correlation of separation factor versus permeability for polymeric membranes. *J. Membr. Sci.* **1991,** *62* (2), 165-85.

9. Robeson, L. M., The upper bound revisited. *J. Membr. Sci.* **2008,** *320* (1+2), 390-400.

10. Ayala, D.; Lozano, A. E.; de Abajo, J.; Garcia-Perez, C.; de la Campa, J. G.; Peinemann, K. V.; Freeman, B. D.; Prabhakar, R., Gas separation properties of aromatic polyimides. *J. Membr. Sci.* **2003,** *215* (1-2), 61-73.

11. Bos, A.; Punt, I. G. M.; Wessling, M.; Strathmann, H., Plasticization-resistant glassy polyimide membranes for CO2/CH4 separations. *Sep. Purif. Technol.* **1998,** *14* (1-3), 27-39.

12. Park, S.-H.; Kim, K.-J.; So, W.-W.; Moon, S.-J.; Lee, S.-B., Gas separation properties of 6FDA-based polyimide membranes with a polar group. *Macromol. Res.* **2003,** *11* (3), 157-162.

13. Stern, S. A.; Liu, Y.; Feld, W. A., Structure/permeability relationships of polyimides with branched or extended diamine moieties. *J. Polym. Sci., Part B: Polym. Phys.* **1993,** *31* (8), 939-51.

14. Liaw, D.-J.; Wang, K.-L.; Huang, Y.-C.; Lee, K.-R.; Lai, J.-Y.; Ha, C.-S., Advanced polyimide materials: Syntheses, physical properties and applications. *Prog. Polym. Sci.* **2012,** *37* (7), 907-974.

15. Wang, Z.; Wang, D.; Jin, J., Microporous Polyimides with Rationally Designed Chain Structure Achieving High Performance for Gas Separation. *Macromolecules (Washington, DC, U. S.)* **2014,** *47* (21), 7477-7483.

16. Xiao, Y.; Low, B. T.; Hosseini, S. S.; Chung, T. S.; Paul, D. R., The strategies of molecular architecture and modification of polyimide-based membranes for CO2 removal from natural gas-A review. *Prog. Polym. Sci.* **2009,** *34* (6), 561-580.

17. Zhuang, Y.; Seong, J. G.; Lee, Y. M., Polyimides containing aliphatic/alicyclic segments in the main chains. *Progress in Polymer Science* **2019,** *92*, 35-88.

18. Escorihuela, S.; Tena, A.; Shishatskiy, S.; Escolástico, S.; Brinkmann, T.; Serra, M. J.; Abetz, V., Gas Separation Properties of Polyimide Thin Films on Ceramic Supports for High Temperature Applications. *Membranes-Basel* **2018,** *8* (1).

19. Kim, T. H.; Koros, W. J.; Husk, G. R.; O'Brien, K. C., Relationship between gas separation properties and chemical structure in a series of aromatic polyimides. *J. Membr. Sci.* **1988,** *37* (1), 45-62.

20. Abedini, A.; Crabtree, E.; Bara, J. E.; Turner, C. H., Molecular Simulation of Ionic Polyimides and Composites with Ionic Liquids as Gas-Separation Membranes. *Langmuir* **2017,** *33* (42), 11377-11389.

21. Bara, J. E.; Carlisle, T. K.; Gabriel, C. J.; Camper, D.; Finotello, A.; Gin, D. L.; Noble, R. D., Guide to CO2 Separations in Imidazolium-Based Room-Temperature Ionic Liquids. *Ind. Eng. Chem. Res.* **2009,** *48* (6), 2739-2751.

22. Moganty, S. S.; Chinthamanipeta, P. S.; Vendra, V. K.; Krishnan, S.; Baltus, R. E., Structure-property relationships in transport and thermodynamic properties of imidazolium bistriflamide ionic liquids for CO2 capture. *Chem. Eng. J. (Amsterdam, Neth.)* **2014,** *250*, 377-389.

23. Ramdin, M.; de Loos, T. W.; Vlugt, T. J. H., State-of-the-Art of CO2 Capture with Ionic Liquids. *Ind. Eng. Chem. Res.* **2012,** *51* (24), 8149-8177.

24. Scovazzo, P., Determination of the upper limits, benchmarks, and critical properties for gas separations using stabilized room temperature ionic liquid membranes (SILMs) for the purpose of guiding future research. *J. Membr. Sci.* **2009,** *343* (1-2), 199-211.

25. Yoo, S.; Won, J.; Kang, S. W.; Kang, Y. S.; Nagase, S., CO2 separation membranes using ionic liquids in a Nafion matrix. *J. Membr. Sci.* **2010,** *363* (1-2), 72-79.

26. Kammakakam, I.; Rao, A. H. N.; Yoon, H. W.; Nam, S.; Park, H. B.; Kim, T.-H., An imidazolium-based ionene blended with crosslinked PEO as a novel polymer membrane for selective CO2 separation. *Macromol. Res.* **2014,** *22* (8), 907-916.

27. Bara, J. E.; Camper, D. E.; Gin, D. L.; Noble, R. D., Room-Temperature Ionic Liquids and Composite Materials: Platform Technologies for CO2 Capture. *Acc. Chem. Res.* **2010,** *43* (1), 152-159.

28. Scott, M. P.; Rahman, M.; Brazel, C. S., Application of ionic liquids as low-volatility plasticizers for PMMA. *Eur. Polym. J.* **2003,** *39* (10), 1947-1953.

29. Chen, H. Z.; Li, P.; Chung, T.-S., PVDF/ionic liquid polymer blends with superior separation performance for removing CO2 from hydrogen and flue gas. *Int. J. Hydrogen Energy* **2012,** *37* (16), 11796-11804.

30. Bara, J. E.; Gabriel, C. J.; Carlisle, T. K.; Camper, D. E.; Finotello, A.; Gin, D. L.; Noble, R. D., Gas separations in fluoroalkyl-functionalized room-temperature ionic liquids using supported liquid membranes. *Chem. Eng. J. (Amsterdam, Neth.)* **2009,** *147* (1), 43-50.

31. Bara, J. E.; Gabriel, C. J.; Hatakeyama, E. S.; Carlisle, T. K.; Lessmann, S.; Noble, R. D.; Gin, D. L., Improving CO2 selectivity in polymerized room-temperature ionic liquid gas separation membranes through incorporation of polar substituents. *J. Membr. Sci.* **2008,** *321* (1), 3-7.

32. Bara, J. E.; O'Harra, K. E., Recent Advances in the Design of Ionenes: Toward Convergence with High-Performance Polymers. *Macromolecular Chemistry and Physics* **2019,** *0* (0), 1900078.

33. Kammakakam, I.; Oharra, K. E.; Bara, J. E.; Jackson, E. M., Design and Synthesis of Imidazolium-Mediated Tröger's Base-Containing Ionene Polymers for Advanced CO2 Separation Membranes. *ACS Omega* **2019,** *4* (2), 3439-3448.

34. Kammakakam, I.; O'Harra, K. E.; Dennis, G. P.; Jackson, E. M.; Bara, J. E., Self-healing imidazolium-based ionene-polyamide membranes: an experimental study on physical and gas transport properties. *Polymer International* **2019,** *68* (6), 1123-1129.

35. O'Harra, K. E.; Kammakakam, I.; Bara, J. E.; Jackson, E. M., Understanding the effects of backbone chemistry and anion type on the structure and thermal behaviors of imidazolium polyimide-ionenes. *Polymer International* **2019**.

36. O'Harra, K. E.; Kammakakam, I.; Devriese, E. M.; Noll, D. M.; Bara, J. E.; Jackson, E. M., Synthesis and Performance of 6FDA-Based Polyimide-Ionenes and Composites with Ionic Liquids as Gas Separation Membranes. *Membranes-Basel* **2019,** *9* (7), 79.

37. Mittenthal, M. S.; Flowers, B. S.; Bara, J. E.; Whitley, J. W.; Spear, S. K.; Roveda, J. D.; Wallace, D. A.; Shannon, M. S.; Holler, R.; Martens, R.; Daly, D. T., Ionic Polyimides: Hybrid

Polymer Architectures and Composites with Ionic Liquids for Advanced Gas Separation Membranes. *Ind. Eng. Chem. Res.* **2017,** *56* (17), 5055-5069.

38. O'Harra, K. E.; Kammakakam, I.; Noll, D. M.; Turflinger, E. M.; Dennis, G. P.; Jackson, E. M.; Bara, J. E., Synthesis and Performance of Aromatic Polyamide Ionenes as Gas Separation Membranes. *Membranes-Basel* **2020,** *10* (3).

39. Fox, T. G.; Loshaek, S., Influence of molecular weight and degree of crosslinking on the specific volume and glass temperature of polymers. *Journal of Polymer Science* **1955,** *15* (80), 371-390.

40. Xu, Y.; Chen, C.; Zhang, P.; Sun, B.; Li, J., Effect of molecular structures on polyimide properties: Comparison between estimations and experiments. *Journal of Applied Polymer Science* **2007,** *103* (2), 998-1003.

41. Shimazu, A.; Miyazaki, T.; Ikeda, K., Interpretation of d-spacing determined by wide angle X-ray scattering in 6FDA-based polyimide by molecular modeling. *Journal of Membrane Science* **2000,** *166* (1), 113-118.

42. Coleman, M. R.; Koros, W. J., The transport properties of polyimide isomers containing hexafluoroisopropylidene in the diamine residue. *J. Polym. Sci., Part B: Polym. Phys.* **1994,** *32* (11), 1915-26.

43. Bara, J. E.; Lessmann, S.; Gabriel, C. J.; Hatakeyama, E. S.; Noble, R. D.; Gin, D. L., Synthesis and Performance of Polymerizable Room-Temperature Ionic Liquids as Gas Separation Membranes. *Ind. Eng. Chem. Res.* **2007,** *46* (16), 5397-5404.

44. Carlisle, T. K.; Bara, J. E.; Lafrate, A. L.; Gin, D. L.; Noble, R. D., Main-chain imidazolium polymer membranes for CO2 separations: An initial study of a new ionic liquid-inspired platform. *J. Membr. Sci.* **2010,** *359* (1-2), 37-43.

45. Li, P.; Coleman, M. R., Synthesis of room temperature ionic liquids based random copolyimides for gas separation applications. *Eur. Polym. J.* **2013,** *49* (2), 482-491.

46. Supasitmongkol, S.; Styring, P., High CO2 solubility in ionic liquids and a tetraalkylammonium-based poly(ionic liquid). *Energy Environ. Sci.* **2010,** *3* (12), 1961-1972.

47. Tome, L. C.; Aboudzadeh, M. A.; Rebelo, L. P. N.; Freire, C. S. R.; Mecerreyes, D.; Marrucho, I. M., Polymeric ionic liquids with mixtures of counter-anions: a new straightforward strategy for designing pyrrolidinium-based CO2 separation membranes. *J. Mater. Chem. A* **2013,** *1* (35), 10403-10411.

2.7 Appendix

^{1}H-NMR Data

The NMR and MS data for 6FDA API and [6FDA API(p)][Tf_2N] have been published by the authors previously. ***6FDA API:*** ^{1}H NMR (500 MHz, DMSO-d6) δ 8.08 (d, 2H), 7.86 (d, 2H), 7.64 (, 2H), 7.27 – 7.11 (dt, 2H), 7.19 (s, 2H), 6.88 (s, 2H), 4.03 (t, J = 7.0 Hz, 4H), 3.58 (t, J = 6.7 Hz, 4H), 2.05 (m, 4H). 13C NMR (126 MHz, DMSO-d6) δ 167.56, 167.43, 137.72, 137.44, 135.96, 133.63, 133.21, 128.78, 124.34, 123.61, 119.68, 44.12, 35.71, 29.98. HRMS [M][H+]: calculated = 658.1761; found = 658.1763. ***[6FDA API(pXy)][Tf_2N]:*** ^{1}H NMR (500 MHz, DMSO-d6) δ 9.28 (br, 2H), 8.08 (br, 2H), 7.83 (br, 2H), 7.78 (br, 4H), 7.69 (br, 2H), 7.47 (br, 4H), 5.43 (br, 4H), 4.25 (br, 4H), 3.64 (br, 4H), 2.16 (br, 4H).[1]

The ^{1}H-NMR spectra and assignments for [6FDA API(mXy)][Tf_2N] and [6FDA API(o)][Tf_2N] are included below.

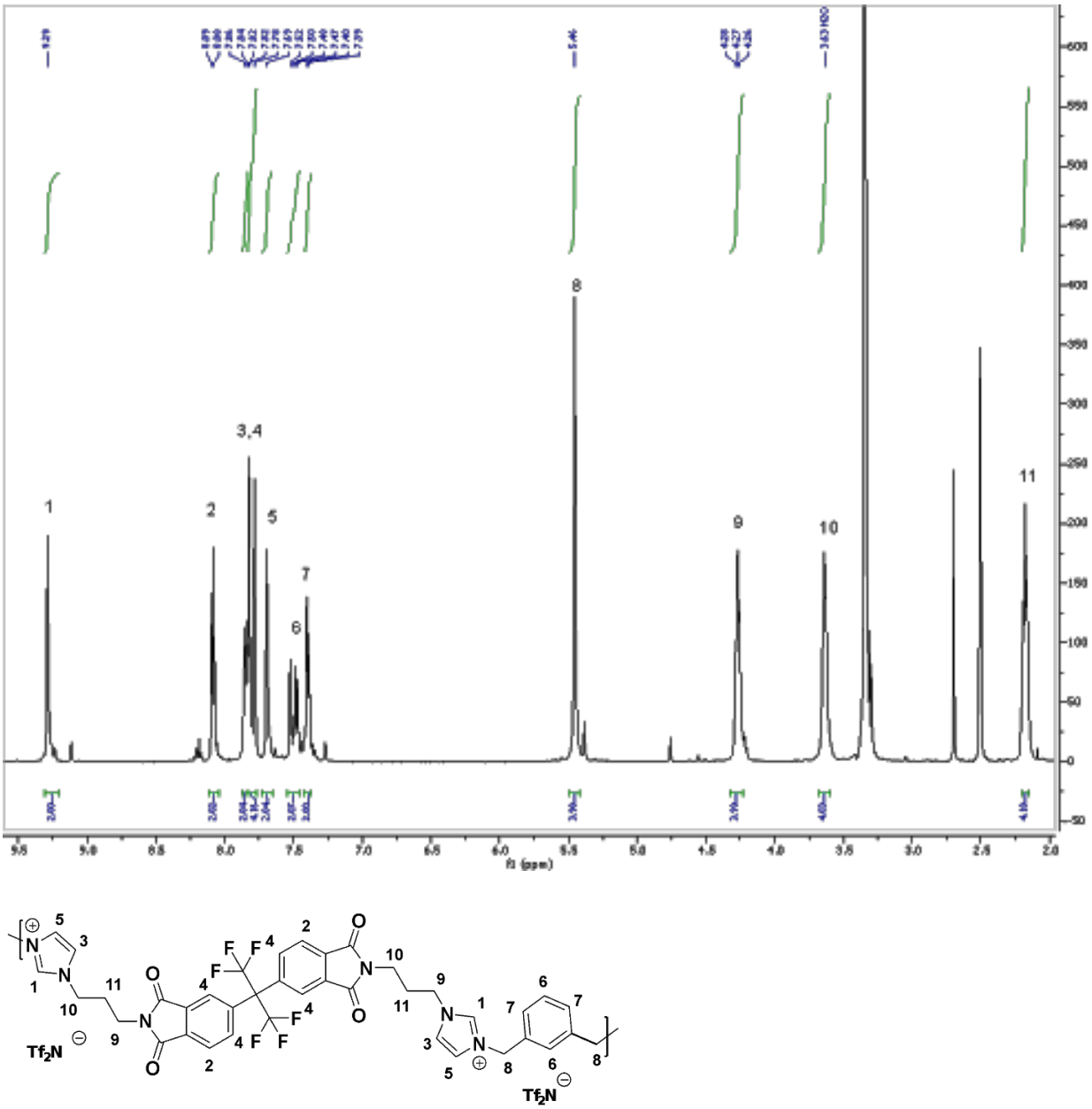

Figure A2.1 ^{1}H-NMR spectrum for [6FDA API(mXy)][Tf_2N]

^{1}H NMR (500 MHz, DMSO-d6) δ 9.37 (br, 2H), 8.08 (d, J = 8.04 Hz, 2H), 7.85 (d, J = 8.30 Hz, 2H), 7.80 (dt, J = 1.19 Hz, 4H) 7.69 (br, 2H), 7.50 (m, J = 7.41 Hz, 2H), 7.40 (d, J = 7.48 Hz, 2H), 5.46 (br, 4H), 4.27 (t, J = 7.24 Hz, 4H), 3.63 (t, J = 5.3 Hz, 4H), 2.18 (m, J = 7.59 Hz, 4H).

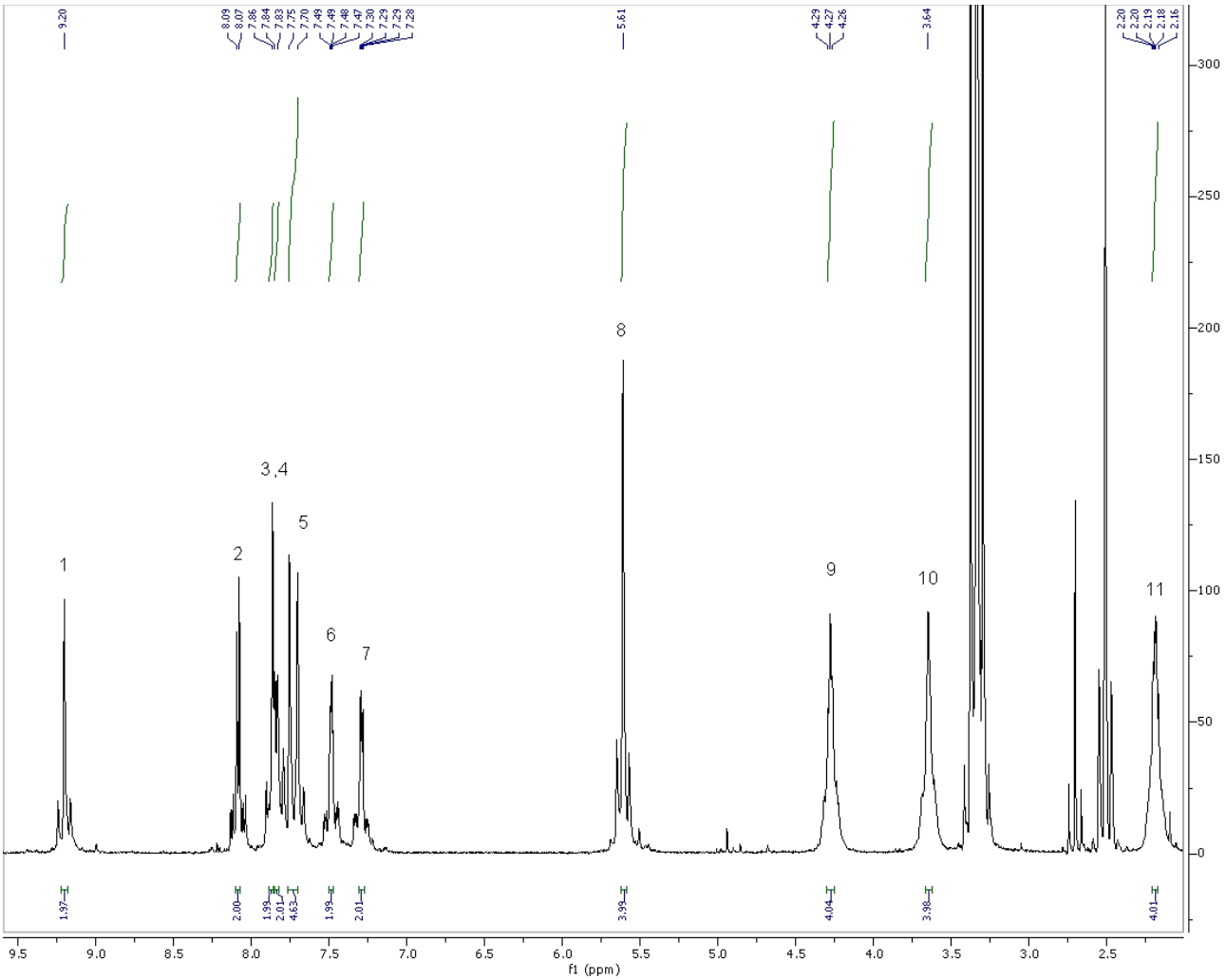

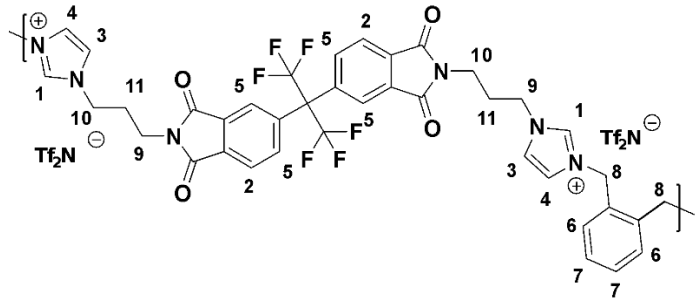

Figure A2.2 ^{1}H-NMR spectrum for [6FDA API(oXy)][Tf_2N]

^{1}H NMR (500 MHz, DMSO-d6) δ 9.21 (br, 2H), 8.08 (d, J = 8.07 Hz, 2H), 7.86 (br, 2H), 7.84 (d, J = 8.65 Hz, 2H), 7.72 (dt, J = 1.20 Hz, 4H), 7.48 (m, J = 2.24, 3.38 Hz, 2H), 7.29 (m, J = 2.18, 3.44 Hz, 2H), 5.59 (br, 4H), 4.27 (t, J = 7.49 Hz, 4H), 3.64 (t, J = 5.4 Hz, 4H), 2.1 (m, J = 2.4, 8.2 Hz, 4H)

MALDI-TOF MS

The number average molecular weights (M_N) for the [6FDA-API(p/m/oXy)][Tf_2N] ionenes were determined using matrix-assisted laser desorption/ionization time-of-flight mass spectrometry (MALDI-TOF MS).

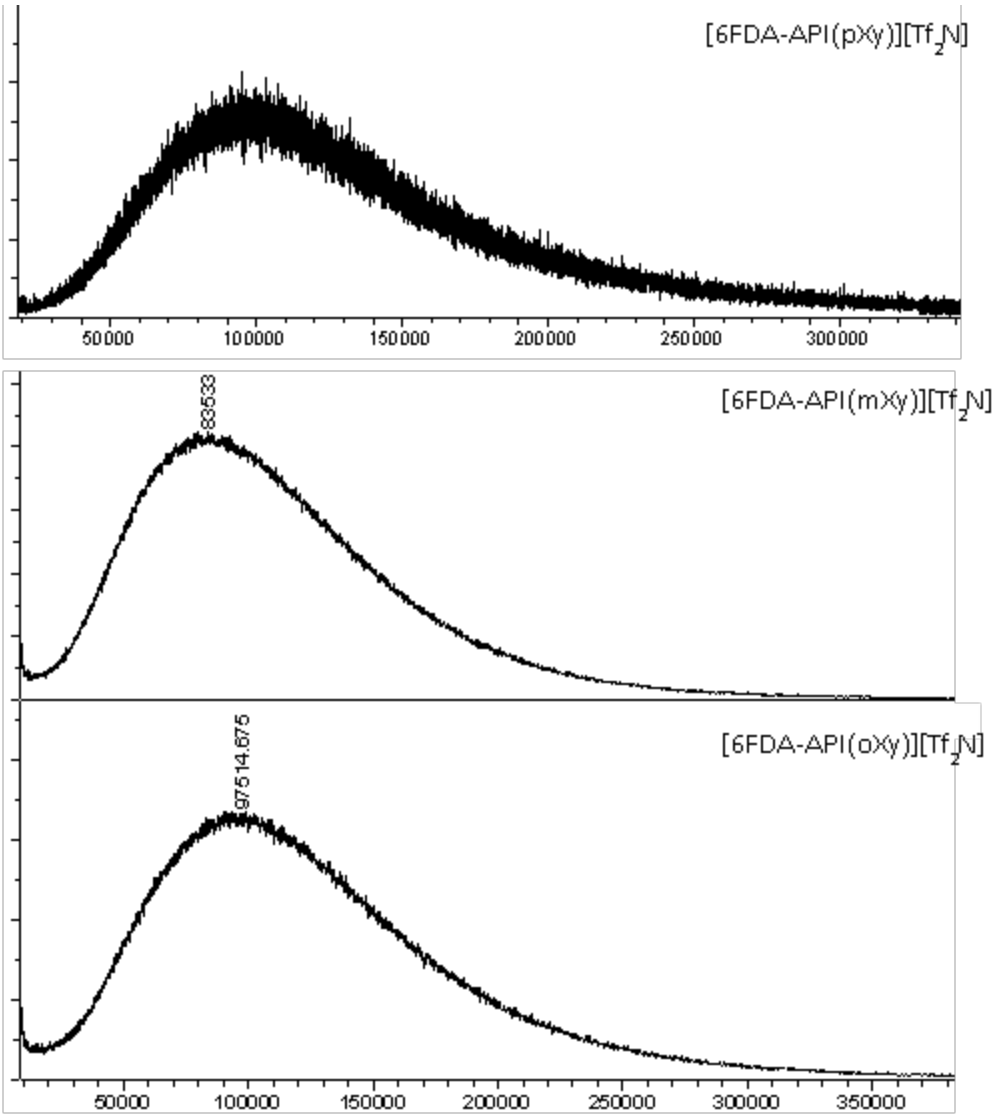

Figure A2.3 MALDI-TOF profile for three neat ionenes, labeled with M_N.

Thermal Data

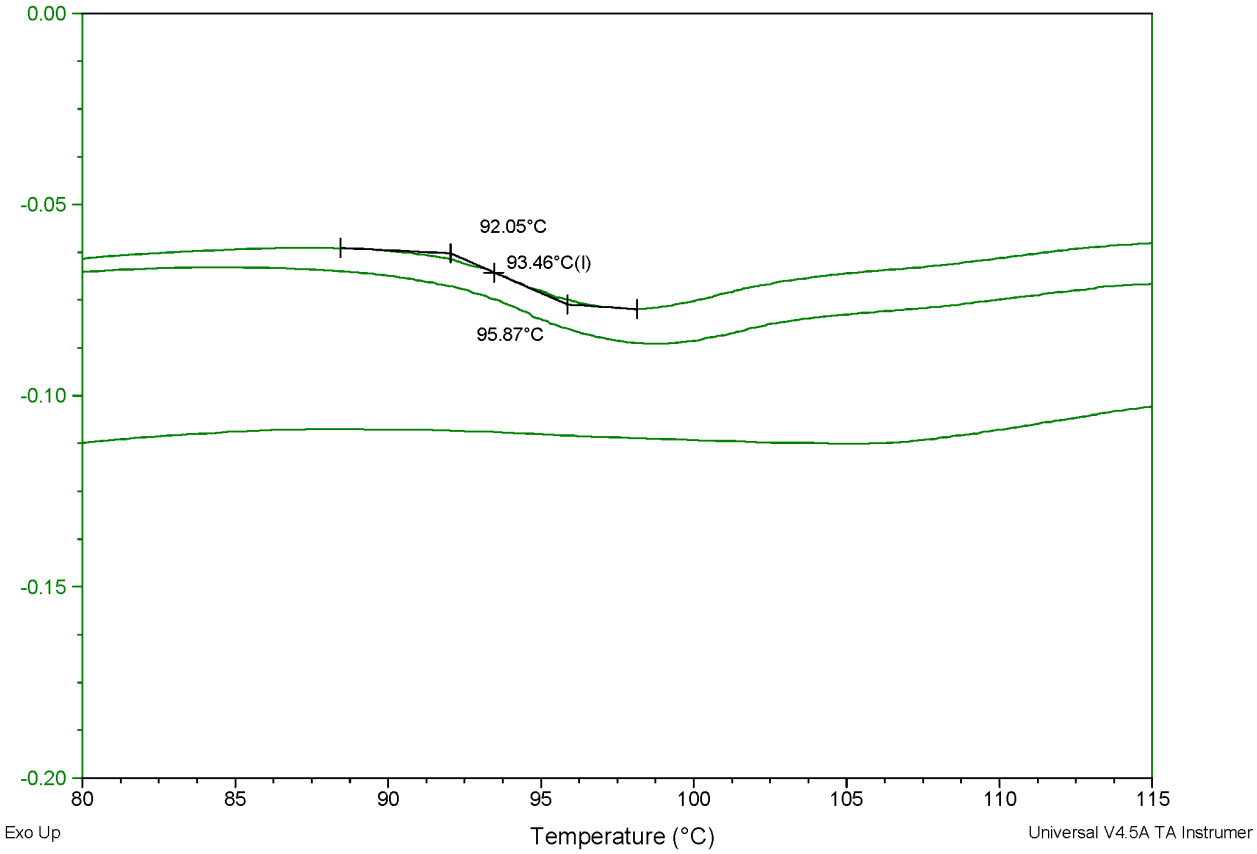

Figure A2.4 DSC profile of [6FDA-API(pXy)][Tf_2N]

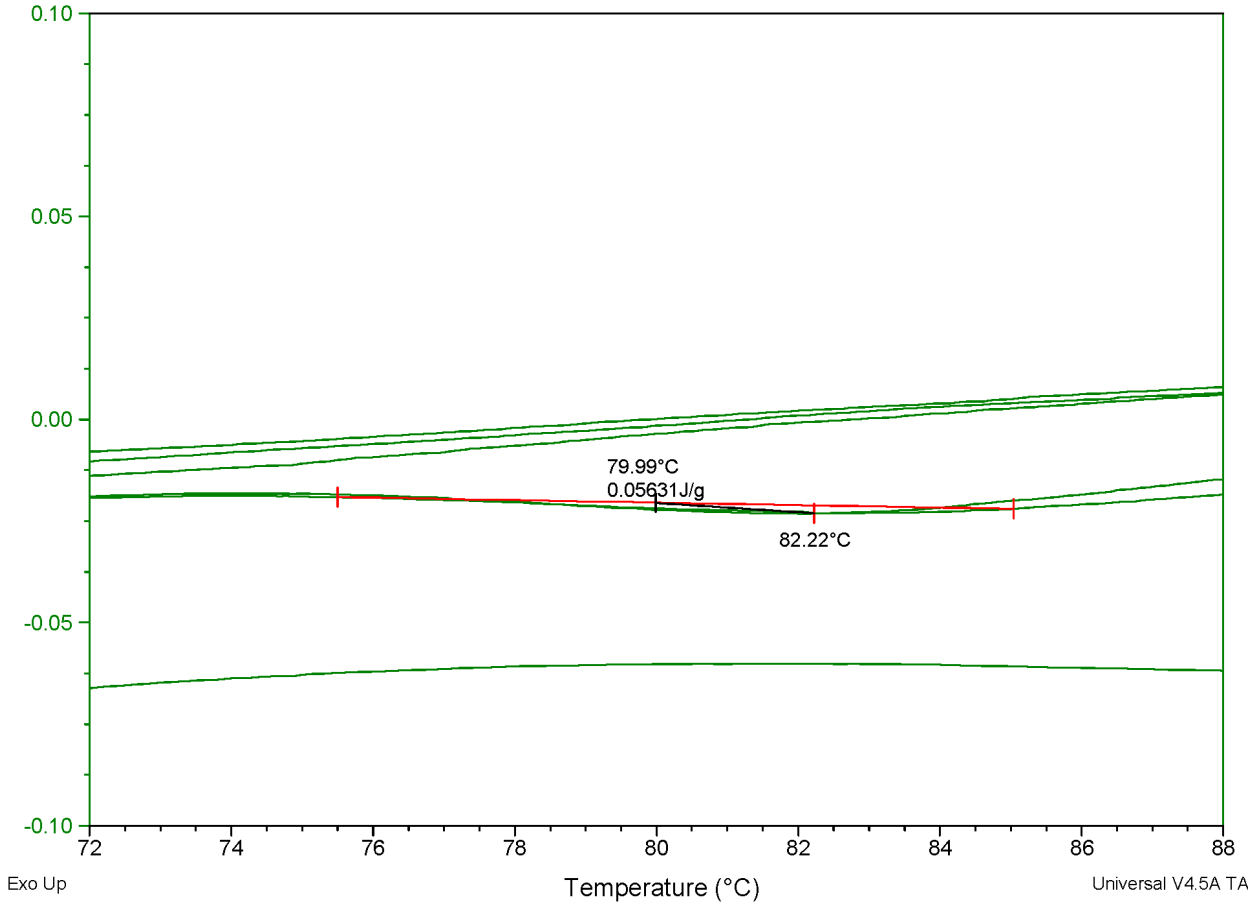

Figure A2.5 DSC profile of [6FDA-API(mXy)][Tf_2N]

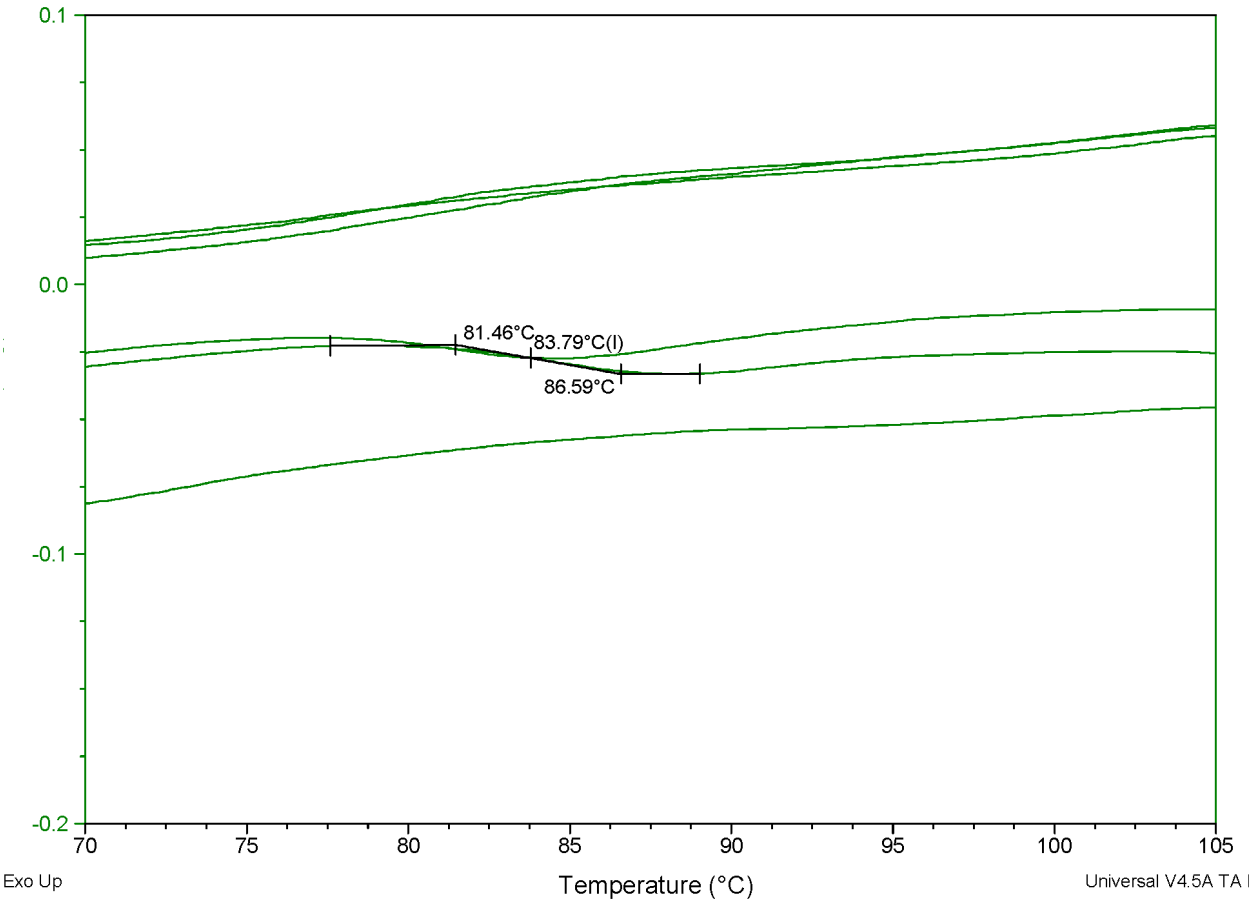

Figure A2.6 DSC profile of [6FDA-API(oXy)][Tf_2N]

FT-IR Analysis

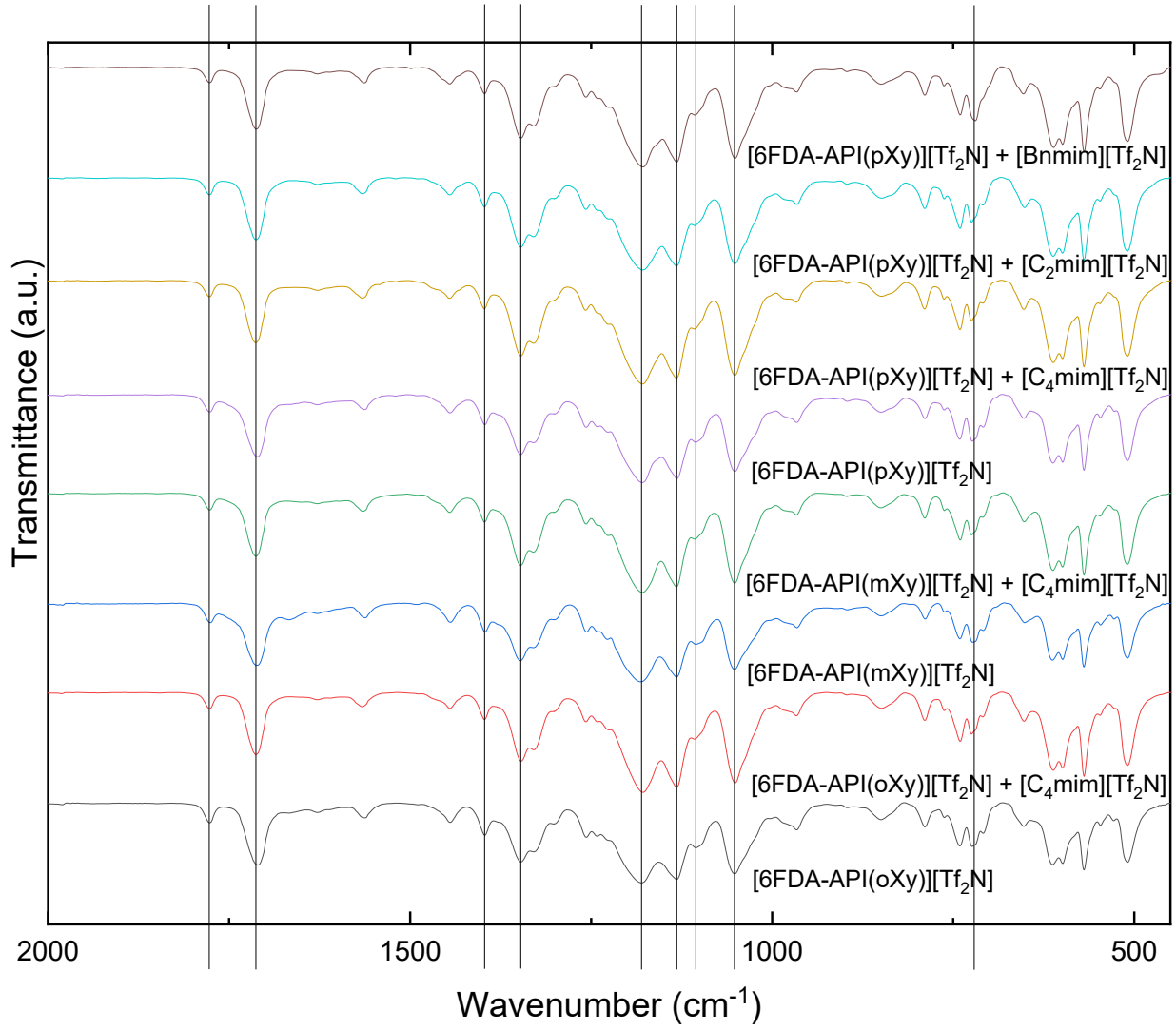

Figure A2.7 FTIR spectra of all neat and composite materials with main groups indicated

CHAPTER 3

EXPERIMENTAL AND COMPUTATIONAL STUDIES ON THE EFFECTS OF C(2) METHYLATION ON THE PROPERTIES AND GAS SEPARATION PERFORMANCE OF POLYIMIDE-IONENES AND COMPOSITES WITH IONIC LIQUIDS

3.1 Abstract

As methylation of the imidazolium C(2) position is known to affect the intermolecular properties of ionic liquids (ILs), polyimide (PI)-ionenes were designed to determine what effects (if any) a C(2)-Me group might have on the properties and membrane performance characteristics relative to analogous PI-ionenes with an imidazolium C(2)-H group. 1-butyl-3-methylimidazolium bistriflimide ([C_4mim][Tf_2N]), a well-known IL, was added to the polymers forming homogeneous PI-ionene + IL composites which were more amenable to the formation of flexible films suitable for membrane testing. The gas permeation behaviors of the resultant membranes were measured for H_2, CO_2, N_2, and CH_4. The 6FDA-containing PI-ionene exhibited greater permeabilities than the PMDA-containing material, while both materials exhibited comparable selectivity for CO_2 relative to other gases. The permeability-selectivity relationships were visualized on Robeson Plots, and these PI-ionene membranes were comparable to other ionene and poly(IL) materials. Molecular dynamics (MD) simulations and quantum mechanics (QM) calculations were performed on

the C(2)-H and C(2)-Me ionic, monomeric units to determine their conformations and other structural properties[-]. The results obtained are useful in the further development of ionene polymers for gas separation membranes

Keywords: Polyimide-ionene; Imidazolium; Ionic liquid; Composite membranes; Gas Separation; CO_2 Selectivity

3.2 Introduction

Although multiple types of processed exist to separate CO_2 from various industrial gas streams, membranes offer inherent advantages of pressure-driven, solution-diffusion (S-D) transport of solutes through dense polymer materials. In the S-D mechanism, separation of gases through polymer membranes is influenced by the available free volume through which diffusion can occur for a given gas (and its relative size) and the thermodynamics of gas-polymer interactions which govern solubility – essentially the product of "*how much*" (i.e., S) and "*how fast*" (i.e., D). Both solubility and diffusion properties of polymer membranes can be controlled/tailored via molecular design.

Among the many different polymer types that have been studied as gas separation membranes, polyimides (PIs) exhibit CO_2 selectivity in addition to robust thermal and mechanical properties. PIs are condensation polymers formed through the reaction of a dianhydride and diamine. Common dianhydrides include pyromellitic dianhydride (PMDA), 4,4'-(hexafluoroisopropylidene)diphthalic anhydride (6FDA), and 3,3',4,4'-benzophenonetetracarboxylic dianhydride (BTDA) (Figure 3.1). Examples of common diamines such as 4,4'-Oxydianiline (ODA), *p*-Phenylenediamine (PPD), and 4,4'-Methylenedianiline (MDA) are also shown in Figure 1.

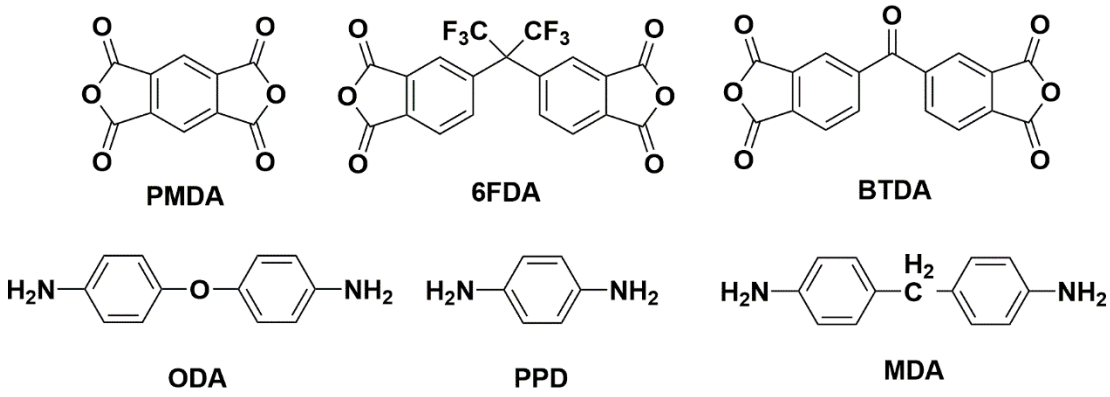

Figure 3.1 Common dianhydrides (top) and diamines (bottom) used in commercial polyimide materials.

Combinations of dianhydrides and diamines in Figure 3.1 can form commercial polymers with desirable chemical, thermal, and mechanical properties, traits which are required for viable membrane formation. Kapton® (Figure 3.2) is formed via a condensation polymerization between PMDA and ODA (Figure 3.1), and is well-known for its high thermal stability, processability. Furthermore, Kapton exhibits selectivity for CO_2 when used as a gas separation membrane.

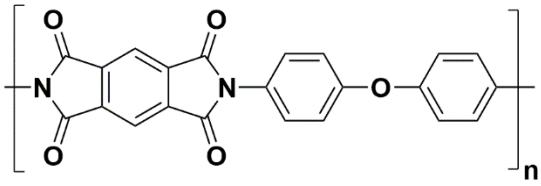

Figure 3.2 Structure of industrially available Kapton®

O'Brien, et al. measured the CO_2 permeability (P_{CO2}) of a commercial sample of Kapton H® to be 0.22 barrer, yet a polymer with an identical backbone synthesized in their work from PMDA + ODA was measured as P_{CO2} = 2.71 barrer. This ~12x increase was attributed to the processing method(s) which influenced the aggregation and orientation of

the film.[1] One of the main conclusions of a review by Hirayama and co-workers on the structure-property relationship of PIs was that the addition of methyl groups to the PI backbone increases P_{CO2}.[2]

The presence of pendant groups on polymer backbones can have significant effects on the performances of gas separation membranes. Stern, et al. showed that the selection of diamines which vary only with the presence of a methyl group to form PI structures greatly affects the polymer microstructure and gas permeation behaviors. When a methyl group was added onto the CH_2CH_2 bridge of 4,4'-(ethane-1,2-diylbis(oxy))dianiline (Figure 3.3) and reacted with 6FDA to form polyimides, the CO_2/CH_4 permselectivities increased by over 50% while P_{CO2} decreased by 30%.[3]

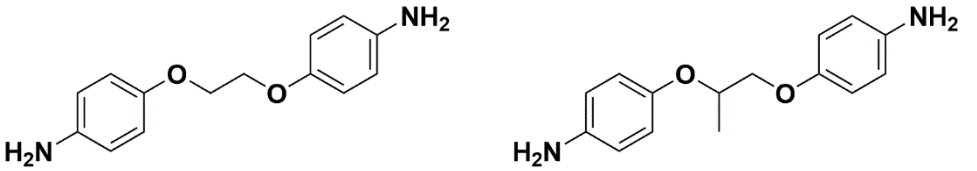

4,4'-(ethane-1,2-diylbis(oxy))dianiline **4,4'-(propane-1,2-diylbis(oxy))dianiline**

Figure 3.3 Structures of 4,4'-(ethane-1,2-diylbis(oxy))dianiline (left) and 4,4'-(propane-1,2-diylbis(oxy))dianiline (right) which were polymerized with 6FDA to form polyimides.

Hirayama and coworkers did an extensive test of over 43 PI homopolymers formed from various combinations of dianhydrides and diamines. Comparing two polyimides formed using 6FDA, 3,3'-dimethyl-4,4'-diaminodiphenylmethane (Figure 3.4a), and 3,3',5,5'-tetramethyl-4,4'-diaminodiphenylmethane (Figure 3.4b), the results show that the addition of methyl groups drastically changed the permeabilities of the resulting materials. The addition of two more methyl groups onto a phenylene diamine caused the resulting 6FDA polyimide to increase in P_{CO2} by 500% while only decreasing the CO_2/CH_4

permselectivity by 33%.[2] Dependent upon the position of the R group(s), the final properties of materials with similar backbones can be markedly different.

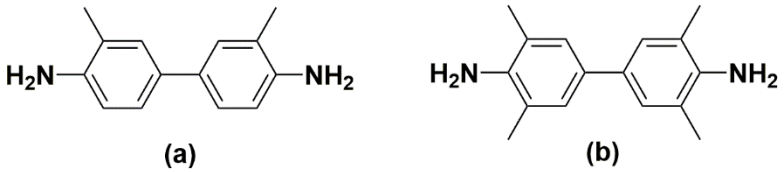

Figure 3.4 Comparable diamine monomers used in Hiryama, et al paper where (a) is 3,3'-dimethyl-4,4'-diaminodiphenylmethane and (b) is 3,3',5,5'-tetramethyl-4,4'-diaminodiphenylmethane.

Ionenes are polymers which contain ionic groups (e.g., ammonium, imidazolium, phosphonium, etc.) directly in the polymer backbone.[4-7] Historically, the vast majority of ionenes in the literature have contained ammonium cations tethered by simple alkyl linkages.[8, 9] However, in more recent years imidazolium ionenes are becoming of greater interest due to the tremendous growth in the study of ionic liquids (ILs) particularly for the separation of CO_2 from various gas streams.[10-13] The numerous synthetic strategies available for imidazolium ionenes present opportunities to create highly tailored polymers that also contain structural elements found in the aforementioned PIs. Due to their "hybrid" characteristics, the design of imidazolium PI-ionenes and composites with ILs present unique possibilities in the design of polymer gas separation membranes.

One example of a PI-ionene was presented by Li where 6FDA-containing polyimide copolymer (random and block) containing imidazolium moieties and MDA which demonstrated good CO_2 selectivities. Although the P_{CO2} decreased with increasing ionic content, the CO_2/CH_4 selectivity increased; however, it should be noted that the number average molecular weight (M_n) of the both random and block copolymers were

considerably lower as the fraction of the ionic components increased, indicating potential difficulties in synthesis when using the imidazolium-containing diamine.[14, 15]

Rather than form PI-ionenes through the reaction of an imidazolium-containing diamine, our group has found that higher molecular weights are achieved by first forming a bis(imidazole) diimide that is then polymerized with a α,ω-dihalide (or similar compound) via the Menshutkin reaction (forming the imidazolium group as the product of polymerization), followed by anion-exchange from the halide to a molecular anion. Mittenthal, et al. demonstrated this concept forming a PMDA-containing PI-ionene (Figure 3.5) which showed excellent film forming qualities.

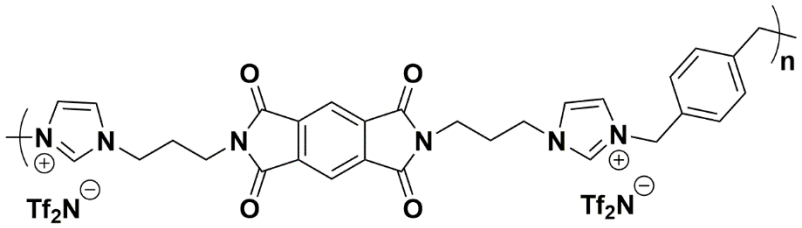

Figure 3.5 PMDA-containing PI-ionene reported by Mittenthal, et al.

Although the neat PI-ionene had a P_{CO2} of ~1 barrer, soaking the film in 1-butyl-3-methylimidazolium bistriflimide ([C_4mim][Tf_2N]) IL (which was absorbed by the polymer matrix) increased P_{CO2} by more than 2000%.[16] Multiple works from O'Harra and coworkers have expanded on the concept of PI-ionenes built from PMDA or 6FDA and have demonstrated that these synthetic methods can be applied to provide great control over the backbone structure, while achieving molecular weights > 100 kDa enabling formation of mechanically stable thin films. Furthermore, each of these PI-ionenes also exhibits favorable interactions with ILs to form composites with ILs with enhanced P_{CO2} relative to the neat PI-ionenes.[17, 18]

Although our group has examined multiple structural variations within PI-ionenes and related polymers, the effects of methyl groups appended to the imidazolium ring has not yet been explored. Within the study of IL properties, there has been a strong focus on understanding the effects of methylation of the C(2) position of the imidazole ring.[19-24] The C(2)-H is considered to be "acidic" and able to experience H-bonding with anions, and this behavior is attributed as a differentiating factor between low melting imidazolium salts and other organic salts (e.g., quaternary ammonium). "Blocking" this H-bonding via introduction of a methyl (or other alkyl) group at the C(2) position is correlated with clear increases in viscosity and melting points compared to analogous ILs with a C(2)-H, although the effects this methylation on CO_2 solubility are not as obvious. These changes indicate that the interactions in imidazolium ILs with C(2)-Me groups are distinctly different than those with C(2)-H groups. Although the exact nature of these interactions are still under debate, Ludwig's group confirms the methylation of the imidazolium's C(2) position causes the H-bonding effect to transition toward coulombic interactions between the ions.[25]

Carlisle, Bara and co-workers have shown that relatively simple imidazolium ionenes can be formed in two steps via the reaction of 2-methylimidazole and 1,10-dibromodecane (Figure 3.6).

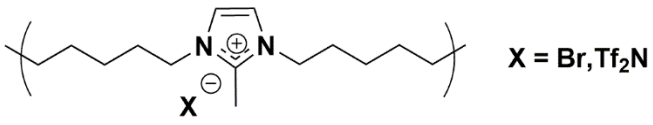

Figure 3.6 "Main-chain imidazolium ionene" formed from 2-methyl imidazole and 1,10-dibromodecane

To the best of our knowledge, the alkyl-linked imidazolium ionene depicted in Figure 6 is the only instance of an imidazolium ionene with an imidazolium C(2)-Me group in the literature. Carlisle's imidazolium ionenes in both the bromide (Br^-) and $[Tf_2N]^-$ forms were amenable to casting into thin films. The gas permeabilities varied greatly depending on the type of anion, with P_{CO2} = 0.13 barrer and 5.3 barrer, for the Br^- and Tf_2N^- forms, respectively.[26] Carlisle and Bara were unable to compare this ionene to a structurally analogous polymer with a C(2)-H group as difficulties were encountered in the synthesis. Prior to the synthesis of an ionene containing 2-methylimidazole, He, et al. formed imidazolium oligomers using 2-methylimidazole. These oligomers had a controlled synthesis allowing for differing anions to be coordinated with the imidazolium cations. Even though these were used in peptide synthesis, their synthesis should be noted likely due to their synthesis scheme being the first polymerization using 2-methylimidazolium.[27]

Thus, the effect of a C(2)-Me group on the properties of imidazolium ionenes and associated gas separation membranes remains unexplored. Herein, we report two new were exchanged PI-ionenes: [PMDA-2MeAPI(pXy)][Tf_2N] and [6FDA-2MeAPI(pXy)][Tf_2N] (Figure 3.7), which are synthesized using 6FDA or PMDA with 1-(3-aminopropyl)-2-methylimidazole (2-MeAPI), followed by polymerization via Menshutkin Reaction with pDCXy and subsequent anion-exchange to the $[Tf_2N]^-$ form. To aid in the formation of thin films suitable for gas separation membranes, IL was added to the dope solution and the IL remains in the polymer film after solvent evaporation. The materials were characterized and tested as gas separation membranes to begin developing an understanding as to how the presence of a methyl group at the C(2) position of the imidazolium cation affects the structure-property relationships in PI-ionenes. Furthermore, quantum mechanics (QM)

and molecular dynamics (MD) simulations were performed on the PMDA-2MeAPI and 6FDA-2MeAPI monomers to gain further insight the effects on the film's characteristics and gas separation ability.

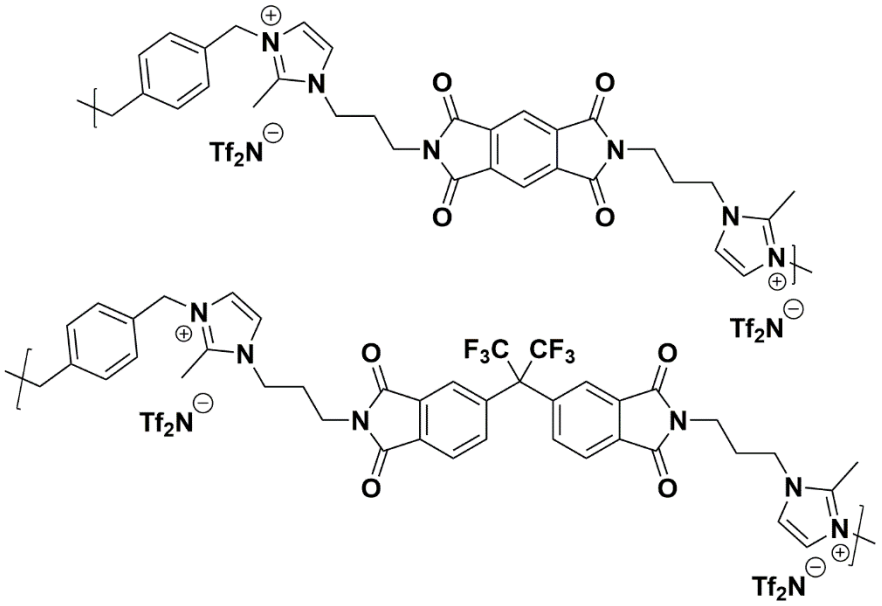

Figure 3.7 Structures of [PMDA-2MeAPI(pXy)][Tf_2N] (top) and [6FDA-2MeAPI(pXy)][Tf_2N] (bottom)

3.3 Materials and Methods

3.3.1 Materials

PMDA (>99%) and 6FDA (>99%) were purchased from Akron Polymer Systems. pDCXy (>98%) was purchased from TCI. $LiTf_2N$ was purchased from 3M. N-methylpyrrolidone (NMP, ACS grade), tetrahydrofuran (THF, ACS grade), diethyl ether (Et_2O, ACS grade), methanol (MeOH), ammonium hydroxide (NH_4OH(aq), 28-30% in water, ACS Grade), and N,N-dimethylformamide (DMF, anhydrous), were purchased from VWR. Raney Nickel®2800 slurry in H_2O and triethylamine (Et_3N) were purchased from Oakwood Chemical. 2-methylimidazole was purchased from Alfa Aesar. Celite® 545 was purchased

from Millipore-Sigma. Acrylonitrile (≥ 99%) was purchased from Sigma-Aldrich. All materials were used as obtained, without further purification. Deionized H_2O (DI H_2O, 12 MW) was obtained from a source in the Department of Chemistry at the University of Alabama.

3.3.2 Synthesis of 3-(2-methyl-1H-imidazol-1-yl)propan-1-amine ("2MeAPI")

The synthesis of 2MeAPI has been detailed in our previous work.[28] The corresponding nitrile (i.e., R-CN) precursor was prepared from 2-methylimidazole, acrylonitrile, and Et_3N in refluxing toluene, and was subsequently reduced to 2MeAPI (i.e., R-NH_2) with H_2 in the presence of Raney nickel in MeOH/NH_4OH(aq).

3.3.3 Synthesis of 2MeAPI-Diimide Monomers

3.3.3.1 Synthesis of 2,6-bis(3-(2-methyl-1H-imidazol-1-yl)propyl)pyrrolo[3,4-f]isoindole-1,3,5,7(2H,6H)-tetraone ("PMDA-2MeAPI")

PMDA (10.00 g, 45.8 mmol) and 2MeAPI (13.4 g, 96.3 mmol) were added with 80 mL DMF to a 250 mL heavy-walled pressure vessel (Ace Glass) sealed with a threaded PTFE cap with a DuPont Kalrez® o-ring. The reaction was heated at 120 °C for 24 h. The product was precipitated in DI H_2O and stirred at RT for 1 h. The solids were washed with 2 x 50 mL DI H_2O and dried in a vacuum oven at 100 °C overnight to yield an off-white powder (18.7 g, 89 %).

Scheme 3.1 Synthesis schematic of PMDA-2MeAPI monomer.

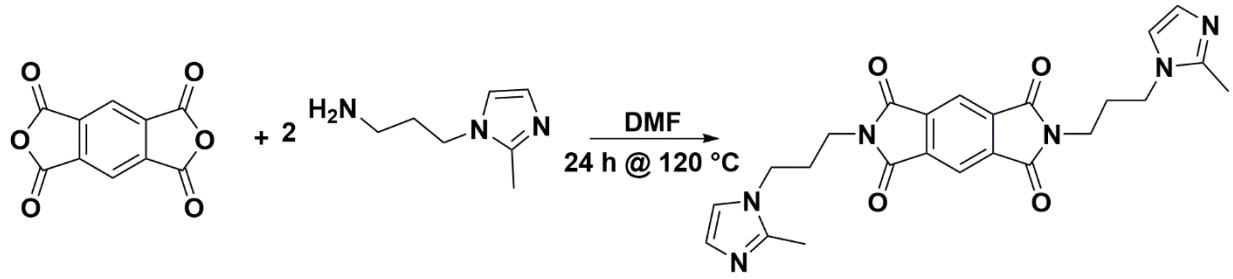

3.3.3.2 Synthesis of 5,5'-(perfluoropropane-2,2-diyl)bis(2-(3-(2-methyl-1H-imidazol-1-yl)propyl) isoindoline-1,3-dione) ("6FDA-2MeAPI")

6FDA-2MeAPI was synthesized via the reaction of 6FDA and 2MeAPI. 6FDA (5.00 g, 11.3 mmol) was added to a 250mL round bottom flask with 30 mL of DMF. The reaction was cooled to 5 °C and stirred for 1h. 2MeAPI (3.45 g, 24.8 mmol) was then added to the flask, the cooling source was removed and the vessel was allowed to warm to room temperature while stirring for 16 h. Toluene (15 mL) was then added and the flask equipped with a reflux condenser. The vessel was heated at 125 °C for 24 h. The solution was cooled, and toluene and some DMF were removed via rotary evaporation. The remaining solution was poured into 400 mL of DI H_2O to precipitate the product. The solids were filtered and washed with 2 x 100mL of DI H_2O. The product was collected and dried for 24 h at 120 °C in a vacuum oven. The product was a tan powder (6.12 g, 82 %).

Scheme 3.2 Synthesis schematic of 6FDA-2MeAPI monomer

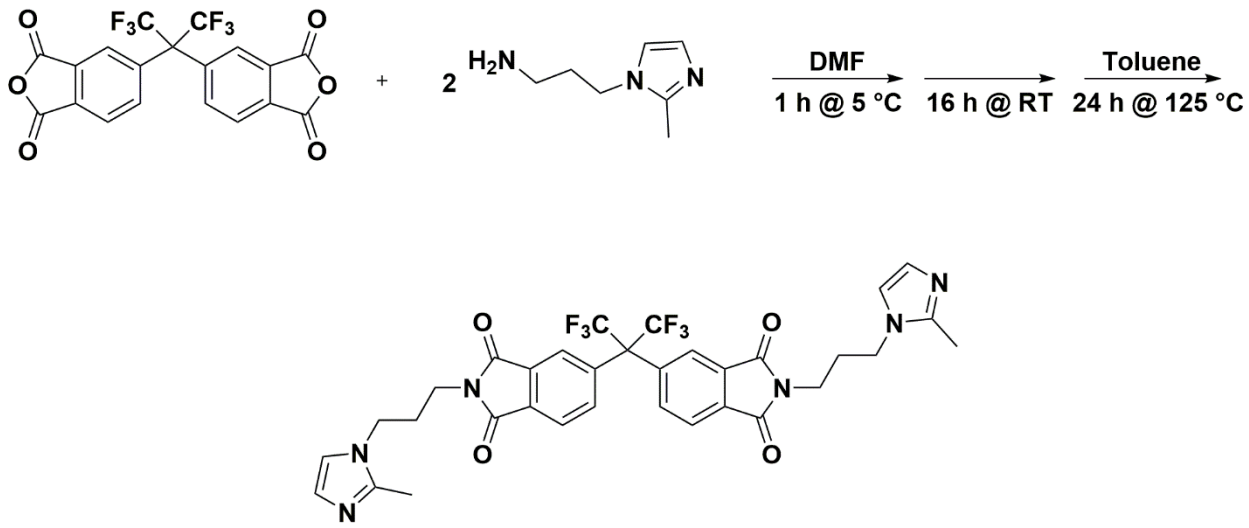

3.3.4 Synthesis of PI-ionenes

3.3.4.1 Synthesis of [PMDA-2MeAPI(pXy)][Tf_2N]

PMDA-2MeAPI was polymerized with an equimolar equivalent of pDCXy to form a PI-ionene with a xylyl linkage via the Menshutkin reaction. PMDA-2MeAPI (5.00 g, 10.9 mmol) and pDCXy (1.90 g, 10.9 mmol) were added with 80 mL of NMP to a 250 mL round-bottom heavy-walled pressure vessel. The reaction was heated at 150 °C for 24 h. The solvent was decanted, and the gel precipitate was dissolved in DI H_2O. This polymer solution was solubilized as the $[Cl]^-$ salt and, subsequently, poured into DI H_2O containing $LiTf_2N$ (2.5 eq., 7.8 g) to promote exchange of the anion. The ionene was vigorously stirred with an overhead mechanical mixer for 24 h at RT to ensure complete anion metathesis to the $[Tf_2N]^-$ form. The product was then filtered and dried in a vacuum oven at 120 °C overnight.

To remove low molecular weight content, THF (100 mL) was added to [PMDA-2MeAPI(pXy)][Tf_2N] and stirred at RT for 4 h. The purified polymer separates as a brown

gel, and the THF layer containing solvent and oligomeric compounds was decanted. Finally, the polymer was reprecipitated in Et_2O and filtered. Again, the ionene product was dried to yield a light tan glassy solid (9.42 g, 77 %).

Scheme 3.3 Synthesis of [PMDA-2MeAPI(pXy)][Tf_2N].

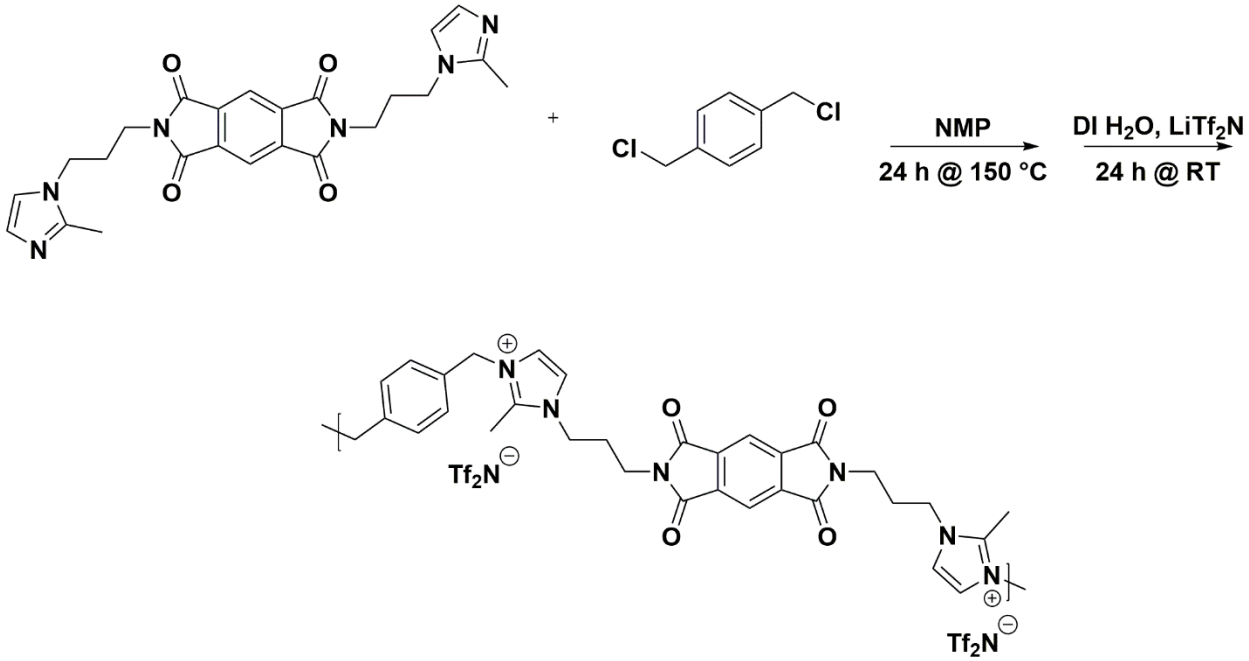

3.3.4.2 Synthesis of [6FDA-2MeAPI(pXy)][Tf_2N]

6FDA-2MeAPI was polymerized with an equimolar equivalent of pDCXy to form a PI-ionene with xylyl linkage via the Menshutkin reaction. 6FDA-2MeAPI (5.00 g, 7.28 mmol) and pDCXy (1.27 g, 7.28 mmol) were added with 50 mL of anhydrous DMF to a round-bottom heavy-walled pressure vessel and was sealed. The reaction was heated to 120 °C for 24 h. The solvent was decanted, and solids were dissolved in DI H_2O. This polymer solution was isolated as the Cl^- salt, and the solution was subsequently poured into DI H_2O containing $LiTf_2N$ (2.5 eq., 5.23 g) to promote exchange of the anion. The [6FDA-2MeAPI(pXy)][Tf_2N] ionene was stirred for 24 h at RT to ensure anion metathesis to the $[Tf_2N]^-$ form. The product was then filtered and dried in a vacuum oven at 120 °C overnight.

Low molecular weight content was removed using THF in an identical manner to that for the PMDA-containing PI-ionene. [6FDA-2MeAPI(pXy)][Tf_2N] was dried to yield an off-white powder (7.57 g, 74 %).

Scheme 3.4 Synthesis Schematic of [6FDA-2MeAPI(pXy)][Tf_2N].

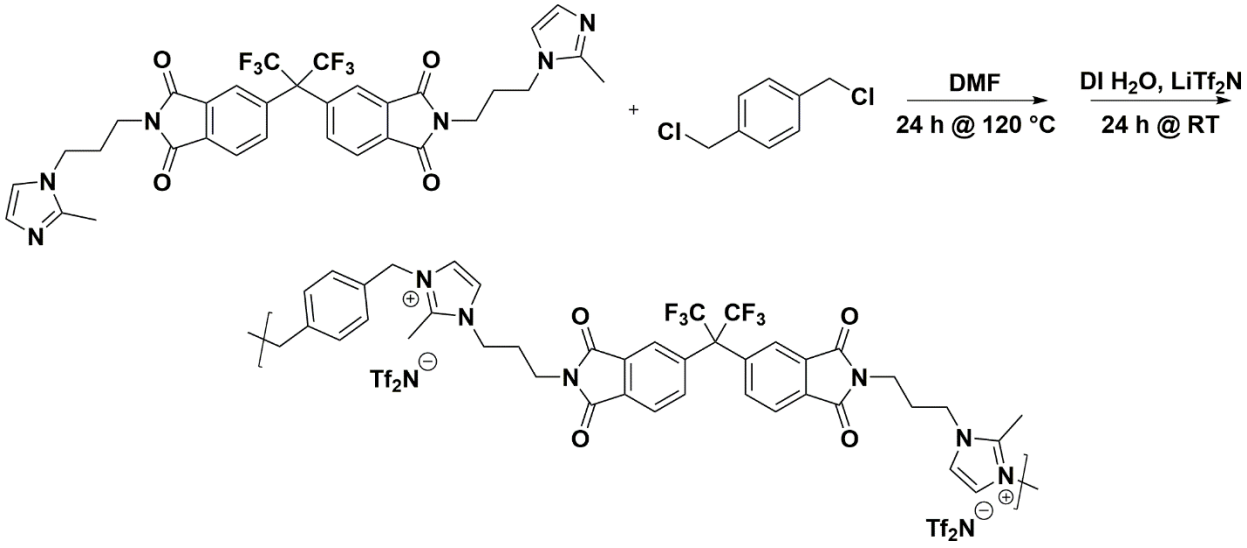

3.3.5 Membrane Preparation

Membranes were prepared by dissolving ~1 g of polymer in ~10 mL of acetone in a 20 mL scintillation vial. One molar equivalent of [C_4mim][Tf_2N] per polymer repeat unit was then dissolved in each solution. Rain-X®, a hydrophobic coating, was buffed onto a 6" x 6" glass plate to aid in the eventual release of the polymer films from the glass surface. The solution was cast onto these glass plates and left at room temperature overnight. The resulting film was then placed into a vacuum oven at 80 °C for 24 h. These films peeled easily from the plates yet were slightly tacky, so the resulting films was placed onto Supor® PES supports prior to insertion in the membrane systems.

3.3.5 Material Characterization

^{1}H and ^{13}C NMR were used to characterize [PMDA-2MeAPI(pXy)][Tf_2N] and [6FDA-2MeAPI(pXy)][Tf_2N] using a Bruker Avance (360 MHz or 500 MHz for ^{1}H, 500 MHz for ^{13}C). ^{1}H- and ^{13}C-NMR spectra are presented in Figures A3.1-A3.4.

FT-IR spectroscopy was performed using a PerkinElmer Spectrum Two spectrometer with the UATR accessory. (Figure A3.5). The spectra were normalized at the carbonyl peak (C=O stretching vibrations at ~1720 cm^{-1}).

Matrix assisted laser deionization/ionization-time of flight (MALDI-TOF) mass spectroscopy was performed using a Bruker Ultraflex on both polymers to determine the number-average molecular weight (M_N). The graphs can be seen in Figure A3.6.

Wide-angle X-ray diffraction (WAXD) was carried out using a Bruker D8 Discover with GADDS using a cobalt source (K_α = 1.79 Å) with a point collimator. The detector was a Vantec 500 area detector. The domain spacing (d-spacing) was determined for each material along with their [C_4mim][Tf_2N] composite counterparts. The d-spacing was calculated using Bragg's law:

$$d = \frac{\lambda}{2 * sin\theta}$$

The 2θ range for WAXD was 5 to 55 °.

Differential scanning calorimetry (DSC) was performed using a TA instruments Q20. Each sample was run in with three cycles from 25 °C to 250 °C at a rate of 10 °C min^{-1} under N_2 atmosphere. Thermal gravimetric analysis (TGA) was carried out on a Seiko TG-DTA 7300. The samples were run starting at room temperature running up to 700 °C at a heating rate of 10 °C.min^{-1} under inert environment. All thermal graphs can be seen in Figures A3.7-A3.9.

Thicknesses of the materials were determined using a Mitutoyo micrometer. Membranes were measured at 5 different spots. Since the PI-IL composites were tacky. To determine the thickness, the difference was taken between the film and PES support were measured, and then known thickness of the Supor® was subtracted. An average of their differences of the membrane-PES and PES was used for the thickness variable within the permeation calculations. The thickness of the film was also observed using SEM to ensure the accuracy of the micrometer.

3.3.6 Gas Separation Units

Gas permeation behavior of ionene composite membranes were analyzed using pure gases (H_2, CO_2, N_2, and CH_4) to determine their permeability, solubility, and diffusivity coefficients. The high vacuum time-lag systems are based on a constant-volume/variable-pressure method and used in this research, as described in our previous works.[16, 17, 29, 30] A 47 mm diameter composite membrane is placed into a Millipore membrane holder with an O-ring. After the feed and permeate are held at dynamic vacuum for 24 h, pure gas is applied to ~3 atm (~44 psia) on the feed while the downstream pressure is at vacuum (~0.01 psia). Through solution-diffusion, the gas permeates through the dense film while the pressure of the downstream is recorded. The pure gas permeations are determined by calculating the linear steady-state increase of the permeate pressure against time (dp/dt). The time lag (θ) is used in part to determine the diffusivity of gas through the membrane. The ideal selectivities ($\alpha_{i/j}$) are determined by dividing the calculated permeability in barrer of one gas by another.

3.4 Results and Discussion

3.4.1 Formation of 2MeAPI Composite Membranes

When casting membranes from this material, the ionic liquid was added due to the extremely fragile nature of the material. The non-methylated counterparts were able to form films without the use of ionic liquid. The membrane forming ability of the non-methylated counterparts demonstrated the necessity of the C(2) position of the imidazolium. The addition of [C_4mim][Tf_2N] to these membranes allowed for thin, flexible membrane formation, yet due to the tackiness of the resulting film the use of PES make it suitable for gas permeation tests since the limiting factor for gas separation would be the dense, amorphous polymer. Although the membrane was supple, it remained as a thin layer upon the Supor® substrate, which can be seen in the SEM images in the Figures A3.10-A3.11.

3.4.2 Simulation Outcomes

3.4.2.1 QM Calculations

All QM calculations were performed with the ORCA[31, 32] program by using the B97-3c functional.[33] This level of theory is generally applicable for estimating the chemical properties of large systems (here, 50~80 atoms) at a low-cost. Frequency calculations at the same level of theory were performed to confirm that all the structures correspond to minima on the potential energy surface. The partial charges of atoms in the charge-neutral molecules were calculated using both the ChelpG[34] method and CM5[35] at the same level using the Multiwfn program.[36] The optimized structures were visualized in GaussView[37] via OfakeG,[38] which converts ORCA output files to a Gaussian-like format. The chemical

structures, optimized structures and the corresponding atomic charges are shown in Figure 3.8, Figure A3.12 and Table A3.1, respectively.

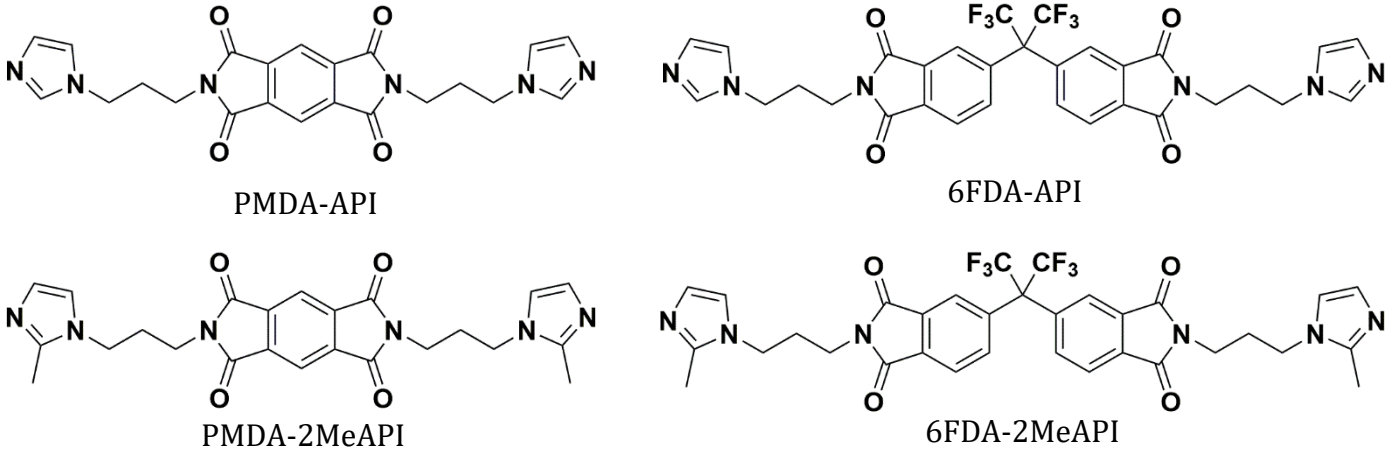

Figure 3.8 Names and structures of studied monomers.

In order to further investigate the structure-property relationships of these molecules, especially how the C(2)-Me group changes the electronic properties around the imidazolium cation, the electrostatic potential (ESP), and the reduced density gradient (RDG)[39] of these molecules were analyzed by Multiwfn and visualized by VMD.[40] The general interaction property functions (GIPF)[41] of these species were also generated to analyze the molecular electrostatic properties. The GIPFs are derived from the molecular surface electrostatic potentials by mapping the electrostatic potential surface according to the van der Waals surfaces, as defined by Bader[42] (with the electron density isosurface corresponding to 0.001 e/Bohr^3).

3.4.2.2 QM Results

The calculated atomic charges using the ChelpG and CM5 methods are listed in Table S1. The charges on the C(2) positions increase after methylation, both for PMDA-API (C24 and C25) and 6FDA-API (C35 and C36). Using the ChelpG method, the charges dramatically increase from ~0.14 e to 0.46 e, while for the CM5 method, the charges slightly increase from ~0.13 e to 0.21 e. The discrepancies are mainly due to the inherent differences of the two calculation methods. For these larger species, the ChelpG method (derived from the electrostatic potential) can suffer from erroneous issues related to "buried atoms", while the CM5 partial atomic charges display more consistent behavior.[35] Furthermore, the C(2) positions in imidazole rings have most positive charges, while C(4) and C(5) positions have less positive charges (0.14~0.15 e lower than C(2) positions) in PMDA-API and 6FDA-API. Thus, based on the charges calculated using the CM5 method, the methylation on the C(2) positions of the imidazolium rings slightly increase their atomic charges (0.08 e). Besides, the C(2) positions in the molecules without methylation show higher positive charges than at the C(4) and C(5) positions, potentially explaining why the methylation at the C(2) positions are more significant than at the C(4) and C(5) positions.

The electrostatic potential surface is mapped to the molecular vdW surface of these four species, as shown in Figure 3.9, and the corresponding ESP distributions and GIPF descriptors are shown in Figure S13 and Table S2, respectively. From the ESP distributions of these molecules, the methylation for both PMDA-API and 6FDA-API makes the ESP curves less positive. For the neutral species, the sites possessing more positive values (i.e. the red spheres distributed on the red surface) have a stronger tendency to attract electrons, and thus, are the most likely interaction sites with the anions or the O atoms of

CO_2. However, from the ESP surfaces, the methylation of PMDA-API and 6FDA-API on the C(2) positions both slightly weaken the ESP values around the C(2) atoms, which potentially decreases the electrostatic intermolecular interactions between these corresponding cationic species in the polymer chains with the anions.

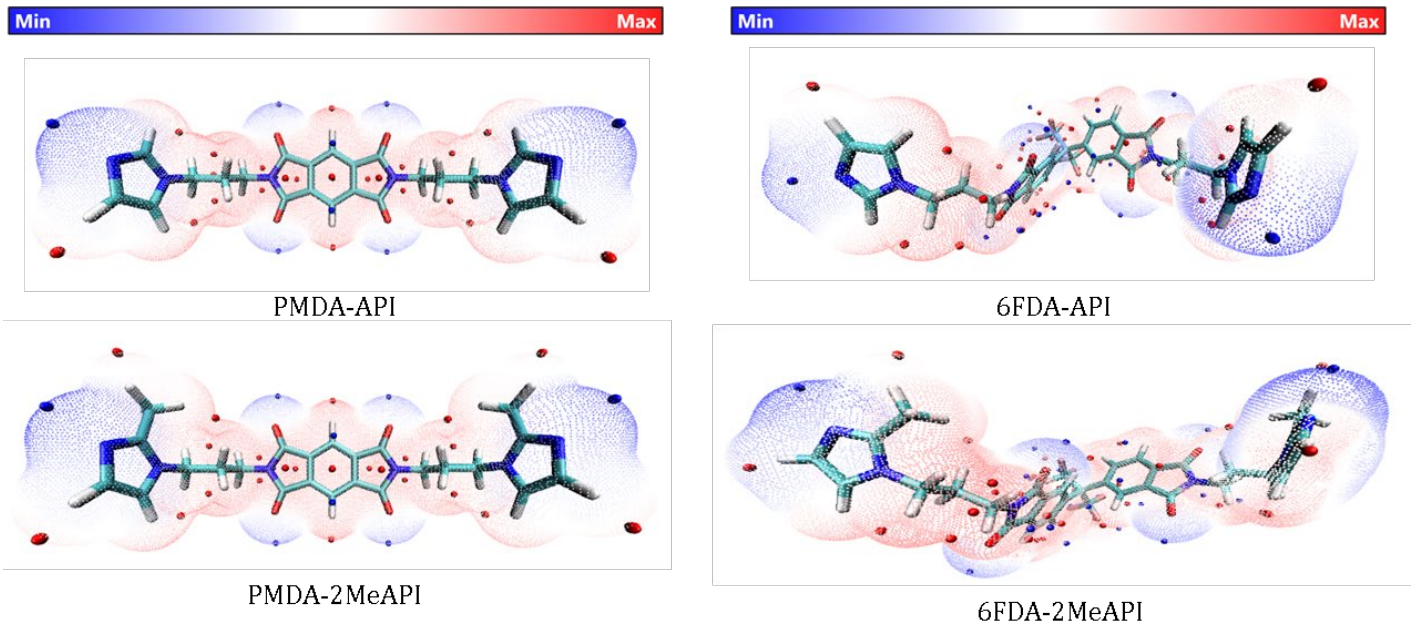

Figure 3.9 ESP-mapped molecular vdW surfaces of the neutral monomers, corresponding to the ρ = 0.001 e/Bohr^3 isosurface. The color scale bar is shown at the top, while the corresponding ESP values (units of kcal/mol) are -50~50 kcal/mol. The local minima and maxima points on the ESP surface are represented as blue and red spheres, respectively. These species are represented as licorice models (cyan: C, white: H, red: O, blue: N, and pink: F).

Furthermore, the reduced density gradient (RDG) analyses based on our density-functional theory (DFT) calculations are shown in Figure 3.10. The RDG images, which help visualize the intramolecular non-covalent interactions, show weaker interactions between the methyl groups with the -CH_2 on the backbones of PMDA-2MeAPI and 6FDA-2MeAPI, while these weaker interactions are not presented in the PMDA-API and 6FDA-API molecules. The RDG results indicate that the methylation on the C(2) positions slightly

increase the intramolecular interactions between the imidazolium rings with the polymer chains in these molecules.

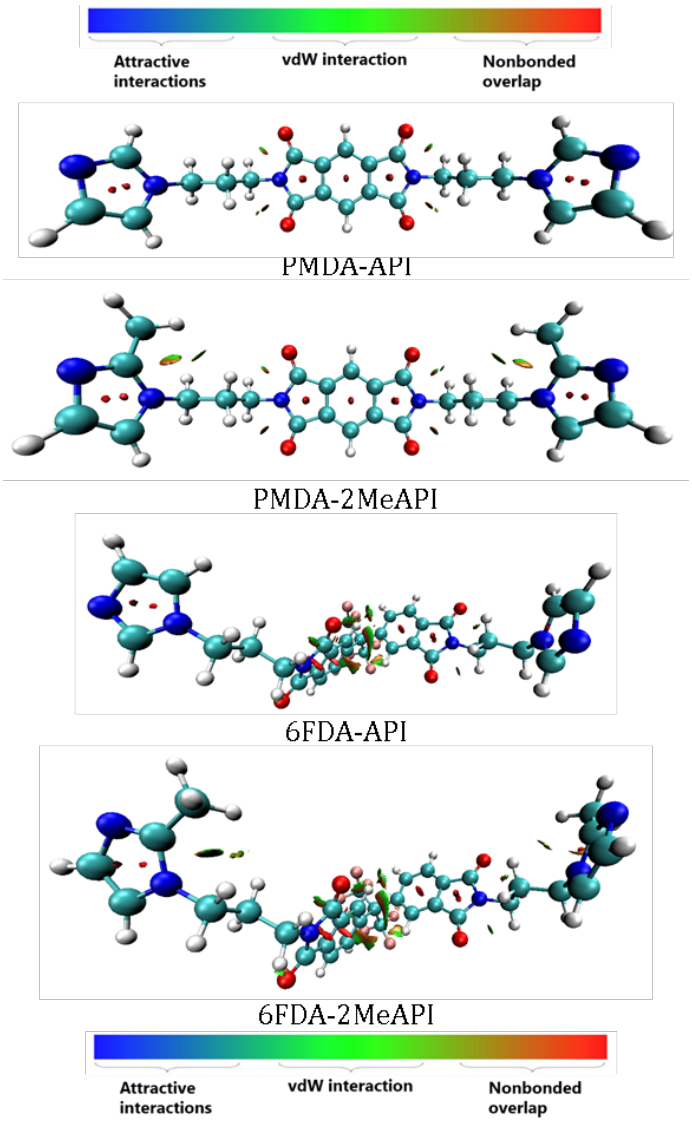

Figure 3.10 Color-filled reduced density gradient (RDG) map of the neutral monomers (isovalue of the RDG is set to 0.5). The value of sign(λ_2)ρ(r) on the surfaces is represented by the color bar at top, where sign(λ_2) is the sign of the second largest eigenvalue of the Hessian of ρ(r). The surfaces are colored on a blue-green-red scale according to values of sign(λ_2)ρ(r), ranging from −0.04 to 0.02 au. Blue indicates strong attractive interactions, and red indicates strong nonbonded overlap. The species are represented as CPK models (cyan: C, white: H, red: O, blue: N, and pink: F).

3.4.2.3 MD Simulations

In order to further investigate the effects of methylation on the C(2) position of the imidazolium rings, simulations of the PI-ionenes were performed. Because of the structural flexibility of these molecules, there are many stable low-lying conformers that can be found. Thus, we performed MD simulations of the corresponding poly-ionic monomers, in order to sample the structural dynamics. These simulations included one positively charged polymer chain (PMDA-API, PMDA-2MeAPI, 6FDA-API and 6FDA-2MeAPI with benzyl groups (-CH_2-C_6H_6) at both termini) with two negatively charged anions ($[Tf_2N]^-$). Although the monomer structures during the MD simulations do not truly emulate the liquid state environment, the main types of anion–cation interactions can still be captured adequately, which helps us theoretically quantify the effect of the C(2) methylation. The MD simulations were performed with the newly-developed GFN-FF[43] using xTb.[44] This approach has been found to yield results nearing the accuracy of semi-empirical QM methods, and in some cases reaching even DFT accuracy.[43]

In order to perform the MD simulations, the optimized geometries of these ionic molecules and the anions were inserted into the simulation boxes at close distances (~5 Å), followed by a few pre-optimization steps to adjust the covalent-bonding network. Then, NVT ensemble simulations (constant volume and temperature) were performed at 300 K using a total of 250 ps for equilibrium, followed by another 250 ps for production (time step of 1 fs). The simulations were accelerated by constraining the X-H bonds in the system. A total of 10000 trajectories were used to generate the spatial distribution function (SDF) and connection matrix (CMat) using the Travis package.[45, 46]

For reference, the initial and final snapshots of these systems are shown in Figure A3.14. The initial molecular geometries optimized using DFT calculations are almost linear structures, while after the MD simulations, the polymer chains tend to fold together. In order to gain a deeper insight into the intermolecular and intramolecular interactions within these polymer chains, the spatial distribution functions (SDF) are shown in Figure 3.11, and the connection matrices (CMats) of all non-carbon atoms in the cationic molecules with the anions and the CMats for the intramolecular interactions within the positively-charged species are shown in Figures A3.15 and A3.16, respectively. In Figure 3.11, the anionic species are located around the O atom sites of the backbones and near the H atoms of the imidazolium rings in PMDA-API and PMDA-2MeAPI. While for 6FDA-API and 6FDA-2MeAPI, the anionic species are located around the O and F atom sites of the backbones and near the H atoms of the imidazolium ring (of 6FDA-API) and near the O atoms and the ring-bound H atoms (of 6FDA-2MeAPI).

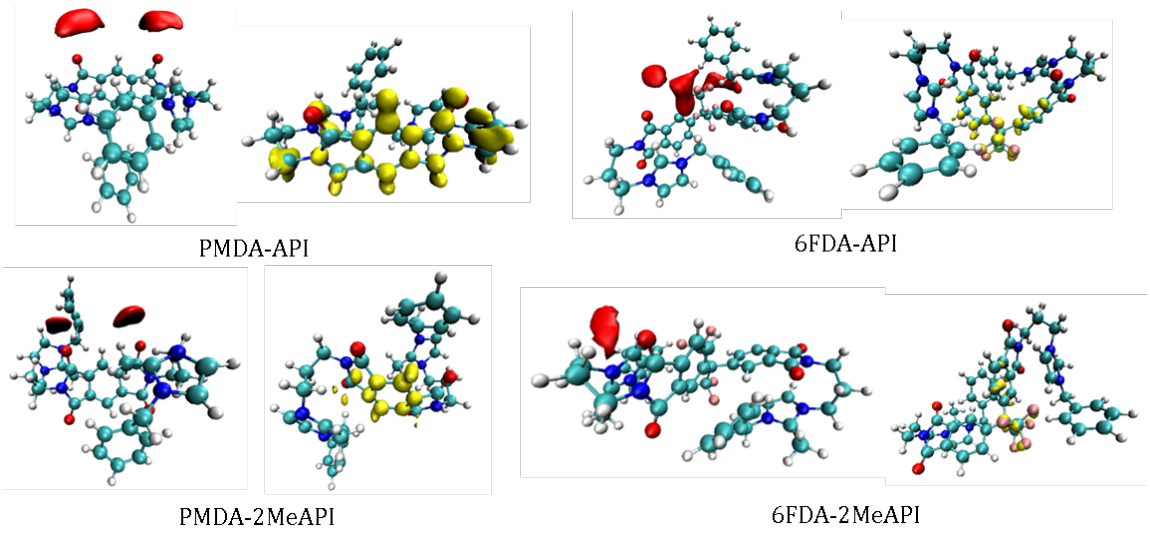

Figure 3.11 The spatial distribution functions (SDFs) of anions (red) and cationic polymer chains (gold) around the positively charged polymer chain. The corresponding isovalues for the anion and cationic species of number densities are 10 nm^{-3} and 4 nm^{-3}, respectively. The central positively charged polymer chain are represented as CPK models.

The CMats for these monomers show the potential binding sites between the cationic species with the anions. Here, we focus on the changes of intermolecular H-bonding between the counter-ions and the intramolecular H-bonding within cationic polymer chains before and after C(2) methylation. We focus on the interactions between the H atoms in PMDA-API (H49 and H50) and 6FDA-API (H 68 and H69) and the H atoms in the -CH_3 groups in PMDA-2MeAPI (H52~54 and H56~58) and 6FDA-2MeAPI (H71~73 and H75~77) with the H-bond acceptors. The slightly stronger H-bonding via the O atom sites, and the weaker H-bonding via the F atom sites of the anions highlight the increased H-bonding interaction after methylation of both PMDA-API and 6FDA-API. Examples of potential H-bonding networks between the -CH_3 groups in PMDA-2MeAPI and 6FDA-2MeAPI with the O atom sites in the $[Tf_2N]^-$ anions during MD simulations are shown in Figure 3.12. Due to thermal fluctuations, the binding sites and bond distances change during the MD simulations. Although the true liquid state is not captured, the main types of anion–cation interactions should still be consistent. Thus, based on the CMat analyses from the MD simulations, the methylation of C(2) positions on the imidazolium ring potentially increase the chance of H-bonding between the cationic species with the anions by providing more binding sites via -CH_3. Furthermore, the SDFs show that the methylation of the C(2) positions slightly decrease the intramolecular interactions via electrostatic interaction, while increasing the hydrogen bonding interactions by providing more H sites in -CH_3 (confirmed by the CMat intramolecular H-bonding analyses in Figure A3.16.

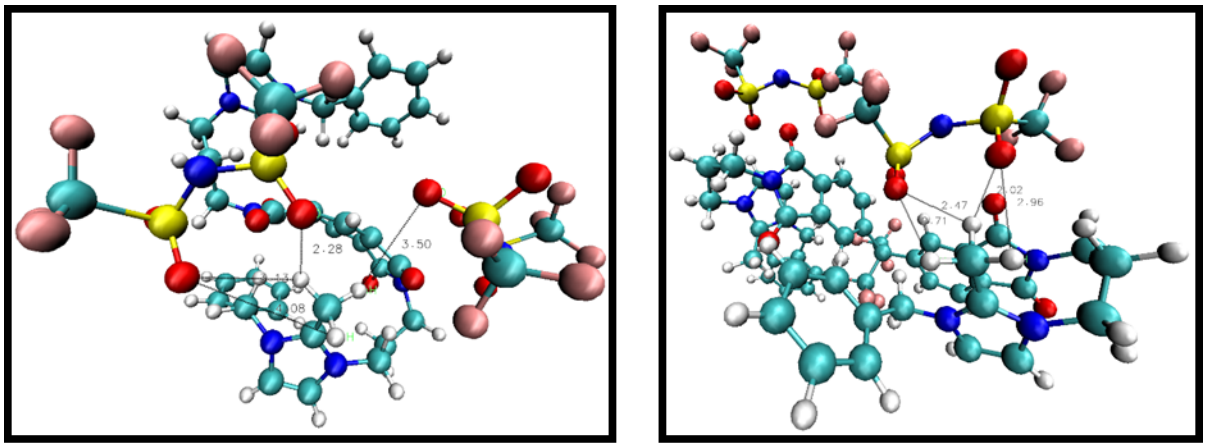

PMDA-2MeAPI 6FDA-2MeAPI

Figure 3.12 Examples of potential H-bonding networks between the -CH_3 groups in PMDA-2MeAPI and 6FDA-2MeAPI with the O atoms in the $[Tf_2N]^-$ anions during the MD simulations. Binding sites and bond distances (listed in the text with units of Å) vary during the MD simulations.

In conclusion, the intermolecular SDF results show that the methylation at the C(2) position of the imidazolium rings decreases the intermolecular interactions (mainly via electrostatic interactions) between the positively-charged polymer chain with the $[Tf_2N]^-$ anions, while slightly increasing the intramolecular H-bonding interaction within positively-charged polymer chains. This is corroborated with the inter- and intra-molecular CMat analyses, along with the ESP and RDG analyses based on DFT calculations.

3.4.3 Material Characterization

Glass transition temperatures (T_g) were determined from the DSC thermograms. The T_g values were less than their counterparts from a previous work.[47] The changes in T_g can be attributed to the reduction of H-bonding within the supramolecular polymer structure of both polymers. Looking at the [PMDA-API(pXy)][Tf_2N] and [PMDA-2MeAPI(pXy)][Tf_2N], the reduction in T_g was from 106.8 ˚C to 87.0 ˚C, , which likely due to

the additional electrostatic charge that is produced that may increase the strain between chains. [PMDA-API(pXy)][Tf_2N] also shows that it a stronger ordered compared to [PMDA-2MeAPI(pXy)][Tf_2N], which can be seen in the XRD measurements (Figure 3.13). The C(2) position causes a distinct structuring in the PMDA ionenes that is disrupted by C(2)-Me. However, the T_g values of [6FDA-API(pXy)][Tf_2N] and [6FDA-2MeAPI(pXy)][Tf_2N] had increased from 93.5 ˚C to 107.4 ˚C, respectively. This increase is likely due to the increase in glassy nature from the C(2)-Me that allows for more coulombic interactions between [Tf_2N] anion and the polymer backbone. This could lead to less chain entanglement when comparing the two 6FDA-based polymers.

FT-IR measurements were performed on all materials to validate the structural composition/functional groups along verifying the presence of IL within the polymer matrix. The spectra are provided in Figure A3.6. FT-IR spectra were normalized to the carbonyl stretching (C=O) peak at 1720 cm^{-1}. The formation of the imide ring and imidazolium can be found in the C-N-C out of plane bending and stretching at 721 cm^{-1} and 1100 cm^{-1}, respectively. The sulfonyl (S=O) stretching within a sulfonimide at peaks 1370-1335 cm^{-1} and the S-N-S stretching at 760 cm^{-1} indicate complete exchange of $[Cl]^-$ to $[Tf_2N]^-$ in the final PI-ionenes. The increase of the S=O and S-N-S were denoted in the composite membranes to demonstrate the incorporation [C_4mim][Tf_2N] into the polymer matrix.

WAXD was used to determine the domain spacings of the polymer films as well as the effects of the IL on the chain-chain spacing, coordinating effects, and molecular interactions. Due to their random nature, amorphous polymers produced a broad halo with a range of 2θ (˚) corresponding to a range of chain-chain spacings of a polymer. [PMDA-

2MeAPI(pXy)][Tf_2N] and [6FDA-2MeAPI(pXy)][Tf_2N] produced profiles with 2θ = 19.5-22.5 ˚ and 2θ = 18.3-20.5 ˚, respectively whereas their counterparts, [PMDA-API(pXy)][Tf_2N] and [6FDA-API(pXy)][Tf_2N], show halos from 2θ = 20-24 ˚and 2θ = 17.5-22.0 ˚ (Figures 3.13-3.14). The d-spacing ranges can be found within Table 3.2 along with the "peak" value. With the presence of a C(2)-Me group on the imidazolium cation, the d-spacing increased. In [PMDA-2MeAPI(pXy)][Tf_2N], the crystalline peak is not present that occurs in the XRD profile of [PMDA-API(pXy)][Tf_2N]. This indicates the C(2) played a vital part in the intermolecular forces present between anion-cation pairs. The C(2) addition caused a reduction in H-bonding which likely led to the increase in d-spacings, yet the halo's peak correlated with other polyimides with d-spacings of 5.5 Å.[48]

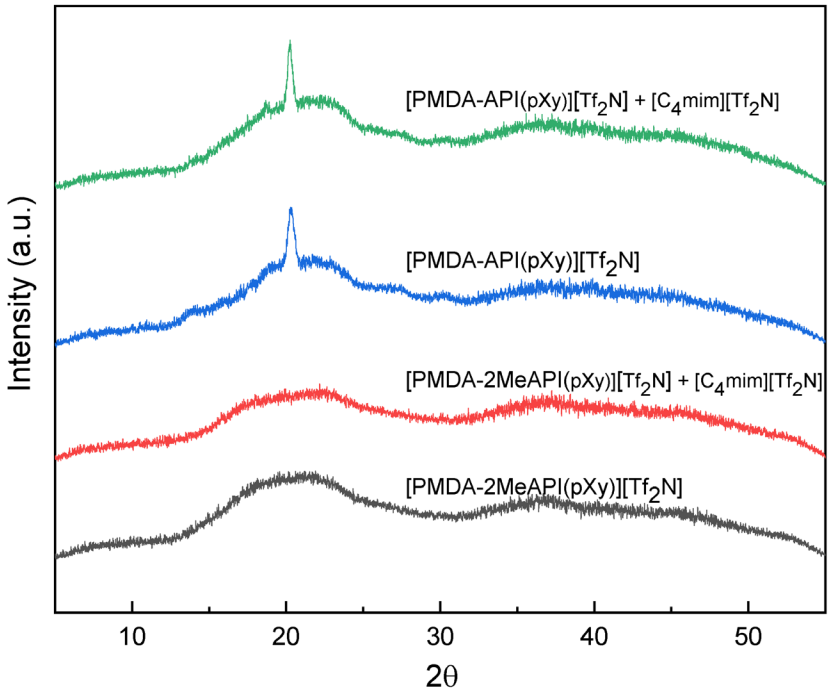

Figure 3.13 XRD Profiles of PMDA C(2)-H and C(2)-Me, both neat and composite, PIs

Addition of [C4mim][Tf2N] decreased the d-spacing range likely due to the addition of H-bonding components within the polymer matrix, yet the decrease is not substantial. The n-butyl group of the [C4mim][Tf2N] may have impeded the packing causing only a slight reduction of 2θ range within both [PMDA-2MeAPI(pXy)][Tf2N] and [6FDA-2MeAPI(pXy)][Tf2N] composites.

Table 3.1 Halo and peak values of neat and IL composites of C(2)-Me materials and C(2)-H materials

	[PMDA-2MeAPI(pXy)][Tf2N]		**[6FDA-2MeAPI(pXy)][Tf2N]**	
	Neat	[C4mim][Tf2N]	Neat	[C4mim][Tf2N]
Halo (Å)	4.77-5.72	4.56-5.72	5.03-5.81	4.51-5.81
Peak (Å)	4.77	4.56	5.15	4.75
	[PMDA-API(pXy)][Tf2N]		**[6FDA-API(pXy)][Tf2N]**	
	Neat	[C4mim][Tf2N]	Neat	[C4mim][Tf2N]
Halo (Å)	4.54-5.36	4.54-5.48	5.10-6.16	4.93-6.23
Peak (Å)	5.05	5.07	5.65	5.15

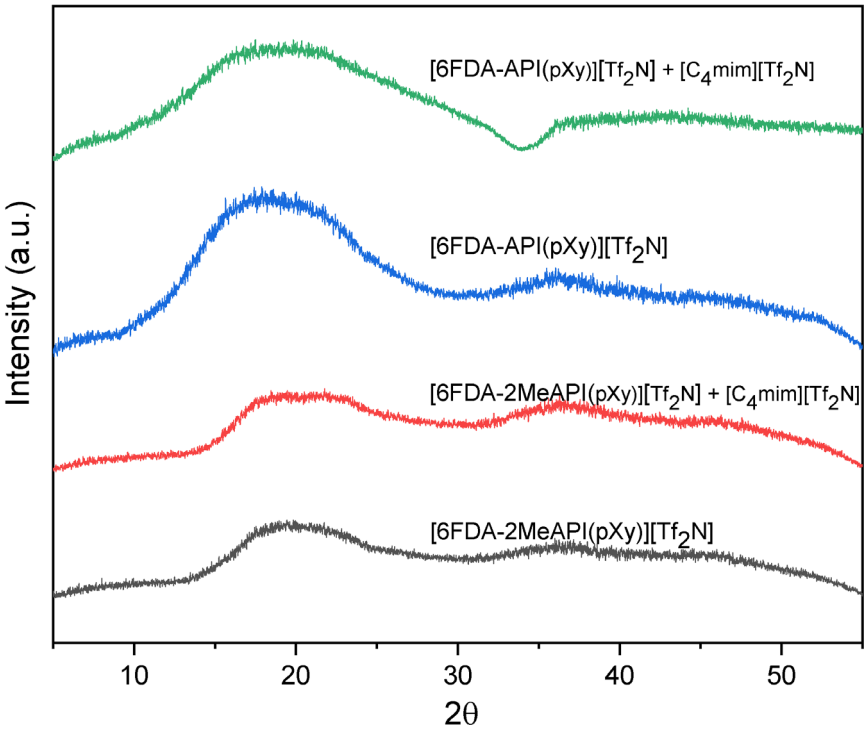

Figure 3.14 XRD Profiles of 6FDA C(2)-H and C(2)-Me, both neat and composite, PIs

3.4.3 Gas Separation Performances of PI-Ionene + IL Composite Membranes

The permeabilities, diffusivities, and solubilities are recorded in Table 3.3. Both the [PMDA-2MeAPI(pXy)][Tf_2N] + [C_4mim][Tf_2N] and [6FDA-2MeAPI(pXy)][Tf_2N] + [C_4mim][Tf_2N] showed moderate gas separation ability for all gases (N_2, CH_4, CO_2, and H_2) where both C(2)-Me composites decreased when compared to their direct counterpart with C(2)-H groups. Comparing the [PMDA-API(pXy)][Tf_2N] + [C_4mim][Tf_2N] and [PMDA-2MeAPI(pXy)][Tf_2N] + [C_4mim][Tf_2N], the addition of the methyl group caused significant decreases in all gas diffusivities by over factors of 10 while slight increases in solubility. As seen in research done with C(2)-Me imidazolium cations, the CO_2 solubility of the material did not change with the addition of a methyl group on the acidic C(2) position. The gas solubility of the IL was determined to be the anion affinity for CO_2 within the IL.[49]

Table 3.2 Permeability, diffusivity and solubility values of [PMDA-2MeAPI(pXy)][Tf_2N] + [C_4mim][Tf_2N] and [6FDA-2MeAPI(pXy)][Tf_2N] + [C_4mim][Tf_2N]

	Permeability[b]		**Diffusivity[c]**		**Solubility[d]**	
	[6FDA-2MeAPI(pXy)][Tf_2N] + [C_4mim][Tf_2N]					
N_2	0.16	±0.01	0.66	±0.22	0.205	±0.08
CH_4	0.16	±0.02	0.69	±0.03	0.171	±0.01
H_2	3.89	±0.05	15.2	±2.74	0.200	±0.07
CO_2	5.57	±0.03	3.3	±0.08	1.300	±0.04
	[PMDA-2MeAPI(pXy)][Tf_2N] + [C_4mim][Tf_2N]					
N_2	0.07	±0.004	0.28	±0.01	0.180	±0.01
CH_4	0.08	±0.004	0.21	±0.03	0.310	±0.05
H_2	1.34	±0.02	3.6	±0.61	0.290	±0.08
CO_2	2.75	±0.03	0.7	±0.01	2.980	±0.03
	[6FDA-API(pXy)][Tf_2N] + [C_4mim][Tf_2N]					
N_2	0.20	±0.03	--	--	--	--
CH_4	0.18	±0.02	--	--	--	--
H_2	3.59	±0.25	--	--	--	--
CO_2	6.58	±0.15	--	--	--	--
	[PMDA-API(pXy)][Tf_2N] + [C_4mim][Tf_2N]					
N_2	0.52	±0.02	13.3	±5.2	0.025	±0.004
CH_4	0.79	±0.02	4.05	±0.53	0.154	±0.026
H_2	5.18	±0.04	67.4	±15.6	0.061	±0.016
CO_2	20.40	±0.1	7.56	±0.34	2.010	±0.19

[a] Three replicate experiments were acquired, so uncertainties are presented as a single standard deviation.
[b] Permeability in barrer.1 barrer=10^{-10} (cm^3 (STP) cm) (cm^2 s cmHg)$^{-1}$.
[c] Diffusivity (10^{-8} cm^2 s^{-1}).
[d] Solubility (cm^3 (STP) cm^{-3} $cmHg^{-1}$).
-- not reported in prior work.

Permeabilities of both [PMDA-2MeAPI(pXy)][Tf_2N] + [C_4mim][Tf_2N] and [6FDA-2MeAPI(pXy)][Tf_2N] + [C_4mim][Tf_2N] can be compared to each other since the only difference was their dianhydride units. Koros and co-workers compared PMDA and 6FDA

in two instances, and the increase in the permeability is alike.[50, 51] In this instance, addition of a methyl group on the C(2) position further concludes that 6FDA could be a better unit than PMDA when looking to improve gas permeabilities by increasing FFV, yet, within ionic polymer architecture, the C(2) position can be seen as an integral part of resulting polymer matrix. When comparing the permeabilities of the IL composites both with and without a methyl group, the non-methylated counterparts have higher permeabilities with respect to all gases tested than either [PMDA-2MeAPI(pXy)][Tf_2N] + [C_4mim][Tf_2N] or [6FDA-2MeAPI(pXy)][Tf_2N] + [C_4mim][Tf_2N]. As an indicator of permeability, the d-spacing can be a correlative factor since the d-spacing is indicative of the chain-chain spacings within a polymer matrix. This phenomenon is also demonstrated here. Although other factors attribute to the gas separation ability, the d-spacing of [6FDA-2MeAPI(pXy)][Tf_2N] + [C_4mim][Tf_2N] was higher than the [PMDA-2MeAPI(pXy)][Tf_2N] + [C_4mim][Tf_2N]. So, the correlation between d-spacing and permeability holds true for these membranes as it had for other similar ionic polymer systems.[17, 18, 29, 30] It should be noted that H_2 permeabilities were still lower than the CO_2 when IL was present in the polymer matrix, as the permselectivity of CO_2/H_2 is > 1.

The QM calculations and MD simulations highly validate the results of the gas permeation and the changes within the d-spacings. As stated in the discussion of QM simulations, both 6FDA-2MeAPI and PMDA-2MeAPI experienced an increase in the electrostatic charge at the C(2)-Me position as well as the MD simulations demonstrating the increase of the H-bonding effects at the same position. The increase in these molecular interactions cause a two-fold basis for the decrease in permeability when comparing the both the API and the 2MeAPI connectivity. Due to the increase in the electrostatic charges

and H-bonding characteristics, the supramolecular structure of the polymer chains is more tightly bound to the anions which leads to the reduction of d-spacings for gas molecules to permeate the polymer matrix. The effects can be seen in the XRD as well as the gas permeation data which these simulations prove that the addition the -Me on the C(2) position has a substantial effect on the structuring of the polymer chains.

Selectivity values were also derived from permeabilities, selectivities, and diffusivities displayed in Table 3.4. Diffusivity and solubility selectivities of both [PMDA-2MeAPI(pXy)][Tf_2N] + [C_4mim][Tf_2N] and [6FDA-2MeAPI(pXy)][Tf_2N] + [C_4mim][Tf_2N] showed that CO_2 favors a solubility-based mechanism whereas H_2 favors a diffusivity-based mechanism, as seen in previous research with ionic polyimide membranes.[16] Permselectivities of the IL-composite membranes coincided with the inverse relationship of permeability/selectivity. The relationship is demonstrated by Robeson's Upper Bound when plotting CO_2 permeability versus CO_2 selectivity.[52, 53] Robeson plots with similar ionic gas separation membranes can be seen in Figures S17-S18. The materials were below the upper bound and within the bulk of other materials when comparing CO_2/N_2 and CO_2/CH_4.

Table 3.3 Permeability, Diffusivity, and solubility selectivities derived from specific gas pairings

	[6FDA-2MeAPI(pXy)][Tf_2N] + [C_4mim][Tf_2N]			**[PMDA-2MeAPI(pXy)][Tf_2N] + [C_4mim][Tf_2N]**		
	P_i/P_j	**D_i/D_j**	**S_i/S_j**	**P_i/P_j**	**D_i/D_j**	**S_i/S_j**
CO_2/N_2	35.41	5.0	6.3	40.99	2.5	16.6
CO_2/CH_4	35.51	4.8	7.6	33.07	3.3	9.6
H_2/N_2	24.73	23.0	1.0	20.00	12.9	1.6
H_2/CH_4	24.81	22.0	1.2	16.14	17.1	0.9
CO_2/H_2	1.43	0.2	6.5	2.05	0.2	10.3

3.5 Conclusions

2MeAPI was reacted with two dianhydrides (PMDA and 6FDA) through a condensation mechanism leading to a two new bisimidazole diimide monomers. These monomers were then polymerized via the Mentshutkin reaction resulting in an ionic polymer with halide anions. Anion metathesis was performed on the materials to exchange the halide with [Tf_2N]. the brittle neat materials and acts to help increase the P_{CO2}. The materials were characterized via NMR and FT-IR to ensure the strucutre of the material . The thermal properties of [PMDA-2MeAPI(pXy)][Tf_2N] and [6FDA-2MeAPI(pXy)][Tf_2N] were also measured. The XRD demonstrated that the C(2)-Me ionenes had a significant decrease in the overall ordering of the materials which lends to the fact that they were more amorphous. [C_4mim][Tf_2N] was added which helped plasticize so that they could form films, and gas separation properties were tested which demonstrated that the C(2)-Me causes the materials diffusivity to significantly decrease while slightly increasing the solubility. These materials did not have higher gas permeabilities than their C(2)-H counterparts likely due to the reduction of hydrogen bonding between the polymer chains which caused a more amorphous film as seen in the XRD, yet due to the ionic nature of the films, it can be seen that they still have distinct CO_2 solubilities when compared to other gases. The QM and MD simulations corroborate the gas spearation properties and the XRD changes from the non-methylated to the methylated which resulted in higher electrostatic charge at the C(2) position.

3.6 References

1. O'Brien, K. C.; Koros, W. J.; Husk, G. R., Influence of casting and curing conditions on gas sorption and transport in polyimide films. *Polymer Engineering & Science* **1987,** *27* (3), 211-217.

2. Hirayama, Y.; Yoshinaga, T.; Kusuki, Y.; Ninomiya, K.; Sakakibara, T.; Tamari, T., Relation of gas permeability with structure of aromatic polyimides I. *Journal of Membrane Science* **1996,** *111* (2), 169-182.

3. Stern, S. A.; Liu, Y.; Feld, W. A., Structure/permeability relationships of polyimides with branched or extended diamine moieties. *J. Polym. Sci., Part B: Polym. Phys.* **1993,** *31* (8), 939-51.

4. Anderson, E. B.; Long, T. E., Imidazole- and imidazolium-containing polymers for biology and material science applications. *Polymer* **2010,** *51* (12), 2447-2454.

5. Green, M. D.; Allen, M. H., Jr.; Dennis, J. M.; Salas-de la Cruz, D.; Gao, R.; Winey, K. I.; Long, T. E., Tailoring macromolecular architecture with imidazole functionality: A perspective for controlled polymerization processes. *Eur. Polym. J.* **2011,** *47* (4), 486-496.

6. Williams, S. R.; Long, T. E., Recent advances in the synthesis and structure-property relationships of ammonium ionenes. *Prog. Polym. Sci.* **2009,** *34* (8), 762-782.

7. Bara, J. E.; O'Harra, K. E., Recent Advances in the Design of Ionenes: Toward Convergence with High-Performance Polymers. *Macromolecular Chemistry and Physics* **2019,** *0* (0), 1900078.

8. Gibbs, C. F.; Littmann, E. R.; Marvel, C. S., Quaternary ammonium salts from halogenated alkyldimethylamines. II. The polymerization of γ-halogenopropyldimethylamines. *J. Am. Chem. Soc.* **1933,** *55*, 753-7.

9. Bogert, M. T., The mechanism of the ionene synthesis. *Science (Washington, DC, U. S.)* **1933,** *77*, 197-8.

10. Ueki, T.; Watanabe, M., Macromolecules in Ionic Liquids: Progress, Challenges, and Opportunities. *Macromolecules* **2008,** *41* (11), 3739-3749.

11. Zhang, H.; Behera, P. K.; Singha, N. K.; Hong, K.; Mays, J. W., Polymerization in Ionic Liquids. *Encyclopedia of Polymer Science and Technology* **2015**, 1-19.

12. Qian, W.; Texter, J.; Yan, F., Frontiers in poly(ionic liquid)s: syntheses and applications. *Chemical Society Reviews* **2017,** *46* (4), 1124-1159.

13. Correia, D. M.; Fernandes, L. C.; Martins, P. M.; García-Astrain, C.; Costa, C. M.; Reguera, J.; Lanceros-Méndez, S., Ionic Liquid–Polymer Composites: A New Platform for Multifunctional Applications. *Adv Funct Mater* **2020,** *n/a* (n/a), 1909736.

14. Li, P.; Paul, D. R.; Chung, T.-S., High performance membranes based on ionic liquid polymers for CO2 separation from the flue gas. *Green Chem.* **2012,** *14* (4), 1052-1063.

15. Li, P.; Zhao, Q.; Anderson, J. L.; Varanasi, S.; Coleman, M. R., Synthesis of copolyimides based on room temperature ionic liquid diamines. *J. Polym. Sci., Part A: Polym. Chem.* **2010,** *48* (18), 4036-4046.

16. Mittenthal, M. S.; Flowers, B. S.; Bara, J. E.; Whitley, J. W.; Spear, S. K.; Roveda, J. D.; Wallace, D. A.; Shannon, M. S.; Holler, R.; Martens, R.; Daly, D. T., Ionic Polyimides: Hybrid Polymer Architectures and Composites with Ionic Liquids for Advanced Gas Separation Membranes. *Ind. Eng. Chem. Res.* **2017,** *56* (17), 5055-5069.

17. O'Harra, K. E.; Kammakakam, I.; Devriese, E. M.; Noll, D. M.; Bara, J. E.; Jackson, E. M., Synthesis and Performance of 6FDA-Based Polyimide-Ionenes and Composites with Ionic Liquids as Gas Separation Membranes. *Membranes-Basel* **2019,** *9* (7), 79.

18. O'Harra, K. E.; Kammakakam, I.; Noll, D. M.; Turflinger, E. M.; Dennis, G. P.; Jackson, E. M.; Bara, J. E., Synthesis and Performance of Aromatic Polyamide Ionenes as Gas Separation Membranes. *Membranes-Basel* **2020,** *10* (3).

19. Bonhôte, P.; Dias, A.-P.; Papageorgiou, N.; Kalyanasundaram, K.; Grätzel, M., Hydrophobic, Highly Conductive Ambient-Temperature Molten Salts. *Inorganic Chemistry* **1996,** *35* (5), 1168-1178.

20. Hunt, P. A., Why Does a Reduction in Hydrogen Bonding Lead to an Increase in Viscosity for the 1-Butyl-2,3-dimethyl-imidazolium-Based Ionic Liquids? *The Journal of Physical Chemistry B* **2007,** *111* (18), 4844-4853.

21. Endo, T.; Kato, T.; Nishikawa, K., Effects of Methylation at the 2 Position of the Cation Ring on Phase Behaviors and Conformational Structures of Imidazolium-Based Ionic Liquids. *The Journal of Physical Chemistry B* **2010,** *114* (28), 9201-9208.

22. Fumino, K.; Wulf, A.; Ludwig, R., Strong, Localized, and Directional Hydrogen Bonds Fluidize Ionic Liquids. *Angewandte Chemie International Edition* **2008,** *47* (45), 8731-8734.

23. Noack, K.; Schulz, P. S.; Paape, N.; Kiefer, J.; Wasserscheid, P.; Leipertz, A., The role of the C2 position in interionic interactions of imidazolium based ionic liquids: a vibrational and NMR spectroscopic study. *Phys Chem Chem Phys* **2010,** *12* (42), 14153-14161.

24. Zahn, S.; Bruns, G.; Thar, J.; Kirchner, B., What keeps ionic liquids in flow? *Phys Chem Chem Phys* **2008,** *10* (46), 6921-6924.

25. Fumino, K.; Peppel, T.; Geppert-Rybczyńska, M.; Zaitsau, D. H.; Lehmann, J. K.; Verevkin, S. P.; Köckerling, M.; Ludwig, R., The influence of hydrogen bonding on the physical properties of ionic liquids. *Phys Chem Chem Phys* **2011,** *13* (31), 14064-14075.

26. Carlisle, T. K.; Bara, J. E.; Lafrate, A. L.; Gin, D. L.; Noble, R. D., Main-chain imidazolium polymer membranes for CO2 separations: An initial study of a new ionic liquid-inspired platform. *J. Membr. Sci.* **2010,** *359* (1-2), 37-43.

27. He, X.; Chan, T. H., Structurally Defined Imidazolium-Type Ionic Oligomers as Soluble/Solid Support for Peptide Synthesis. *Organic Letters* **2007,** *9* (14), 2681-2684.

28. Demarteau, J.; O'Harra, K. E.; Bara, J. E.; Sardon, H., Valorization of Plastic Wastes for the Synthesis of Imidazolium-Based Self-Supported Elastomeric Ionenes. *ChemSusChem* **2020,** *13* (12), 3122-3126.

29. Kammakakam, I.; Oharra, K. E.; Bara, J. E.; Jackson, E. M., Design and Synthesis of Imidazolium-Mediated Tröger's Base-Containing Ionene Polymers for Advanced CO2 Separation Membranes. *ACS Omega* **2019,** *4* (2), 3439-3448.

30. Kammakakam, I.; O'Harra, K. E.; Dennis, G. P.; Jackson, E. M.; Bara, J. E., Self-healing imidazolium-based ionene-polyamide membranes: an experimental study on physical and gas transport properties. *Polymer International* **2019,** *68* (6), 1123-1129.

31. Neese, F., The ORCA Program System. *Wiley Interdiscip. Rev.: Comput. Mol. Sci.* **2012,** *2*, 73-78.

32. Neese, F., Software Update: the ORCA Program System, Version 4.0. *Wiley Interdiscip. Rev.: Comput. Mol. Sci.* **2018,** *8*, e1327.

33. Brandenburg, J. G.; Bannwarth, C.; Hansen, A.; Grimme, S., B97-3c: A Revised Low-Cost Variant of the B97-D Density Functional Method. *J. Chem. Phys.* **2018,** *148*, 064104.

34. Breneman, C. M.; Wiberg, K. B., Determining Atom-Centered Monopoles from Molecular Electrostatic potentials. The Need for High Sampling Density in Formamide Conformational Analysis. *J. Comput. Chem.* **1990,** *11*, 361-373.

35. Marenich, A. V.; Jerome, S. V.; Cramer, C. J.; Truhlar, D. G., Charge Model 5: An Extension of Hirshfeld Population Analysis for the Accurate Description of Molecular Interactions in Gaseous and Condensed Phases. *J. Chem. Theory Comput.* **2012,** *8*, 527-541.

36. Lu, T.; Chen, F., Multiwfn: A Multifunctional Wavefunction Analyzer. *J. Comput. Chem.* **2012,** *33*, 580-592.

37. Dennington, R.; Keith, T.; Millam, J. *GaussView, Version 5*, 2009.

38. Tian Lu *OfakeG program*, 1.0.6; http://sobereva.com/soft/OfakeG, (accessed May, 2020)

39. Johnson, E. R.; Keinan, S.; Mori-Sánchez, P.; Contreras-García, J.; Cohen, A. J.; Yang, W., Revealing Noncovalent Interactions. *J. Am. Chem. Soc.* **2010,** *132*, 6498-6506.

40. Humphrey, W.; Dalke, A.; Schulten, K., VMD: Visual Molecular Dynamics. *J. Mol. Graphics* **1996,** *14*, 33-38.

41. Murray, J. S.; Brinck, T.; Lane, P.; Paulsen, K.; Politzer, P., Statistically-Based Interaction Indices Derived from Molecular Surface Electrostatic Potentials: A General Interaction Properties Function (GIPF). *J. Mol. Struct. THEOCHEM* **1994,** *307*, 55-64.

42. Bader, R. F.; Carroll, M. T.; Cheeseman, J. R.; Chang, C., Properties of Atoms in Molecules: Atomic Volumes. *J. Am. Chem. Soc.* **1987,** *109*, 7968-7979.

43. Spicher, S.; Grimme, S., Robust Atomistic Modeling of Materials, Organometallic, and Biochemical Systems. *Angew. Chem. Int. Ed.* **2020,** *59*.

44. Grimme, S.; Bannwarth, C.; Shushkov, P., A Robust and Accurate Tight-Binding Quantum Chemical Method for Structures, Vibrational Frequencies, and Noncovalent Interactions of Large Molecular Systems Parametrized for All spd-Block Elements (Z = 1–86). *J. Chem. Theory Comput.* **2017,** *13*, 1989-2009.

45. Martin, B.; Kirchner, B., TRAVIS-A Free Analyzer and Visualizer for Monte Carlo and Molecular Dynamics Trajectories. *J. Chem. Inf. Model.* **2011,** *51*, 2007-2023.

46. Brehm, M.; Thomas, M.; Gehrke, S.; Kirchner, B., TRAVIS—A Free Analyzer for Trajectories from Molecular Simulation. *J. Chem. Phys.* **2020,** *152*, 164105.

47. O'Harra, K. E.; Kammakakam, I.; Bara, J. E.; Jackson, E. M., Understanding the effects of backbone chemistry and anion type on the structure and thermal behaviors of imidazolium polyimide-ionenes. *Polymer International* **2019**.

48. Shimazu, A.; Miyazaki, T.; Ikeda, K., Interpretation of d-spacing determined by wide angle X-ray scattering in 6FDA-based polyimide by molecular modeling. *Journal of Membrane Science* **2000,** *166* (1), 113-118.

49. Cadena, C.; Anthony, J. L.; Shah, J. K.; Morrow, T. I.; Brennecke, J. F.; Maginn, E. J., Why Is CO2 So Soluble in Imidazolium-Based Ionic Liquids? *J. Am. Chem. Soc.* **2004,** *126* (16), 5300-5308.

50. Kim, T. H.; Koros, W. J.; Husk, G. R., Advanced gas separation membrane materials: rigid aromatic polyimides. *Sep. Sci. Technol.* **1988,** *23* (12-13), 1611-26.

51. Kim, T. H.; Koros, W. J.; Husk, G. R.; O'Brien, K. C., Relationship between gas separation properties and chemical structure in a series of aromatic polyimides. *J. Membr. Sci.* **1988,** *37* (1), 45-62.

52. Robeson, L. M., Correlation of separation factor versus permeability for polymeric membranes. *J. Membr. Sci.* **1991,** *62* (2), 165-85.

53. Robeson, L. M., The upper bound revisited. *J. Membr. Sci.* **2008,** *320* (1+2), 390-400.

3.7 Appendix

^{1}H- and ^{13}C-NMR

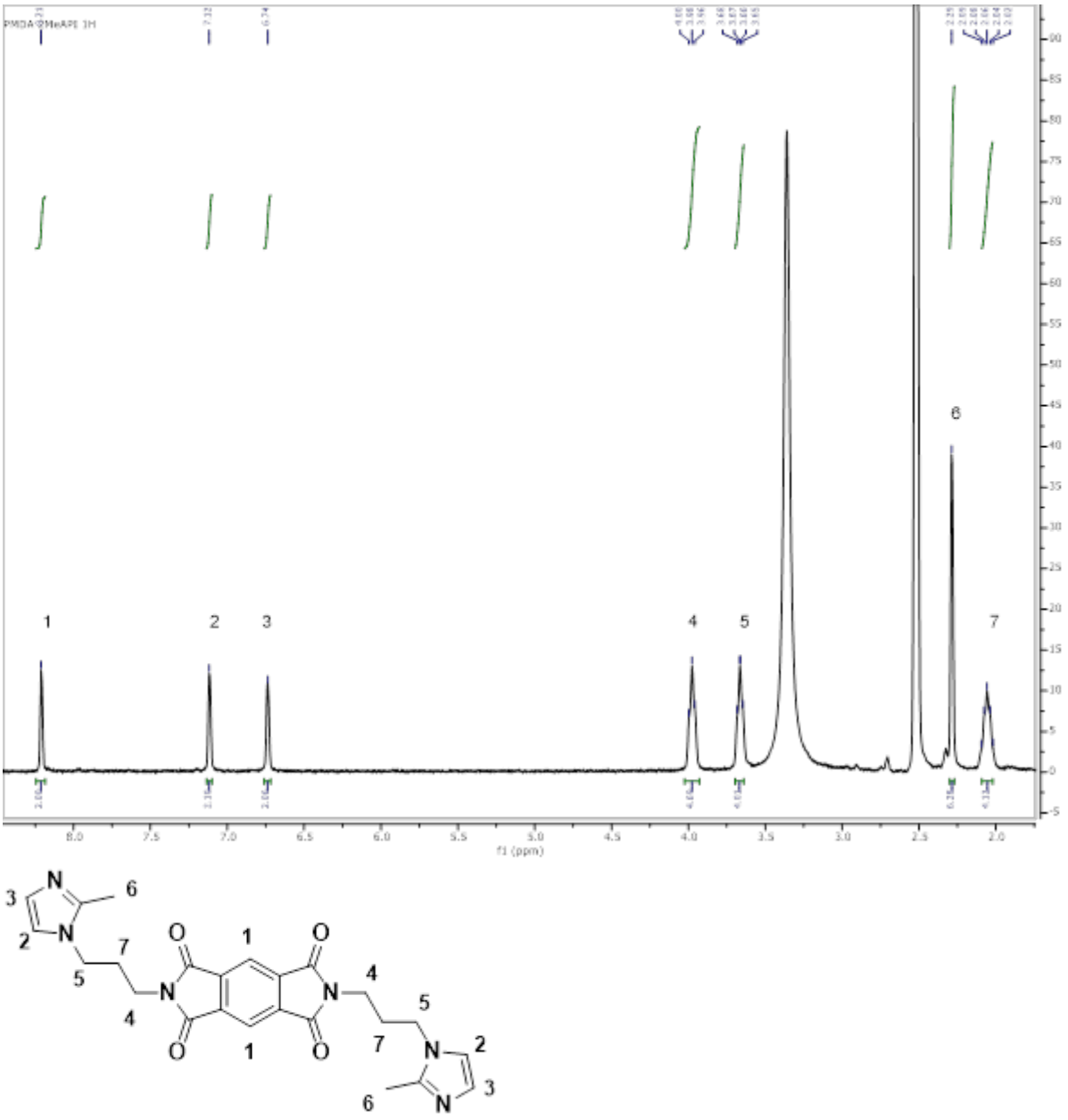

Figure A3.1 ^{1}H-NMR spectrum for [PMDA-2MeAPI(pXy)][Tf_2N]
^{1}H-NMR (500MHz, d6-DMSO) δ 8.21 (s, 2H), 7.12 (s, 2H), 6.74 (s, 2H), 3.98 (t, J = 7.24 Hz, 4H), 3.66 (t, J = 6.10 Hz, 4H), 2.29 (s, 6H), 2.06 (p, J = 6.51, 6.71 Hz, 4H).

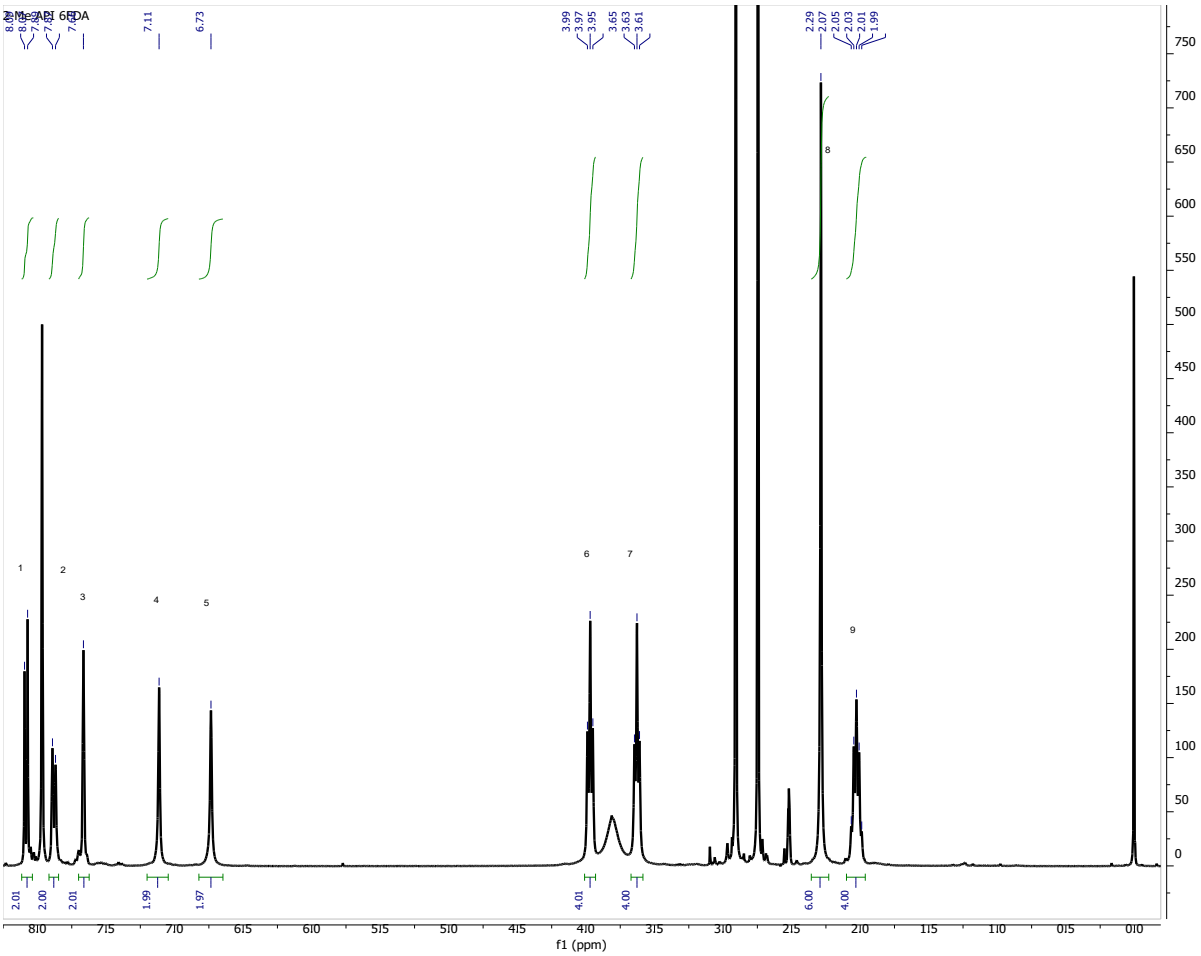

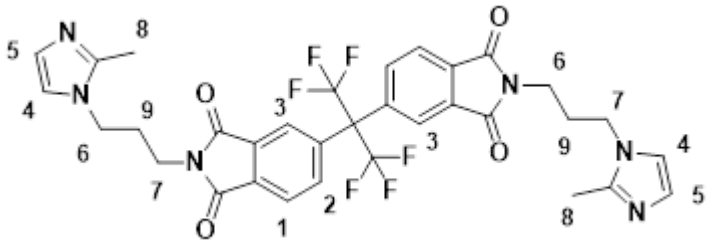

Figure A3.2 ^{1}H-NMR spectrum for [6FDA-2MeAPI(pXy)][Tf_2N]
^{1}H-NMR (500MHz, d6-DMSO) δ 8.08 (d, J = 8.06 Hz, 2H), 7.88 (d, J = 7.99 Hz, 2H), 7.66 (s, 2H), 7.11(s, 2H), 6.73 (s, 2H), 3.97 (t, J = 7.11 Hz, 4H), 3.63 (t, J = 6.62 Hz, 4H), 2.29 (s, 6H), 2.03 (p, J = 6.76, 6.93 Hz, 4H).

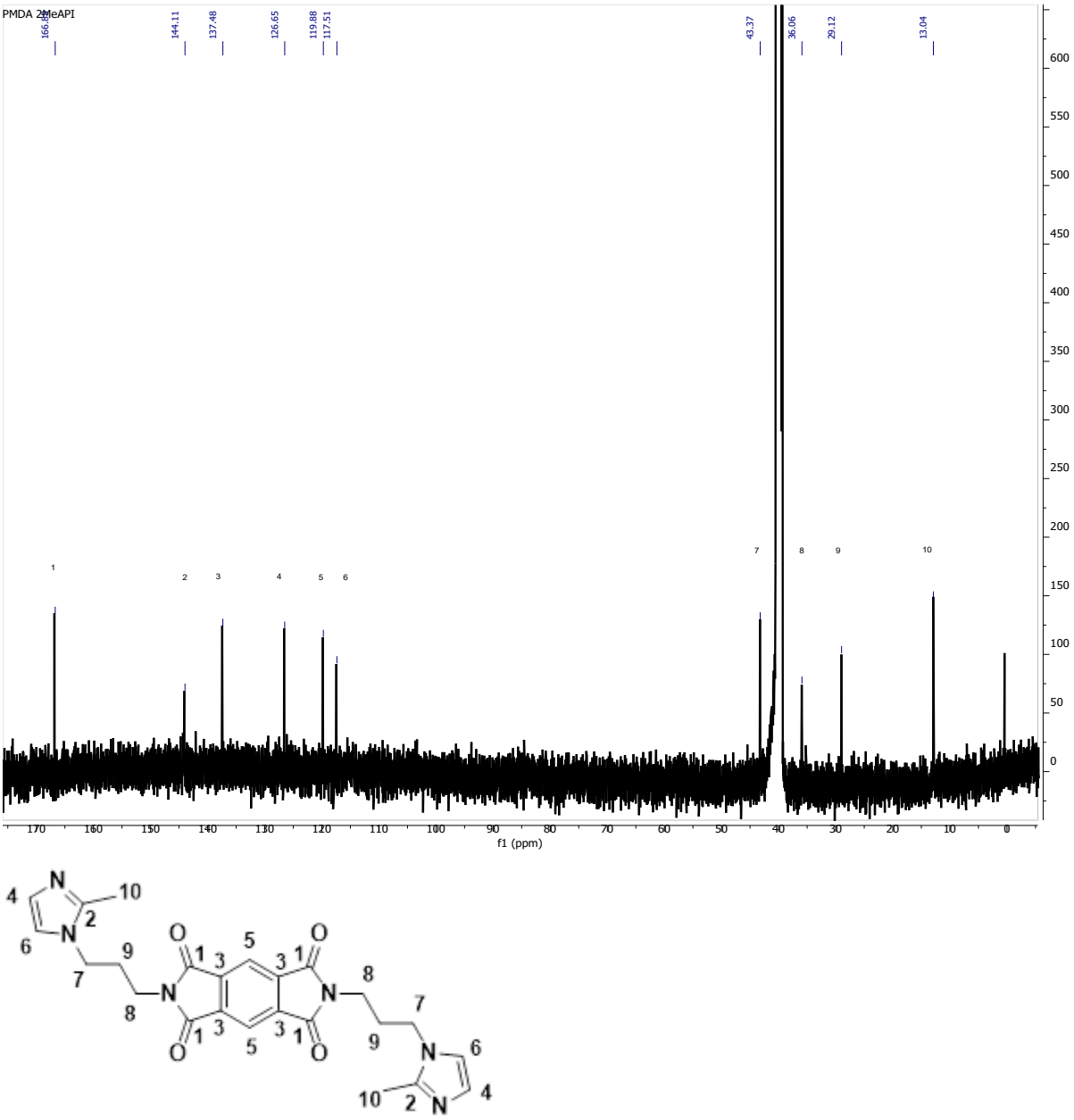

Figure A3.3 ^{13}C-NMR spectrum for [PMDA-2MeAPI(pXy)][Tf_2N]
^{13}C-NMR (500MHz, d6-DMSO) δ 166.85 (C-1, 4C), 144.11 (C-2,2C), 137.48 (C-3,4C), 126.65 (C-4,2C), 119.88 (C-5,2C), 117.51 (C-6,2C), 43.37 (C-7,2C), 36.06 (C-8, 2C), 29.12 (C-9, 2C), 13.04 (C-10, 2C).

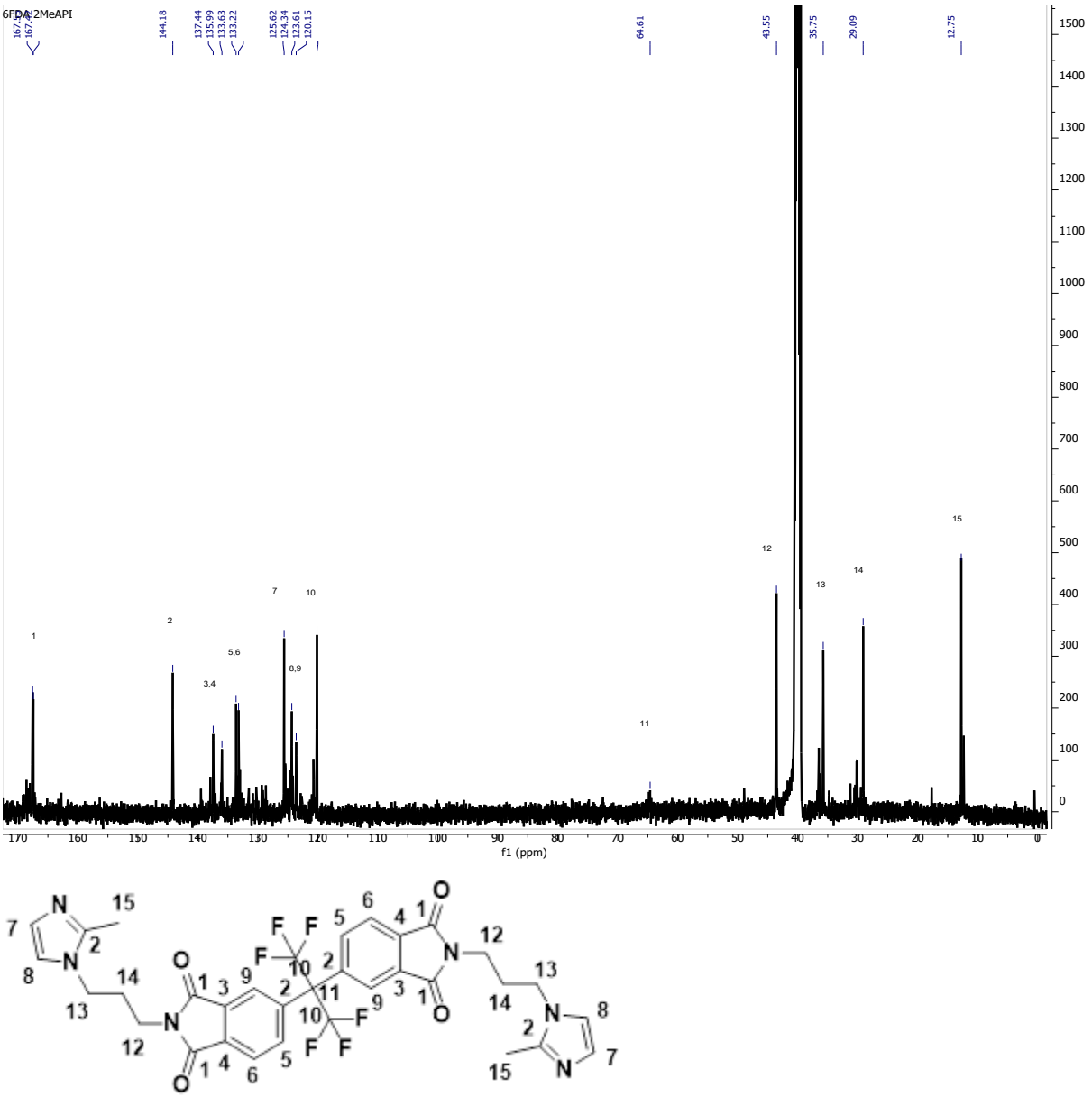

Figure A3.4 ^{13}C-NMR spectrum for [6FDA-2MeAPI(pXy)][Tf_2N]
^{13}C-NMR (500MHz, d6-DMSO) δ167.55, 167.42, 144.18, 137.44, 135.99, 133.63, 133.22, 125.62, 124.34, 123.61, 120.15, 64.61, 43.55, 35.75, 29.09,12.75.

FT-IR Analysis

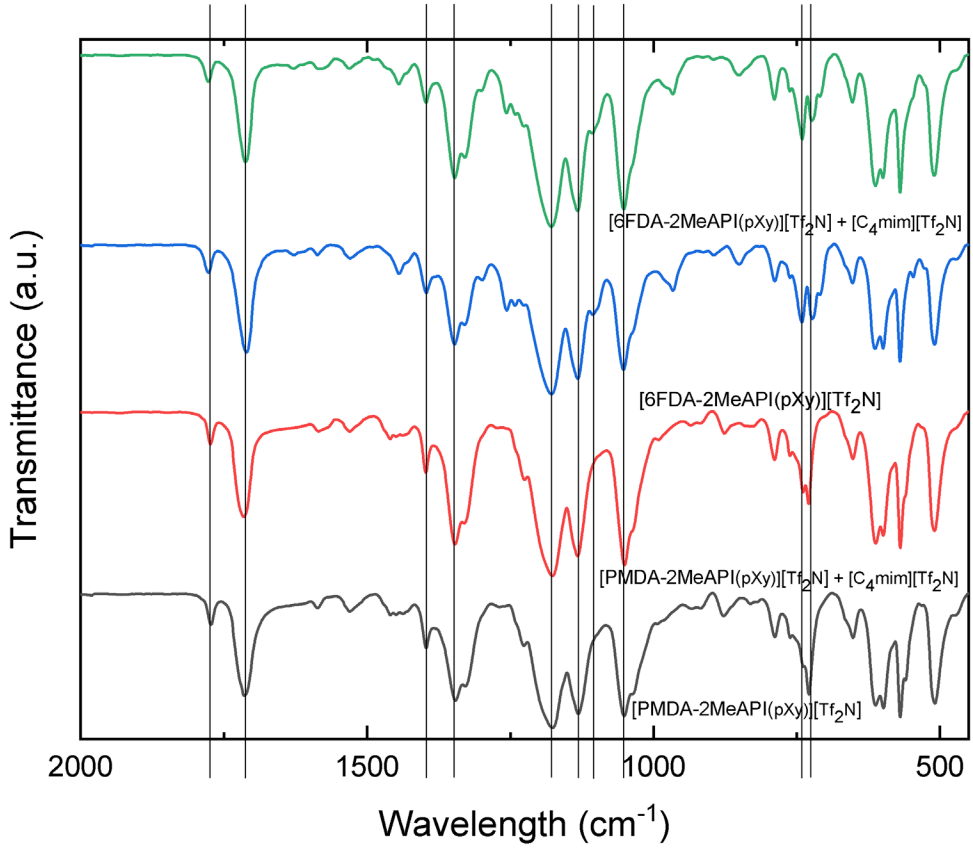

Figure A3.5 FT-IR spectra of all neat and composite materials with main groups indicated

MALDI-TOF MS

The number average molecular weights (M_N) for both [PMDA-2MeAPI(pXy)][Tf_2N] and [6FDA-2MeAPI(pXy)][Tf_2N] ionenes were determined using matrix-assisted laser desorption/ionization time-of-flight mass spectrometry (MALDI-TOF MS).

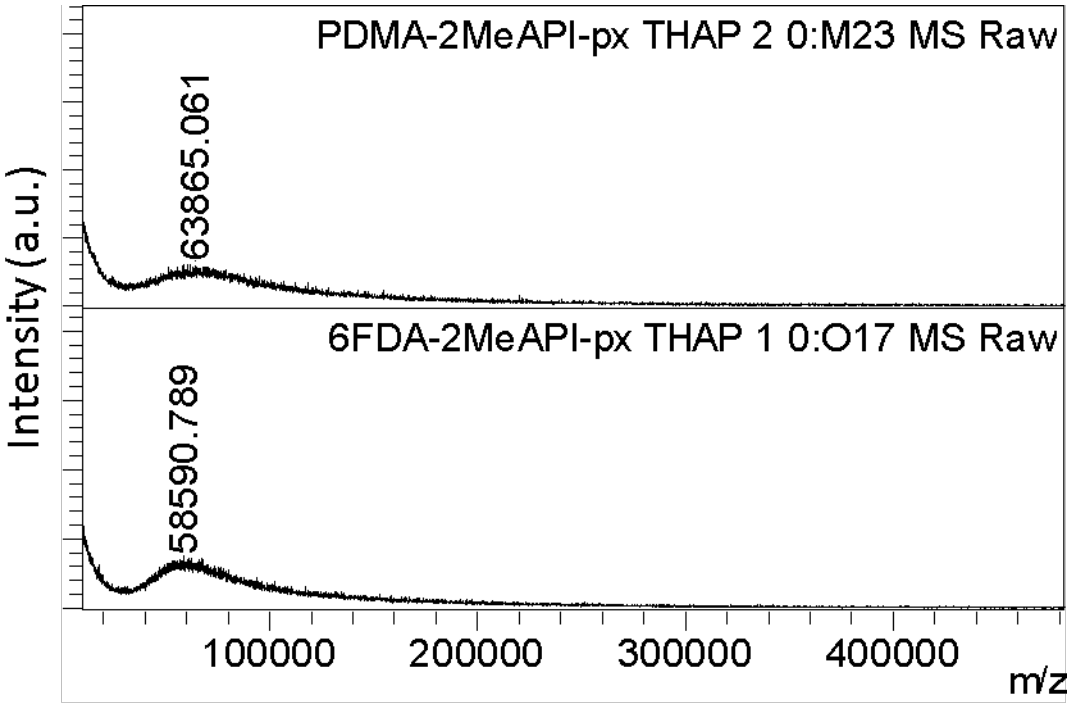

Figure A3.6 MALDI-TOF profile for ionenes, labeled with M_N.

Thermal Data

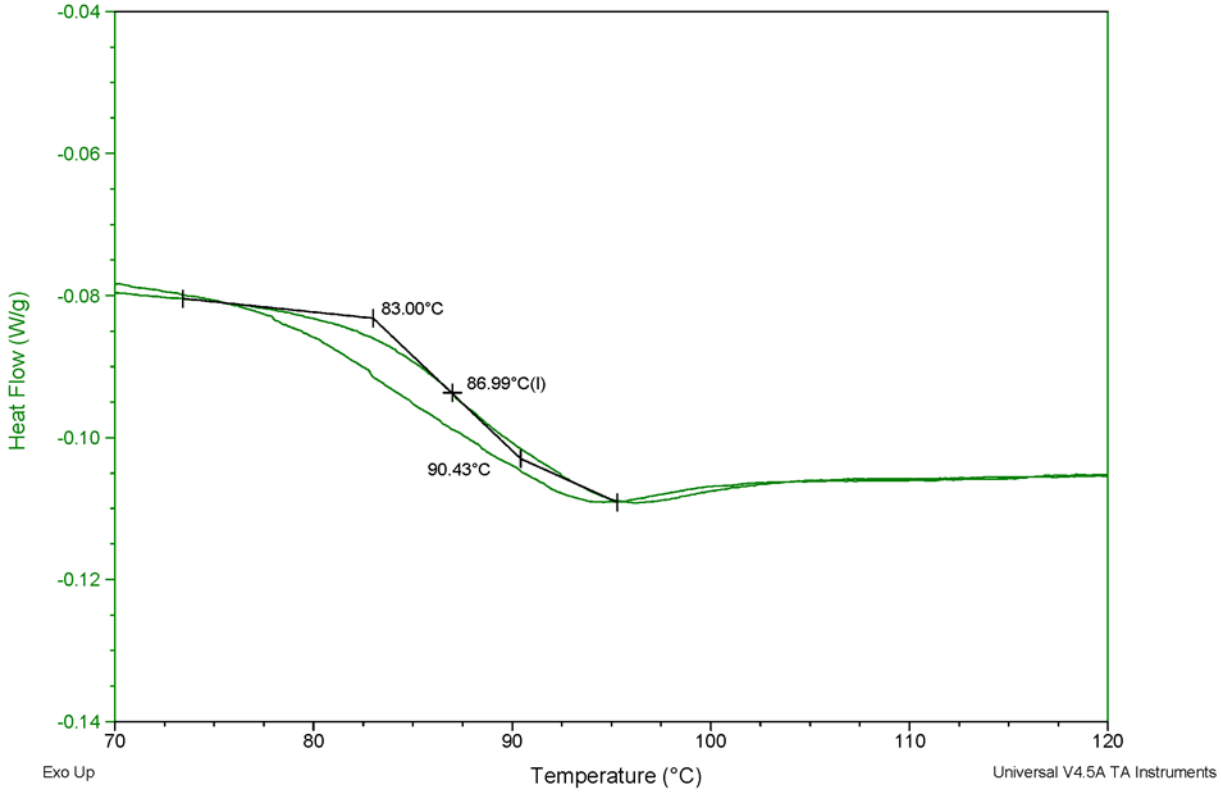

Figure A3.7 DSC profile of [PMDA-2MeAPI(pXy)][Tf_2N]

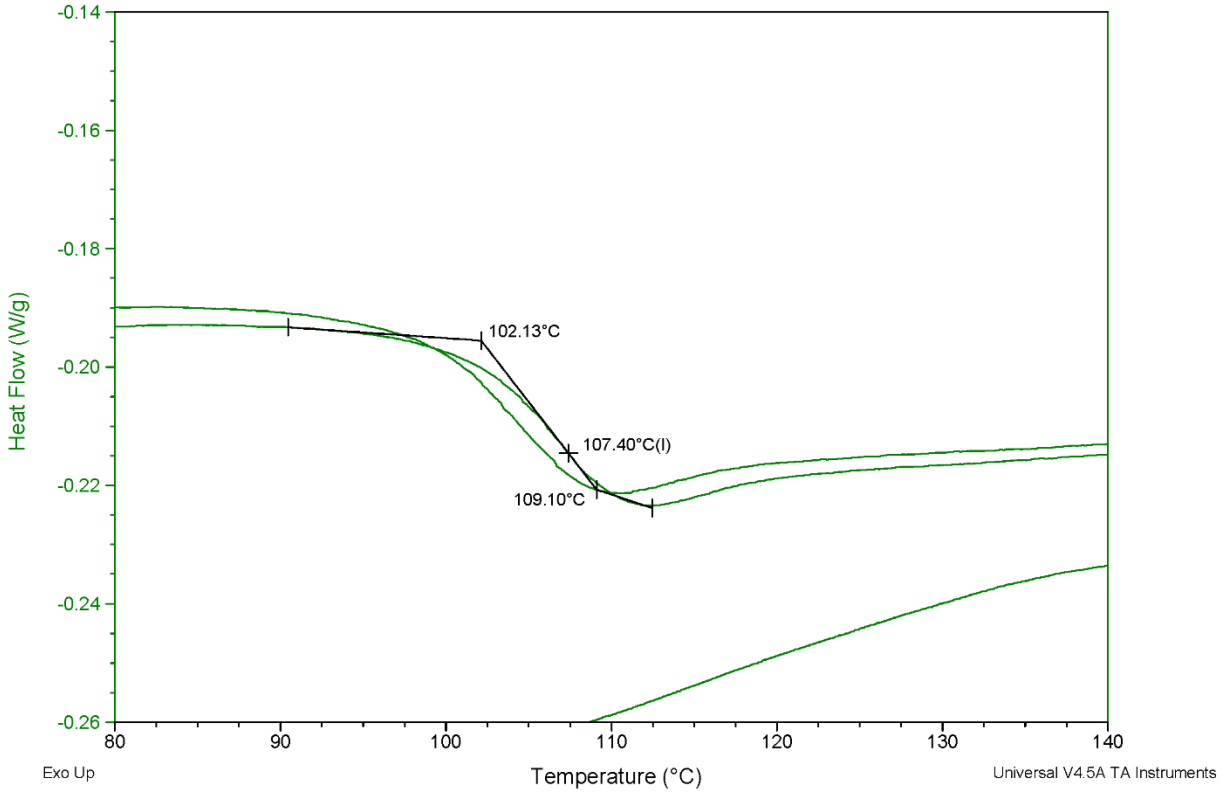

Figure A3.8 DSC profile of [6FDA-2MeAPI(pXy)][Tf_2N]

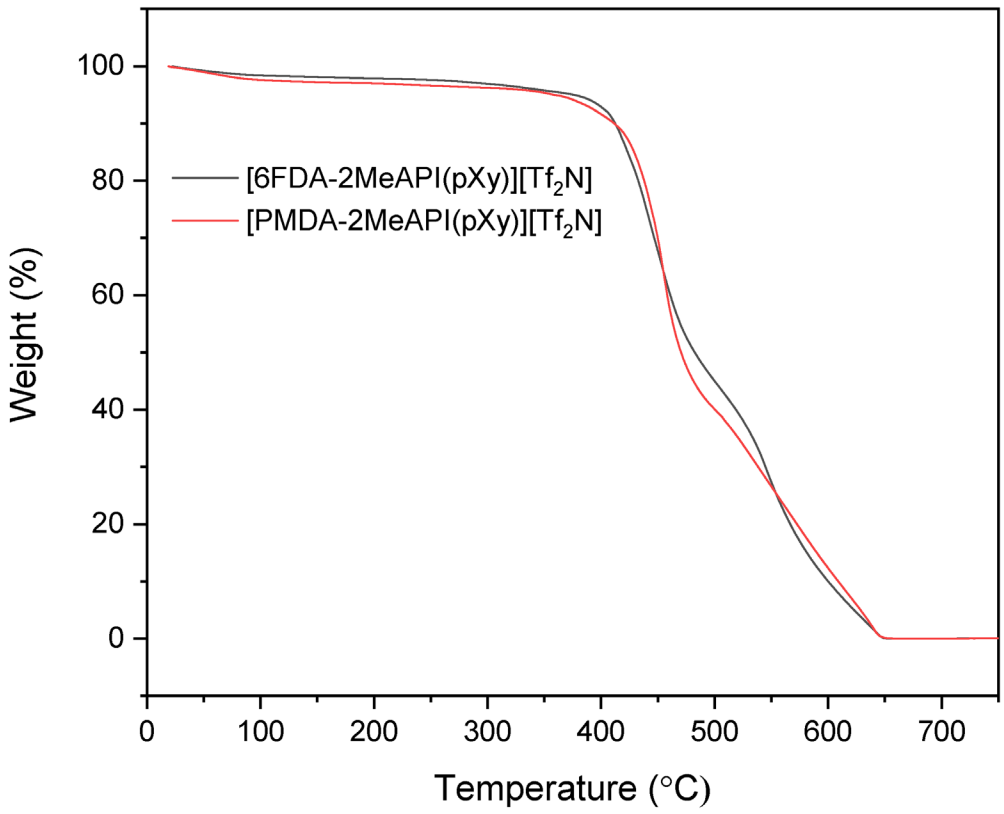

Figure A3.9 TGA plots of both [PMDA-2MeAPI(pXy)][Tf_2N] and [PMDA-2MeAPI(pXy)][Tf_2N]

SEM Images

Figure A3.10 SEM image of [PMDA-2MeAPI(pXy)][Tf_2N] + [C_4mim][Tf_2N] on a Supor ® PES support

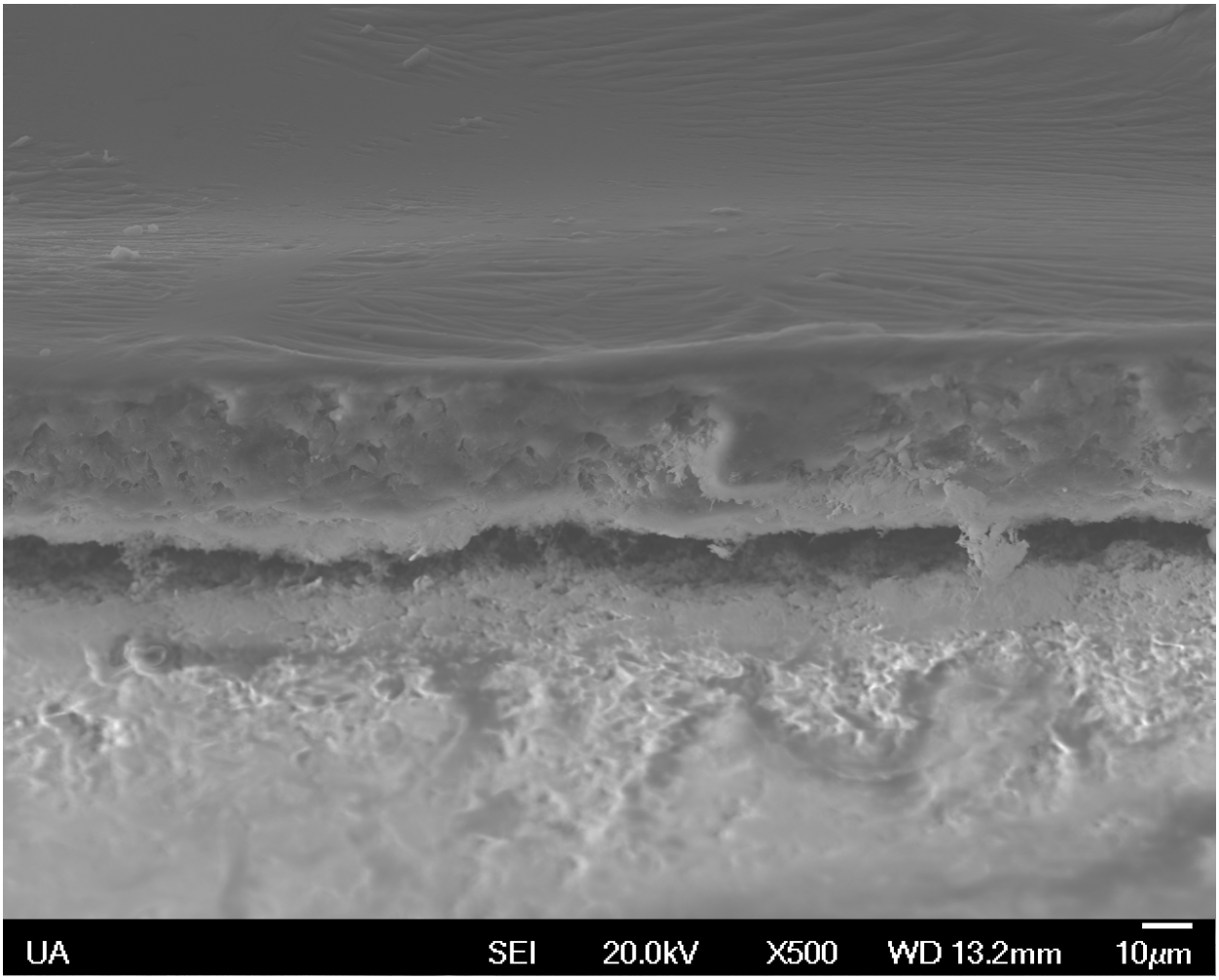

Figure A3.11. SEM image of [6FDA-2MeAPI(pXy)][Tf_2N] + [C_4mim][Tf_2N] on a Supor ® PES support

PMDA-API

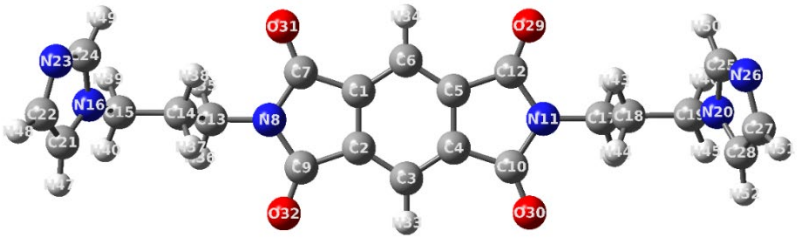

PMDA-2MeAPI

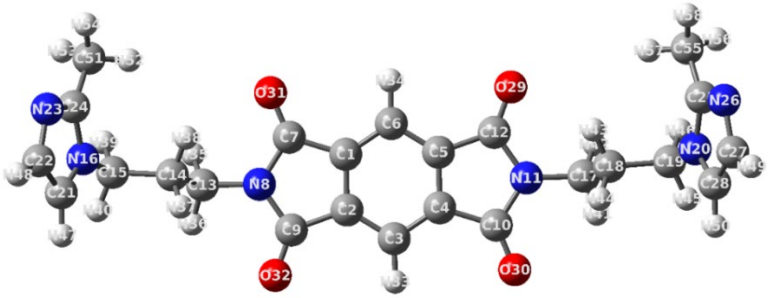

6FDA-API

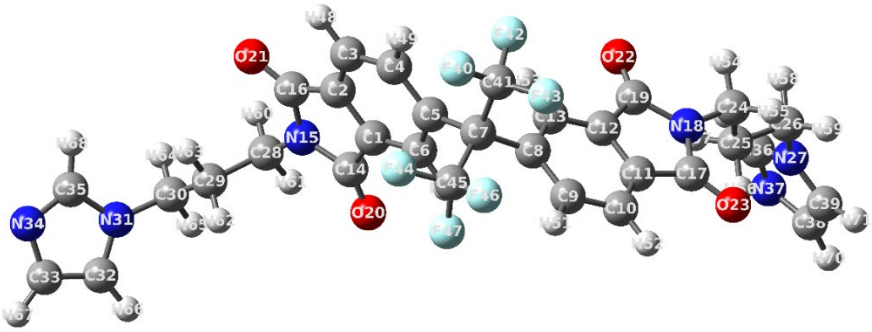

6FDA-2MeAPI

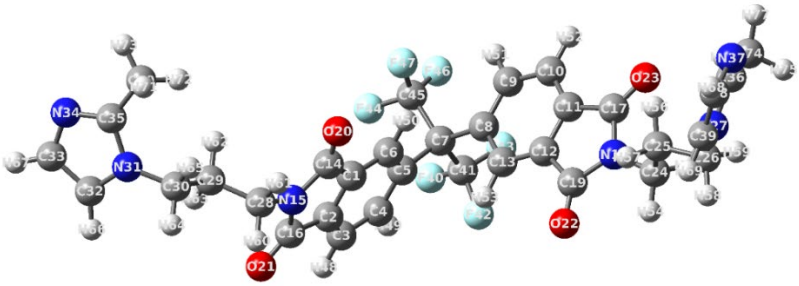

Figure A3.12. Optimized geometries of the studied molecules

Table A3.1 Atomic charges (units of e) calculated by ChelpG and CM5 methods.*

	PMDA-API			PMDA-2MeAPI			6FDA-API			6FDA-2MeAPI		
No.	Atom	ChelpG	CM5	Atom	ChelpG	CM5	Atom	ChelpG	CM5	Atom	ChelpG	CM5
1	C	0.00	0.02	C	-0.05	0.01	C	-0.09	0.00	C	-0.10	0.00
2	C	-0.05	0.02	C	-0.03	0.01	C	-0.06	0.01	C	-0.08	0.00
3	C	-0.02	-0.03	C	-0.03	-0.03	C	-0.08	-0.05	C	-0.07	-0.05
4	C	-0.06	0.02	C	-0.04	0.01	C	-0.07	-0.06	C	-0.08	-0.06
5	C	-0.02	0.02	C	-0.05	0.01	C	0.29	0.01	C	0.34	0.00
6	C	-0.06	-0.03	C	-0.04	-0.03	C	-0.05	-0.06	C	-0.06	-0.06
7	C	0.48	0.28	C	0.52	0.28	C	-0.68	0.00	C	-0.78	0.00
8	N	-0.30	-0.25	N	-0.30	-0.26	C	0.33	0.01	C	0.30	0.00
9	C	0.51	0.28	C	0.49	0.28	C	-0.10	-0.06	C	-0.06	-0.06
10	C	0.52	0.28	C	0.50	0.28	C	-0.05	-0.05	C	-0.10	-0.05
11	N	-0.31	-0.25	N	-0.31	-0.26	C	-0.07	0.01	C	-0.05	0.00
12	C	0.50	0.28	C	0.52	0.28	C	-0.08	0.00	C	-0.12	0.00
13	C	0.13	-0.03	C	0.12	-0.03	C	-0.07	-0.06	C	-0.03	-0.06
14	C	0.06	-0.15	C	0.00	-0.15	C	0.56	0.28	C	0.57	0.27
15	C	-0.22	-0.02	C	-0.16	-0.03	N	-0.39	-0.25	N	-0.39	-0.26
16	N	0.18	-0.23	N	0.06	-0.23	C	0.55	0.28	C	0.57	0.28
17	C	0.12	-0.03	C	0.14	-0.03	C	0.53	0.28	C	0.56	0.28
18	C	0.06	-0.15	C	0.02	-0.15	N	-0.32	-0.25	N	-0.34	-0.26
19	C	-0.21	-0.02	C	-0.18	-0.03	C	0.54	0.28	C	0.56	0.28
20	N	0.18	-0.23	N	0.07	-0.23	O	-0.39	-0.25	O	-0.41	-0.26
21	C	-0.21	0.11	C	-0.18	0.11	O	-0.39	-0.24	O	-0.41	-0.25
22	C	0.36	0.12	C	0.32	0.11	O	-0.39	-0.24	O	-0.40	-0.25
23	N	-0.47	-0.31	N	-0.51	-0.32	O	-0.38	-0.24	O	-0.42	-0.25
24	**C**	**0.28**	**0.23**	**C**	**0.55**	**0.29**	C	0.13	-0.03	C	0.13	-0.03
25	**C**	**0.27**	**0.23**	**C**	**0.55**	**0.29**	C	0.07	-0.15	C	0.01	-0.15
26	N	-0.47	-0.31	N	-0.52	-0.32	C	-0.20	-0.02	C	-0.11	-0.03
27	C	0.36	0.12	C	0.32	0.11	N	0.18	-0.23	N	0.06	-0.23
28	C	-0.20	0.11	C	-0.18	0.11	C	0.20	-0.03	C	0.21	-0.03
29	O	-0.36	-0.23	O	-0.39	-0.25	C	0.10	-0.15	C	0.05	-0.15
30	O	-0.36	-0.23	O	-0.37	-0.23	C	-0.29	-0.02	C	-0.22	-0.03
31	O	-0.36	-0.23	O	-0.39	-0.25	N	0.21	-0.23	N	0.07	-0.23

32	O	-0.36	-0.22	O	-0.37	-0.23	C	-0.23	0.09	C	-0.19	0.10
33	H	0.13	0.15	H	0.13	0.14	C	0.34	0.11	C	0.29	0.11
34	H	0.14	0.15	H	0.13	0.14	N	-0.47	-0.32	N	-0.52	-0.32
35	H	0.07	0.13	H	0.07	0.13	**C**	**0.25**	**0.22**	**C**	**0.55**	**0.29**
36	H	0.06	0.13	H	0.07	0.13	**C**	**0.26**	**0.22**	**C**	**0.56**	**0.29**
37	H	0.03	0.11	H	0.05	0.11	N	-0.48	-0.32	N	-0.52	-0.32
38	H	0.01	0.11	H	0.01	0.10	C	0.35	0.11	C	0.30	0.10
39	H	0.10	0.14	H	0.08	0.13	C	-0.23	0.10	C	-0.20	0.10
40	H	0.15	0.14	H	0.14	0.14	F	-0.14	-0.09	F	-0.14	-0.09
41	H	0.07	0.13	H	0.06	0.13	C	0.63	0.34	C	0.63	0.34
42	H	0.08	0.13	H	0.07	0.13	F	-0.17	-0.10	F	-0.17	-0.10
43	H	0.01	0.11	H	0.00	0.10	F	-0.17	-0.10	F	-0.16	-0.10
44	H	0.03	0.11	H	0.05	0.11	F	-0.16	-0.10	F	-0.17	-0.10
45	H	0.15	0.14	H	0.15	0.14	C	0.60	0.34	C	0.61	0.34
46	H	0.10	0.14	H	0.09	0.13	F	-0.13	-0.09	F	-0.13	-0.09
47	H	0.21	0.17	H	0.21	0.17	F	-0.17	-0.10	F	-0.17	-0.10
48	H	0.10	0.17	H	0.11	0.16	H	0.14	0.14	H	0.14	0.14
49	H	0.15	0.17	H	0.11	0.16	H	0.14	0.12	H	0.14	0.12
50	H	0.15	0.17	H	0.21	0.17	H	0.06	0.12	H	0.07	0.12
51	H	0.10	0.17	C	-0.39	-0.19	H	0.15	0.12	H	0.14	0.12
52	H	0.21	0.17	H	0.16	0.12	H	0.14	0.14	H	0.14	0.13
53				H	0.17	0.14	H	0.08	0.12	H	0.07	0.12
54				H	0.17	0.14	H	0.07	0.13	H	0.06	0.13
55				C	-0.40	-0.19	H	0.06	0.13	H	0.07	0.12
56				H	0.17	0.14	H	0.03	0.11	H	0.00	0.10
57				H	0.16	0.12	H	0.00	0.11	H	0.04	0.11
58				H	0.17	0.14	H	0.09	0.13	H	0.13	0.13
59							H	0.14	0.14	H	0.06	0.13
60							H	0.05	0.13	H	0.03	0.13
61							H	0.03	0.13	H	0.04	0.13
62							H	0.02	0.11	H	0.01	0.10
63							H	0.00	0.11	H	0.04	0.11
64							H	0.11	0.13	H	0.15	0.13
65							H	0.16	0.13	H	0.09	0.13

66					H	0.21	0.16
67					H	0.11	0.16
68					H	0.11	0.16
69					H	0.21	0.16
70					C	-0.42	-0.20
71					H	0.17	0.13
72					H	0.16	0.12
73					H	0.17	0.14
74					C	-0.42	-0.20
75					H	0.16	0.13
76					H	0.17	0.12
77					H	0.17	0.14

*The C atoms shown in bold are the C(2) sites, which are linked with the substituted -H atoms or -CH_3 atoms.

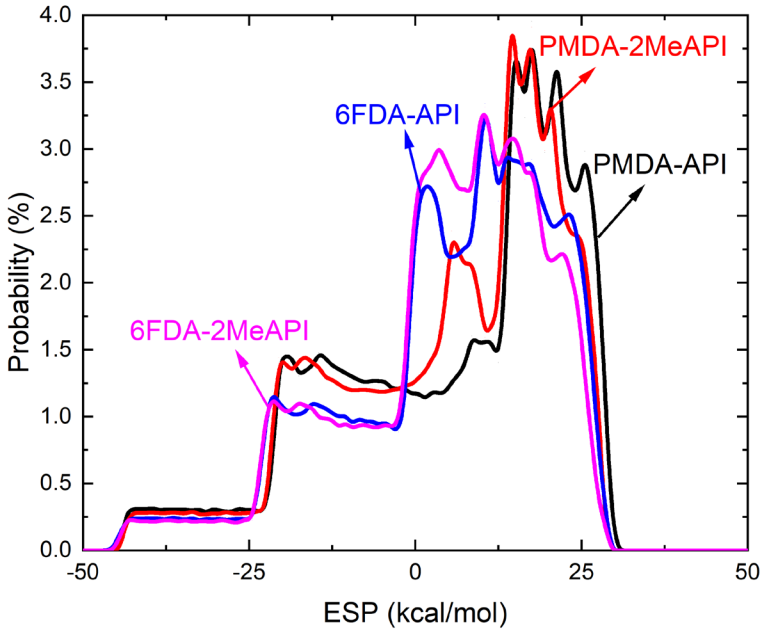

Figure A3.13 Electrostatic potential distribution (units of kcal/mol) of studied molecules.

Table A3.2 General interaction properties function (GIPF) descriptors of studied molecules.

	SA	V_{ion}	$\bar{V}$	V_{min}	V_{max}	Π	σ_{tot}^2
	Å^2	Å^3	kcal/mol				(kcal/mol)^2
PMDA-API	459	497	5.6	-15.3	16.8	15.0	166
PMDA-2MeAPI	494	542	4.8	-15.1	15.0	13.8	161
6FDA-API	601	684	4.9	-15.2	13.4	12.6	177
6FDA-2MeAPI	635	729	4.4	-14.8	12.4	11.9	171

First frame	Last frame
PMDA-API	
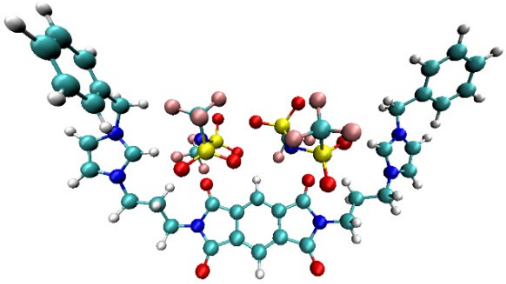	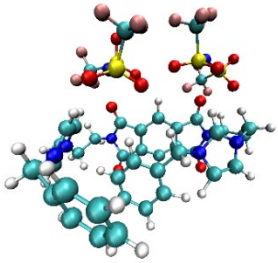
PMDA-2MeAPI	
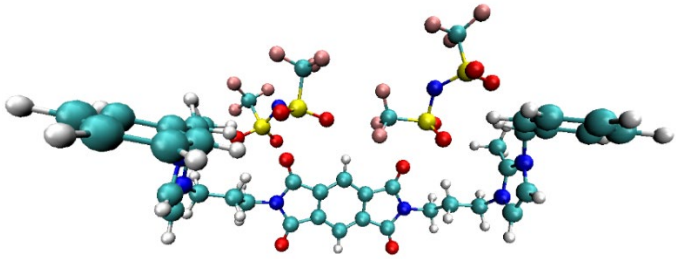	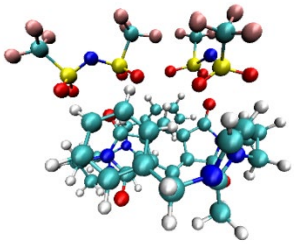
6FDA-API	
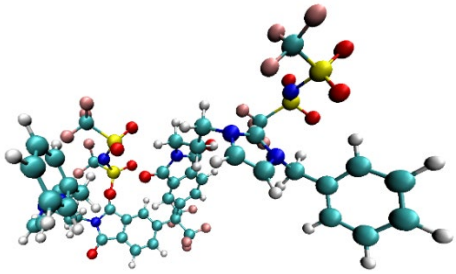	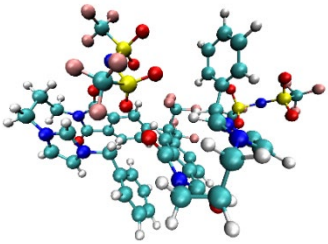
6FDA-2MeAPI	
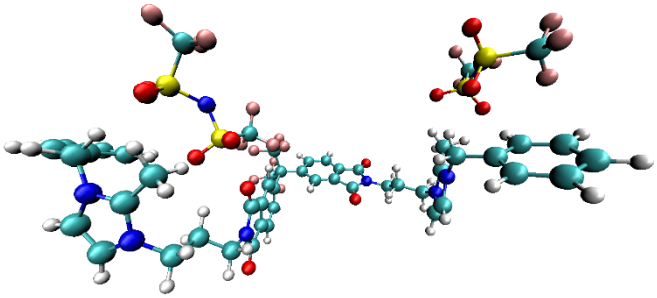	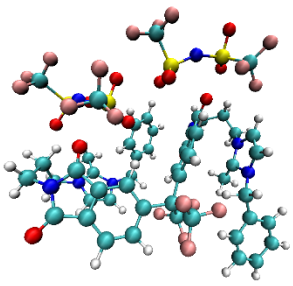

Figure A3.14 Representative snapshots of the studied monomers during MD simulations

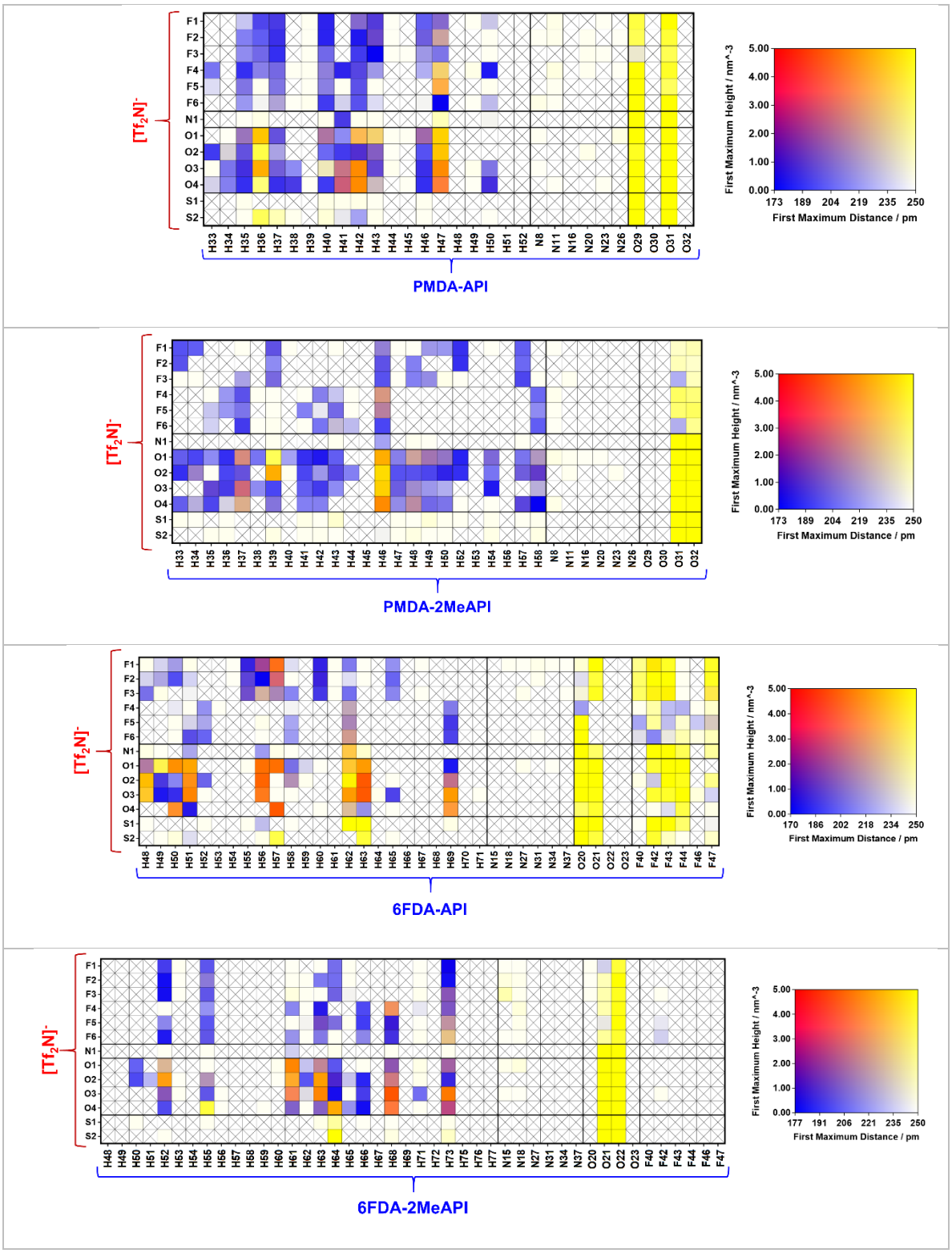

Figure A3.15 Connection matrices (CMats) for all non-carbon atoms within the monomers, taken from the MD simulations. The color in each square represents both the peak height and the distance to the first maximum in the corresponding RDF (for color scale, see the right-hand side). The individual grids are labeled according to the assignments shown in Figure A3.1.

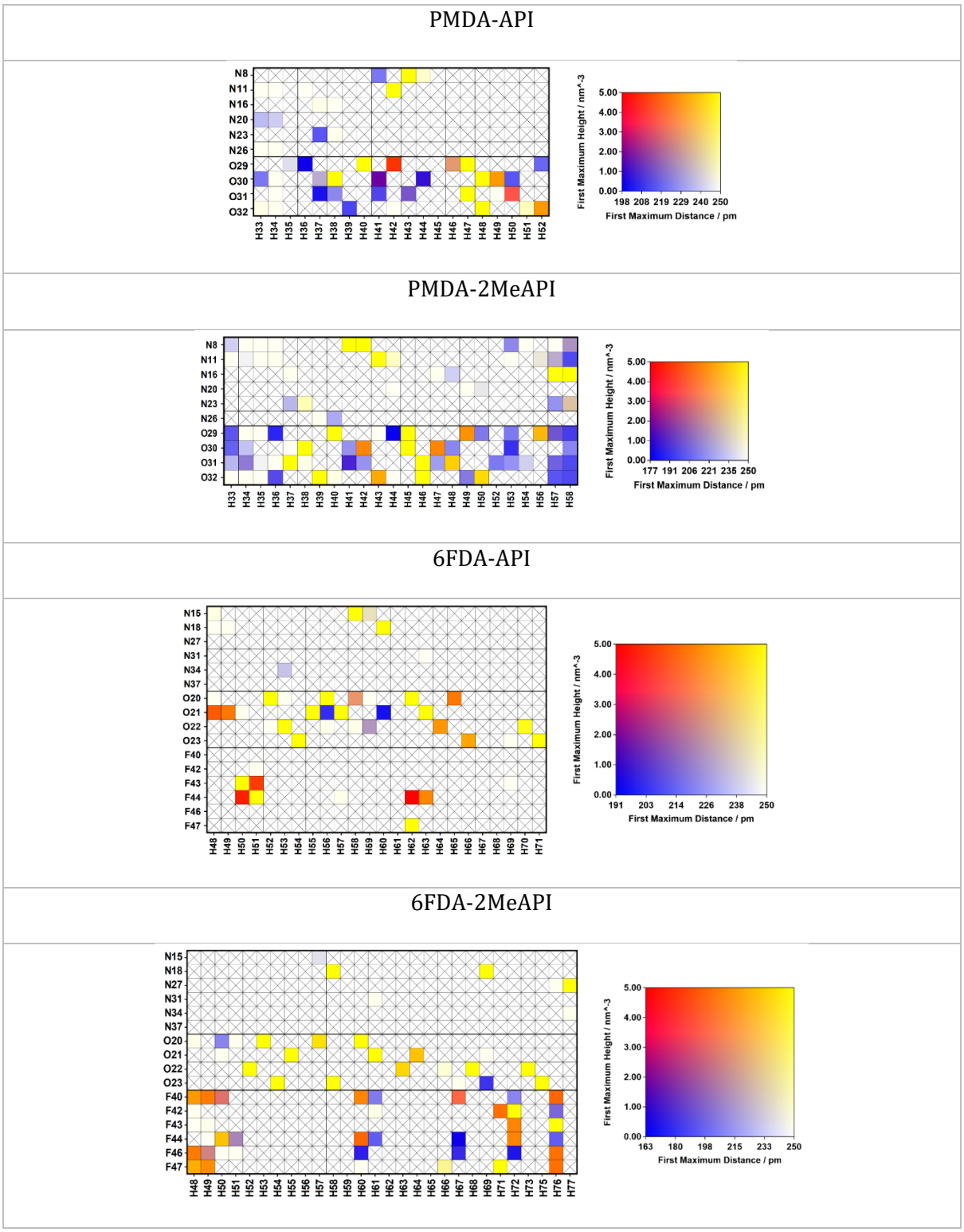

Figure A3.16 Intramolecular connection matrices (CMats) for all non-carbon atoms within the positively charged monomers, taken from the MD simulations. Rows represent hydrogen bond acceptors, and columns correspond to hydrogen bond donors. The color in each square represents both the peak height and the distance to the first maximum in the corresponding RDF (for color scale, see the right-hand side). The individual grids are labeled according to the assignments shown in Figure A3.1

Robeson Plots

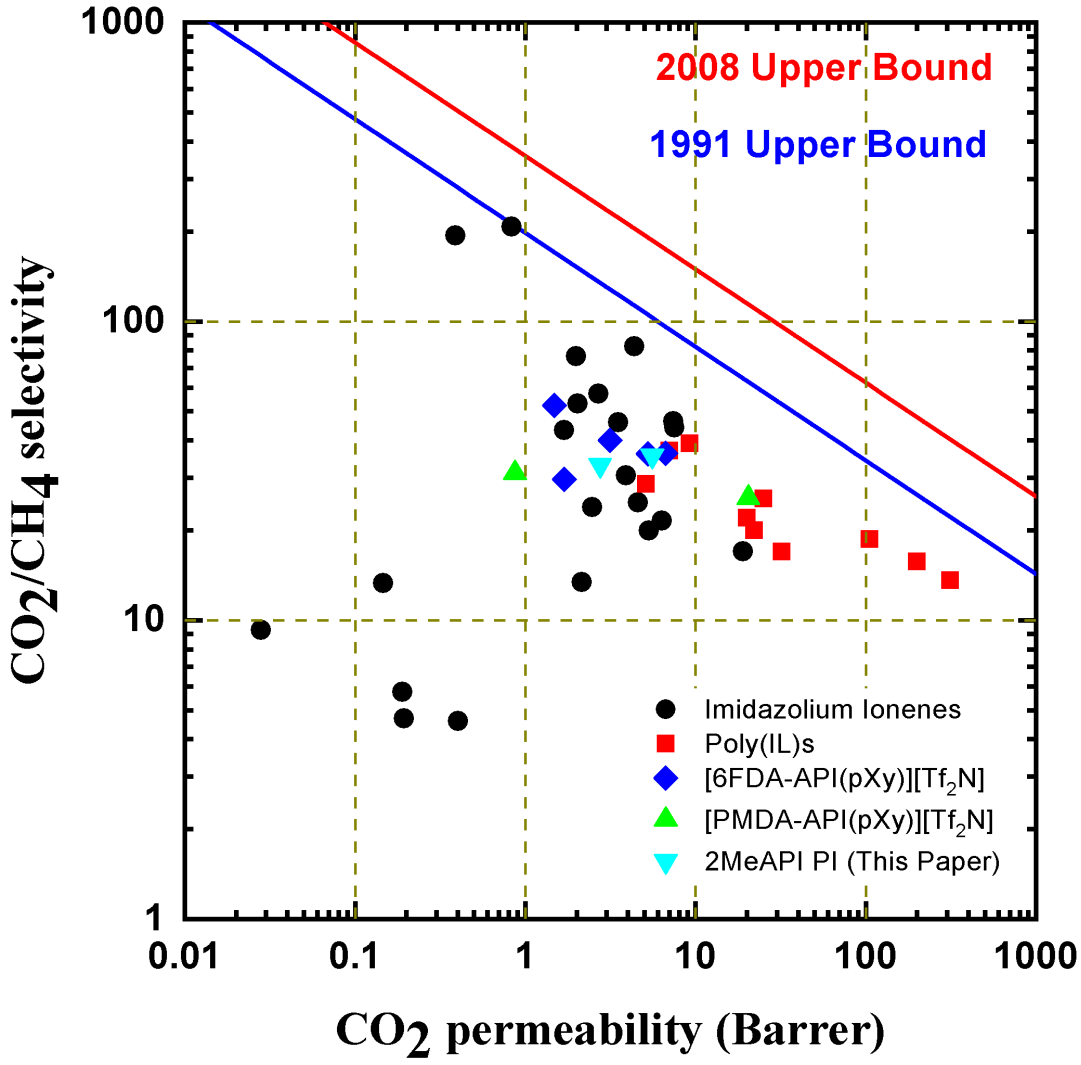

Figure A3.17 CO_2/CH_4 Robeson Plot of [6FDA-2MeAPI(pXy)][Tf_2N] + [C_4mim][Tf_2N] and [6FDA-2MeAPI(pXy)][Tf_2N] + [C_4mim][Tf_2N] along with other ionic materials.

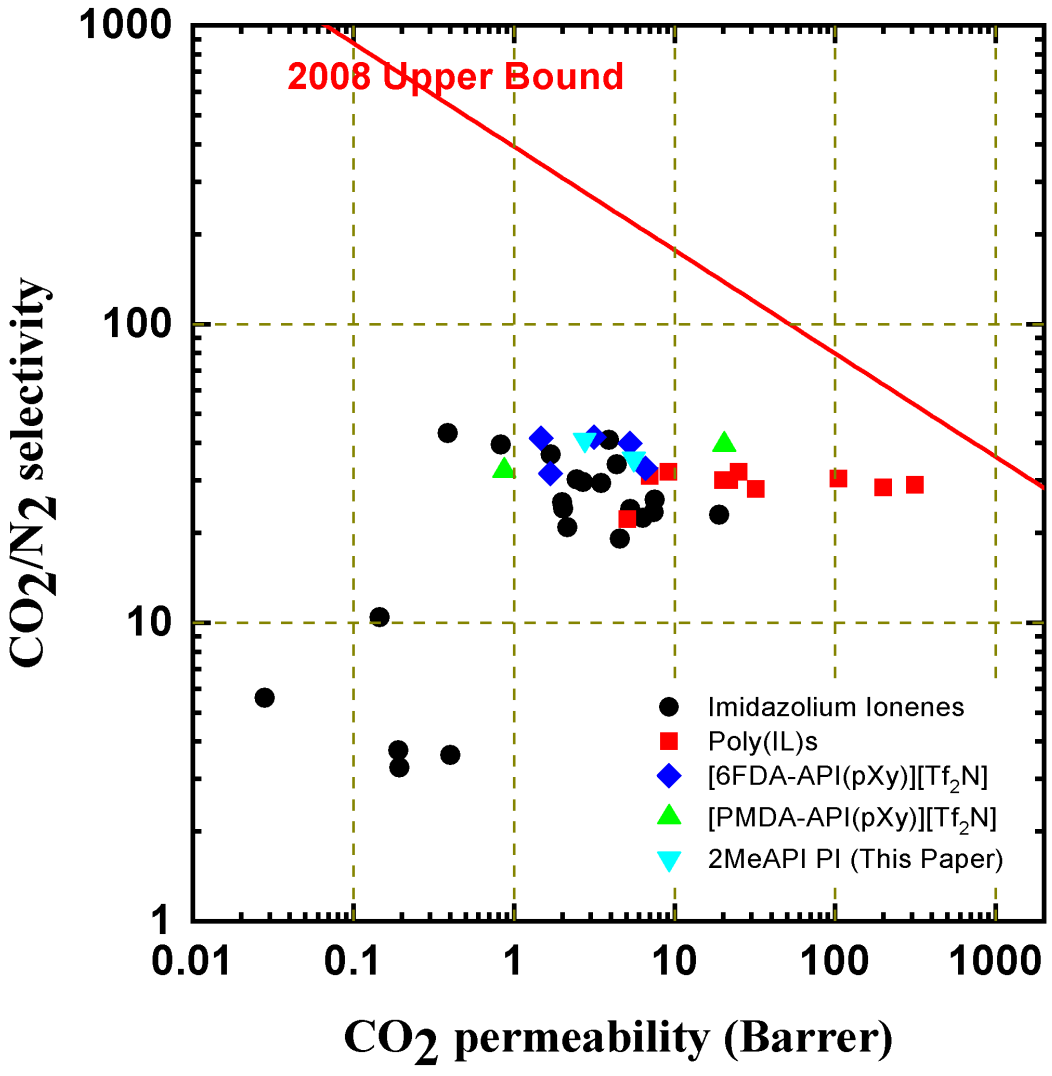

Figure A3.18 CO_2/N_2 Robeson Plot of [6FDA-2MeAPI(pXy)][Tf_2N] + [C_4mim][Tf_2N] and [6FDA-2MeAPI(pXy)][Tf_2N] + [C_4mim][Tf_2N] along with other ionic materials.

CHAPTER 4

EFFECTS OF PROCESSING ON PMDA-BASED IONENES AND IONIC LIQUID COMPOSITES

4.1 Abstract

The processing effects, whether the polymer is solvent-cast or melt-pressed, have major effects on the final state of the polymer's chain-chain interactions. The processing methods of ionic polymers has yet to be determined which can lead to forming thinner films and increasing gas permeabilities and coordination. Two new ionic polymers with varying regiochemistry formed using a previously made PMDA-API monomers are polymerized going through the *meta*- and *ortho*- xylyl connectivities. The resulting polymers formed are ionic and have bistriflimide as the anionic component. Herein, these polymers are denoted as [PMDA-API(pXy)][Tf_2N], [PMDA-API(mXy)][Tf_2N], and [PMDA-API(oXy)][Tf_2N]. The processing effects of these polymers demonstrated using x-ray diffractometry demonstrating that the *para*- linkage has an ordered structure when solvent cast. Due to its localized coordinated nature, [PMDA-API(pXy)][Tf_2N] is selected to form composites with various ILs to determine the effects on ordering. [PMDA-API(pXy)][Tf_2N] and its composites are tested as gas separation membranes.

Keywords: 6FDA-Ionenes, Ionic Liquid Composites, Gas Separation Membranes

4.2 Introduction

Ionic liquid (IL)-based membranes have recently received more interest due to their negligible vapor pressures and high CO_2 solubilities which lends to their ability to have extremely high CO_2 permeabilities (>1000 barrer) which allows them to have CO_2/CH_4 and CO_2/N_2 selectivity.[1] This ability allows ILs to be used in CO_2-based separation systems especially in natural gas processing and post-combustion separations. Imidazolium-based ionic materials have garnered even more interest since their formation by Wilkes and co-workers in 1992.[2] These materials are based upon the Menshutkin reaction that allows for the formation of quaternary, cationic amines through the reaction of a tertiary amine and an alkyl halide. Imidazolium has gained interest due to the hydrogen bond effects of the -CH groups as well as the resonance structures that are present and the C(2) position sharing the cationic charge upon the formation of a quaternary amine.[3, 4] Imidazolium ionic liquids have low melting points and are typically liquids at room temperature yet are completely ionic without any solvating groups.

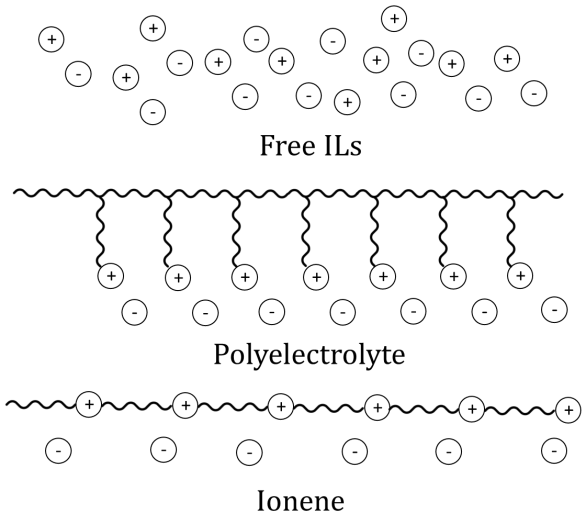

Figure 4.1 Graphical representation of ionic based materials used in membrane separations

The first membranes that featured imidazolium ILs were supported ionic liquid membranes (SILMs) where "free" ILs were within a supported polymer matrix (Figure 4.1). SILMs formed the basis for membrane separations with ionic materials. Ionic liquids are polymerized and soaked into different materials such as PVDF[5, 6], PES[7-10], PMMA[11-13], and other such porous materials[14, 15] via capillary forces or impregnation within the materials. Although materials tested as SILMs had very high permeability values, dependent on the porous support, their pressure differential between feed and permeate typically needs to be kept relatively low, or the IL would be displaced due to the weak capillary forces holding the ILs within the porous structure.[6, 7, 9, 10] Their mechanical stability and thick membrane formation are unable to withstand the industrial limits for real-world application. Addition of polymerizable groups (vinyl and styrene) within ILs allow for formation of polymers with imidazolium units pendant to the main polymer chain allowing thin and mechanically stable membranes.[16-20] These materials are called poly(ionic liquids) (PILs) and known as polyelectrolytes within the ionic polymer field (Figure 4.1).

PILs are formed from a radical addition polymerization reaction initiated via a thermal or photo initiator. They have shown to also be good gas separation membranes having higher CO_2 permeabilities yet can resist higher pressures (>2 bar). When comparing PILs and SILMs the very large reduction in permeability occurs due to the immobilized cation-anion that cannot interact as freely. This reduction is obviously disadvantageous to the viability of PILs, so in multiple instances, Bara, et al. added "free" ILs into the polymerizable ILs which greatly affected the permeability of the material (Figure 4.2).[17, 21, 22] In one instance upon loading free ILs into polymerizable ionic liquids, the CO_2

permeabilities of the composite materials increased by 400% while maintaining CO_2/N_2 and CO_2/CH_4 permselectivities.[17]

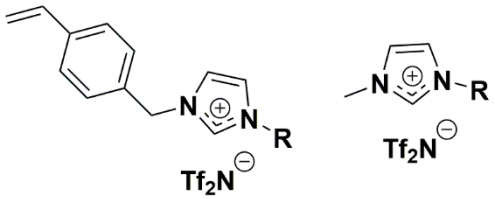

Figure 4.2 Styrene functionalized polymerizable ionic liquids and their free IL substituents

Yet issues still exist with industrial applications of PILs due to their thermal stabilities and membrane supports that are typically necessary for film formation. Carlisle, et al. later showed that imidazolium units can be polymerized in a polymer backbone (Figure 4.3) forming materials called ionenes (Figure 4.1).[23] Ionene demonstrated film forming abilities as a neat materials as well as forming composite materials with ILs. The IL composites had a significant increase in their CO_2 permeabilities due to IL's nature to have high CO_2 solubilities. The future of ionic materials lies in the ionic moiety's ability to be polymerized within other materials whether it is as a free, pendant, or backbone group. One feature that has been demonstrated is the incorporation of ionic moieties into polymer backbones featuring high free fractional volume components which highly influences their thermal properties and mechanical strengths.

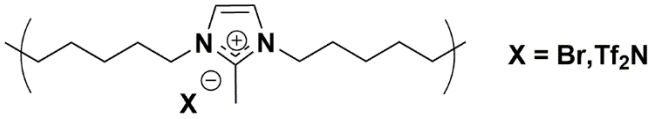

Figure 4.3 Ionene polymerized by Carlisle, et al. featuring either bromide or bistriflimide anions

To the best of our knowledge, ionic moieties were polymerized within a polyimide backbone by Li, et al. in 2010.[24] Although the block copolyimide featured decreasing CO_2 permeabilities, their CO_2/CH_4 and CO_2/N_2 selectivities increased. In 2013, Li demonstrated a random copolymer (Figure 4.4) which featured the similar units to the previous paper.[25] The increase in ionic moieties within the polymer backbone slightly increased permselectivity values while decreasing the permeability values, yet formation of highly ionic high-performance materials was yet to be introduced. The Bara group has furthered the field of high-performance ionic materials by formulating a polymerization method to create such ionic polyimides with high molecular weight in 2017. The PMDA-based ionene absorbed free IL which increased the CO_2 permeabilities by over 2000%.[26] Multiple ionic-based membranes have been formed since which include polyamide[27], Tröger's Base[28], and more aromatic[29, 30] functionalities within these high-performance polymers. These materials have been shown to create composites with ILs which have increased their permeabilities.

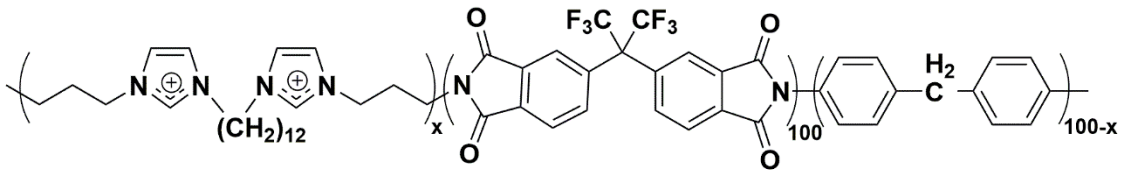

Figure 4.4 Random ionic copolyimide polymerized in Li, et al. paper.

Herein, two new constitutional isomers of [PMDA-API(Xy)][Tf_2N] polymer were polymerized through the *meta*- and *ortho*- xylyl connectivities. Along with their polymerization, the structuring of the polymer is demonstrated using XRD. Even though the polymerization and gas permeation properties of these PMDA-based polymers have been previously reported, the use of different ILs and processing methods are demonstrated. We

also report the effect of solvent casting as the best processing methods which greatly affects the overall structuring of [PMDA-API(pXy)][Tf_2N] as well as incorporating different ionic liquids ([Bnmim][Tf_2N] and [PEGmim][Tf_2N] (Figure 4.5)) into the polymer matrix to determine their effects on the structuring and gas separation of these ionic PIs.

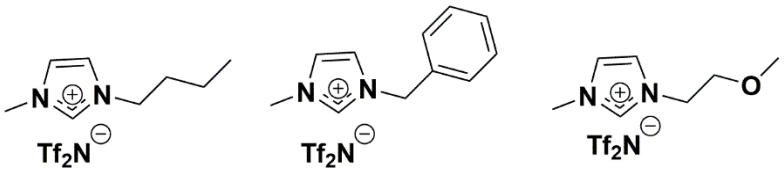

Figure 4.5 Ionic liquid used to form composite membranes with [PMDA-API(pXy)][Tf_2N]

The changing regiochemistry of these polymers is examined through x-ray diffraction, differential scanning calorimetry, and thermal gravimetric analysis, yet similar to the 6FDA-based ionenes previously reported, the film forming ability is hindered due to changing the xylyl linkage (*meta*- and *ortho*-).[31]

4.3 Materials and Methods

4.3.1 Materials

PMDA (>99%) was purchased from Akron Polymer Systems. 1,4-bis(chloromethyl)benzene (pDCXy, >98%), 1,4-bis(chloromethyl)benzene (mDCXy, >96%), 1,2-bis(chloromethyl)benzene (oDCXy, >97%), and 1-(3-aminopropyl)imidazole (API) were purchased from TCI. Lithium bis-trifluoromethanesulfonimide ($LiTf_2N$) was purchased from 3M. N-methylpyrrolidone (NMP, ACS grade), tetrahydrofuran (THF, ACS grade), diethyl ether (Et_2O, ACS grade), N,N-dimethylformamide (DMF, anhydrous) were purchased from VWR. All materials were used as obtained, without further purification.

4.3.2 Synthesis of 2,6-bis(3-(1H-imidazol-1-yl)propyl)pyrrolo[3,4-f]isoindole-1,3,5,7(2H,6H)-tetraone (PMDA-API)

The synthesis of "PMDA-API" has been introduced in our previous work,[26] formed from the condensation of PMDA (1 eq.) and API (2.05 eq.) in NMP. The product was precipitated in water, purified, and dried as outlined in literature. ^{1}H NMR was consistent with published values.

4.3.3 Synthesis of PMDA Ionenes

PMDA API was subsequently polymerized with an equimolar equivalent of pDCXy, mDCXy, and oDCXy to form a xylyl linkage via the Menshutkin reaction. Following ion exchange from the Cl^- to the $[Tf_2N]^-$ salt, the polyimide ionenes were cleaned to remove any oligomeric content.

4.3.3.1 Synthesis of [PMDA-API(pXy)][Tf_2N]

PMDA-API (10.0 g, 23.1 mmol) and pDCXy (4.05 g, 23.1mmol) were added with 80 mL of NMP to a 250 mL round-bottom heavy-walled pressure vessel (Ace Glass) sealed with a threaded PTFE cap with a DuPont Kalrez® O-Ring. The reaction was heated to 150 °C for 24 h. The solvent was decanted, and gel precipitate was dissolved in DI H_2O. This polymer solution was solubilized as the Cl^- salt, and subsequently poured into DI H_2O containing $LiTf_2N$ (2.5 eq., 16.6 g) to promote exchange of the anion. The [PMDA-API(pXy)][Tf_2N] ionene was stirred for 24 h at RT. The product was then filtered and dried in a vacuum oven at 120 °C overnight.

To remove low molecular weight content, 100 mL of THF was added to [PMDA-API(pXy)][Tf_2N] and stirred at RT for 4 hrs. The purified polymer separates as a brown gel, and the THF layer containing solvent and oligomeric compounds was decanted. Finally, the

polymer was reprecipitated in Et_2O and filtered. Again, the ionene product was dried to yield a light tan powder (21.83 g, 86%).

4.3.3.2 Synthesis of [PMDA-API(mXy)][Tf_2N]

The *meta*- derivative follows the same synthetic procedure as above, utilizing PMDA-API (10.0 g, 23.1 mmol) and mDCXY (4.05 g, 23.1 mmol). The [PMDA-API(mXy)][Tf_2N] was cleaned via a similar procedure and dried, yielding the product as an off-white powder (20.53 g, 81%).

4.3.3.3 Synthesis of [PMDA-API(oXy)][Tf_2N]

The *ortho*- derivative follows the same synthetic procedure as above, utilizing PMDA-API (10.0 g, 23.1 mmol) and oDCXy (4.05 g, 23.1 mmol). The [PMDA-API(oXy)][Tf_2N] was cleaned via a similar procedure and dried, yielding the product as an off-white powder (17.25 g, 68%).

4.3.4 Membrane Preparation

Membrane composites were formed using 1 g of [PMDA-API(pXy)][Tf_2N] with 10 mL of acetone as a casting solution. One molar equivalent of IL was added per backbone unit of polymer to be consistent with previous works on amounts of IL this polymer absorbs. Three different ILs ([C_4mim][Tf_2N], [Bnmim][Tf_2N], and [PEGmim][Tf_2N]) were used to make composites membranes with [PMDA-API(pXy)][Tf_2N]. These casting solutions were poured onto glass disk that have Rain-X ® applied to the casting surface, which allowed for easy delamination from the glass plate.

4.3.5 Material Characterization

^{1}H-NMR was performed on [PMDA-API(mXy)][Tf_2N] and [PMDA-API(oXy)][Tf_2N] using a Bruker Avance (360 MHz or 500 MHz). Both ^{1}H-NMR spectra are presented in Figure A4.1-A4.2.

Matrix assisted laser deionization/ionization-time of flight (MALDI-TOF) mass spectrometry was performed using a Bruker Ultraflex on both polymers to determine the number-average molecular weight (M_N).

FTIR spectra were taken to ensure the exchange of the Cl^- anion to the $[Tf_2N]^-$ anion as well as the imide formation. The spectra of the IL composite membranes were also included to show the increase in the sulfonimide bands which correspond to the addition of IL. All spectra were normalized at the carbonyl peak (C=O stretching vibrations at ~1720 cm^{-1}).

Wide-angle x-ray diffraction (WAXD) was carried out using a Bruker D8 Discover with GADDS using a cobalt source (K_α = 1.79 Å) with a point collimator. The detector was a Vantec 500 area detector. The domain spacing (d-spacing) was determined for each material along with [PMDA-API(pXy)][Tf_2N] + IL composite counterparts. The d-spacing was calculated using Bragg's law:

$$d = \frac{\lambda}{2 * sin\theta}$$

The 2θ range for WAXD was 5 to 55 °.

Thicknesses of the materials were determined using a Mitutoyo micrometer (model 3). Membranes were measured at 5 different spots and an average of the measurements were taken. The thickness of the film was also observed using SEM to ensure the accuracy of the micrometer. SEM images of the films are in the Appendix (Figure A4.3-A4.6).

4.3.6 Gas Separation Units

The gas separation units had been outlined within multiple other papers. These units were used as they had been prepared in prior research. These units are high vacuum time lag units that have a large gas reservoir to ensure the feed volume was always higher than the permeate. Through a solution diffusion model, the steady state permeation was used to determine the permeability of the materials. These values were then used to determine the diffusivity and solubility.

4.4 Results and Discussion

4.4.1 [PMDA-API(pXy)][Tf_2N] + IL Composite Membranes

Composite materials formed from solution casting were highly flexible and plasticized compared to the neat [PMDA-API(pXy)][Tf_2N] (Figure 4.6). The neat [PMDA-API(pXy)][Tf_2N] was soaking in IL to determine the effects of soaking on the solvent cast material. The neat [PMDA-API(pXy)][Tf_2N] absorbed [C_4mim][Tf_2N] similar to the last trial, but the material absorbed more [C_4mim][Tf_2N] up to 1.3:1 polymer:IL molar ratio. Previous renditions of soaking film caused the [PMDA-API(pXy)][Tf_2N] to break apart and tear indicating [C_4mim][Tf_2N] was disrupting the polymer matrix. Along with these values, the wt % of IL in [PMDA-API(pXy)][Tf_2N] is also displayed in the Table 4.1.

Table 4.1 Molar ratio of Polymer:IL and Weight % of IL added to the polymer

	[PMDA-API(pXy)][Tf_2N]		
	[C_4mim][Tf_2N]	**[PEGmim][Tf_2N]**	**[Bnmim][Tf_2N]**
Molar ratio	1:1	1:1	1:1
Wt % IL	0.383	0.384	0.414

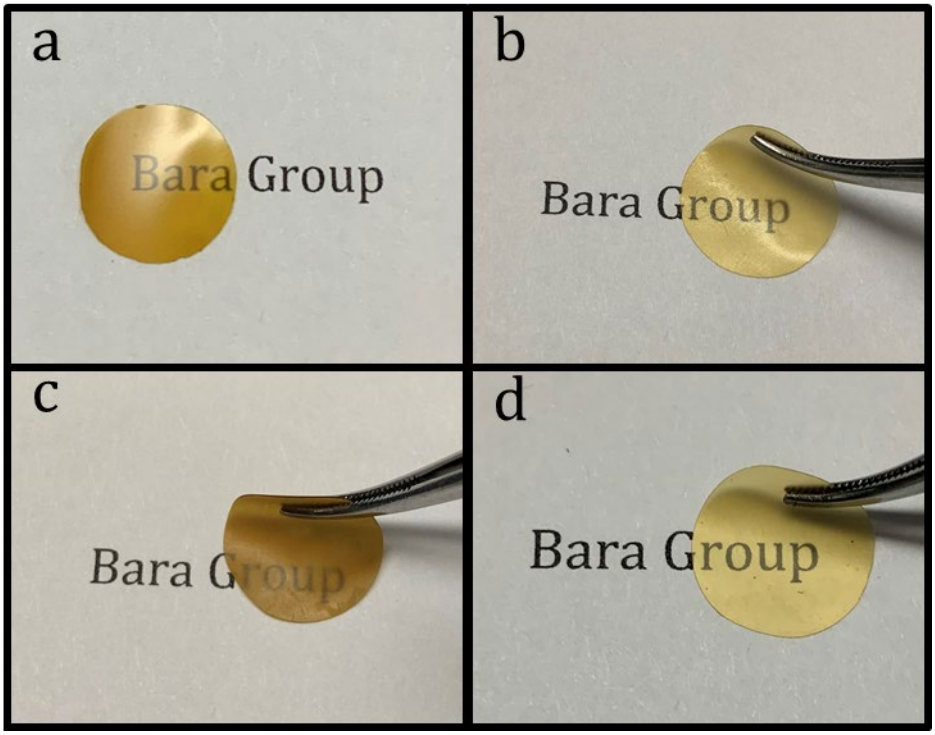

Figure 4.6 Thin film forming ability of (a) [PMDA-API(pXy)][Tf_2N], (b) [PMDA-API(pXy)][Tf_2N] + [C_4mim][Tf_2N], (c) [PMDA-API(pXy)][Tf_2N] + [Bnmim][Tf_2N], and (d) [PMDA-API(pXy)][Tf_2N] + [PEGmim][Tf_2N]

4.4.2 Material Characterization

The MALDI-TOF MS spectra for [PMDA-API(mXy)][Tf_2N], and [PMDA-API(oXy)][Tf_2N] are displayed in Figure A2.5-A6. [PMDA-API(pXy)][Tf_2N], [PMDA-API(mXy)][Tf_2N], and [PMDA-API(oXy)][Tf_2N] were shown to form high molecular weight polymers, yet even with the high molecular weight the film forming abilities of the *meta-* and *ortho-* were hindered likely due to the large amount of ring strain placed on the polymer whereas the *para-* linkage allowed for a higher degree of chain aggregation.

FT-IR measurements were performed to evaluate functional groups while also verifying the addition of IL to the polymer matrix. The spectra are provided in Figure A4.6. FT-IR spectra were normalized to the carbonyl stretching (C=O) peak at 1720 cm^{-1}. The

formation of the imide ring and imidazolium can be found in the C-N-C out of plane bending and stretching at 721 cm^{-1} and 1100 cm^{-1}, respectively. The sulfonyl (S=O) stretching within a sulfonimide of the Tf_2N anion at peaks 1370-1335 cm^{-1} and the S-N-S stretching at 760 cm^{-1} indicate anion metathesis. The increase of the S=O and S-N-S were denoted in the composite membranes to demonstrate the incorporation IL.

XRD profiles of neat and composite materials are shown in Figures 4.7-4.9. The neat materials contained the typical polymer halo ranging between 2θ = 10-30 ˚. The neat materials had XRD profiles that corresponded to previously reported materials that contain *para-*, *meta-*, and *ortho-* regiochemistry where both the *meta-* and *ortho-* had very similar halos with larger ranges than the *para-*. The broader halo was due to the packing of the polymer chains; as the position within the xylyl linkages got closer together, the peak became broader leading to a broader range of domain spacings. [PMDA-API(pXy)][Tf_2N] had a distinct crystalline peak at 2θ = 20.3 ˚ which corresponded to a d-spacing value of 5.07 Å. This local ordered region was indicative of coordination between polymer which was likely the chain-chain interactions coordinating and stacking in sheets.

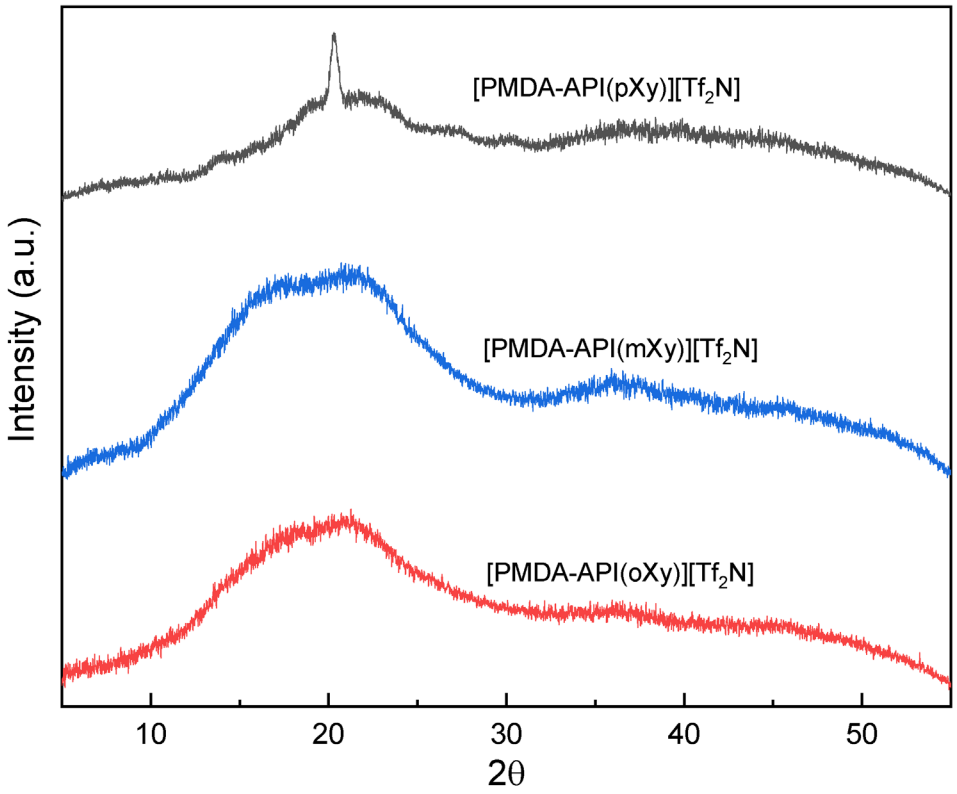

Figure 4.7 XRD profiles of [PMDA-API(pXy)][Tf_2N], [PMDA-API(mXy)][Tf_2N], and [PMDA-API(oXy)][Tf_2N]

Formation of IL-composite membranes did not demonstrate any significant changes in the XRD profiles (Figure 4.8). The predominant peak within the [PMDA-API(pXy)][Tf_2N] profile did not change within the XRD profiles which was an indication that the PMDA was unaffected by the addition of any IL into the polymer matrix. Contrary to our previous conceptions about the organization effects of ILs within PMDA-API structure, this XRD presented that [PMDA-API(pXy)][Tf_2N] organized into a highly ordered structure which was not caused by the introduction of IL. The main reason for the material's ordering likely was due to the solvating effects of IL with ionic polymers. In previous scenarios, [PMDA-API(pXy)][Tf_2N] was melt-pressed into a membrane, so the polymer chains did not have the ability to organize into their best conformation and lowest energy state, resulting in a

more amorphous polymer halo. Soaking the [PMDA-API(pXy)][Tf_2N] in [C_4mim][Tf_2N] allowed for the polymer to structure itself as it absorbs a solvent which helped plasticize the membrane as the neat material was brittle while the soaked and mixed composites were highly flexible. It should be noted that upon soaking different ionenes in [C_4mim][Tf_2N], the materials would completely dissolve. The dissolution is likely due to the excess [Tf_2N] anions that were present can start to interact with the polymer matrix solvating the polymer chain as they started to interact with more [C_4mim][Tf_2N]. Obviously, more investigation is necessary to determine the exact effects of excess IL on polymer structure.

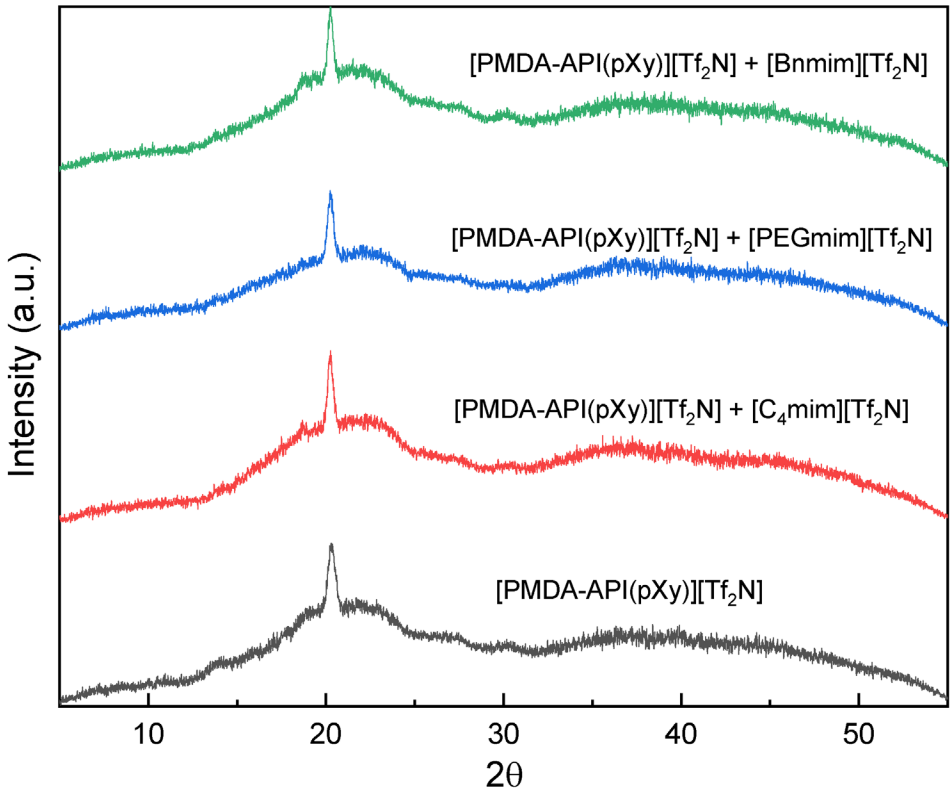

Figure 4.8 XRD profiles of composites materials formed using [PMDA-API(pXy)][Tf_2N] as the polymer and either [C_4mim][Tf_2N], [PEGmim][Tf_2N], or [Bnmim][Tf_2N]

Determination of the effects of soaking versus casting methods were investigated to determine the effects on the final membranes. Obviously, casting acquired a higher degree of localized ordering within the film compared to melt-pressing; however, [PMDA-API(pXy)][Tf_2N] still absorbed IL when cast, yet the higher concentration of [C_4mim][Tf_2N] caused the XRD profile to become broader, and the local ordering peak was not as strong when comparing the both of the [PMDA-API(pXy)][Tf_2N] + [C_4mim][Tf_2N] (Figure 4.9). [PMDA-API(pXy)][Tf_2N] had strong coordinating abilities denoted by the localized ordering peak which was likely the contributing factor to its ability to not completely dissolve in the presence of excess[C_4mim][Tf_2N]. Yet, the polymer matrix had a board halo and lower peak of the soaked film which indicated that the polymer matrix had been disrupted causing a more amorphous structure than the respective cast composite.

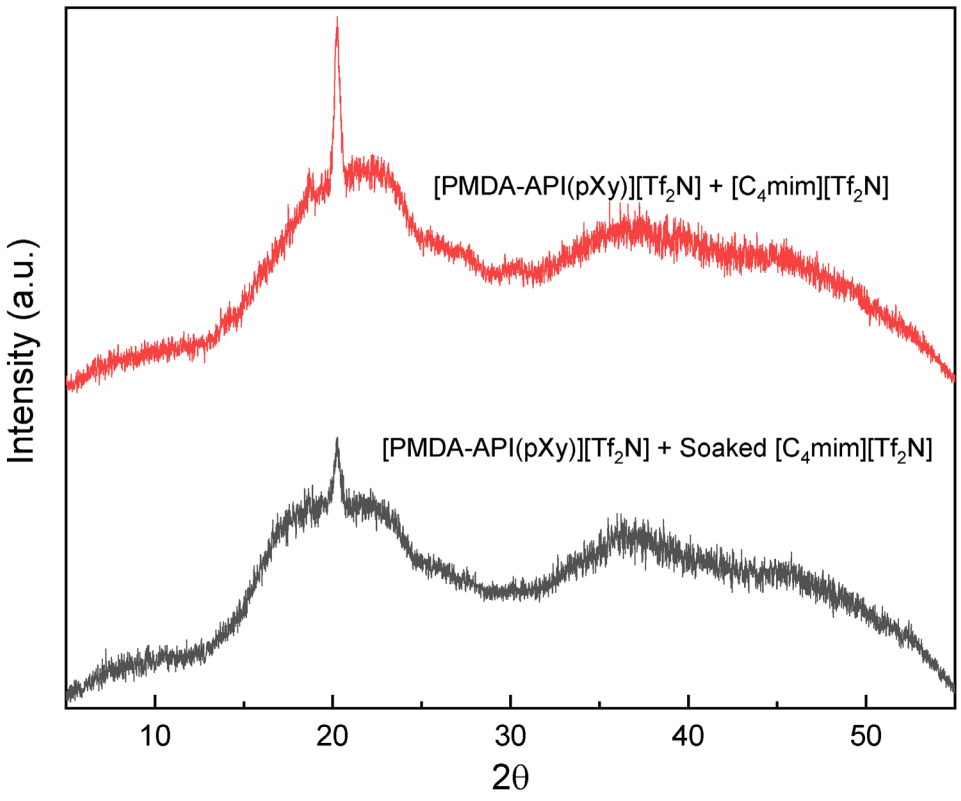

Figure 4.9 XRD profiles comparing [PMDA-API(pXy)][Tf_2N] + [C_4mim][Tf_2N] membranes formed from mixing IL and soaking IL

4.4.3 Gas Separation Properties

The permeability, solubility, and diffusivity of both neat [PMDA-API(pXy)][Tf_2N] and [PMDA-API(pXy)][Tf_2N] + IL composites are presented in Table 4.2. The permeabilities of the neat material (i.e. the material without any IL) showed similarities to its neat melt-pressed counterpart, yet the N_2, CH_4, and CO_2 permeabilities had substantially increased by over 1100%, 800%, and 300%, respectively. The increase in permeabilities corresponded to the XRD profiles where previously an amorphous halo can be seen from 2θ = 18-25 ˚, yet the solvent cast film had a distinct peak occurring at 2θ = 20.3 ˚. As stated in the prior section, the d-spacing was indicative of chain-chain interactions and distances. These qualities can correlate to the overall permeability of a membrane. The increase in ordering

allowed for a higher permeability since the chain spacings were not completely random. The permselectivities of the solvent cast [PMDA-API(pXy)][Tf_2N] were shown to be less than that of melt-pressed film. Previous reports had noted that melt-pressing and solvent casting had significant effects on the permeability of a membrane where the highly processed films were typically lower than the solvent cast.[32] Due to the significant increase of the N_2 and CH_4 permeabilities and only slight increase in CO_2 permeability, the permselectivity values were much less than previously report.

Table 4.2 Permeability, Diffusivity and Solubility values of Neat [PMDA-API(pXy)][Tf_2N] and [PMDA-API(pXy)][Tf_2N] + IL composites

	[PMDA-API(pXy)][Tf_2N]	**[PMDA-API(pXy)][Tf_2N] - [C_4mim][Tf2N]**	**[PMDA-API(pXy)][Tf_2N] - [PEGmim][Tf2N]**	**[PMDA-API(pXy)][Tf_2N] - [Bnmim][Tf2N]**
	Permeability[b]			
N_2	0.30 ±0.01	0.64 ±0.014	0.58 ±0.018	0.23 ±0.02
CH_4	0.23 ±0.02	0.89 ±0.057	0.64 ±0.035	0.32 ±0.02
CO_2	2.72 ±0.06	22.31 ±0.37	18.96 ±0.04	9.32 ±0.18
	Diffusivity[c]			
N_2	1.53 ±0.03	1.39 ±0.01	2.3 ±0.13	1.42 ±0.04
CH_4	0.72 ±0.02	2.72 ±0.07	2.88 ±0.05	0.66 ±0.04
CO_2	0.6 ±0.03	4.8 ±0.1	8.3 ±0.57	2.2 ±0.08
	Solubility[d]			
N_2	0.149 ±0.01	0.350 ±0.004	0.190 ±0.005	0.130 ±0.01
CH_4	0.244 ±0.02	0.250 ±0.02	0.170 ±0.01	0.370 ±0.03
CO_2	3.500 ±0.18	3.500 ±0.03	1.740 ±0.12	3.150 ±0.07

[a] Three replicate experiments were acquired, so uncertainties are presented as a single standard deviation.
[b] Permeability in barrer. 1 barrer=10^{-10} (cm^3 (STP) cm) (cm^2 s cmHg)$^{-1}$.
[c] Diffusivity (10^{-8} cm^2 s^{-1}).
[d] Solubility (cm^3 (STP) cm^{-3} $cmHg^{-1}$).

Though the [PMDA-API(pXy)][Tf_2N] + IL composites did not change drastically in their XRD profiles, the substituent on the imidazolium ring had a significant effect on the N_2, CH_4, and CO_2 permeabilities. [PMDA-API(pXy)][Tf_2N] + [C_4mim][Tf_2N] had very similar

N_2, CH_4, and CO_2 permeabilities compared to the previously soaked material. The similarity in the permeabilities was expected since they had the same composition. Looking at the changing ILs within the polymer showed that the changing functionalities had a major effect on the permeability. The addition of an ether group onto the IL caused a slight decrease in all permeabilities which was expected since the ether group was electron donating, yet the permeability was only slightly decreased when comparing the [C_4mim][Tf_2N] and [PEGmim][Tf_2N] since the "tail" of the IL was the same length which can disrupt the packing of the polymer matrix. The addition of the aromatic IL, [Bnmim][Tf_2N], aromatic substituent on the imidazolium ring caused a very significant decrease in the permeabilities since the aromatic ring can coordinate with the other aromatic portions in the polymer matrix blocking the gas from permeating through the polymer matrix versus the chain which can cause the polymer to pack slightly worse as it coordinated with the polymer. The significant decrease in the permeability was consistent with the 6FDA-IL composite where the [Bnmim][Tf_2N] decreased the permeability of all gases.

Table 4.3 Permeability, diffusivity, and solubility selectivity values of [PMDA-API(pXy)][Tf_2N] and [PMDA-API(pXy)][Tf_2N] + IL composites

	[PMDA-API(pXy)][Tf_2N]			
	Neat	**[C_4mim][Tf_2N]**	**[PEGmim][Tf_2N]**	**[Bnmim][Tf_2N]**
	P_i/P_j			
CO_2/N_2	9.1	34.7	32.7	39.9
CO_2/CH_4	11.8	25.0	29.6	29.0
	D_i/D_j			
CO_2/N_2	0.4	3.5	3.6	1.5
CO_2/CH_4	0.8	1.8	2.9	3.3
	S_i/S_j			
CO_2/N_2	23.5	10.0	9.2	24.2
CO_2/CH_4	14.3	14.0	10.2	8.5

The [PMDA-API(pXy)][Tf_2N] + IL materials demonstrated significantly higher permselectivities compared to the neat [PMDA-API(pXy)][Tf_2N]. The CO_2/CH_4 permselectivity increased by at least 200% for all IL composites while the CO_2/N_2 increased by over 300%. The permselectivities of the solvent cast were significantly lower than the previously-made melt-pressed membrane.[26] [PMDA-API(pXy)][Tf_2N] + [C_4mim][Tf_2N] showed previous CO_2/CH_4 and CO_2/N_2 permselective of 25.7 and 39.5, respectively, which corresponded to this paper's permselectivities very well. [PMDA-API(pXy)][Tf_2N] + [PEGmim][Tf_2N] was also similar to the [PMDA-API(pXy)][Tf_2N] + [C_4mim][Tf_2N] which can be expected as the chain length is similar. Due to the reduction in permeability and the permeability-selectivity tradeoff, the increase in permselectivities for [PMDA-API(pXy)][Tf_2N] + [Bnmim][Tf_2N] was expected. The permeability-selectivity relationship was plotted against the Robeson upper bound with other ionic polymers[16, 17, 23, 25, 26, 28-30, 33, 34] (Figure A4.8-A4.9). Both the diffusivity and solubility selectivities of the gases were not affected significantly comparing the IL composite materials. Since these values were relatively similar, it can be said that PMDA composite were predominately solubility selective materials. Even looking at the neat [PMDA-API(pXy)][Tf_2N], the solubility selectivity was the predominant factor. Addition of ILs increased the diffusivity selectivity compared to the neat material which was likely due to the disruption in packing from the side groups.

4.5 Conclusion

The polymerization of *para*-, *meta*-, and *ortho*-[PMDA-API(Xy)][Tf_2N] isomers was demonstrated along with their formation of composite IL membranes. [PMDA-API(pXy)][Tf_2N] was shown to form a coordinated material due to the solvent casting

methods. Solvent casting allows for the polymer chains to relax as the solvent evaporates allowing the polymer to be in a lower energy state as compared to melt-pressing which "locks" the chains into place. The addition of IL did not affect the localized ordering of the material as it was the predominant structuring present through the XRD analysis. The addition of IL was shown to not affect the neat [PMDA-API(pXy)][Tf_2N] based upon the XRD analysis. Soaking neat [PMDA-API(pXy)][Tf_2N] still produced a similar result, but absorbed slightly more IL, causing the halo of the composite to became broader than solvent casted counterparts. More work needs to be done on the solvating effects of ILs with ionenes. When used as gas separation membranes, solvent casted membranes had a much higher permeability due to the inherent effects of solvent casting. The incorporation of [C_4mim][Tf_2N] and [PEGmim][Tf_2N] into the polymer matrix caused N_2, CH_4, and CO_2 permeabilities to increase similar to their previously reported values. The addition of [Bnmim][Tf_2N] maintained N_2 and CH_4 permeabilities that were close to the neat film while only slightly increasing the CO_2 permeability likely due to the higher number of ionic and aromatic moieties within the polymer matrix.

4.6. References

1. Han, X.; Armstrong, D. W., Ionic liquids in separations. *Acc. Chem. Res.* **2007,** *40* (11), 1079-1086.

2. Wilkes, J. S.; Zaworotko, M. J., Air and water stable 1-ethyl-3-methylimidazolium based ionic liquids. *Journal of the Chemical Society, Chemical Communications* **1992,** (13), 965-967.

3. Fumino, K.; Peppel, T.; Geppert-Rybczyńska, M.; Zaitsau, D. H.; Lehmann, J. K.; Verevkin, S. P.; Köckerling, M.; Ludwig, R., The influence of hydrogen bonding on the physical properties of ionic liquids. *Phys Chem Chem Phys* **2011,** *13* (31), 14064-14075.

4. Fumino, K.; Wulf, A.; Ludwig, R., Strong, Localized, and Directional Hydrogen Bonds Fluidize Ionic Liquids. *Angewandte Chemie International Edition* **2008,** *47* (45), 8731-8734.

5. Cserjesi, P.; Nemestothy, N.; Belafi-Bako, K., Gas separation properties of supported liquid membranes prepared with unconventional ionic liquids. *J. Membr. Sci.* **2010,** *349* (1-2), 6-11.

6. Santos, E.; Albo, J.; Irabien, A., Acetate based Supported Ionic Liquid Membranes (SILMs) for CO2 separation: Influence of the temperature. *J. Membr. Sci.* **2014,** *452*, 277-283.

7. Bara, J. E.; Gabriel, C. J.; Carlisle, T. K.; Camper, D. E.; Finotello, A.; Gin, D. L.; Noble, R. D., Gas separations in fluoroalkyl-functionalized room-temperature ionic liquids using supported liquid membranes. *Chem. Eng. J. (Amsterdam, Neth.)* **2009,** *147* (1), 43-50.

8. Scovazzo, P.; Kieft, J.; Finan, D. A.; Koval, C.; DuBois, D.; Noble, R., Gas separations using non-hexafluorophosphate [PF6]- anion supported ionic liquid membranes. *J. Membr. Sci.* **2004,** *238* (1-2), 57-63.

9. Lan, W.; Li, S.; Xu, J.; Luo, G., Preparation and Carbon Dioxide Separation Performance of a Hollow Fiber Supported Ionic Liquid Membrane. *Ind. Eng. Chem. Res.* **2013,** *52* (20), 6770-6777.

10. Ilconich, J.; Myers, C.; Pennline, H.; Luebke, D., Experimental investigation of the permeability and selectivity of supported ionic liquid membranes for CO2/He separation at temperatures up to 125°C. *J. Membr. Sci.* **2007,** *298* (1+2), 41-47.

11. Scott, M. P.; Rahman, M.; Brazel, C. S., Application of ionic liquids as low-volatility plasticizers for PMMA. *Eur. Polym. J.* **2003,** *39* (10), 1947-1953.

12. Scott, M. P.; Brazel, C. S.; Benton, M. G.; Mays, J. W.; Holbrey, J. D.; Rogers, R. D., Application of ionic liquids as plasticizers for poly(methyl methacrylate). *Chem Commun* **2002,** (13), 1370-1371.

13. Ueki, T.; Watanabe, M., Macromolecules in Ionic Liquids: Progress, Challenges, and Opportunities. *Macromolecules* **2008,** *41* (11), 3739-3749.

14. Gan, Q.; Rooney, D.; Xue, M.; Thompson, G.; Zou, Y., An experimental study of gas transport and separation properties of ionic liquids supported on nanofiltration membranes. *J. Membr. Sci.* **2006,** *280* (1+2), 948-956.

15. Gan, Q.; Rooney, D.; Zou, Y., Supported ionic liquid membranes in nanopore structure for gas separation and transport studies. *Desalination* **2006,** *199* (1-3), 535-537.

16. Bara, J. E.; Gabriel, C. J.; Hatakeyama, E. S.; Carlisle, T. K.; Lessmann, S.; Noble, R. D.; Gin, D. L., Improving CO2 selectivity in polymerized room-temperature ionic liquid gas separation membranes through incorporation of polar substituents. *J. Membr. Sci.* **2008,** *321* (1), 3-7.

17. Bara, J. E.; Hatakeyama, E. S.; Gin, D. L.; Noble, R. D., Improving CO2 permeability in polymerized room-temperature ionic liquid gas separation membranes through the formation of a solid composite with a room-temperature ionic liquid. *Polym. Adv. Technol.* **2008,** *19* (10), 1415-1420.

18. Blasig, A.; Tang, J.; Hu, X.; Tan, S. P.; Shen, Y.; Radosz, M., Carbon Dioxide Solubility in Polymerized Ionic Liquids Containing Ammonium and Imidazolium Cations from Magnetic Suspension Balance: P[VBTMA][BF4] and P[VBMI][BF4]. *Ind. Eng. Chem. Res.* **2007,** *46* (17), 5542-5547.

19. Gu, Y.-Y.; Lodge, T. P., Synthesis and Gas Separation Performance of Triblock Copolymer Ion Gels with a Polymerized Ionic Liquid Mid-Block. *Macromolecules (Washington, DC, U. S.)* **2011,** *44* (7), 1732-1736.

20. Simons, K.; Nijmeijer, K.; Bara, J. E.; Noble, R. D.; Wessling, M., How do polymerized room-temperature ionic liquid membranes plasticize during high pressure CO2 permeation? *J. Membr. Sci.* **2010,** *360* (1-2), 202-209.

21. Bara, J. E.; Gin, D. L.; Noble, R. D., Effect of Anion on Gas Separation Performance of Polymer-Room-Temperature Ionic Liquid Composite Membranes. *Industrial & Engineering Chemistry Research* **2008,** *47* (24), 9919-9924.

22. Bara, J. E.; Noble, R. D.; Gin, D. L., Effect of "Free" Cation Substituent on Gas Separation Performance of Polymer-Room-Temperature Ionic Liquid Composite Membranes. *Ind. Eng. Chem. Res.* **2009,** *48* (9), 4607-4610.

23. Carlisle, T. K.; Bara, J. E.; Lafrate, A. L.; Gin, D. L.; Noble, R. D., Main-chain imidazolium polymer membranes for CO2 separations: An initial study of a new ionic liquid-inspired platform. *J. Membr. Sci.* **2010,** *359* (1-2), 37-43.

24. Li, P.; Zhao, Q.; Anderson, J. L.; Varanasi, S.; Coleman, M. R., Synthesis of copolyimides based on room temperature ionic liquid diamines. *J. Polym. Sci., Part A: Polym. Chem.* **2010,** *48* (18), 4036-4046.

25. Li, P.; Coleman, M. R., Synthesis of room temperature ionic liquids based random copolyimides for gas separation applications. *Eur. Polym. J.* **2013,** *49* (2), 482-491.

26. Mittenthal, M. S.; Flowers, B. S.; Bara, J. E.; Whitley, J. W.; Spear, S. K.; Roveda, J. D.; Wallace, D. A.; Shannon, M. S.; Holler, R.; Martens, R.; Daly, D. T., Ionic Polyimides: Hybrid Polymer Architectures and Composites with Ionic Liquids for Advanced Gas Separation Membranes. *Ind. Eng. Chem. Res.* **2017,** *56* (17), 5055-5069.

27. Kammakakam, I.; O'Harra, K. E.; Dennis, G. P.; Jackson, E. M.; Bara, J. E., Self-healing imidazolium-based ionene-polyamide membranes: an experimental study on physical and gas transport properties. *Polymer International* **2019,** *68* (6), 1123-1129.

28. Kammakakam, I.; Oharra, K. E.; Bara, J. E.; Jackson, E. M., Design and Synthesis of Imidazolium-Mediated Tröger's Base-Containing Ionene Polymers for Advanced CO2 Separation Membranes. *ACS Omega* **2019,** *4* (2), 3439-3448.

29. O'Harra, K. E.; Kammakakam, I.; Noll, D. M.; Turflinger, E. M.; Dennis, G. P.; Jackson, E. M.; Bara, J. E., Synthesis and Performance of Aromatic Polyamide Ionenes as Gas Separation Membranes. *Membranes-Basel* **2020,** *10* (3).

30. O'Harra, K. E.; Kammakakam, I.; Devriese, E. M.; Noll, D. M.; Bara, J. E.; Jackson, E. M., Synthesis and Performance of 6FDA-Based Polyimide-Ionenes and Composites with Ionic Liquids as Gas Separation Membranes. *Membranes-Basel* **2019,** *9* (7), 79.

31. Dennis, G. P.; O'Harra, K. E.; Kammakakam, I.; Jones, T. A.; Mittenthal, M. S.; Flowers, B. S.; Tuan, Y.; Jackson, E. M.; Bara, J. E., 6FDA-containing polyimide-ionene + ionic liquid gas separation membranes. *Journal of Polymer Science* **2020,** *58* (18), 2664-2674.

32. O'Brien, K. C.; Koros, W. J.; Husk, G. R., Influence of casting and curing conditions on gas sorption and transport in polyimide films. *Polymer Engineering & Science* **1987,** *27* (3), 211-217.

33. Supasitmongkol, S.; Styring, P., High CO2 solubility in ionic liquids and a tetraalkylammonium-based poly(ionic liquid). *Energy Environ. Sci.* **2010,** *3* (12), 1961-1972.

34. Tome, L. C.; Mecerreyes, D.; Freire, C. S. R.; Rebelo, L. P. N.; Marrucho, I. M., Pyrrolidinium-based polymeric ionic liquid materials: New perspectives for CO2 separation membranes. *J. Membr. Sci.* **2013,** *428*, 260-266.

4.7 Appendix

^{1}H-NMR

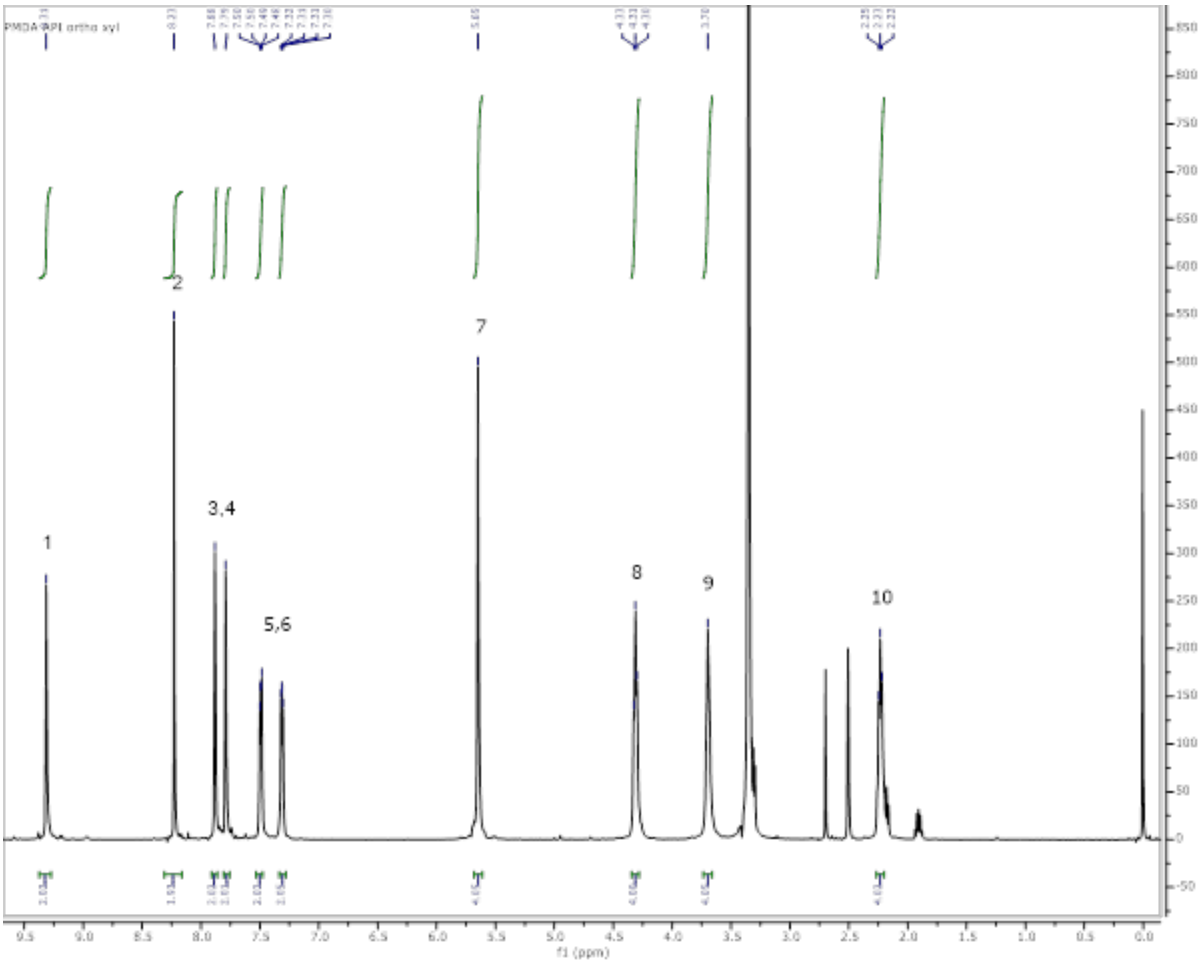

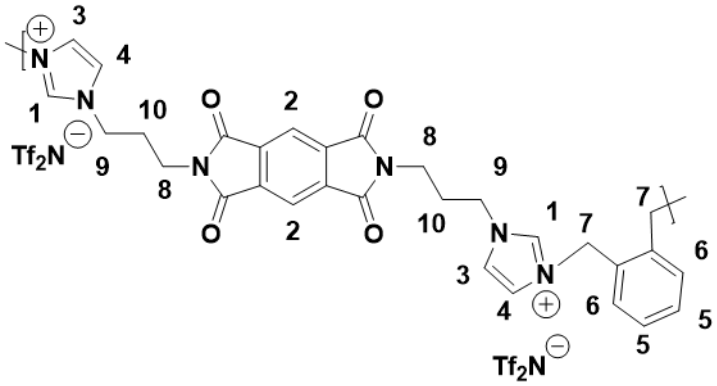

Figure A4.1 ^{1}H-NMR spectrum of [PMDA-API(oXy)][Tf_2N]
δ 9.31 (s, 2H), 8.23 (s, 2H), 7.88 (s, 2H), 7.79 (s, 2H), 7.49 (dd, J = 5.64, 3.29 Hz, 2H), 7.31 (dd, J = 5.56, 3.44Hz, 2H), 5.65 (s, 4H), 4.31 (t, J = 6.81 Hz, 4H), 3.70 (t, J = 6.79 Hz, 4H), 2.23 (m, J = 6.87 Hz, 4H).

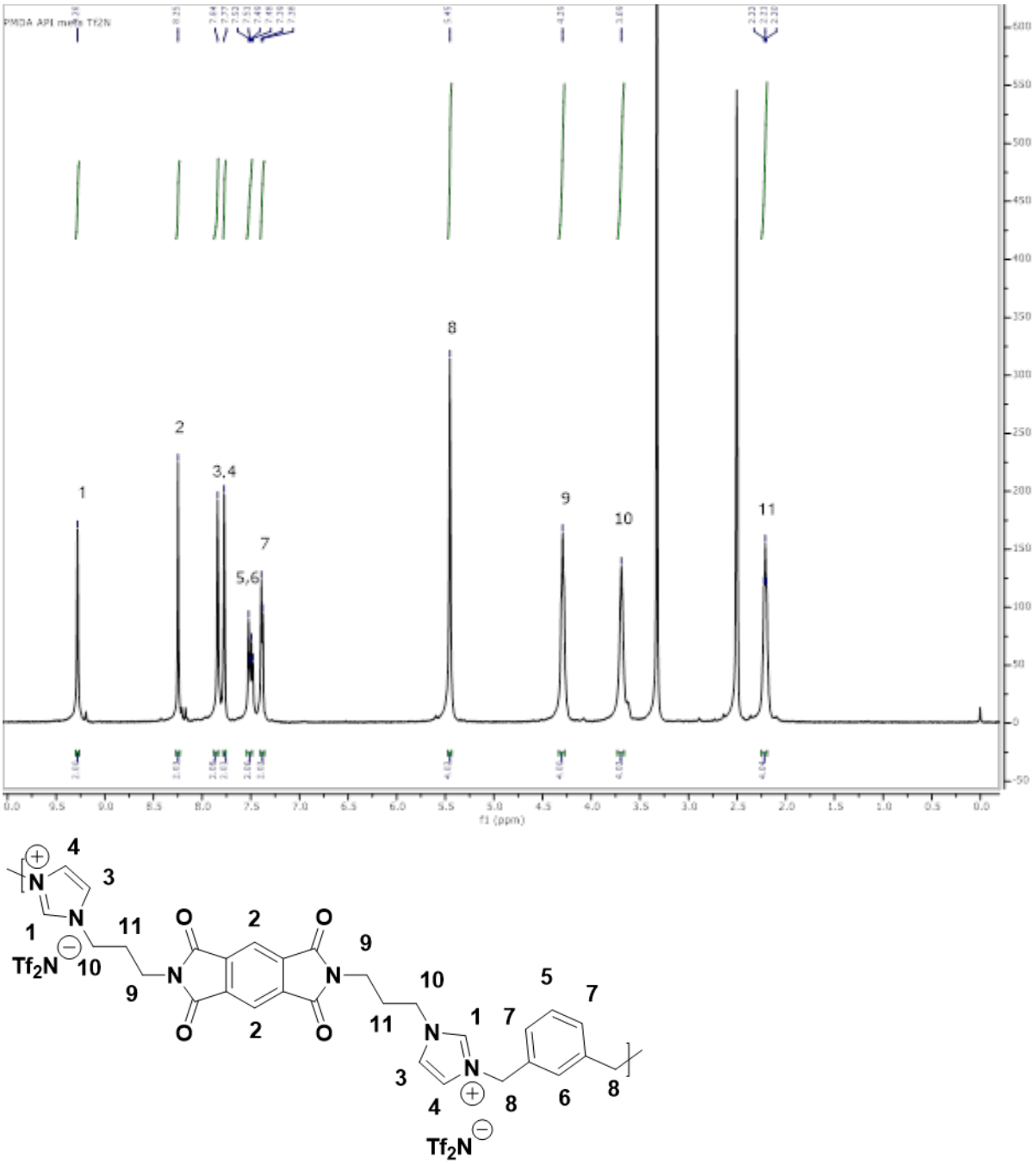

Figure A4.2 ^{1}H-NMR spectrum of [PMDA-API(mXy)][Tf_2N]
δ 9.28 (s, 2H), 8.25 (s, 2H), 7.84 (s, 2H), 7.77 (s, 2H), 7.52 (s, 1H), 7.49 (t, J = 7.51 Hz, 1H), 7.38 (d, J = 7.37 Hz, 2H), 5.45 (s, 4H), 4.29 (t, J = 6.78 Hz, 4H), 3.69 (t, J = 6.81 Hz, 4H), 2.21 (m, J = 6.26 Hz, 4H).

SEM images

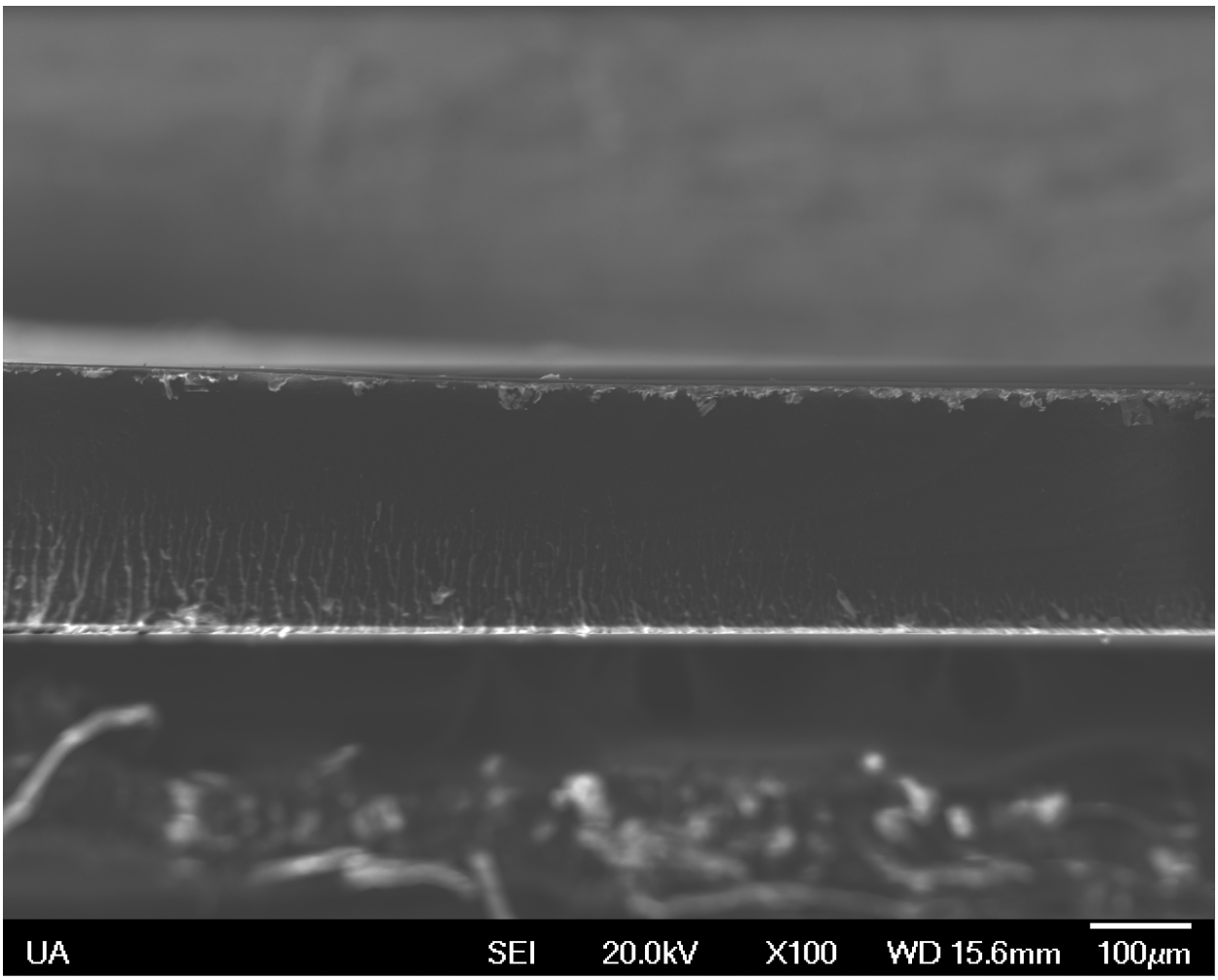

Figure A4.3 SEM image of [PMDA-API(pXy)][Tf_2N]

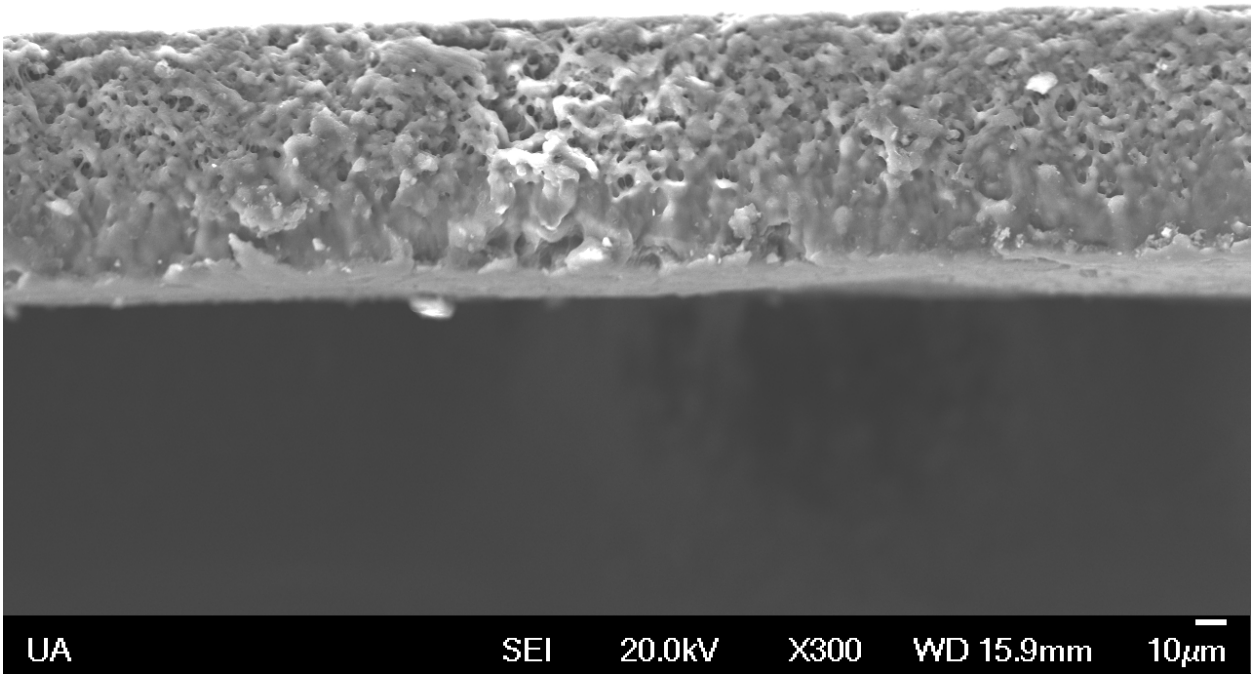

Figure A4.4 SEM image of [PMDA-API(pXy)][Tf_2N] + [C_4mim][Tf_2N]

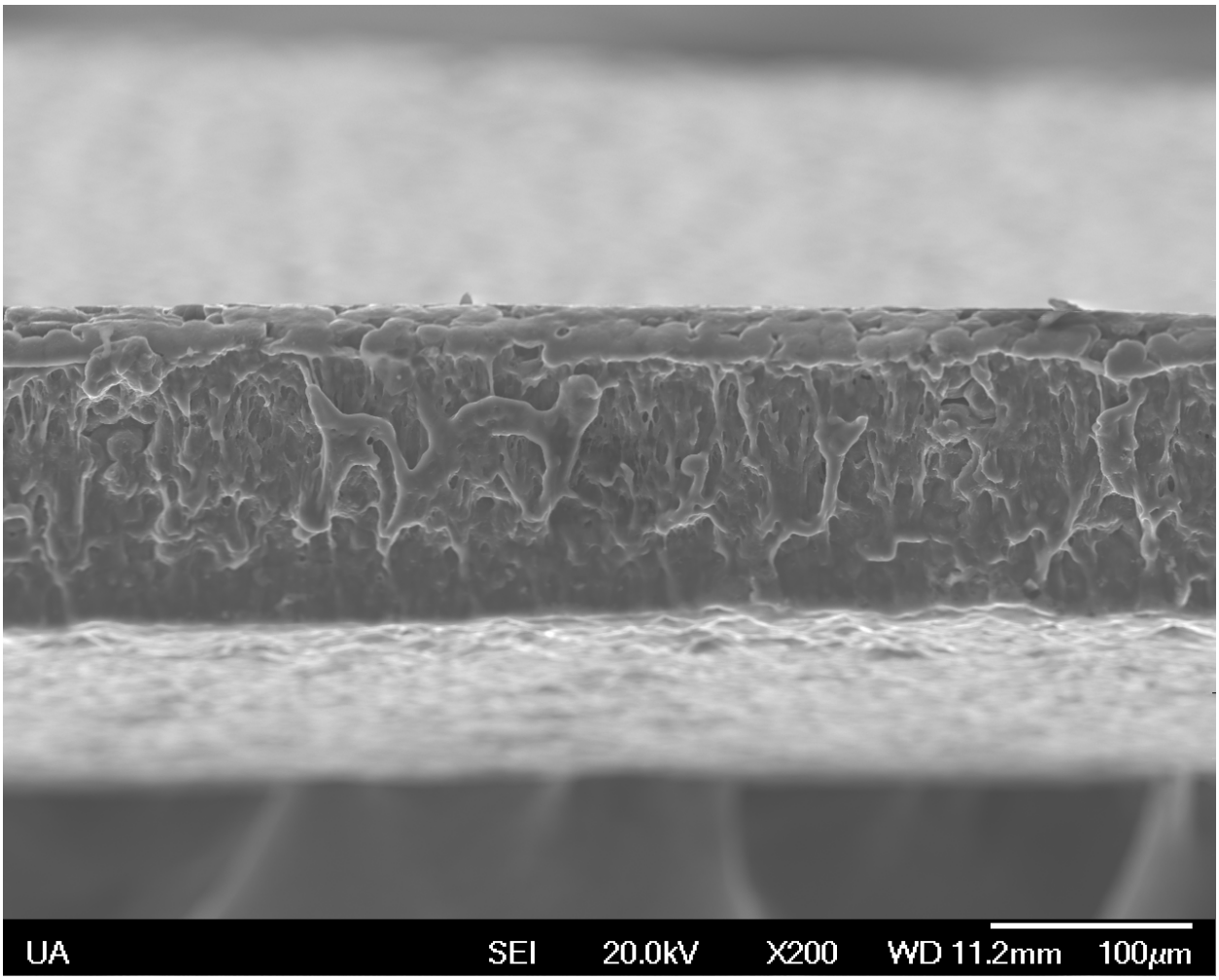

Figure A4.5 SEM image of [PMDA-API(pXy)][Tf_2N] + [PEGmim][Tf_2N]

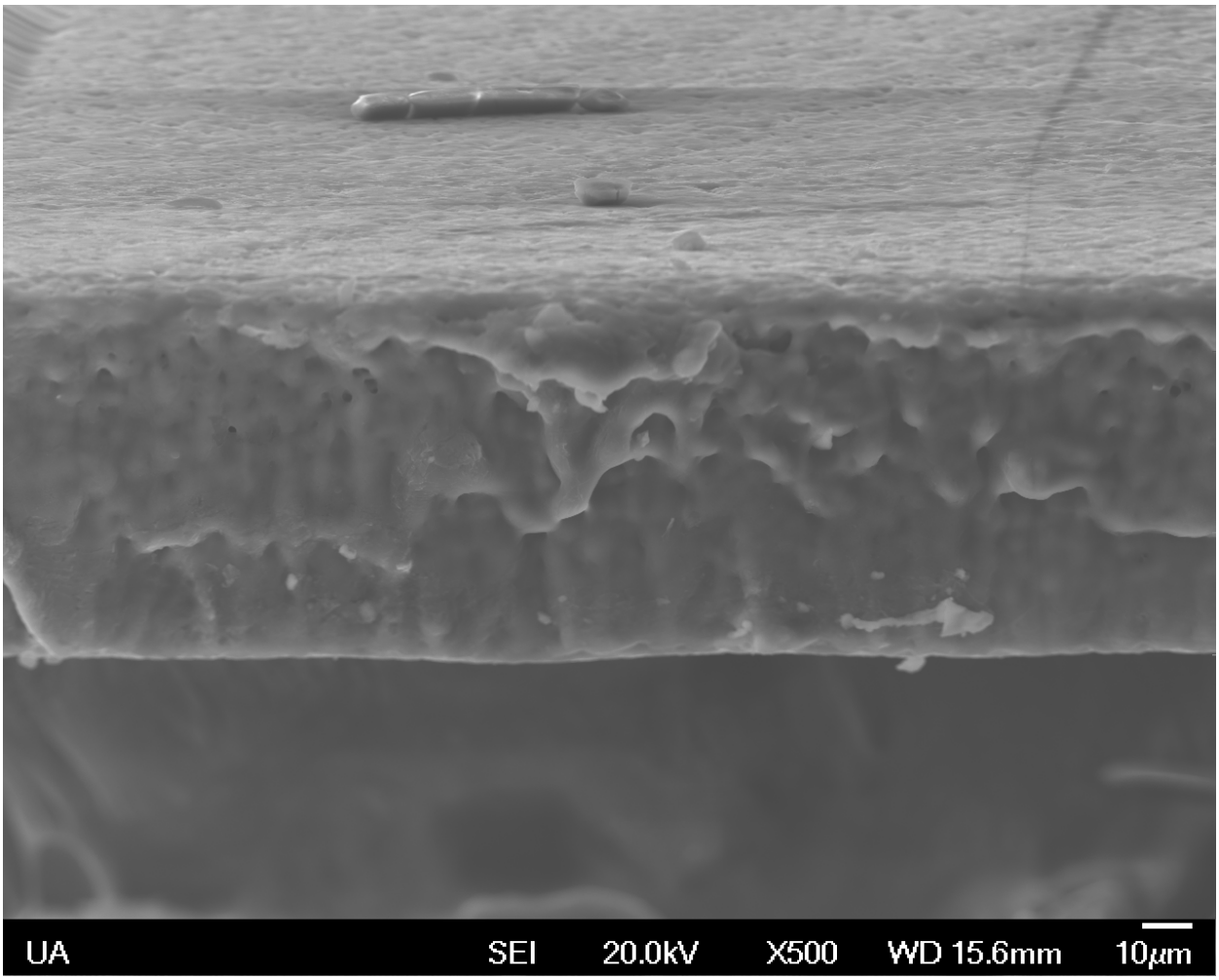

Figure A4.6 SEM image of [PMDA-API(pXy)][Tf_2N] + [Bnmim][Tf_2N]

MALDI-TOF MS

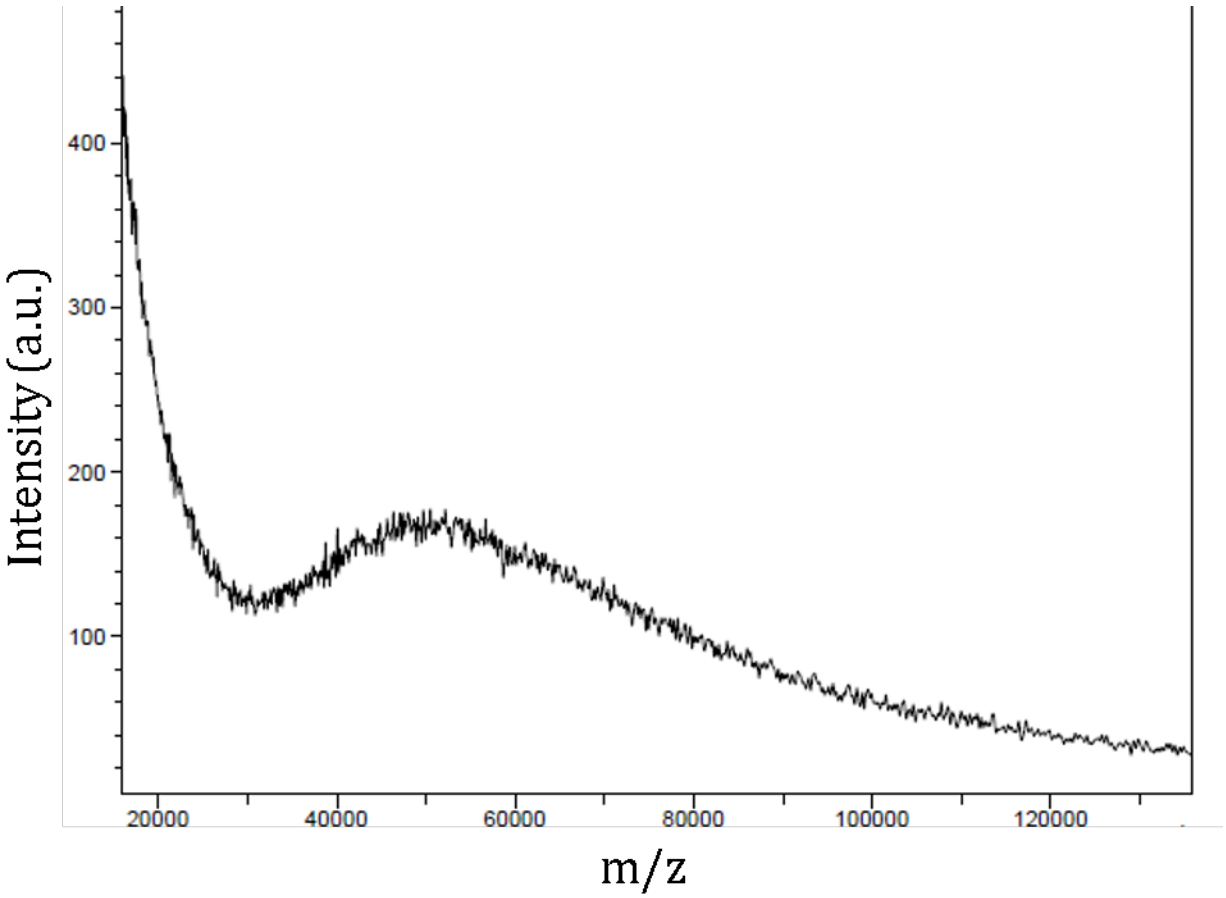

Figure A4.7 MALDI-TOF MS of [PMDA-API(mXy)][Tf_2N]

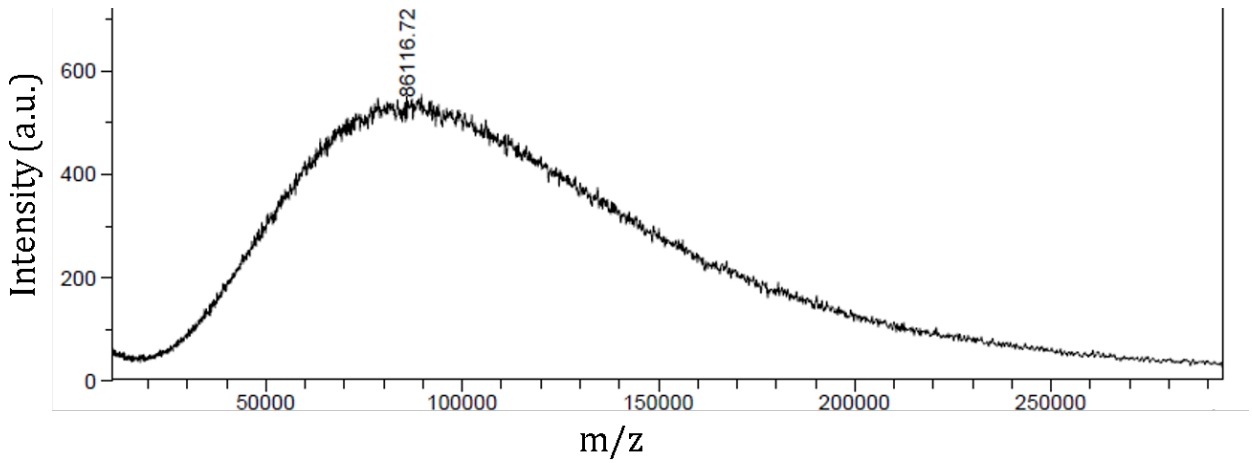

Figure A4.8 MALDI-TOF MS of [PMDA-API(oXy)][Tf_2N]

FTIR

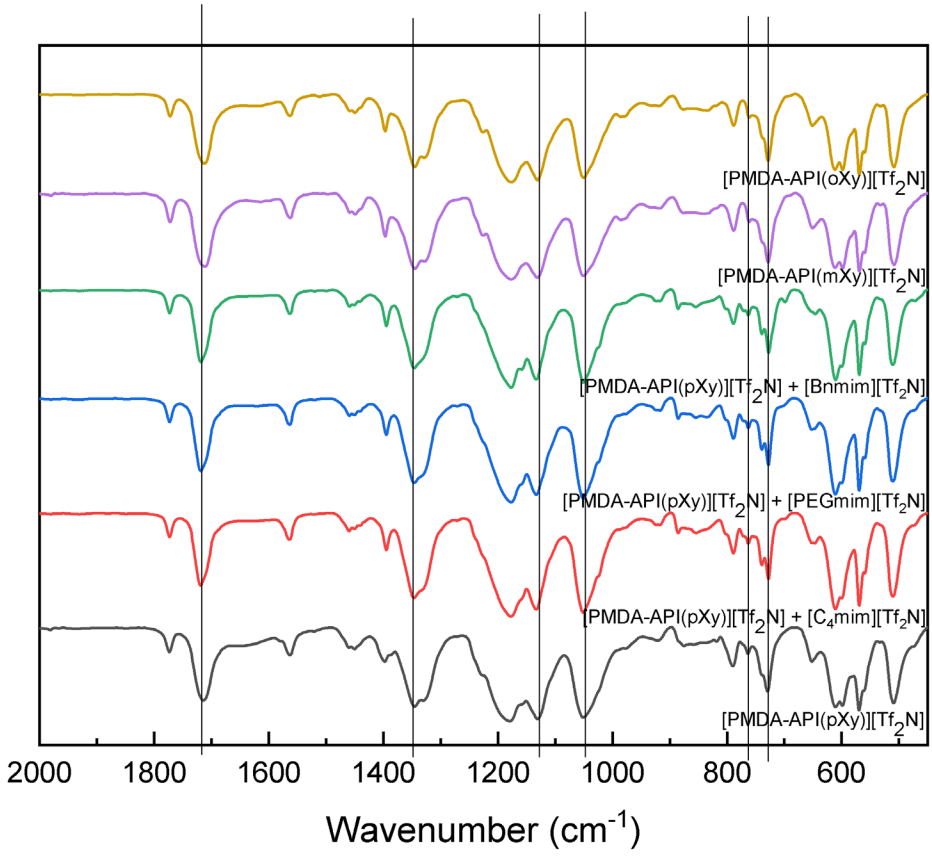

Figure A4.9 FTIR spectra of [PMDA-API(pXy)][Tf_2N], [PMDA-API(mXy)][Tf_2N], [PMDA-API(oXy)][Tf_2N], and [PMDA-API(pXy)][Tf_2N] + IL composites

Robeson Plot

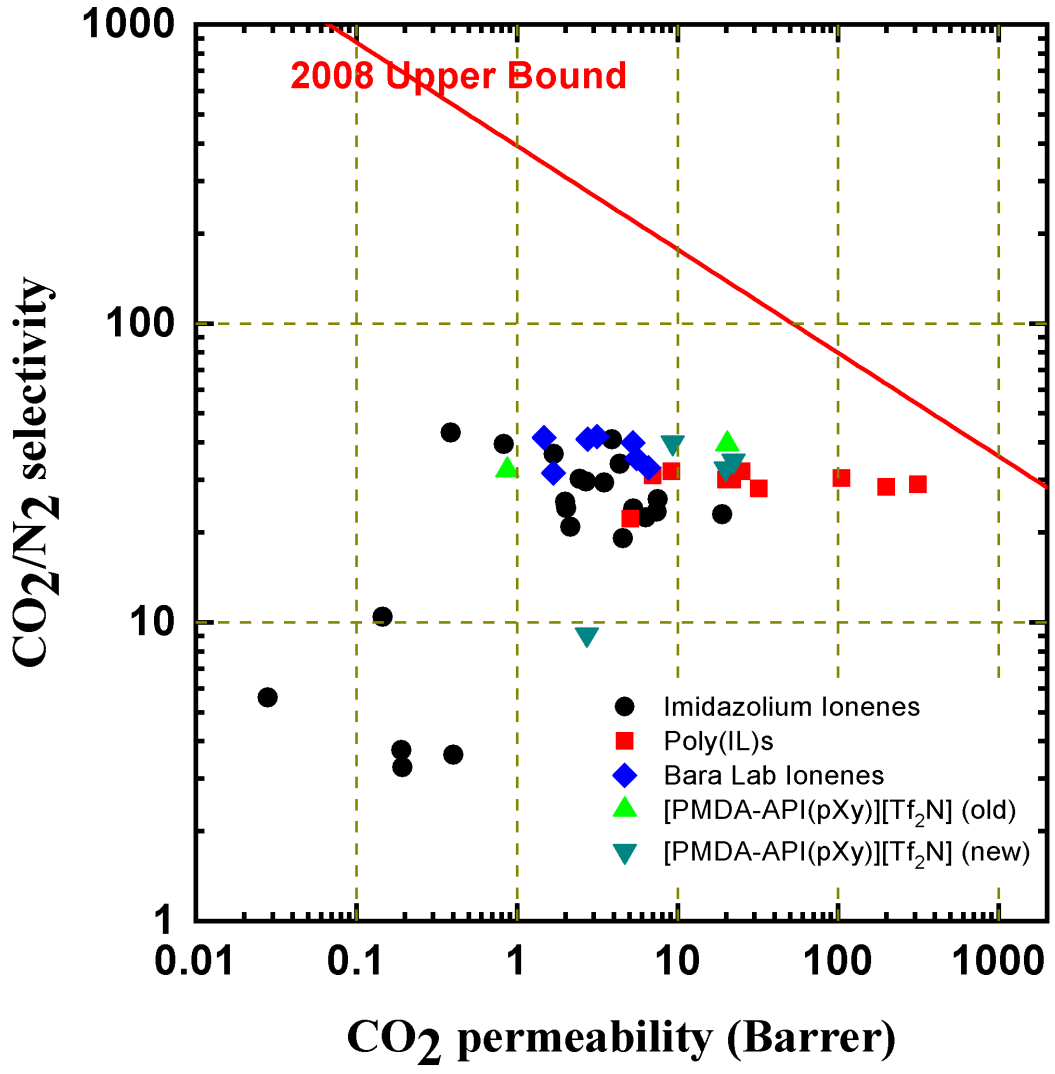

Figure A4.10 Robeson Plot of CO_2/N_2 Selectivity versus CO_2 permeability with relevant ionene compounds

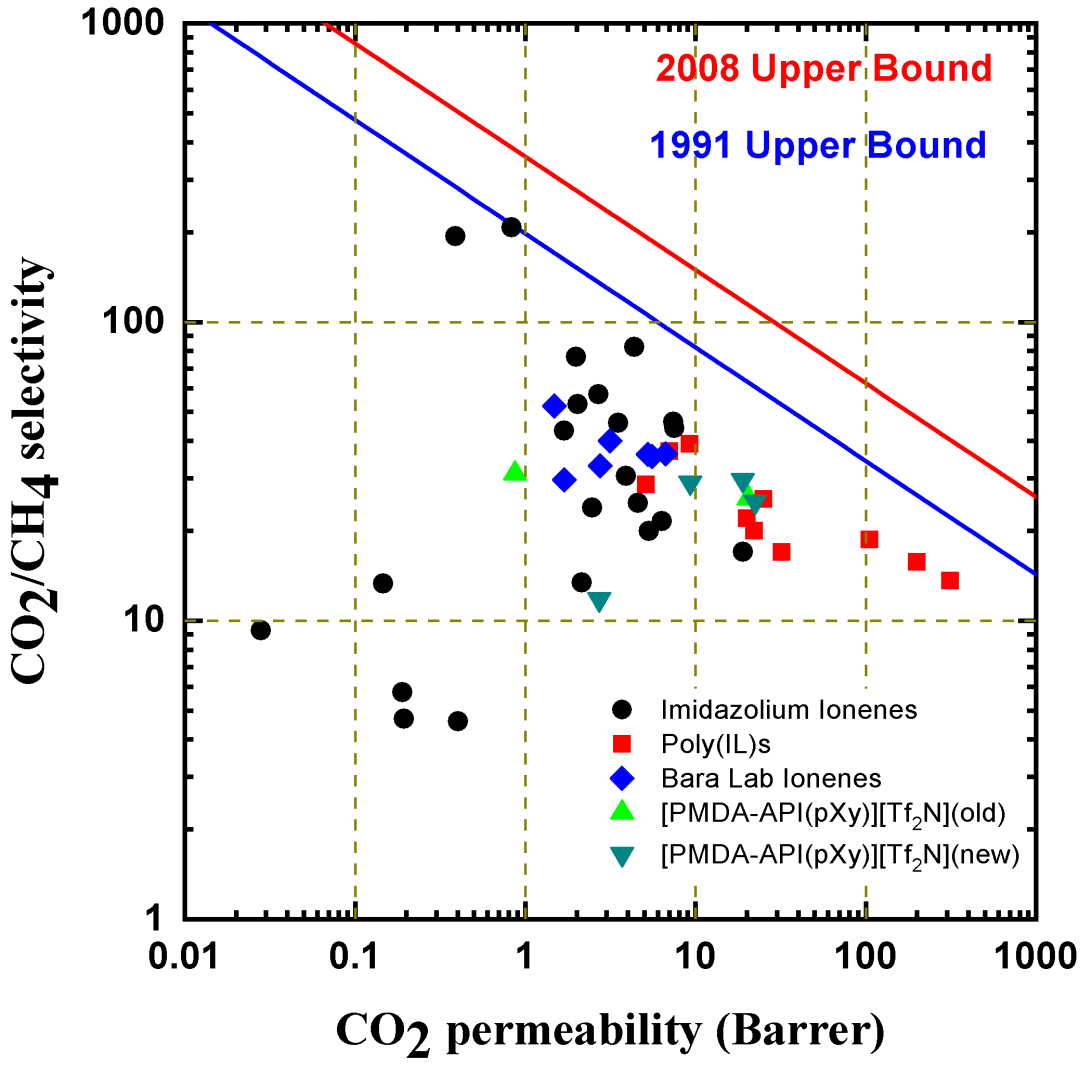

Figure A4.11 Robeson Plot of CO_2/N_2 Selectivity versus CO_2 permeability with relevant ionene compounds

CHAPTER 5

SUPPLEMENTARY INFORMATION & WORKS IN PROGRESS

5.1 Ionic Polyamides as Gas Separation Membranes

5.1.1 Introduction

Though polyamides are not used as gas separation membranes due to their structure containing high amounts of intramolecular H-bonding which result in improved properties (thermal, mechanical, etc.) relative to other polymers. By taking advantage of this class and adding ionic moieties to the backbone, the polymers can be of interest. In this study, ionic polyamides were formed using terephthaloyl chloride (TC) and isophthaloyl chloride (IC) with two equivalents of 1-(3-aminopropyl)imidazole (API). The resultant monomer, denoted as TC-API and IC-API, was reacted via Menshutkin reaction with α,α'-dichloro-(p/m/o)-xylene to form xylene linked polyamides. Subsequently, an ion exchange was performed to form the final [TC-API(p/m/oXy)][Tf_2N] and [IC-API((p/m/o)Xy)][Tf_2N] products. The [TC-API(pXy)][Tf_2N] and [IC-API(mXy)][Tf_2N] can self-heal while also being very elastomeric. All the resulting polymers were used in gas separation tests with CO_2, N_2 and CH_4 to determine the permeability, solubility, and diffusivity associated with each gas. The permeability data were used to then look at the selectivity of relevant gas pairs.

5.1.2 Experimental Section

Six distinct ionic polyamides were polymerized using TC, IC, API, and α,α'-dichloro-(p/m/o)-xylene. First, either TC or IC were dissolved with API in acetonitrile in the presence of K_2CO_3 and heated to 130 °C for 12 h. The resulting solution was had a white precipitate formed. The acetonitrile was decanted off and the subsequent powder was poured into DI water. After letting the compound stir, the precipitate was filtered and dried under vacuum. Then either TC-API or IC-API is dissolved into NMP and α,α'-dichloro-(p/m/o)-xylene and reacted at 150 °C and 24 h to form the six isomers. These isomers were dried under vacuum at 100 °C for 48 h. An overview of the synthesis is shown in scheme 5.1.

Scheme 5.1 Synthesis scheme of [TC-API(pXy)][Tf_2N] and [IC-API(mXy)][Tf_2N]

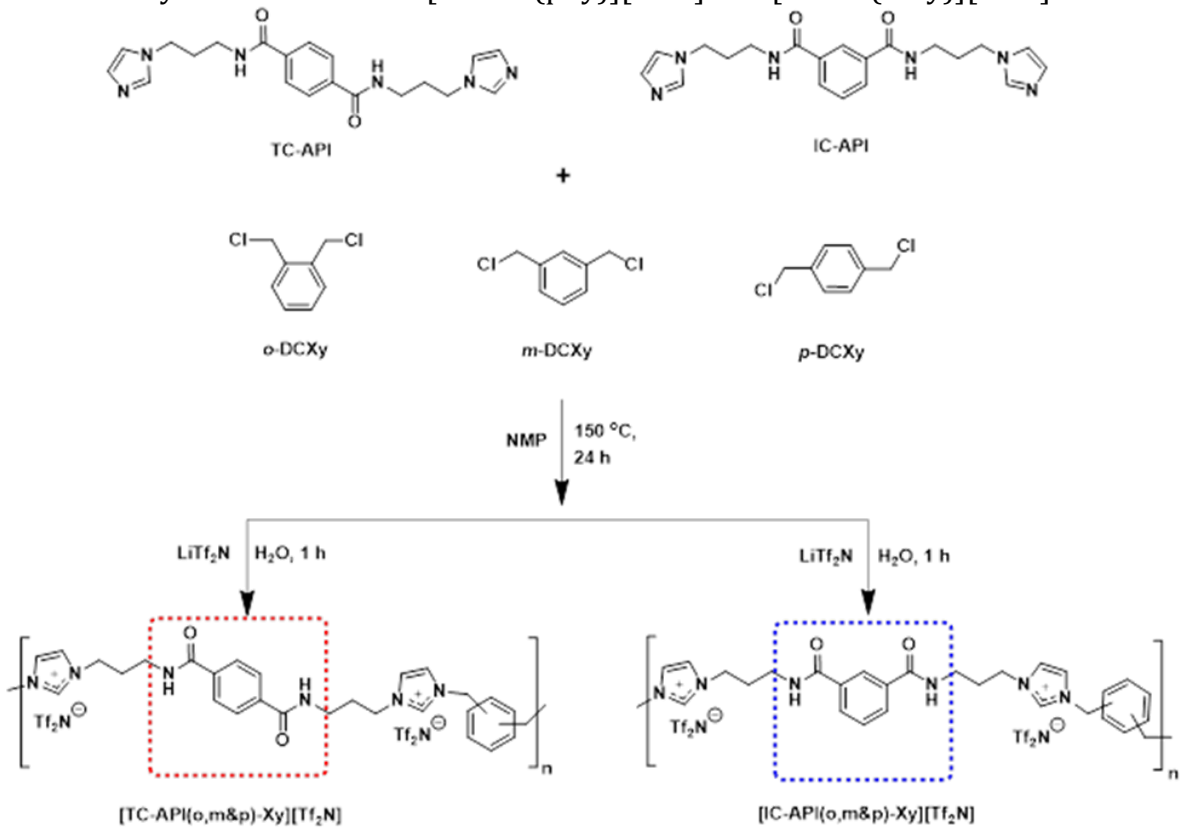

The monomers and polymers were characterized using ^{1}H-NMR to ensure the structure. MALDI-TOF was used to determine the number average molecular weight (Mn). They were melt-pressed at 100 °C and 3000 psi using a Carver press (model 4386) with heated platens to form thin layer membranes. Wide angle x-ray diffraction (WAXD) was performed using a Bruker D8 Discover on the thin layer membranes to determine the d spacing of the material using Bragg's Law (Eqn. 5.1) as stated below:

$$d=\lambda/(2*\sin\theta) \qquad (5.1)$$

Differential scanning calorimetry (DSC) was carried out on the materials using a TA instruments DSC Q2000 from 20 °C to 300 °C with a rate of 10 °C min^{-1}. DSC helps determine the glass transition of the polymer. Thermogravimetric analysis (TGA) was performed on each material using a Seiko Tg-DTA 7300 from room temperature to 750 °C at 10 °C min^{-1} under N_2 atmosphere. TGA helps determine the stability of the polymer. Bulk [TC-API(pXy)][Tf_2N] was formed into a tensile bar (ASTM D638-10 Type IV) using a Teflon mold. An MTS QTest 25 using either 5.66 lb_f or 450 lb_f load cells at 1.2-inch min^{-1} determined the stress-strain curve which was used to determine the Young's modulus. Due to the thermoelastic character of these materials, a tensile bar of [TC-API(pXy)][Tf2N] was reformed to perform replicate testing. To make the membranes for gas separation testing, two 47 mm aluminum tabs were punched that had adhesive on the back. The square piece was cut from the bulk membrane. Once the membrane was adhered to one aluminum tab, the other aluminum tab was placed on top giving a ½-inch testing area. The "tabbed" membrane was loaded into Millipore holder with a sintered disk. Gas permeation tests were performed using time lag systems as described in our previously published manuscript.[1] These time lag systems use a solution-diffusion method to determine the

permeation of gas through the membrane. Due to the pressure differential between the top and bottom of the unit, the gas is absorbed into the membrane, it will reach a maximum load capacity, and gas will flow and start to desorb from the membrane into the permeate. Both the top and bottom pressures were recorded and used to determine the moles within the permeate. A few updates have occurred to our membrane systems since they were last published. We have added NPT thermocouples that allows us to ensure the temperatures were considered. Also, the connections to the systems were changed to VCR fittings rather than tube fittings. VCR connectors use a metal gasket to seal the connections of the system. All tubing was also changed to metal-braided PTFE-lined tubing. All these changes make sure the gases applied to the system do not leak from the tube fittings and tubing. A more detailed description of the advances to our gas separation systems can be seen in section 5.5.

Dynamic vacuum was applied to both the top and bottom to ensure the membrane was devoid of any gas and the feed and permeate pressure were ~0 psia. Steady state permeation curves of CO_2, N_2, and CH_4 were used to determine the single gas permeability as well as the solubility, and diffusivity.

Using the permeation data in barrer, the relevant selectivities were determined. Methods and procedures can be seen in full in the published manuscript.[1]

5.1.3 Results and Discussion

5.1.3.1 Wide Angle X-ray Diffraction

The XRD profiles (Figure 5.1) showed that the materials had peaks that were bimodal, yet $2\theta = 21°$ is the dominating d spacing since the polyamide were known for their d spacing being around 4.9 Å. This peak ($2\theta = 21°$) likely occurs due to the high amount of H-bonding

present in the polyamide. This substantial amount of bonding dominates the overall chain-chain packing and chain entanglement. The lower peak (2θ = 17 °) demonstrated the chains that do not pack as well since the triflate anion as well as the xylene linkages is within that portion of the backbone. This can be seen in figure 5.1.

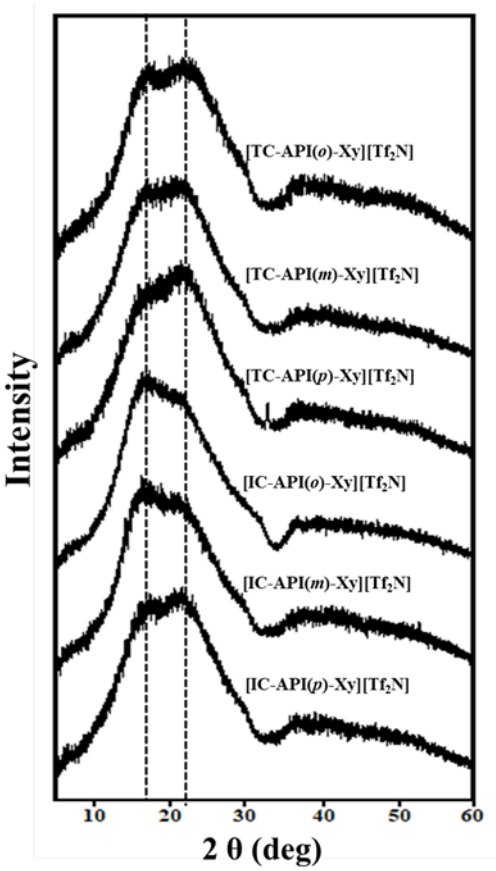

Figure 5.1 Wide angle x-ray diffraction profiles of ionic polyamide membranes.

5.1.3.2 Tensile Testing

The material was melt-molded using a Teflon mold with ASTM D638 Type IV wells that had been fabricated by CNC, and after each trial, the same bar was molded again using the Teflon mold. These materials demonstrated highly elastomeric characteristics. Upon elongation, these materials would become opaque, perhaps indicating alignment induced by stretching. Multiple tests were run on the same [TC-API(pXy)][Tf_2N] due to the elastomeric

character of the films. Initially, the material had little stress (Pa) but high strain (% elongation).

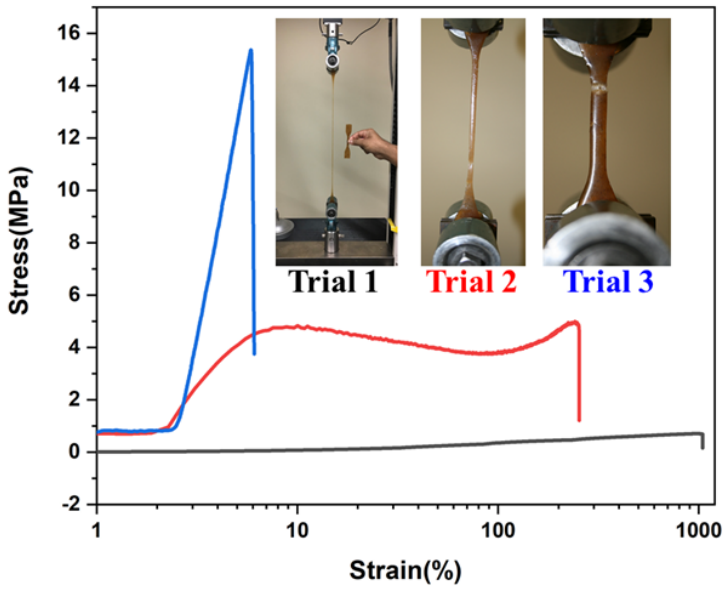

Figure 5.2 Stress-Strain Graph of multiple trails of [TC-API(pXy)]Tf_2N]

Each subsequent test revealed a higher stress but lower strain which increased to a peak at 15 MPa. Trial 3 stress peaked at nearly 30 times higher than trial 1. The increase in stress is likely due to the h-bonding characteristics. The heat applied to the material along with multiple stress tests can cause annealing and chain entanglement of the polymer. The elongation when stretching the chains highly decreases the amorphous character of the polymer aligning the chains increasing the chain-chain interactions of the H-bonding.

5.1.3.3 Gas Permeation Testing

The gas separation parameters can be seen in Tables 5.1 & 5.2. These values follow the same trends as conventional polymer systems and are representative of the kinetic diameters of each gas: CO_2 > N_2 > CH_4. However irrespective of their regioselective orientation, [TC-API(pXy)][Tf_2N] exhibits the highest CO_2 permeability which is likely due

to the lower chain entanglement as denoted by the T_g of the polymer. [IC-API(mXy)][Tf_2N] had the second highest CO_2 permeability. These gas separation factors can be attributed to the amide and xylyl linkages being in the para-para or meta-meta formation. In both [TC-API(pXy)][Tf_2N] and [IC-API(mXy)][Tf_2N], the CO_2 permeabilities were significantly higher than either the N_2 or CH_4 permeabilities with the [TC-API(pXy)][Tf_2N] outperforming the [IC-API(mXy)][Tf_2N] by a factor of over two. The CO_2/CH_4 and CO_2/N_2 permselectivity values of [TC-API(pXy)][Tf_2N] and [IC-API(mXy)][Tf_2N] were rather high where the values were 193 and 39.2, and 168 and 43.6, respectively. The solubilities and diffusivities demonstrate that these materials were solubility dependent rather than diffusion dependent as noted by the much high solubility selectivity versus the diffusion selectivity.The gas permeation tests confirmed the high amount of chain-chain interactions likely due to the H-bonding which caused the low permeabilities.

Table 5.1 Pure gas permeabilities (P)[a] and permselectivities (α) of ionene-PA membranes at 3 atm and 20°C

Membrane	P_{CO2}	P_{N2}	P_{CH4}	$\alpha_{CO2/N2}$	$\alpha_{CO2/CH4}$
[TC-API(*o*Xy)][Tf_2N]	0.19	0.051	0.033	3.74	5.76
[TC-API(*m*Xy)][Tf_2N]	0.028	0.005	0.003	5.35	9.2
[TC-API(*p*Xy)][Tf_2N]	0.83	0.021	0.00	39.2	193
[IC-API(*o*Xy)][Tf_2N]	0.15	0.014	0.011	10.8	13.2
[IC-API(*m*Xy)][Tf_2N]	0.39	0.009	0.002	43.6	168
[IC-API(*p*Xy)][Tf_2N]	0.19	0.059	0.041	3.27	4.77

[a]*P* in barrers, where 1 barrer = 10^{-10} [cm^3 (STP) cm]/(cm^2 s cmHg)

Table 5.2 Pure gas diffusivity coefficients[a] and solubility coefficients[b] at 3 atm and 20 °C

Membrane	D_{CO2}	D_{N2}	D_{CH4}	S_{CO2}	S_{N2}	S_{CH4}
[TC-API(*o*Xy)][Tf_2N]	0.57	0.3	0.21	0.33	0.17	0.16
[TC-API(*m*Xy)][Tf_2N]	0.20	0.17	0.10	0.14	0.031	0.029
[TC-API(pXy)][Tf_2N]	0.79	0.535	0.03	1.05	0.039	0.14
[IC-API(*o*Xy)][Tf_2N]	0.57	0.854	0.11	0.26	0.016	0.1
[IC-API(*m*Xy)][Tf_2N]	0.16	0.548	0.20	2.4	0.016	0.011
[IC-API(*p*Xy)][Tf_2N]	0.32	0.407	0.26	0.61	0.15	0.16

[a]Diffusivity coefficient (10^{-8} cm^2 s^{-1}).
[b]Solubility coefficient (cm^3 (STP) cm^{-3} $cmHg^{-1}$).

5.1.4 Conclusions

Six distinct ionic polyamides were formed and confirmed via ^{1}H-NMR and FT-IR. The number average molecular weight was determined using MALDI-TOF MS. The ionic polymers had highly unique properties such as self-healing and elasticity proven by the

tensile testing. The materials were melt-pressed and formed thin layer membranes that were used in XRD and gas separation tests. The XRD showed a bimodal peak which can be attributed to the h-bonding between chains. The d spacing acquired from the XRD profiles as well as the thermal data correlates to the gas separation abilities of the polymers. The [TC-API(pXy)][Tf_2N] had the highest CO_2 permeability which is attributed to the flexibility of the chains between the terephthalic acid segments. Having similar regioselective portions of amide and xylyl linkages (i.e. para-para and meta-meta) increases the CO_2 permeabilities as well as the diffusivities and solubilities. The materials were useful for CO_2/light gas separations given the correct formation of amide and xylyl linkages.

This work has been published in Polymer International as "Self-healing imidazolium-based ionene-polyamide membranes: an experimental study on physical and gas transport properties." By Irshad Kammakakam, Kathryn O'Harra, ***Grayson Dennis****, Enrique Jackson, and Jason Bara on 5 Mar 2019.*

5.2 Ether-Based Linkages within Ionic PMDA Polyimides for Gas Separation

5.2.1 Introduction

Few cases exist where PIs have been polymerized containing ether linkages, yet from these few instances, some conclusions can be determined and applied to the effects of having these types of linkages which contained either alkyl or aromatic groups. Stern, et al polymerized a 6FDA with extended diamines containing PEG-like linkages (Figure 5.3).[2] The corresponding polymers were named as follows: 6FDA-PEPE (n = 1), 6FDA-PBEPE (n = 2), and 6FDA-PTEPE (n = 3). These polymers were tested for their T_g, Density, d-spacing

and finally their gas permeation using CO_2, CH_4, N_2, and O_2. As the length of the PEG-like linkages are extended, the gas permeation of all gases decreased. The P_{CO2} is 68.8 barrer for 6FDA-PEPE decreasing to a value of 19.4 barrer for 6FDA-PTEPE. In another instance, Hirayama and coworkers polymerized phenyl ethers of varying lengths with BPDA.[3] The polymers were then tested as gas separation membranes where the increasing amount of phenyl ethers the decreased the CO_2 permeability of the materials. Although, in this case, the polymers had increasing aromatic character, addition of ether functionalities can change the inter- and intra-molecular interactions within the polymer matrix.

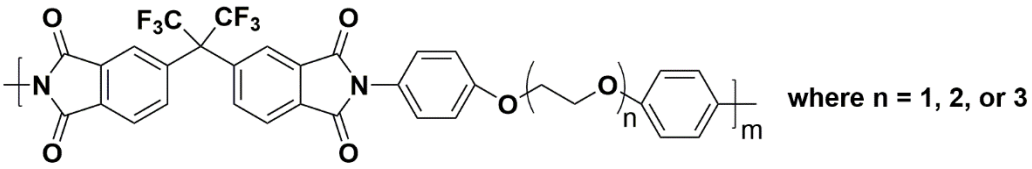

Figure 5.3 Structure of polyimide from Stern, et al. with OEG-like linkages

ILs form an interesting platform for the use of ether or oligo(ethylene glycol) (OEG) linkage. ILs have been previously tested with the addition of OEG for their bulk physical properties (e.g. density, polarity, viscosity, heat capacity). Ethylene glycol functionalized ILs have been shown to have lower viscosities compared to their alkyl counterparts.[4, 5] Looking into the molecular effects of OEG on ILs has been investigated in recent years.[4, 6, 7] Zeng, et al. elucidated the effects of OEG functionalized ILs through the use of Gaussian MD simulations. MD simulations of the OEG-functionalized ILs at their minimum energy structure showed that the ether groups will coordinate with the acidic C(2) position of the IL even at longer OEG lengths. Though the addition of these OEG functionalities has not been used in many polymer systems, their use in ionic polymers could be of interest due to the inherent CO_2-philic properties of ethylene glycol and ILs.

Two PI ionenes were polymerized and tested with differing OEG-based linkages to determine the effects of ether linkages on an ionene matrix. The formation of these OEG-containing polyimide ionenes was made through the use of our previously made PMDA-API monomer and 1-iodo-2-(2-iodoethoxy)ethane, 1,2-bis(2-iodoethoxy)ethane, and 1-iodo-2-(2-(2-(2-iodoethoxy)ethoxy)ethoxy)ethane. These materials were tested using MALDI and FT-IR. The gas properties were determined in only preliminary testing, so more investigation of these materials is necessary. However, the introduction of OEG linkages into ionic Polyimides can cause inter- and intramolecular interactions that have yet to be determined and can be favorable to the supramolecular structure and overall membrane formation ability.

5.2.2 Experimental Section

The polymerization reaction for OEG-containing ionic polyimides can be seen in Scheme 5.2. PMDA-API monomer and dihalide OEG were added to NMP in a heavy-walled pressure vessel and reacted for 24 h at 150 ˚C. Once the reaction finished, it was cooled to RT, and the NMP was roto-evaporated off. Excess $LiTf_2N$ was mixed into DI H_2O, and the $[PMDA\text{-}API(PEG)_n][I]$ was also dissolved in DI H_2O. The $[PMDA\text{-}API(PEG)_n][I]$ was poured into the aqueous $LiTf_2N$ to perform an ion metathesis exchanging the halide anion with $[Tf_2N]^-$. Upon precipitation of the $[PMDA\text{-}API(PEG)_n][Tf_2N]$, it was stirred overnight for 24 h to ensure complete exchange of the anions

Scheme 5.2 Polymerization scheme for the formation of [PMDA-API(PEG)$_n$][Tf$_2$N] (n = 1, 2, 3) polymers

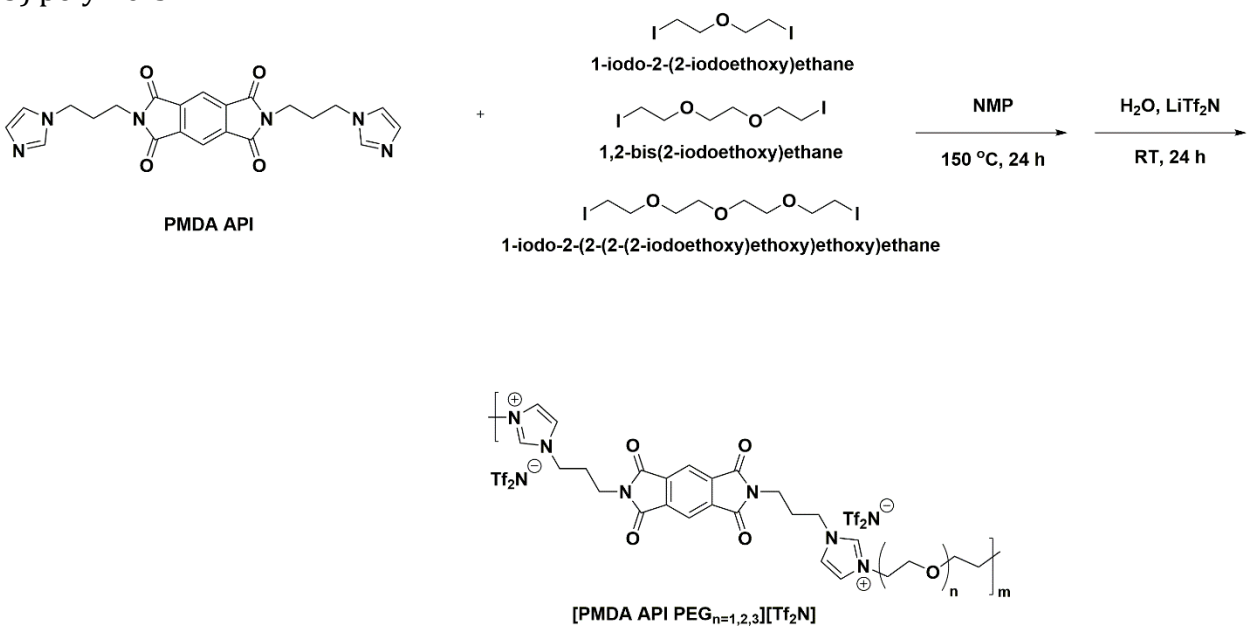

To form films of this material, they were pressed under heat between two glass plates that had Rain-X applied to them beforehand. The films delaminated very easily from the highly hydrophobic surface. MALDI-TOF MS was used to determine the M_n of the polymer. FT-IR was performed on the materials using a PerkinElmer Spectrum Two with the ATR accessory, and XRD was performed on the films using a Bruker D8 Discover with a Cobalt x-ray source (λ = 1.7902 Å) with a point collimator. Lastly, the films were tested with pure gas runs of N_2, CH_4, and CO_2 using our high vacuum time lag systems that have been described in previous publications.

5.2.3 Results and Discussion

The FT-IR spectra were produced in the Figure A5.1. Functionalities of interest were denoted by lines demonstrating their presence throughout the spectra. The MALDI-TOF MS showed that the [PMDA-API(PEG)$_n$][Tf$_2$N] (n = 1, 2, 3) were found to have M_n values of 68 kDa, 57 kDa and 55 kDa, respectively. The MALDI spectra can be seen in Figures A5.2

XRD profiles of these materials are provided in Figure 5.4. The profiles show that [PMDA-API(PEG)$_n$][Tf$_2$N] (n = 1 and 3) have nearly indistinguishable profiles which peak at 2θ = 16.6 ˚ which corresponds to a d-spacing of 6.20 Å. A secondary small peak also occurs at a median value of 2θ = 35.8 ˚ (d-spacing = 2.9 Å). The main d-spacing value is higher than typical of other polyimides as well as ionic materials. The likely factor that produced both d-spacings was the coordination of the ether groups with the imidazolium groups which corresponded extremely closely with the values of a molecular dynamics simulation done by Zeng, et al., which found that the C(2)-H position of an imidazolium coordinated with the ether linkages at over 2 Å.[8] The larger PMDA moiety likely causes the packing to be restricted which produces the higher 2θ peak.

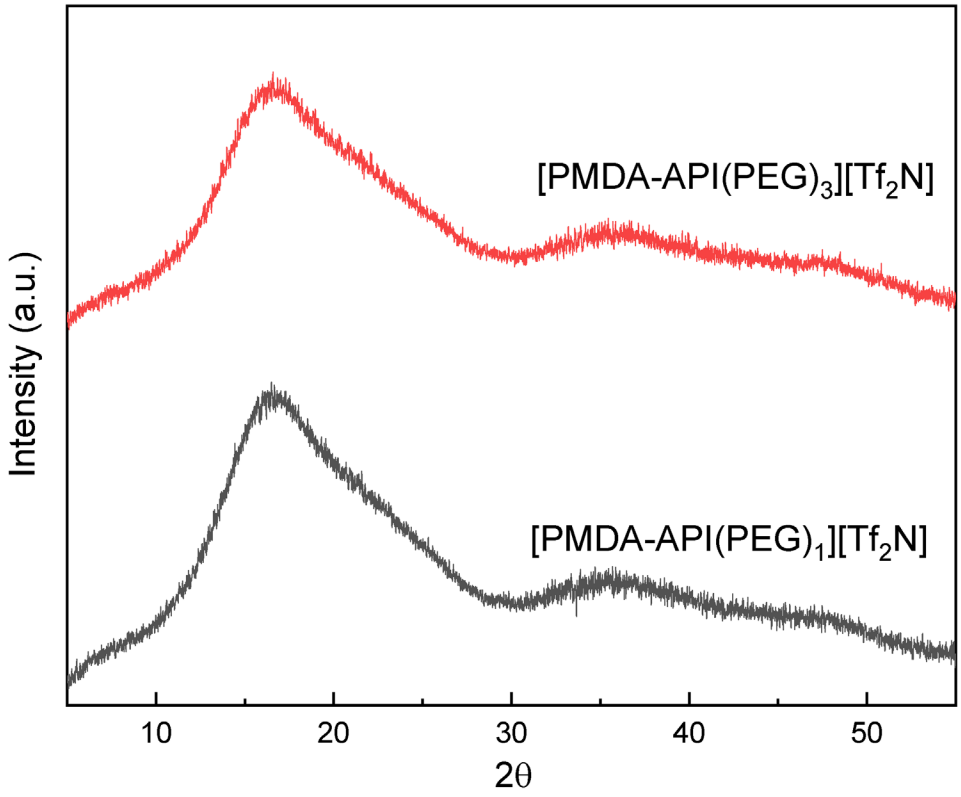

Figure 5.4 XRD Profiles of [PMDA-API(PEG)$_1$][Tf$_2$N] and [PMDA-API(PEG)$_3$][Tf$_2$N]

For the sake of time, only [PMDA-API(PEG)$_1$][Tf$_2$N] and [PMDA-API(PEG)$_3$][Tf$_2$N] were tested as gas separation membranes, and the gas permeation data was determined and is presented in Table 5.3. The initial gas separation testing demonstrated that [PMDA-API(PEG)$_3$][Tf$_2$N] had a higher permeability than the [PMDA-API(PEG)$_1$][Tf$_2$N], which diverged from some of the literature which showed that the [PMDA-API(PEG)$_1$][Tf$_2$N] should have a higher permeability. The neat materials, however, were extremely different in their thermal properties, which have yet to be tested. Through qualitative observation, the [PMDA-API(PEG)$_1$][Tf$_2$N] was glassy at RT while the [PMDA-API(PEG)$_3$][Tf$_2$N] was slightly rubbery at RT. These properties need to be elucidated before any conclusion about the permeabilities of these materials can be concluded. One conclusion that can be made is that the Selectivity of the materials is hindered through the formation of the high d-spacings since gas molecules can more easily permeate through the resulting polymer matrix.

Table 5.3 Permeability values of [PMDA-API(PEG)$_1$][Tf$_2$N] and [PMDA-API(PEG)$_3$][Tf$_2$N]

	Permeability (Barrer)	
	[PMDA-API(PEG)$_1$][Tf$_2$N]	[PMDA-API(PEG)$_3$][Tf$_2$N]
N_2	0.33	1.19
CH_4	0.39	1.31
CO_2	0.52	2.93

5.2.4 Conclusions

Even though this study is only a preliminary investigation into the use of OEG linkages in ionic polyimides, more testing needs to be completed to fully understand the OEG linkage in ionic polymers. In this small study, the polymers were polymerized and formed into membranes which were tested using our high vacuum time lag systems. The XRD profiles of

[PMDA-API(PEG)$_1$][Tf_2N] and [PMDA-API(PEG)$_3$][Tf_2N] were determined which had a high d-spacing with indistinguishable profiles. The permeabilities showed that the increasing amount of OEG content increased the gas permeabilities. Longer gas testing is necessary to determine the overall mechanism of gas permeation through the membrane. Determination of its mechanistic behavior with gases could be linked to other research involving solubility of gases with respect to their OEG content.

5.3 Effects of Mixed Anions on Ionene + IL Composites

5.3.1 Introduction

The effects of anions on the structuring of ILs has been a heavily research topic ranging from halide anions to larger and bulky non-coordinating anions such as [BF_4], [PF_6], [OTf], [BETI], etc.[9-13] The bulk of research on ILs and their ionic counterparts occurs using the [Tf_2N] anion due to the higher CO_2 solubility associated with it. However, through differing methods the anion has been shown to also have coordinating effects within the IL. These affect the intermolecular interactions of the ILs and allow for the side group to play more of a role in the IL, as the C(2) position is seen as integral to the coordination of the imidazolium component.[14, 15]

Few instances exist were combinations of differing anion have been used within ILs. One case from Bara, et al. showed the addition of an IL featuring differing anions (e.g. [Tf_2N], [dca], [SbF_6], and [OTf]) into a polymerizable IL.[11] The PIL-IL composite membranes with [dca], [SbF_6], and [OTf] did not outperform the Tf_2N composites. The [dca], [SbF_6], and [OTf] containing membranes also had very similar gas separation permeabilities and selectivities. Anthony, et al. also investigated the effect of anions on gas solubility of ILs, yet this research used different anions (e.g. [BF_4] and [PF_6]) while also looking at ammonium

and pyrridium ionic liquids.[10] The overall effect on the Henry's constant of the imidazolium based ILs that were tested showed that the [Tf_2N] anion increases gas solubilities compared to either [BF_4] or [PF_6] while [BF_4] and [PF_6] did not have any distinguishable differences.

Through our previous research into polyimide ionenes, [PMDA-API(pXy)] and [6FDA-API(pXy)] were exchanged with different noncoordinating anions such as [BF_4], [PF_6], [OTf], or [BETI], which greatly affected the coordination as seen through the XRD patterns produced.[16] Due to the highly coordinating nature of the smaller anions, namely [PF_6] and [BF_4], the XRD Profiles were highly crystalline which lead to processing issues when trying to form thin films. These anions are also known to stability issues and their effects in polymers was highly unknown.[17] To elucidate the exact coordinating effects of the anions within an ionene + IL blended composite, in particular, [PMDA-API(pXy)][X] (X = BF_4, PF_6, OTf, and BETI), [C_4mim][Tf_2N] was added to the materials, and they were solvent cast to determine the effects of multiple anions on the polymer structure. In another case, [PMDA-API(pXy)][Tf_2N] was mixed with [C_4mim][X], as to determine the effects of the IL anions on the typical ionene structure. The materials were tested using XRD and FT-IR and then as gas separation membranes.

5.3.2 Experimental Section

To form membranes with differing anions, [PMDA-API(pXy)][Cl] was formed using the same procedure from Chapter 4. Upon formation of the polymer, anion metathesis using either LiOTf, LiBETI, KPF_6, or $NaBF_4$ was performed by dissolving both polymer in DI H_2O and salt in DI H_2O and precipitating the polymer in the salt solution forming four distinct polymers with differing anions. This procedure is outlined in full in a previously

published manuscript.[16] After the polymer is formed, the polymer is dissolved into solvent and one molar equivalent of [C_4mim][Tf_2N] was added to the solution. The solution was cast onto a 3-inch glass plate. After the solution completely evaporated, the film was placed into an oven to ensure that the film is completely dried. Ionic liquids with differing anion have also been synthesized which can be used in conjunction with the [PMDA-API(pXy)][Tf_2N] to determine the effects of small anions within IL as plasticizers rather than [C_4mim][Tf_2N].

5.3.3 Results and Discussion

Determining the effects of anion mixtures within ionenes + IL composites could lead to more permeable membranes. Two differing combination of ionenes and ILs can be used so that the anion composition is in a molar ratio of 2:1 being the two anions within the backbone to the one anion within the IL. Many combinations on this type of structuring can be completed to determine the exact effects of having mixtures of anions within an ionene backbone. Investigation of the attractiveness between non-coordinating anion and the imidazolium would be a good study to determine whether anion will be bound to the polymer backbone. The coordination can be determined using low mass MALDI-TOF MS which will determine if the non-coordinating ion flying with the polymer backbone. Images of the [PMDA-API(pXy)][PF_6] + [C_4mim][Tf_2N] and [PMDA-API(pXy)][BF_4] + [C_4mim][Tf_2N] flexibility as a membrane can be seen in Figure 5.5.

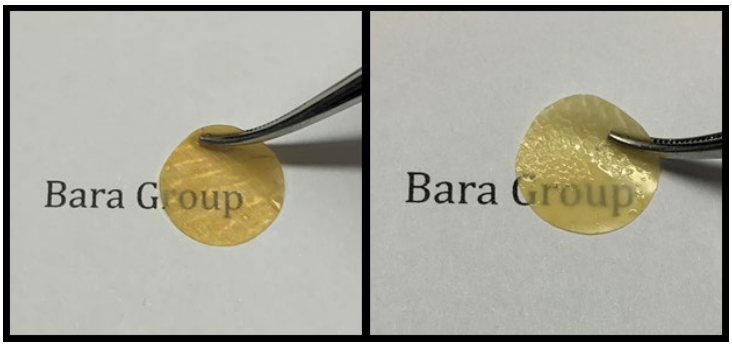

Figure 5.5 Film formation ability of [PMDA-API(pXy)][BF_4] + [C_4mim][Tf_2N] (Left) and [PMDA-API(pXy)][PF_6] + [C_4mim][Tf_2N] (Right)

The XRD profiles of these materials had shown the addition of [C_4mim][Tf_2N] caused an amorphous halos between 2θ = 5˚ to 25˚ to form in nearly all the XRD profiles (Figure 5.6) except the [PMDA-API(pXy)][PF_6] + [C_4mim][Tf_2N] which formed a highly order composite. More XRD patterns will need to be taken to determine if ordering occurs over time after casting the films. It can be noted that the BETI anion, which was the largest has the highest d-spacing value at 6.12 Å. Triflate, BF_4, and PF_6 had the d-spacings which were all very similar at around 4.5 Å. [PMDA-API(pXy)][PF_6] + [C_4mim][Tf_2N], however, had multiple peaks of ordering throughout its profile which indicated coordination.

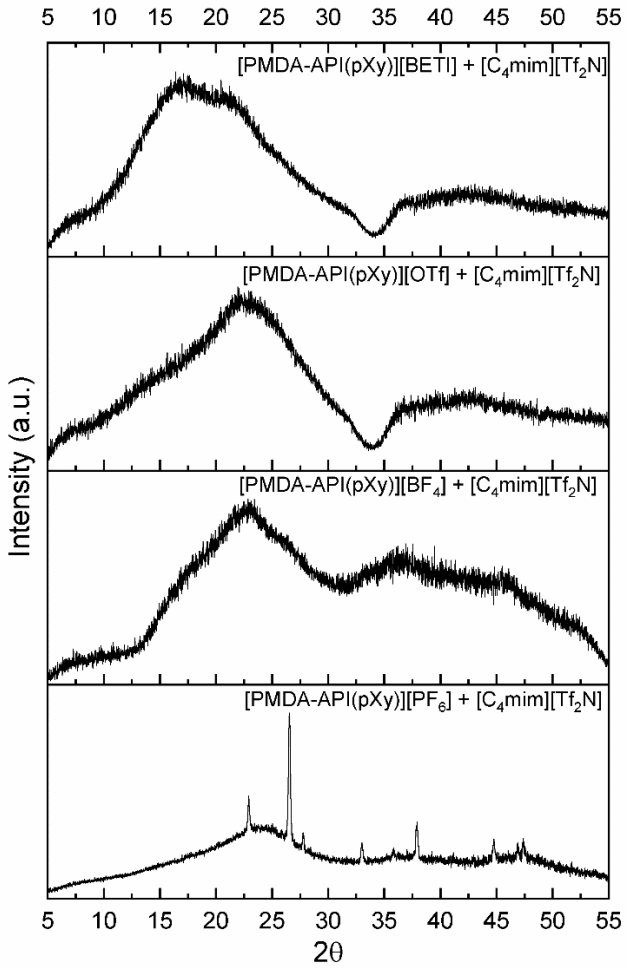

Figure 5.6 XRD profiles of [PMDA-API(pXy)][BETI] + [C_4mim][Tf_2N], [PMDA-API(pXy)][OTf] + [C_4mim][Tf_2N], [PMDA-API(pXy)][PF_6] + [C_4mim][Tf_2N], and [PMDA-API(pXy)][BF_4] + [C_4mim][Tf_2N].

The addition of [C_4mim][PF_6] to [PMDA-API(pXy)][Tf_2N] caused the ordered structure which was typically seen in either [PMDA-API(pXy)][Tf_2N] or [PMDA-API(pXy)][PF_6] + [C_4mim][Tf_2N] to completely disappear (Figure 5.7). The introduction of the [PF_6] anion cannot coordinate with the polymer as [C_4mim][PF_6] was highly bound together, which demonstrated that the [Tf_2N] anions were also tightly bound to the imidazolium cations within the backbone. The standard amorphous halo can still be seen when comparing [PMDA-API(pXy)][Tf_2N] + [C_4mim][PF_6] and [PMDA-API(pXy)][PF_6] + [C_4mim][Tf_2N].

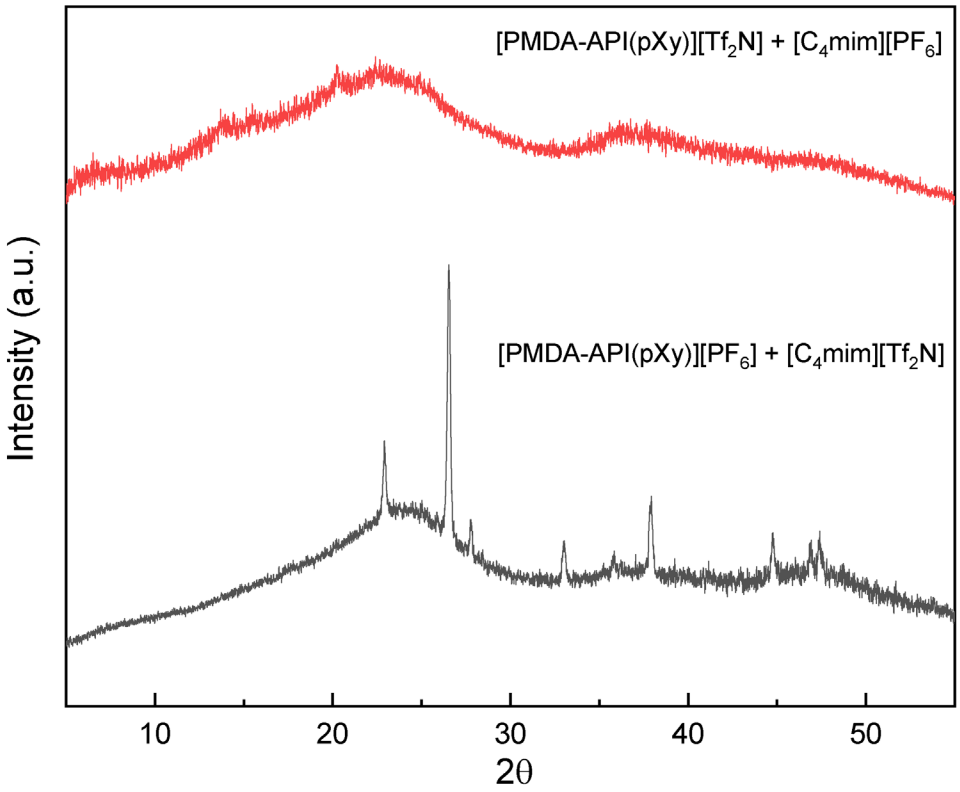

Figure 5.7 XRD profile of [PMDA-API(pXy)][Tf_2N] + [C_4mim][PF_6] and [PMDA-API(pXy)][PF_6] + [C_4mim][Tf_2N]

Currently, one material had been tested in gas separation using a mixture of these anions, so a few more materials needed to be tested to have a good overview of anion effects on permeabilities. [PMDA-API(pXy)][PF_6] + [C_4mim][Tf_2N] was tested using N_2, CH_4, and CO_2 to determine the Permeability, diffusivity, and solubility as seen in Table 5.4. This composite membrane was compared to [PMDA-API(pXy)][Tf_2N] + [C_4mim][Tf_2N] as this composite was most comparable to the anion. The CO_2 permeability decreased with the [PF_6] anion coordinated with the [PMDA-API(pXy)] likely due to the increase in chain-chain interactions that occurred with the smaller anion compared to the [Tf_2N] anion.

Table 5.4 Permeability, diffusivity, and solubility values of [PMDA-API(pXy)][PF_6] + [C4mim][Tf_2N] compared to [PMDA-API(pXy)][Tf_2N] + [C4mim][Tf_2N]

	[PMDA-API(pXy)][Tf_2N] + [C_4mim][Tf_2N]	**[PMDA-API(pXy)][PF_6] + [C4mim][Tf_2N]**
	Permeability	
N_2	0.64 ±0.01	0.15 ±0.007
CH_4	0.89 ±0.06	0.13 ±0.011
CO_2	22.31 ±0.37	3.70 ±0.08
	Diffusivity	
N_2	1.39 ±0.01	0.28 ±0.02
CH_4	2.72 ±0.07	0.49 ±0.02
CO_2	4.8 ±0.1	1.01 ±0.1
	Solubility	
N_2	0.352 ±0.01	0.420 ±0.04
CH_4	0.250 ±0.02	0.210 ±0.02
CO_2	3.500 ±0.03	2.810 ±0.31

The diffusivity changed pretty substantially comparing [PMDA-API(pXy)][PF_6] + [C4mim][Tf_2N] to [PMDA-API(pXy)][Tf_2N] + [C4mim][Tf_2N] demonstrating that the larger [Tf_2N] anion allowed for a higher diffusivity than the [PF_6] anion. The solubility values did not change substantially comparing [PMDA-API(pXy)][PF_6] + [C4mim][Tf_2N] to [PMDA-API(pXy)][Tf_2N] + [C4mim][Tf_2N]. The [PF_6] anion decreased slightly compared to the [Tf_2N] anion which was congruent with what was seen in changing anions within ILs.[10-12]

The selectivity values for permeability, diffusivity, and solubility can be seen in Table 5.5. These values were relatively similar, yet it should be noted that the permselectivity values were slightly different which again can be influenced by the chain-chain spacing of the materials. Looking at the diffusivity and solubility selectivities, the values of the [PMDA-API(pXy)][PF_6] + [C4mim][Tf_2N] and [PMDA-API(pXy)][Tf_2N] +

[C4mim][Tf_2N] were within the same scale which was good since the values were scaling within the same range.

Table 5.5 Permeability, diffusivity, and solubility selectivities of [PMDA-API(pXy)][PF_6] + [C4mim][Tf_2N] compared to [PMDA-API(pXy)][Tf_2N] + [C4mim][Tf_2N]

	[PMDA-API(pXy)][Tf_2N] - [C_4mim][Tf_2N]	**[PMDA-API(pXy)][PF_6] - [C_4mim][Tf_2N]**
	P_i/P_j	
CO_2/N_2	34.7	24.2
CO_2/CH_4	25.0	27.9
	D_i/D_j	
CO_2/N_2	3.5	3.6
CO_2/CH_4	1.8	2.1
	S_i/S_j	
CO_2/N_2	9.9	6.7
CO_2/CH_4	14.0	13.4

5.3.4 Conclusions

Investigation of changing the anions can cause significant differences in the XRD patterns of the film. This further showed that the higher crystalline materials will likely have lower permeabilities compared to their larger anion, more amorphous counterparts. To make further determinations of the effects of anions, more materials need to be tested as gas separation membranes, and the use of different molar ratios of anions needs to be investigated as this can have major structuring effects on the polymer. Lastly, the binding of anions to the cationic polymer backbone needs to be determined as this can also have effects on the exchange of ions between IL and polymer.

5.4 Effects of Interpenetrating Ionene Networks in Polymerized Ionic liquids

5.4.1 Introduction

Macromolecules have been previously studied as a vehicle for ionic liquids (ILs).[18, 19] ILs have unique properties such as electrical and ionic conductivity, thermal and chemical stability, and nonflammability along with negligible vapor pressures. These properties can be imparted to other the polymeric matrices when ILs are added to the bulk to enhance the gas solubility, electrical conductivity, and chemical and physical resistances. ILs have been used within PVDF[20, 21], PMMA[22-24], PEO[25], and even other polymerizable ionic liquids[11, 26, 27]. In most cases, "free" ILs are added to improve the gas permeability of these materials. The act of "locking" materials into a polymerized IL (PIL) can allow for testing of the materials to determine their effects within the PIL structures. This includes larger ionic components that have been proposed in a recent work.[28] Testing PILs with dissolved large molecules can lead to materials that have higher free fractional volume due to the PIL coordinating with the large molecules.

Within the first paper that was published on ionic polyimides by Mittenthal, et al., ionene-IL composite membranes were formed using IL soaked membranes seemed to be the best way for ionene-IL composite membranes.[29] Upon using other polyimide and polyamide ionenes in this type of procedure, the ionene would dissolve within the IL. This dissolution of polymer caused issues as the ionene and IL are rendered useless; however, this concept was taken advantage of to form interpenetrating ionene networks within polymerizable ILs. Although this concept is in its infancy since one IIN had been tested so far. This concept would lead to the use of multivalent imidazolium molecules for IINs in the future.

5.4.2 Experimental Section

To form IINs, 1-vinyl-3-butylimdiazolium bistriflimide ([VC_4im][Tf_2N]) was polymerized using 1-vinylimidazole and 1-bromobutane in ACN under reflux conditions. The resulting bromide was exchanged with bistriflimide to form [VC_4im][Tf_2N] which was our PIL of interest. The [6FDA-API(pXy)][Tf_2N] was made as stated in the Chapter 2. A solution of IL and [6FDA-API(pXy)][Tf_2N] was made with 25 wt% of [6FDA-API(pXy)][Tf_2N], which produced a highly viscous mixture. The polymer + IL solution was placed into an oven at 80 ˚C for 48 h. The solution was mixed intermittently during its time in the oven to help encourage mixing. After bringing the solution to RT. 2-hydroxy-2-methylpropiophenone (a UV initiator) was then added to the solution and mixed carefully to not introduce air into the mixture. Rain-X was applied to two quartz plates. A piece of Supor® PES was cut and placed onto a quartz plate and the mixture was evenly spread across the membrane, and a quartz plate was placed on top to sandwich the film together. A UV-light (λ = 254 nm) was applied to the material which was left for 2 h to polymerize. To ensure completely polymerization, the material was flipped and left to polymerize for 1 h longer. The resulting film easily delaminated from the quartz plates.

To determine the effective thickness of the material, the density of the photopolymerized IIN was found. The addition of weight of the IIN was also determined using five measurements of PES disks and PES + IIN disks. Knowing the weight, density and area, the effective thickness of the material can be back calculated. The thickness is integral in calculations of the gas solubility and diffusivity values.

5.4.3 Results and Discussion

Only two materials had been made using this method, [VC_4im][Tf_2N] + [6FDA-API(pXy)][Tf_2N] and [VC_4im][Tf_2N] + [TC-API(pXy)][Tf_2N] which demonstrated nice flexibility and film forming ability. The XRD profiles (Figure 5.8) were compared to the neat [VC_4im][Tf_2N] to ensure that the shifting in amorphous halo can be seen from the addition of either [6FDA-API(pXy)][Tf_2N] or [TC-API(pXy)][Tf_2N]. The neat [VC_4im][Tf_2N] showed a very strong peak at $2\theta = 17.0^\circ$ while the IIN materials had very similar profiles to each other. Both [VC_4im][Tf_2N] + [6FDA-API(pXy)][Tf_2N] and [VC_4im][Tf_2N] + [TC-API(pXy)][Tf_2N] had peaks that demonstrated lower d-spacing but came to a peak at $2\theta = 22.0^\circ$. This was likely due to the polymer chains coordinating with the PIL shifting the overall d-spacing to come much broader. Recasting the [VC_4im][Tf_2N] + [TC-API(pXy)][Tf_2N] demonstrated a rearrangement of the IIN which pushed the d-spacing to become closer to the value of the neat [VC_4im][Tf_2N]. More investigation needs to be completed on the IIN to determine its effects on the dissolved component before and after dissolution.

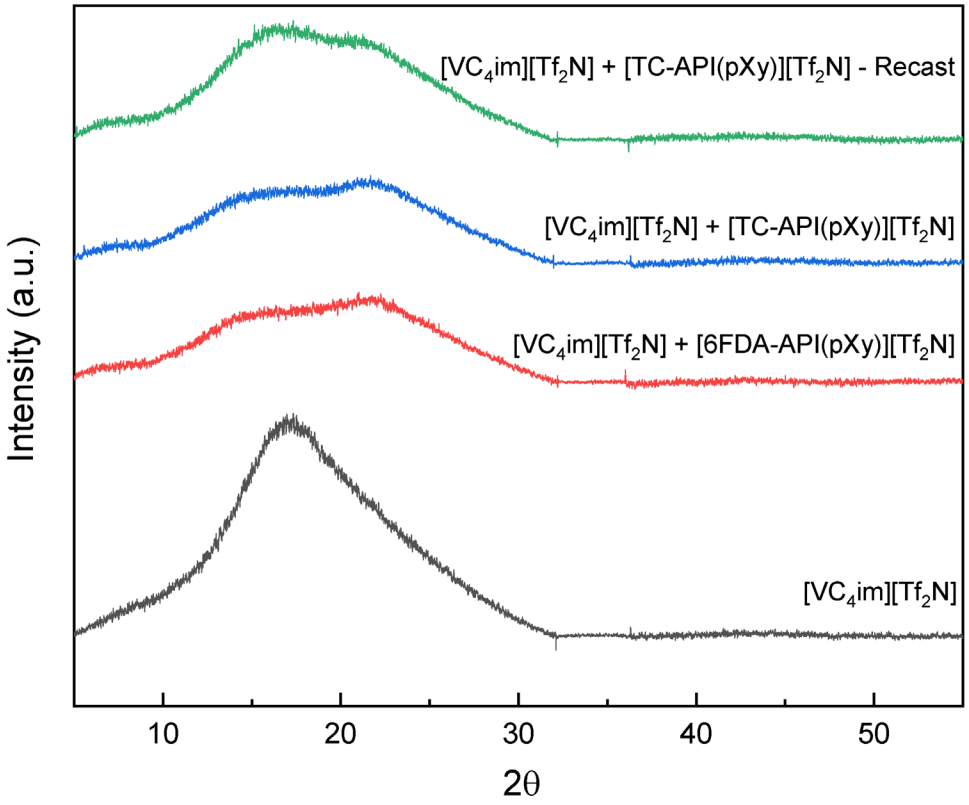

Figure 5.8 XRD Profiles of [VC4im][Tf2N], [VC4im][Tf2N] + [6FDA-API(pXy)][Tf2N] and [VC4im][Tf2N] + [TC-API(pXy)][Tf2N] as well as a recast [VC4im][Tf2N] + [TC-API(pXy)][Tf2N]

The gas separation properties of the [VC4im][Tf2N] and the [VC4im][Tf2N] + [6FDA-API(pXy)][Tf2N] can be seen in Table 5.6. These two materials were chosen to compare the addition of the ionene to the PIL as to determine what the effects of an IIN would be on the overall gas separation abilities of the resulting film. Neat [VC4im][Tf2N] showed the highest permeabilities which correlates to its d-spacing. Comparing [VC4im][Tf2N] + [6FDA-API(pXy)][Tf2N] to [VC4im][Tf2N], [VC4im][Tf2N] had relatively high diffusivity and solubility values which corresponded to IL's ability to facilitate CO_2 adsorption and desorption through the polymer matrix. Looking at the permeability values of the [VC4im][Tf2N] + [6FDA-API(pXy)][Tf2N] compared to [6FDA-API(pXy)][Tf2N] +

[C_4mim][Tf_2N] the permeabilities decreased which was interesting due to the volume of IL that is in the IIN. The reason for the decrease was likely due to the very random nature of the IIN. This feature could be determined to be the case by dissolution of the IIN and recasting the material to look at the rearrangement of the polymer matrix to its lowest energy state through slow evaporation of solvent.

Table 5.6 Permeability, Diffusivity and Solubility values of [VC_4im][Tf_2N] and [VC_4im][Tf_2N] + [6FDA-API(pXy)][Tf_2N] compared to an ionene-IL composite, [6FDA-API(pXy)][Tf_2N] + [C_4mim][Tf_2N]

	[VC_4im][Tf_2N]	**[VC_4im][Tf_2N] + [6FDA-API(pXy)][Tf_2N]**	**[6FDA-API(pXy)][Tf_2N] + [C_4mim][Tf_2N]**
	Permeability		
N_2	1.41 ±0.05	0.27 ±0.034	0.20 ±0.031
CH_4	1.99 ±0.17	0.19 ±0.022	0.18 ±0.017
CO_2	37.00 ±0.16	5.00 ±0.1	6.58 ±0.147
	Diffusivity		
N_2	2.51 ±0.07	0.6 ±0.01	-- --
CH_4	1.65 ±0.28	0.36 ±0.02	-- --
CO_2	5.2 ±0.26	1.2 ±0.09	-- --
	Solubility		
N_2	0.427 ±0	0.340 ±0.03	-- --
CH_4	0.937 ±0.14	0.410 ±0.01	-- --
CO_2	5.390 ±0.26	3.310 ±0.21	-- --

5.4.4 Conclusions

Although the permeability values of this decrease overall when comparing the two materials in their neat states, this method of forming two distinct polymers within each other had not been observed or reported to our knowledge. More work is necessary to determine the exact effects of introduction of ionenes into these polyelectrolyte structures. PILs can be a platform to form new and interesting materials that did not have the ability to

form interconnected networks such as larger molecules that contain multiple imidazolium ions as demonstrated by O'Harra, et al.

5.5 Gas separation Units: Upgrades and Advances

During my time as a graduate student, a lot of work was done to improve and upgrade the gas separation units within the Bara lab (Figure 5.9). The first change that was performed allowed for no leaks within the gas separation systems. The contribution of no leaks allowed for no corrections within final data analysis since the outside atmosphere was not affecting the top or bottom pressure sensors as both sensors were isolated to their respective volumes. Another update that allowed for the reduction of leaks was the exchanging of tube fittings to VCR fittings. Leaks can occur around the tube fittings much more easily that the VCR since the tubing was more fragile than the robust VCR connection that compress around a stainless-steel washer. The tubing connecting the VCR was also changed to be braided Stainless Steel, PTFE-lined tubing. Larger volumes were added to the feed of the gas separation units to help ensure that the permeate volume was nearly infinitesimal to the feed volume. NPT temperature probes were integrated into the feed and permeate of the units to account for the temperature swings that were present in our lab as the units were not temperature-controlled in any manner. This allowed for the temperature to be integrated into the calculations of the permeate.

The next upgrade had to do with the numbers of units and the positioning of the units. A large desk was dedicated solely to gas separation. Super strut ® was bolted and built onto the desk and upwards of 3 units can be run on a single computer. Previously, only one unit was working, so the throughput of our gas separation testing has increased six-fold and will increase even further as we are getting two more gas separation units. the

control panels were added to the units when the units were converted to VCR. This allows easy access to the units on-off valve when applying gas. It also was a reminder to others in the lab the type of membrane that was in the units since it can be written there. The position of the 3-way valves can be difficult to see, so the control panel indicates the on-off-atmosphere positions.

Figure 5.9 Wall of gas separation units added during my time with The Bara Lab

The data processing of the file generated from a gas permeation test had been greatly streamlined as well. A perl program was written which will read the file and create a .xlsx of the permeation data. The program creates a graph, and a table of permeability, diffusivity, and solubility values to help with the ease of processing the data. Addition of statements that generated an easier way for the user to change the range of values within the document to ensure that the user had the final say in what values were being taken and the permeabilities were within the range they should be.

Lastly, an SOP had been formulated. The procedure gave new users a very solid breakdown of the operation of the units without any prior experience. This told the user how to start the units from a complete shutdown of the building's power. The SOP helped

to ensure proper operation of the separation units as well as loading of the film. The procedure went through the applying of gas onto a single unit and the vacuuming of gas on the units. Operation of the perl program was also demonstrated in the SOP since new users may not know how to run the program properly. The SOP can be seen in the appendix of this chapter.

5.6 Membrane Formation Techniques

The main method of membrane formation that was used throughout was melt-pressing. Thought this method can be used for membrane formation, the act of melting and pressing the film can cause a more amorphous structure to occur while not allowing the polymer chains to relax in their lowest energy conformation. By melt pressing films, this can adversely affect the XRD pattern and most importantly the permeability of the resulting membrane. The results of this can be seen in Mittenthal, et al. where the neat [PMDA-API(pXy)][Tf_2N] had an amorphous halo upon melt-pressing, but more recently with a solvent-cast film, the material has local order which is only seen upon soaking the melt-pressed film. Obviously, melt-pressing films can cause issues because ionic polyimides other than [PMDA-API(pXy)][Tf_2N] will dissolve in excess ILs, so modifying the ionene after melt-pressing caused difficulties. However, some materials are still processed through this method, especially materials and IL composites with lower T_g values. To aid in the pressing of materials, different substrates have been chosen so that tacky materials will not stick. Kapton was the typical pressing substrate, yet through trial and error methods, parchment paper, a common baking implement, has been a very good choice for tacky materials as they do not stick to the surface. Another substrate to use for pressing materials has been Teflon sheets. The only issue with Teflon is its soft material characteristics where it can

easily deform once heated especially when the material being pressed is stiff. So, Teflon and parchment paper have been good addition to the formation of melt-pressed films, yet the best method for film formation is still solvent casting.

Figure 5.10 Example of Teflon plate with casting solution in a CNC cut well

Formation methods for solvent cast membrane films can be difficult due to the extremely differing properties such as T_g, T_m, fragility, tackiness, solubility, and chain-chain interactions. To help ameliorate the casting process, different substrates have also been implemented in our casting processes. Many researchers use either glass petri dishes or flat glass plates as to cast membranes due to ease of use and inexpensive costs when casting. Due to the inert and chemical resistance, Teflon has also been used as a casting substrate.[30] In our case, Teflon blocks were cut using CNC to create small wells which are used as a casting surface (Figure 5.10). Only a couple of issues exist with the Teflon which is its soft nature which cause it to mar very easily. Also, due to the walled nature of the cut

Teflon block, the films can be difficult to get out of the Teflon well. Glass, however, is still a very good casting surface as it is very flat as well as inert. It can also be hydrophobic with the use of Rain-X® which helps with the delamination of the film from the glass. Ensuring the compound is completely buffed into the glass is essential as it could have adverse effects on the film if this is not done.

Some general rules for casting films are that no matter the casting surface, the resulting film will not change characteristics drastically (e.g. if the film is brittle on glass, it will have the same features on Teflon). Stickier materials tend to cast better on Teflon due to its inert behavior and anti-adhesion properties. Allowing the film to evaporate at RT will allow for the film to get to its lowest energy state by not forcing the solvent off the material. This technique can aid in the formation of brittle films that would crack and fissure if left in an oven to evaporate. Addition of IL can help plasticize and aid in membrane formation; if a membrane is difficult to cast and delaminate from the casting surface, IL can help lower the T_g of the material which causes it to become rubberier. This technique will allow films to form that are flexible and durable. The use of Rain-X® around the edge of a casting surface can aid in the delamination of the film from its casting substrate. The solvent cast material needs a surface in the center that allows for it to adhere, so by "edging" the glass with the Rain-X® the film will delaminate around that edge much more easily which aids in getting whole films from the casting surface.

5.7 References

1. Kammakakam, I.; O'Harra, K. E.; Dennis, G. P.; Jackson, E. M.; Bara, J. E., Self-healing imidazolium-based ionene-polyamide membranes: an experimental study on physical and gas transport properties. *Polymer International* **2019,** *68* (6), 1123-1129.

2. Stern, S. A.; Liu, Y.; Feld, W. A., Structure/permeability relationships of polyimides with branched or extended diamine moieties. *J. Polym. Sci., Part B: Polym. Phys.* **1993,** *31* (8), 939-51.

3. Hirayama, Y.; Yoshinaga, T.; Kusuki, Y.; Ninomiya, K.; Sakakibara, T.; Tamari, T., Relation of gas permeability with structure of aromatic polyimides I. *Journal of Membrane Science* **1996,** *111* (2), 169-182.

4. Lall-Ramnarine, S. I.; Zhao, M.; Rodriguez, C.; Fernandez, R.; Zmich, N.; Fernandez, E. D.; Dhiman, S. B.; Castner, E. W.; Wishart, J. F., Connecting Structural and Transport Properties of Ionic Liquids with Cationic Oligoether Chains. *J Electrochem Soc* **2017,** *164* (8), H5247-H5262.

5. Tang, S.; Baker, G. A.; Zhao, H., Ether- and alcohol-functionalized task-specific ionic liquids: attractive properties and applications. *Chemical Society Reviews* **2012,** *41* (10), 4030-4066.

6. Chen, Z.; Huo, Y.; Cao, J.; Xu, L.; Zhang, S., Physicochemical Properties of Ether-Functionalized Ionic Liquids: Understanding Their Irregular Variations with the Ether Chain Length. *Industrial & Engineering Chemistry Research* **2016,** *55* (44), 11589-11596.

7. Chen, Z. J.; Xue, T.; Lee, J.-M., What causes the low viscosity of ether-functionalized ionic liquids? Its dependence on the increase of free volume. *Rsc Adv* **2012,** *2* (28), 10564-10574.

8. Zeng, H. J.; Johnson, M. A.; Ramdihal, J. D.; Sumner, R. A.; Rodriguez, C.; Lall-Ramnarine, S. I.; Wishart, J. F., Spectroscopic Assessment of Intra- and Intermolecular Hydrogen Bonding in Ether-Functionalized Imidazolium Ionic Liquids. *The Journal of Physical Chemistry A* **2019,** *123* (39), 8370-8376.

9. Tokuda, H.; Hayamizu, K.; Ishii, K.; Susan, M. A. B. H.; Watanabe, M., Physicochemical Properties and Structures of Room Temperature Ionic Liquids. 1. Variation of Anionic Species. *The Journal of Physical Chemistry B* **2004,** *108* (42), 16593-16600.

10. Anthony, J. L.; Anderson, J. L.; Maginn, E. J.; Brennecke, J. F., Anion Effects on Gas Solubility in Ionic Liquids. *The Journal of Physical Chemistry B* **2005,** *109* (13), 6366-6374.

11. Bara, J. E.; Gin, D. L.; Noble, R. D., Effect of Anion on Gas Separation Performance of Polymer-Room-Temperature Ionic Liquid Composite Membranes. *Industrial & Engineering Chemistry Research* **2008,** *47* (24), 9919-9924.

12. Tome, L. C.; Aboudzadeh, M. A.; Rebelo, L. P. N.; Freire, C. S. R.; Mecerreyes, D.; Marrucho, I. M., Polymeric ionic liquids with mixtures of counter-anions: a new straightforward strategy for designing pyrrolidinium-based CO2 separation membranes. *J. Mater. Chem. A* **2013,** *1* (35), 10403-10411.

13. Cadena, C.; Anthony, J. L.; Shah, J. K.; Morrow, T. I.; Brennecke, J. F.; Maginn, E. J., Why Is CO2 So Soluble in Imidazolium-Based Ionic Liquids? *J. Am. Chem. Soc.* **2004,** *126* (16), 5300-5308.

14. Hunt, P. A., Why Does a Reduction in Hydrogen Bonding Lead to an Increase in Viscosity for the 1-Butyl-2,3-dimethyl-imidazolium-Based Ionic Liquids? *The Journal of Physical Chemistry B* **2007,** *111* (18), 4844-4853.

15. Fumino, K.; Peppel, T.; Geppert-Rybczyńska, M.; Zaitsau, D. H.; Lehmann, J. K.; Verevkin, S. P.; Köckerling, M.; Ludwig, R., The influence of hydrogen bonding on the physical properties of ionic liquids. *Phys Chem Chem Phys* **2011,** *13* (31), 14064-14075.

16. O'Harra, K. E.; Kammakakam, I.; Bara, J. E.; Jackson, E. M., Understanding the effects of backbone chemistry and anion type on the structure and thermal behaviors of imidazolium polyimide-ionenes. *Polymer International* **2019**.

17. Scovazzo, P.; Kieft, J.; Finan, D. A.; Koval, C.; DuBois, D.; Noble, R., Gas separations using non-hexafluorophosphate [PF6]- anion supported ionic liquid membranes. *J. Membr. Sci.* **2004,** *238* (1-2), 57-63.

18. Brazel, R. S. A. P. C. E. C. S.; Brazel, C. S.; Rogers, R. D.; Society, A. C.; Chemistry, A. C. S. D. o. P.; Meeting, A. C. S., *Ionic Liquids in Polymer Systems: Solvents, Additives, and Novel Applications*. American Chemical Society: 2005.

19. Kubisa, P., Application of ionic liquids as solvents for polymerization processes. *Progress in Polymer Science* **2004,** *29* (1), 3-12.

20. Correia, D. M.; Fernandes, L. C.; Martins, P. M.; García-Astrain, C.; Costa, C. M.; Reguera, J.; Lanceros-Méndez, S., Ionic Liquid–Polymer Composites: A New Platform for Multifunctional Applications. *Adv Funct Mater* **2020,** *n/a* (n/a), 1909736.

21. Chen, H. Z.; Li, P.; Chung, T.-S., PVDF/ionic liquid polymer blends with superior separation performance for removing CO2 from hydrogen and flue gas. *Int. J. Hydrogen Energy* **2012,** *37* (16), 11796-11804.

22. Benton, M. G.; Brazel, C. S., An investigation into the degree and rate of polymerization of poly(methyl methacrylate) in the ionic liquid 1-butyl-3-methylimidazolium hexafluorophosphate. *Polym. Int.* **2004,** *53* (8), 1113-1117.

23. Scott, M. P.; Benton, M. G.; Rahman, M.; Brazel, C. S., Plasticizing effects of imidazolium salts in PMMA: high-temperature stable flexible engineering materials. *ACS Symp. Ser.* **2003,** *856* (Ionic Liquids as Green Solvents), 468-477.

24. Scott, M. P.; Rahman, M.; Brazel, C. S., Application of ionic liquids as low-volatility plasticizers for PMMA. *Eur. Polym. J.* **2003,** *39* (10), 1947-1953.

25. Kusuma, V. A.; Macala, M. K.; Baker, J. S.; Hopkinson, D., Cross-Linked Poly(ethylene oxide) Ion Gels Containing Functionalized Imidazolium Ionic Liquids as Carbon Dioxide Separation Membranes. *Industrial & Engineering Chemistry Research* **2018,** *57* (34), 11658-11667.

26. Bara, J. E.; Hatakeyama, E. S.; Gin, D. L.; Noble, R. D., Improving CO2 permeability in polymerized room-temperature ionic liquid gas separation membranes through the formation of a solid composite with a room-temperature ionic liquid. *Polym. Adv. Technol.* **2008,** *19* (10), 1415-1420.

27. Hudiono, Y. C.; Carlisle, T. K.; LaFrate, A. L.; Gin, D. L.; Noble, R. D., Novel mixed matrix membranes based on polymerizable room-temperature ionic liquids and SAPO-34 particles to improve CO2 separation. *J. Membr. Sci.* **2011,** *370* (1-2), 141-148.

28. O'Harra, K. E.; Noll, D. M.; Kammakakam, I.; DeVriese, E. M.; Solis, G.; Jackson, E. M.; Bara, J. E., Designing Imidazolium Poly(amide-amide) and Poly(amide-imide) Ionenes and Their Interactions with Mono- and Tris(imidazolium) Ionic Liquids. *Polymers-Basel* **2020,** *12* (6), 1254.

29. Mittenthal, M. S.; Flowers, B. S.; Bara, J. E.; Whitley, J. W.; Spear, S. K.; Roveda, J. D.; Wallace, D. A.; Shannon, M. S.; Holler, R.; Martens, R.; Daly, D. T., Ionic Polyimides: Hybrid Polymer Architectures and Composites with Ionic Liquids for Advanced Gas Separation Membranes. *Ind. Eng. Chem. Res.* **2017,** *56* (17), 5055-5069.

30. Lin, H.; Freeman, B. D., Gas solubility, diffusivity and permeability in poly(ethylene oxide). *Journal of Membrane Science* **2004,** *239* (1), 105-117.

5.8 Appendix

MALDI-TOF MS

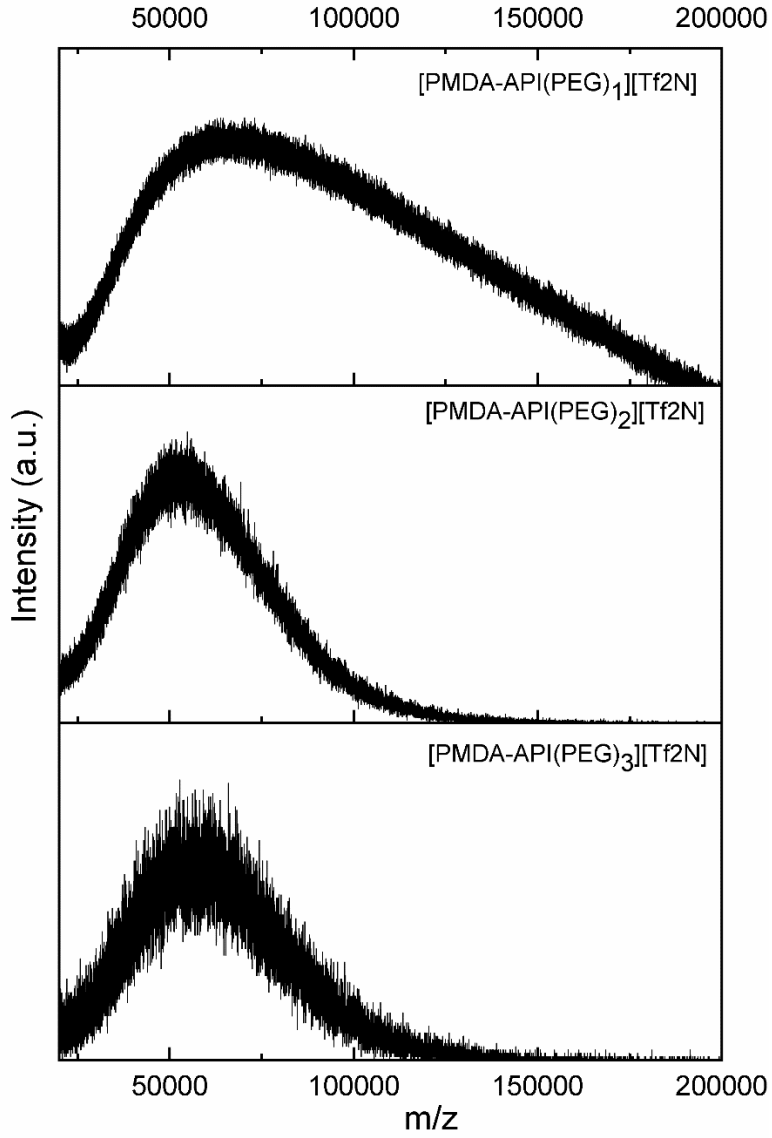

Figure A5.1 MALDI-TOF spectra of [PMDA-API(PEG)$_n$][Tf$_2$N]

FT-IR analysis

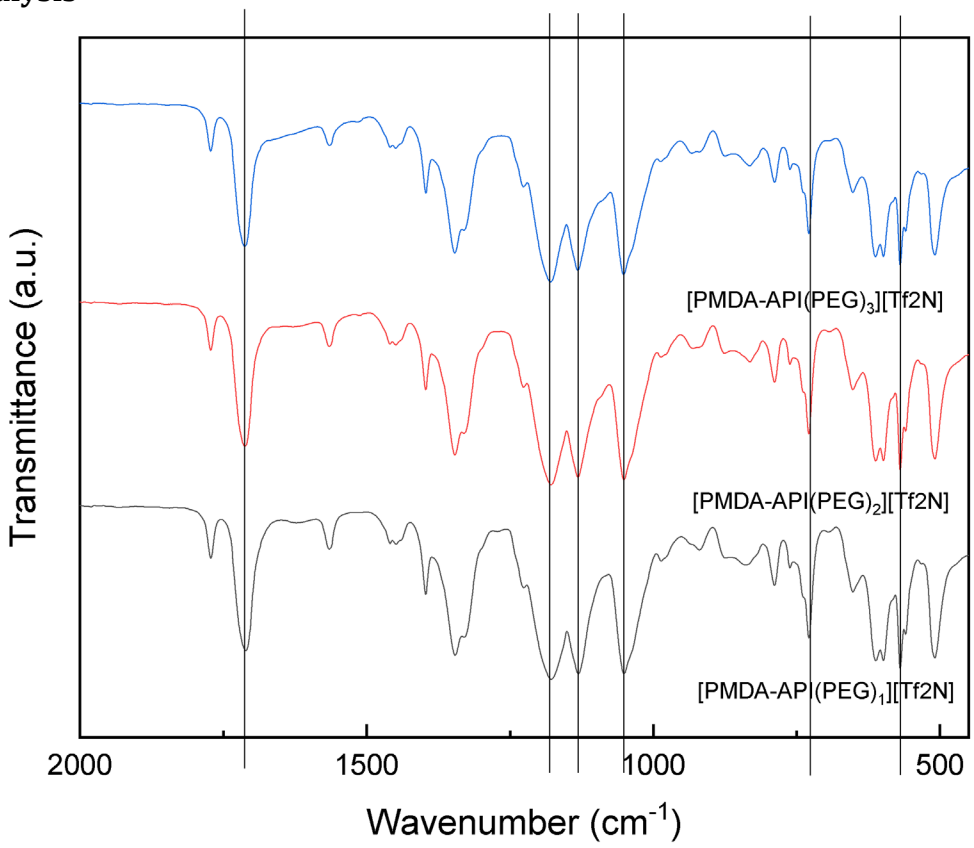

Figure A5.2 FT-IR spectra of [PMDA-API(PEG)$_n$][Tf_2N] with relevant groups marked

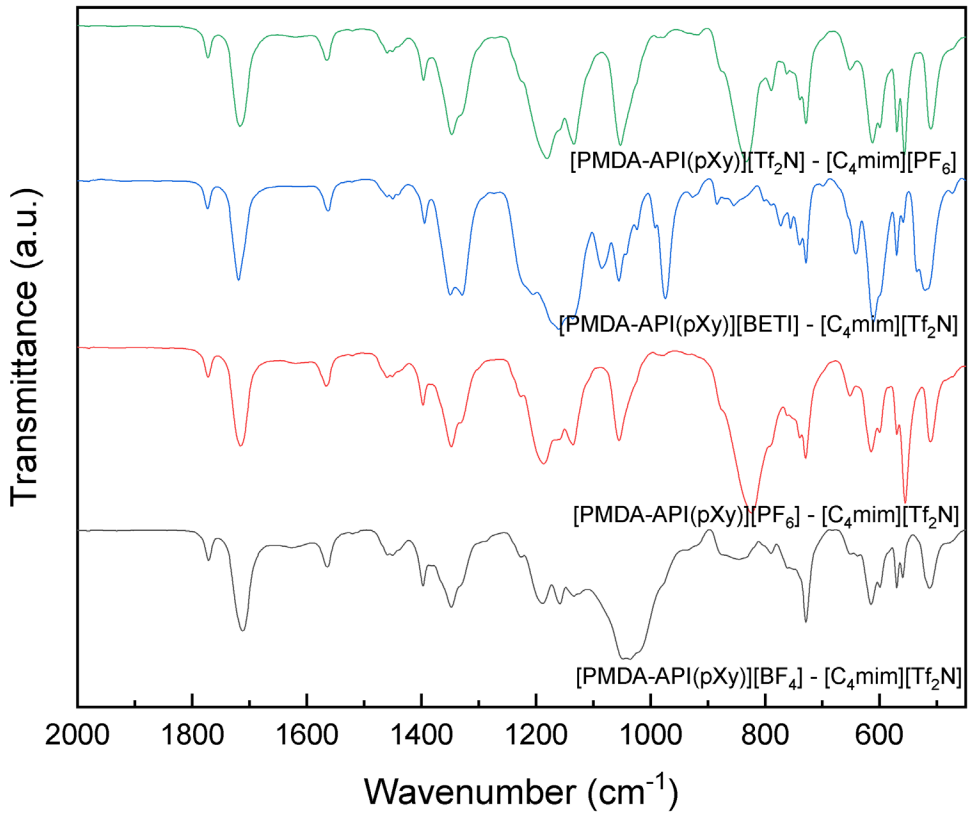

Figure A5.3 FT-IR spectra of [PMDA-API(pXy)][BF_4] – [C_4mim][Tf_2N], [PMDA-API(pXy)][PF_6] – [C_4mim][Tf_2N], [PMDA-API(pXy)][BETI] – [C_4mim][Tf_2N] , and [PMDA-API(pXy)][Tf_2N] – [C_4mim][PF_6]

SOP for Gas Separation Units
Gas separation units

General notes about systems

- It is typically good practice to charge units before vacuuming other units. This will ensure that no gas left in lines is accidentally applied to the already vacuumed units.
- Units that are closed at the top and bottom TYPICALLY have gas applied, whereas units that are open are TYPICALLY vacuuming. There are two exceptions to this rule: Sometimes units get closed and not opened back to vacuum. Check the labview of the unit. If the values of the top and bottom are near or at ZERO, then it is at vacuum. If the value of the top of the unit is at ~45 psi (3 atm), then gas is permeating through the membrane. The second is if the unit is open to atmosphere (ATM on the control panel) These units are at atmosphere likely because a membrane broke or did not get loaded yet into the unit. This should help for you to understand what needs to be done next.

Charging/applying gas onto top of unit (Daily activity):

1. NOTE: Other units should be open to vacuum. Turn off the units that are currently open to VACUUM in the order of TOP (feed), then BOTTOM (permeate), and then CONTROL PANEL. Repeat for ALL vacuuming units.
2. You are free to disconnect the quick connect to the vacuum pump.
3. Once ALL the units are turned off, gather your gas (CH_4, N_2, CO_2, H_2) line you would like to apply and turn on the tank.
4. Check the Regulator (the left side gauge) on the tank so that the GAUGE pressure reads ~2 atm. This will translate to 3 atm ABSOLUTE pressure. Bleed gas line into HOOD. This will allow for any air in the line to be purged by pure gas.
5. Plug in your gas line to the quick connect.
6. Go to the labview. Stop the current test (There are two ways to do this: a stop button on the front panel, and a stop "sign" in the toolbar). In the file path, change the "test" file to the gas (CH_4, N_2, CO_2, H_2) name along with the test number. It should look like this "Membrane_Name_CH4_001". If you would like to find the test number, you can click on the file next to the file path and check the test numbers in the file explorer. Click cancel once you are finished browsing.
7. Once the path has been changed, you can now start the labview using the arrow in the tool bar, and it will run and start saving your file. The pressure values should be near their initial value that you saw when you stopped the "test" file. You can right click both the pressure graphs and reset the graph using the "clear chart" function.
8. Next open the valve on the control panel that you want to charge.
9. While watching the top pressure graph, SLOWLY open the TOP valve. Once you see the pressure start to rise by about 0.1 psi. let it rise to about 4-5 psi. You can now open it slightly more and let it rise to 14 psi. Once it reaches that value, you are free to open it. Wait 2-3 mins for gas to charge

10. The unit is now charged, so close the top valve, and the control panel
11. Repeat steps 6-10 for charging other units. If applying a different gas, apply vacuum before changing gas lines
12. Once you are finished charging the units coil up the gas line and turn off the tank, bleeding the gas line to ensure the thank is off. When you bleed the line, bleed it into the hood when at all possible. Plug the vacuum pump back into the control panel.

Vacuuming gas from a unit:

1. The vacuum should be connected to the control panel. If it is not, you are free to do that now.
2. Go to the labview and stop the current test (There are two ways to do this: a stop button on the front panel, and a stop "sign" in the toolbar). In the file path, change the gas and file number to "test". Whenever your "test" file gets too large, you can delete the "test" file in the file explorer since it is run to see what the pressure gauges are at and is taking up space. Start the labview. You should see the pressures start running again.
3. Ensure all the other valves (top, bottom, and panel) are off to ISOLATE the unit you wish to vacuum. Wait for a ~1-2 minutes to purge gas in the lines to the unit.
4. Open the valve on the CONTROL PANEL to the unit you are vacuuming. Then open the BOTTOM valve. The bottom pressure should drop to zero.
5. SLOWLY open the TOP valve to evacuate the pressurized top. NOTE: The pressure on the top should ALWAYS be 10x the pressure of the bottom. A good "rule of thumb" is that the BOTTOMS pressure should jump to ~1.5 psi but NEVER go above 2 psi.
6. Allow the TOP to get to ~0.2-0.3 psi before SLOWLY opening the top valve. NOTE: Let the unit have vacuum for ~5 minutes before going about vacuuming other charged units.
7. Repeat steps 2-6 to vacuum other units.
8. Once units have been vacuumed, ensure all the other valves (top, bottom, and panel) are off to ISOLATE the unit you wish to vacuum. And vacuum using the BOTTOM and then TOP method to purge gas that may have built up in the membrane.
9. After units have been vacuumed to purge the little amount of gas in them, you are free to open them all to the vacuum pump.

If the computer SHUTDOWN, do the following:

1. Make sure the computer is on. It should always restart to be on.
2. The password for these unit computers is imidazoleAlpha#. This corresponds to the computer name
3. Once you are logged on locate the labview file on the desktop to open all three units' control panels.
4. Change the timing interval to 1 and locate the file path you are going to run and pull up the test file. It can be helpful to look toward the control board to see what membranes are in the units.

5. Start running the test file to see what the status of the membrane is.
6. At this point you can determine whether to charge or vacuum the unit.

Working up data

1. In the file explorer, you wish to create your excel file, there should be an "excel_writer…pl" file. This is the PERL file that writes your data. If there is not locate one and copy it to your folder.
2. While not having a file selected, SHIFT + RIGHT CLICK. This should bring up a menu that displays "Open PowerShell window here".
3. Click the PowerShell, and the UP-arrow key. The shell should display the last command run, which looks like this: "perl excel_writer…pl membrane_name_CH4_001". This being the command to run the data. Change the two last phrases to what you would like to run.
4. Press enter and it will ask for a thickness and then a diameter of your film.
5. After pressing enter it will make your excel file.
6. Wait for it to display the elapsed time which can take ~2 mins.

CHAPTER 6

CONCLUSIONS AND OUTLOOKS

Membrane separation has been proven to be a cost-effective and efficient method to separate gases compared to its other more expensive counterparts. The introduction of ionic moieties within high performance polymer backbones was demonstrated in a facile, modular approach which can lead to the polymerization of many different polymers containing the imidazolium cation. A polyimide-based ionene was the first synthesized ionic polymer which acquired high gas permeability upon adsorption of ionic liquid into its polymer matrix. Using this idea as a platform, a higher FFV unit (PMDA versus 6FDA) was introduced into the polyimide structure. The change in dianhydride unit demonstrated major changes in the polymer structuring leading to a better understanding of the structure-property relationships of polyimide ionenes.

The C(2) position of the imidazolium unit had been shown to be an integral part of ILs and their intermolecular interactions. Methylation of the C(2) position can cause interesting effects on the polymer's chain-chain interactions. Through MD simulations, QM calculations, and experimentation, the C(2) position was determined to have profound effects on the polymer's ability to form thin film membranes without IL as a plasticizer. The MD simulations and QM calculations demonstrated that the electrostatic forces between the polymer are highly increased through the methylation of the C(2) group.

Because of these finding, introduction of other ILs and effects of film processing were investigated within the first polyimide ionene, [PMDA-API(pXy)][Tf_2N]. ILs with differing aromatic, ether, and alkyl groups were added to the polymer to examine the effects on structuring through the XRD patterns. Though the patterns did not change, distinct gas separation properties arose for the differing R groups, and this polyimide ionene had localized ordering which was unusual for amorphous polymers. However, these gas separation properties were congruent with our previous findings of changing the R groups of the IL.

The structure-property relationships of these polymers have always been the utmost priority to determine the direction and outlook for polyimide ionenes. The juxtaposition of differing, yet similar ideas helps provide the driving force, so where do we go next? Ionic polyimides and polyamides have been demonstrated where polyimides have superior gas separation properties, yet formation of polymers with higher FFV units such as Tröger's Base, Triptycene, and PIM can lead to higher gas permeabilities. The methylation of an integral position in the imidazolium moiety was found to not increase the gas permeation abilities although the C(4) and C(5) positions have yet to be explored. Lastly, other works in progress need to be fulfilled to determine their viability in the field of gas separation, where the introduction of inter-spaced ionic charge, more charge density at these locations, and ILs with multiple imidazolium moieties. Much work is still needed to skim the surface of structure-property relationship of ionic polymers and their composites with ILs.

REFERENCES

1. Friedlingstein, P.; Jones, M. W.; O'Sullivan, M.; Andrew, R. M.; Hauck, J.; Peters, G. P.; Peters, W.; Pongratz, J.; Sitch, S.; Le Quéré, C.; Bakker, D. C. E.; Canadell, J. G.; Ciais, P.; Jackson, R. B.; Anthoni, P.; Barbero, L.; Bastos, A.; Bastrikov, V.; Becker, M.; Bopp, L.; Buitenhuis, E.; Chandra, N.; Chevallier, F.; Chini, L. P.; Currie, K. I.; Feely, R. A.; Gehlen, M.; Gilfillan, D.; Gkritzalis, T.; Goll, D. S.; Gruber, N.; Gutekunst, S.; Harris, I.; Haverd, V.; Houghton, R. A.; Hurtt, G.; Ilyina, T.; Jain, A. K.; Joetzjer, E.; Kaplan, J. O.; Kato, E.; Klein Goldewijk, K.; Korsbakken, J. I.; Landschützer, P.; Lauvset, S. K.; Lefèvre, N.; Lenton, A.; Lienert, S.; Lombardozzi, D.; Marland, G.; McGuire, P. C.; Melton, J. R.; Metzl, N.; Munro, D. R.; Nabel, J. E. M. S.; Nakaoka, S. I.; Neill, C.; Omar, A. M.; Ono, T.; Peregon, A.; Pierrot, D.; Poulter, B.; Rehder, G.; Resplandy, L.; Robertson, E.; Rödenbeck, C.; Séférian, R.; Schwinger, J.; Smith, N.; Tans, P. P.; Tian, H.; Tilbrook, B.; Tubiello, F. N.; van der Werf, G. R.; Wiltshire, A. J.; Zaehle, S., Global Carbon Budget 2019. *Earth Syst. Sci. Data* **2019,** *11* (4), 1783-1838.

2. Bernardo, P.; Drioli, E.; Golemme, G., Membrane Gas Separation: A Review/State of the Art. *Ind. Eng. Chem. Res.* **2009,** *48* (10), 4638-4663.

3. Aaron, D.; Tsouris, C., Separation of CO2 from Flue Gas: A Review. *Separ Sci Technol* **2005,** *40* (1-3), 321-348.

4. Bara, J. E., What chemicals will we need to capture CO2? *Greenhouse Gases: Sci. Technol.* **2012,** *2* (3), 162-171.

5. Brennecke, J. F.; Gurkan, B. E., Ionic liquids for CO2 capture and emission reduction. *J. Phys. Chem. Lett.* **2010,** *1* (24), 3459-3464.

6. Freeman, S. A.; Dugas, R.; van Wagener, D. H.; Nguyen, T.; Rochelle, G. T., Carbon dioxide capture with concentrated, aqueous piperazine. *Int. J. Greenhouse Gas Control* **2010,** *4* (2), 119-124.

7. Ramdin, M.; de Loos, T. W.; Vlugt, T. J. H., State-of-the-Art of CO2 Capture with Ionic Liquids. *Ind. Eng. Chem. Res.* **2012,** *51* (24), 8149-8177.

8. Rochelle, G. T., Amine Scrubbing for CO2 Capture. *Science (Washington, DC, U. S.)* **2009,** *325* (5948), 1652-1654.

9. Tennyson, R. N.; Schaaf, R. P., Guidelines can help choose proper processes for gas-treating plants. *Oil Gas J.* **1977,** *75* (2), 78-80, 85-6.

10. Vrachnos, A.; Kontogeorgis, G.; Voutsas, E., Thermodynamic Modeling of Acidic Gas Solubility in Aqueous Solutions of MEA, MDEA and MEA-MDEA Blends. *Ind. Eng. Chem. Res.* **2006,** *45* (14), 5148-5154.

11. Baker, R. W., Future Directions of Membrane Gas Separation Technology. *Ind. Eng. Chem. Res.* **2002,** *41* (6), 1393-1411.

12. Chen, H. Z.; Li, P.; Chung, T.-S., PVDF/ionic liquid polymer blends with superior separation performance for removing CO2 from hydrogen and flue gas. *Int. J. Hydrogen Energy* **2012,** *37* (16), 11796-11804.

13. Du, N.; Park, H. B.; Dal-Cin, M. M.; Guiver, M. D., Advances in high permeability polymeric membrane materials for CO2 separations. *Energy Environ. Sci.* **2012,** *5* (6), 7306-7322.

14. Faiz, R.; Li, K., Polymeric membranes for light olefin/paraffin separation. *Desalination* **2012,** *287*, 82-97.

15. Sanders, D. F.; Smith, Z. P.; Guo, R.; Robeson, L. M.; McGrath, J. E.; Paul, D. R.; Freeman, B. D., Energy-efficient polymeric gas separation membranes for a sustainable future: A review. *Polymer* **2013,** *54* (18), 4729-4761.

16. Scholes, C. A.; Stevens, G. W.; Kentish, S. E., Membrane gas separation applications in natural gas processing. *Fuel* **2012,** *96*, 15-28.

17. Stern, S. A., Polymers for gas separations: the next decade. *J. Membr. Sci.* **1994,** *94* (1-3), 1-65.

18. Wessling, M.; Schoeman, S.; Van der Boomgaard, T.; Smolders, C. A., Plasticization of gas separation membranes. *Gas Sep. Purif.* **1991,** *5* (4), 222-8.

19. Baker, R. W.; Lokhandwala, K., Natural Gas Processing with Membranes: An Overview. *Ind. Eng. Chem. Res.* **2008,** *47* (7), 2109-2121.

20. Budd, P. M.; Msayib, K. J.; Tattershall, C. E.; Ghanem, B. S.; Reynolds, K. J.; McKeown, N. B.; Fritsch, D., Gas separation membranes from polymers of intrinsic microporosity. *J. Membr. Sci.* **2005,** *251* (1-2), 263-269.

21. Carta, M.; Croad, M.; Bugler, K.; Msayib, K. J.; McKeown, N. B., Heterogeneous organocatalysts composed of microporous polymer networks assembled by Tröger's base formation. *Polym. Chem.* **2014,** *5* (18), 5262-5266.

22. Wang, Z.; Wang, D.; Jin, J., Microporous Polyimides with Rationally Designed Chain Structure Achieving High Performance for Gas Separation. *Macromolecules (Washington, DC, U. S.)* **2014,** *47* (21), 7477-7483.

23. Wang, Z.; Wang, D.; Zhang, F.; Jin, J., Tröger's Base-Based Microporous Polyimide Membranes for High-Performance Gas Separation. *ACS Macro Lett.* **2014,** *3* (7), 597-601.

24. Zhuang, Y.; Seong, J. G.; Do, Y. S.; Jo, H. J.; Cui, Z.; Lee, J.; Lee, Y. M.; Guiver, M. D., Intrinsically Microporous Soluble Polyimides Incorporating Tröger's Base for Membrane Gas Separation. *Macromolecules (Washington, DC, U. S.)* **2014,** *47* (10), 3254-3262.

25. Budd, P. M.; McKeown, N. B.; Fritsch, D., Free volume and intrinsic microporosity in polymers. *J Mater Chem* **2005,** *15* (20), 1977-1986.

26. McKeown, N. B.; Budd, P. M., Exploitation of Intrinsic Microporosity in Polymer-Based Materials. *Macromolecules (Washington, DC, U. S.)* **2010,** *43* (12), 5163-5176.

27. Swaidan, R.; Ghanem, B.; Litwiller, E.; Pinnau, I., Physical Aging, Plasticization and Their Effects on Gas Permeation in "Rigid" Polymers of Intrinsic Microporosity. *Macromolecules (Washington, DC, U. S.)* **2015,** *48* (18), 6553-6561.

28. Zhao, S.; Liao, J.; Li, D.; Wang, X.; Li, N., Blending of compatible polymer of intrinsic microporosity (PIM-1) with Tröger's Base polymer for gas separation membranes. *J. Membr. Sci.* **2018,** *566*, 77-86.

29. Al-Juaied, M.; Koros, W. J., Performance of natural gas membranes in the presence of heavy hydrocarbons. *J. Membr. Sci.* **2006,** *274* (1-2), 227-243.

30. Ayala, D.; Lozano, A. E.; de Abajo, J.; Garcia-Perez, C.; de la Campa, J. G.; Peinemann, K. V.; Freeman, B. D.; Prabhakar, R., Gas separation properties of aromatic polyimides. *J. Membr. Sci.* **2003,** *215* (1-2), 61-73.

31. Bos, A.; Punt, I. G. M.; Wessling, M.; Strathmann, H., Plasticization-resistant glassy polyimide membranes for CO2/CH4 separations. *Sep. Purif. Technol.* **1998,** *14* (1-3), 27-39.

32. Calle, M.; Lozano, A. E.; de Abajo, J.; de la Campa, J. G.; Álvarez, C., Design of gas separation membranes derived of rigid aromatic polyimides. 1. Polymers from diamines containing di-tert-butyl side groups. *Journal of Membrane Science* **2010,** *365* (1), 145-153.

33. Costello, L. M.; Koros, W. J., Thermally stable polyimide isomers for membrane-based gas separations at elevated temperatures. *Journal of Polymer Science Part B: Polymer Physics* **1995,** *33* (1), 135-146.

34. Hirayama, Y.; Yoshinaga, T.; Kusuki, Y.; Ninomiya, K.; Sakakibara, T.; Tamari, T., Relation of gas permeability with structure of aromatic polyimides I. *Journal of Membrane Science* **1996,** *111* (2), 169-182.

35. Misra, A. C.; Tesoro, G.; Hougham, G.; Pendharkar, S. M., Synthesis and properties of some new fluorine-containing polyimides. *Polymer* **1992,** *33* (5), 1078-1082.

36. Niwa, M.; Nagaoka, S.; Kawakami, H., Preparation of novel fluorinated block copolyimide membranes for gas separation. *J. Appl. Polym. Sci.* **2006,** *100* (3), 2436-2442.

37. Sanaeepur, H.; Ebadi Amooghin, A.; Bandehali, S.; Moghadassi, A.; Matsuura, T.; Van der Bruggen, B., Polyimides in membrane gas separation: Monomer's molecular design and structural engineering. *Progress in Polymer Science* **2019,** *91*, 80-125.

38. Staudt-Bickel, C.; J. Koros, W., Improvement of CO2/CH4 separation characteristics of polyimides by chemical crosslinking. *Journal of Membrane Science* **1999,** *155* (1), 145-154.

39. Stern, S. A.; Liu, Y.; Feld, W. A., Structure/permeability relationships of polyimides with branched or extended diamine moieties. *J. Polym. Sci., Part B: Polym. Phys.* **1993,** *31* (8), 939-51.

40. Stern, S. A.; Mi, Y.; Yamamoto, H.; Clair, A. K. S., Structure/permeability relationships of polyimide membranes. Applications to the separation of gas mixtures. *Journal of Polymer Science Part B: Polymer Physics* **1989,** *27* (9), 1887-1909.

41. Park, S.-H.; Kim, K.-J.; So, W.-W.; Moon, S.-J.; Lee, S.-B., Gas separation properties of 6FDA-based polyimide membranes with a polar group. *Macromol. Res.* **2003,** *11* (3), 157-162.

42. Liaw, D.-J.; Wang, K.-L.; Huang, Y.-C.; Lee, K.-R.; Lai, J.-Y.; Ha, C.-S., Advanced polyimide materials: Syntheses, physical properties and applications. *Prog. Polym. Sci.* **2012,** *37* (7), 907-974.

43. Xiao, Y.; Low, B. T.; Hosseini, S. S.; Chung, T. S.; Paul, D. R., The strategies of molecular architecture and modification of polyimide-based membranes for CO2 removal from natural gas-A review. *Prog. Polym. Sci.* **2009,** *34* (6), 561-580.

44. Robeson, L. M., Correlation of separation factor versus permeability for polymeric membranes. *J. Membr. Sci.* **1991,** *62* (2), 165-85.

45. Comesaña-Gándara, B.; Chen, J.; Bezzu, C. G.; Carta, M.; Rose, I.; Ferrari, M.-C.; Esposito, E.; Fuoco, A.; Jansen, J. C.; McKeown, N. B., Redefining the Robeson upper bounds for CO2/CH4 and CO2/N2 separations using a series of ultrapermeable benzotriptycene-based polymers of intrinsic microporosity. *Energ Environ Sci* **2019,** *12* (9), 2733-2740.

46. Robeson, L. M., The upper bound revisited. *J. Membr. Sci.* **2008,** *320* (1+2), 390-400.

47. Robeson, L. M.; Smith, Z. P.; Freeman, B. D.; Paul, D. R., Contributions of diffusion and solubility selectivity to the upper bound analysis for glassy gas separation membranes. *Journal of Membrane Science* **2014,** *453*, 71-83.

48. O'Brien, K. C.; Koros, W. J.; Husk, G. R., Influence of casting and curing conditions on gas sorption and transport in polyimide films. *Polymer Engineering & Science* **1987,** *27* (3), 211-217.

49. Coleman, M. R.; Koros, W. J., Conditioning of Fluorine Containing Polyimides. 1. Effect of Exposure to High Pressure Carbon Dioxide on Permeability. *Macromolecules* **1997,** *30* (22), 6899-6905.

50. Kim, T. H.; Koros, W. J.; Husk, G. R.; O'Brien, K. C., Relationship between gas separation properties and chemical structure in a series of aromatic polyimides. *J. Membr. Sci.* **1988,** *37* (1), 45-62.

51. Okamoto, K.-i.; Tanaka, K.; Kita, H.; Ishida, M.; Kakimoto, M.; Imai, Y., Gas Permeability and Permselectivity of Polyimides Prepared from 4,4′-Diaminotriphenylamine. *Polym J* **1992,** *24* (5), 451-457.

52. Tanaka, K.; Taguchi, A.; Hao, J.; Kita, H.; Okamoto, K., Permeation and separation properties of polyimide membranes to olefins and paraffins. *Journal of Membrane Science* **1996,** *121* (2), 197-207.

53. Lin, W.-H.; Chung, T.-S., Gas permeability, diffusivity, solubility, and aging characteristics of 6FDA-durene polyimide membranes. *Journal of Membrane Science* **2001,** *186* (2), 183-193.

54. Coleman, M. R.; Koros, W. J., Isomeric polyimides based on fluorinated dianhydrides and diamines for gas separation applications. *Journal of Membrane Science* **1990,** *50* (3), 285-297.

55. Tanaka, K.; Osada, Y.; Kita, H.; Okamoto, K.-i., Gas permeability and permselectivity of polyimides with large aromatic rings. *Journal of Polymer Science Part B: Polymer Physics* **1995,** *33* (13), 1907-1915.

56. Tanaka, K.; Okano, M.; Toshino, H.; Kita, H.; Okamoto, K.-I., Effect of methyl substituents on permeability and permselectivity of gases in polyimides prepared from methyl-substituted phenylenediamines. *Journal of Polymer Science Part B: Polymer Physics* **1992,** *30* (8), 907-914.

57. Park, J. Y.; Paul, D. R., Correlation and prediction of gas permeability in glassy polymer membrane materials via a modified free volume based group contribution method. *Journal of Membrane Science* **1997,** *125* (1), 23-39.

58. Koros, W. J.; Fleming, G. K.; Jordan, S. M.; Kim, T. H.; Hoehn, H. H., Polymeric membrane materials for solution-diffusion based permeation separations. *Progress in Polymer Science* **1988,** *13* (4), 339-401.

59. Tanaka, K.; Kita, H.; Okano, M.; Okamoto, K.-i., Permeability and permselectivity of gases in fluorinated and non-fluorinated polyimides. *Polymer* **1992,** *33* (3), 585-592.

60. Bara, J. E.; O'Harra, K. E., Recent Advances in the Design of Ionenes: Toward Convergence with High-Performance Polymers. *Macromolecular Chemistry and Physics* **2019,** *0* (0), 1900078.

61. Shaplov, A. S.; Morozova, S. M.; Lozinskaya, E. I.; Vlasov, P. S.; Gouveia, A. S. L.; Tome, L. C.; Marrucho, I. M.; Vygodskii, Y. S., Turning into poly(ionic liquid)s as a tool for polyimide modification: synthesis, characterization and CO2 separation properties. *Polym. Chem.* **2016,** *7* (3), 580-591.

62. Sun, X.; Yang, Y.-K.; Lu, F., Synthesis and properties of ionic, rigid-rod, and thermally stable polyimides containing bipyridinium triflates. *Macromolecules* **1998,** *31* (13), 4291-4296.

63. Bara, J. E.; Carlisle, T. K.; Gabriel, C. J.; Camper, D.; Finotello, A.; Gin, D. L.; Noble, R. D., Guide to CO2 Separations in Imidazolium-Based Room-Temperature Ionic Liquids. *Ind. Eng. Chem. Res.* **2009,** *48* (6), 2739-2751.

64. Han, X.; Armstrong, D. W., Ionic liquids in separations. *Acc. Chem. Res.* **2007,** *40* (11), 1079-1086.

65. Bara, J. E.; Gabriel, C. J.; Carlisle, T. K.; Camper, D. E.; Finotello, A.; Gin, D. L.; Noble, R. D., Gas separations in fluoroalkyl-functionalized room-temperature ionic liquids using supported liquid membranes. *Chem. Eng. J. (Amsterdam, Neth.)* **2009,** *147* (1), 43-50.

66. Cserjesi, P.; Nemestothy, N.; Belafi-Bako, K., Gas separation properties of supported liquid membranes prepared with unconventional ionic liquids. *J. Membr. Sci.* **2010,** *349* (1-2), 6-11.

67. Gan, Q.; Rooney, D.; Zou, Y., Supported ionic liquid membranes in nanopore structure for gas separation and transport studies. *Desalination* **2006,** *199* (1-3), 535-537.

68. Ilconich, J.; Myers, C.; Pennline, H.; Luebke, D., Experimental investigation of the permeability and selectivity of supported ionic liquid membranes for CO2/He separation at temperatures up to 125°C. *J. Membr. Sci.* **2007,** *298* (1+2), 41-47.

69. Lan, W.; Li, S.; Xu, J.; Luo, G., Preparation and Carbon Dioxide Separation Performance of a Hollow Fiber Supported Ionic Liquid Membrane. *Ind. Eng. Chem. Res.* **2013,** *52* (20), 6770-6777.

70. Santos, E.; Albo, J.; Irabien, A., Acetate based Supported Ionic Liquid Membranes (SILMs) for CO2 separation: Influence of the temperature. *J. Membr. Sci.* **2014,** *452*, 277-283.

71. Yoo, S.; Won, J.; Kang, S. W.; Kang, Y. S.; Nagase, S., CO2 separation membranes using ionic liquids in a Nafion matrix. *J. Membr. Sci.* **2010,** *363* (1-2), 72-79.

72. Li, P.; Paul, D. R.; Chung, T.-S., High performance membranes based on ionic liquid polymers for CO2 separation from the flue gas. *Green Chem.* **2012,** *14* (4), 1052-1063.

73. Li, P.; Pramoda, K. P.; Chung, T.-S., CO2 Separation from Flue Gas Using Polyvinyl-(Room Temperature Ionic Liquid)-Room Temperature Ionic Liquid Composite Membranes. *Ind. Eng. Chem. Res.* **2011,** *50* (15), 9344-9353.

74. Bara, J. E.; Hatakeyama, E. S.; Gabriel, C. J.; Zeng, X.; Lessmann, S.; Gin, D. L.; Noble, R. D., Synthesis and light gas separations in cross-linked gemini room temperature ionic liquid polymer membranes. *J. Membr. Sci.* **2008,** *316* (1+2), 186-191.

75. Bara, J. E.; Hatakeyama, E. S.; Gin, D. L.; Noble, R. D., Improving CO2 permeability in polymerized room-temperature ionic liquid gas separation membranes through the formation of a solid composite with a room-temperature ionic liquid. *Polym. Adv. Technol.* **2008,** *19* (10), 1415-1420.

76. Bara, J. E.; Lessmann, S.; Gabriel, C. J.; Hatakeyama, E. S.; Noble, R. D.; Gin, D. L., Synthesis and Performance of Polymerizable Room-Temperature Ionic Liquids as Gas Separation Membranes. *Ind. Eng. Chem. Res.* **2007,** *46* (16), 5397-5404.

77. Blasig, A.; Tang, J.; Hu, X.; Tan, S. P.; Shen, Y.; Radosz, M., Carbon Dioxide Solubility in Polymerized Ionic Liquids Containing Ammonium and Imidazolium Cations from Magnetic Suspension Balance: P[VBTMA][BF4] and P[VBMI][BF4]. *Ind. Eng. Chem. Res.* **2007,** *46* (17), 5542-5547.

78. Carlisle, T. K.; McDanel, W. M.; Cowan, M. G.; Noble, R. D.; Gin, D. L., Vinyl-Functionalized Poly(imidazolium)s: A Curable Polymer Platform for Cross-Linked Ionic Liquid Gel Synthesis. *Chem Mater* **2014,** *26* (3), 1294-1296.

79. Qian, W.; Texter, J.; Yan, F., Frontiers in poly(ionic liquid)s: syntheses and applications. *Chemical Society Reviews* **2017,** *46* (4), 1124-1159.

80. Shaplov, A. S.; Ponkratov, D. O.; Vygodskii, Y. S., Poly(ionic liquid)s: Synthesis, properties, and application. *Polym. Sci., Ser. B* **2016,** *58* (2), 73-142.

81. Tang, J.; Shen, Y.; Radosz, M.; Sun, W., Isothermal Carbon Dioxide Sorption in Poly(ionic liquid)s. *Ind. Eng. Chem. Res.* **2009,** *48* (20), 9113-9118.

82. Tang, J.; Tang, H.; Sun, W.; Plancher, H.; Radosz, M.; Shen, Y., Poly(ionic liquid)s: a new material with enhanced and fast CO2 absorption. *Chem. Commun. (Cambridge, U. K.)* **2005,** (26), 3325-3327.

83. Yuan, J.; Mecerreyes, D.; Antonietti, M., Poly(ionic liquid)s: An update. *Prog. Polym. Sci.* **2013,** *38* (7), 1009-1036.

84. Simons, K.; Nijmeijer, K.; Bara, J. E.; Noble, R. D.; Wessling, M., How do polymerized room-temperature ionic liquid membranes plasticize during high pressure CO2 permeation? *J. Membr. Sci.* **2010,** *360* (1-2), 202-209.

85. Li, P.; Zhao, Q.; Anderson, J. L.; Varanasi, S.; Coleman, M. R., Synthesis of copolyimides based on room temperature ionic liquid diamines. *J. Polym. Sci., Part A: Polym. Chem.* **2010,** *48* (18), 4036-4046.

86. Li, P.; Coleman, M. R., Synthesis of room temperature ionic liquids based random copolyimides for gas separation applications. *Eur. Polym. J.* **2013,** *49* (2), 482-491.

87. Bogert, M. T., The mechanism of the ionene synthesis. *Science (Washington, DC, U. S.)* **1933,** *77*, 197-8.

88. Gibbs, C. F.; Littmann, E. R.; Marvel, C. S., Quaternary ammonium salts from halogenated alkyldimethylamines. II. The polymerization of γ-halogenopropyldimethylamines. *J. Am. Chem. Soc.* **1933,** *55*, 753-7.

89. Mittenthal, M. S.; Flowers, B. S.; Bara, J. E.; Whitley, J. W.; Spear, S. K.; Roveda, J. D.; Wallace, D. A.; Shannon, M. S.; Holler, R.; Martens, R.; Daly, D. T., Ionic Polyimides: Hybrid Polymer Architectures and Composites with Ionic Liquids for Advanced Gas Separation Membranes. *Ind. Eng. Chem. Res.* **2017,** *56* (17), 5055-5069.

90. O'Harra, K. E.; Kammakakam, I.; Noll, D. M.; Turflinger, E. M.; Dennis, G. P.; Jackson, E. M.; Bara, J. E., Synthesis and Performance of Aromatic Polyamide Ionenes as Gas Separation Membranes. *Membranes-Basel* **2020,** *10* (3).

91. O'Harra, K. E.; Kammakakam, I.; Devriese, E. M.; Noll, D. M.; Bara, J. E.; Jackson, E. M., Synthesis and Performance of 6FDA-Based Polyimide-Ionenes and Composites with Ionic Liquids as Gas Separation Membranes. *Membranes-Basel* **2019,** *9* (7), 79.

92. O'Harra, K. E.; Kammakakam, I.; Bara, J. E.; Jackson, E. M., Understanding the effects of backbone chemistry and anion type on the structure and thermal behaviors of imidazolium polyimide-ionenes. *Polymer International* **2019**.

93. Dennis, G. P.; O'Harra, K. E.; Kammakakam, I.; Jones, T. A.; Mittenthal, M. S.; Flowers, B. S.; Tuan, Y.; Jackson, E. M.; Bara, J. E., 6FDA-containing polyimide-ionene + ionic liquid gas separation membranes. *Journal of Polymer Science* **2020,** *58* (18), 2664-2674.

94. Bonhôte, P.; Dias, A.-P.; Papageorgiou, N.; Kalyanasundaram, K.; Grätzel, M., Hydrophobic, Highly Conductive Ambient-Temperature Molten Salts. *Inorganic Chemistry* **1996,** *35* (5), 1168-1178.

95. Endo, T.; Kato, T.; Nishikawa, K., Effects of Methylation at the 2 Position of the Cation Ring on Phase Behaviors and Conformational Structures of Imidazolium-Based Ionic Liquids. *The Journal of Physical Chemistry B* **2010,** *114* (28), 9201-9208.

96. Fumino, K.; Wulf, A.; Ludwig, R., Strong, Localized, and Directional Hydrogen Bonds Fluidize Ionic Liquids. *Angewandte Chemie International Edition* **2008,** *47* (45), 8731-8734.

97. Hunt, P. A., Why Does a Reduction in Hydrogen Bonding Lead to an Increase in Viscosity for the 1-Butyl-2,3-dimethyl-imidazolium-Based Ionic Liquids? *The Journal of Physical Chemistry B* **2007,** *111* (18), 4844-4853.

98. Noack, K.; Schulz, P. S.; Paape, N.; Kiefer, J.; Wasserscheid, P.; Leipertz, A., The role of the C2 position in interionic interactions of imidazolium based ionic liquids: a vibrational and NMR spectroscopic study. *Phys Chem Chem Phys* **2010,** *12* (42), 14153-14161.

99. Zahn, S.; Bruns, G.; Thar, J.; Kirchner, B., What keeps ionic liquids in flow? *Phys Chem Chem Phys* **2008,** *10* (46), 6921-6924.

100. Fumino, K.; Peppel, T.; Geppert-Rybczyńska, M.; Zaitsau, D. H.; Lehmann, J. K.; Verevkin, S. P.; Köckerling, M.; Ludwig, R., The influence of hydrogen bonding on the physical properties of ionic liquids. *Phys Chem Chem Phys* **2011,** *13* (31), 14064-14075.

101. Stassen, H. K.; Ludwig, R.; Wulf, A.; Dupont, J., Imidazolium Salt Ion Pairs in Solution. *Chemistry – A European Journal* **2015,** *21* (23), 8324-8335.

102. Kammakakam, I.; O'Harra, K. E.; Dennis, G. P.; Jackson, E. M.; Bara, J. E., Self-healing imidazolium-based ionene-polyamide membranes: an experimental study on physical and gas transport properties. *Polymer International* **2019,** *68* (6), 1123-1129.